

SURFACE WATER AND GROUNDWATER INTERACTIONS IN NATURAL AND
MINING IMPACTED MOUNTAIN CATCHMENTS

By

Rory Cowie

B. A., The Colorado College, 2004

M. A., University of Colorado, 2010

A dissertation submitted to the
Faculty of the Graduate School of the
University of Colorado for the degree of
Doctor of Philosophy
Department of Geography
2014

This dissertation for the Doctor of Philosophy entitled:
Surface Water and Groundwater Interactions in Natural
and Mining Impacted Mountain Catchments
Written by Rory M Cowie
has been approved for the Department of Geography

Mark W. Williams

Diane M. McKnight

Noah P. Molotch

Holly R. Barnard

Robert L. Runkel

Date

The final copy of this dissertation has been examined by the signatories,
and we find that both the content and the form meet acceptable presentation standards
of scholarly work in the above mentioned discipline.

ABSTRACT

Cowie, Rory (Ph.D., Geography)

Surface water and groundwater interactions in natural and mining impacted mountain catchments

Dissertation directed by Professor Mark W. Williams

Understanding source waters, flow paths, and residence times of water in mountain ecosystems is important when considering critical issues including the sustainability of downstream use, contaminant transport, and the predictive capabilities of hydrologic modeling. Critical Zone development, climatic conditions, and ecosystem characteristics all influence water movement between surface and sub-surface environments in mountain catchments. Additionally, past and present impacts from hardrock mining have significantly influenced the hydrology and geochemistry of many mountain catchments. An improved understanding of surface water and groundwater interaction in natural- and human-influenced mountain environments is therefore critical to adequately manage water resources derived from the mountains.

This work uses hydrologic measurements and mixing models to address surface water and groundwater interactions in three headwater catchments along an elevational gradient (2446 m to 4084 m) within the Boulder Creek Watershed. Isotopic ($\delta^{18}\text{O}$ and $\delta^2\text{H}$) and geochemical (Na^+ , K^+ , Si , Ca^{2+} , Mg^{2+} , Cl^- , SO_4^{2-} ANC) tracers are analyzed with End Member Mixing Analysis (EMMA) to identify temporal changes in the relative contributions of source waters to streamflow generation. Results show that streamflow is derived from groundwater, rain, and snow in the montane and sub-alpine catchments, and from groundwater, talus water, and snow in the alpine catchment. Results also

demonstrate that total precipitation, the fraction occurring as snow, and runoff efficiency increased with elevation. In contrast, the relative contributions of groundwater to streamflow decreased with elevation.

This dissertation also includes two investigations of water sources and pathways leading to the generation of Acid Mine Drainage (AMD) at abandoned hardrock mines. At the Argentine mine in Rico, CO hydrologic connections were identified using natural and applied tracers including isotopes, ionic tracers, and fluorescent dyes. Stable water isotopes ($\delta^{18}\text{O}/\delta\text{D}$) identified a well-mixed hydrological system, while tritium levels in mine waters supported a fast flow-through system with mean residence times of months to years. At the Nelson Tunnel in Creede, CO a combined suite of physical hydrologic parameters, hydrogeologic information, solute chemistry, applied tracers, and isotopic tracers (^3H , $\delta^{18}\text{O}/\delta\text{D}$, $^{87}\text{Sr}/^{86}\text{Sr}$, and $\delta^{14}\text{C}$ of DIC/DOC) were used to determine the sources, pathways, and sub-surface residence times of water contributing to AMD. Results indicated a well-mixed hydrological system where mine waters were not receiving significant direct meteoric inputs or flow from locally recharged groundwater. Instead the most significant contributions to mine discharge were from a deep groundwater flow system with apparent mean residence times of 5,000 to 10,000 years. Results from the mine studies will aid in developing targeted remediation strategies to reduce the impact of AMD to nearby surface waters.

ACKNOWLEDGEMENTS

This research would not have been possible without the support and guidance I received from many professionals. First of all, I would like to thank Dr. Mark Williams, my advisor and committee chair, for his significant contributions to the success of this dissertation research. Through his generous collaboration and funding opportunities I was able to participate in a unique blend of research projects.

Secondly, I would like to thank my committee of Dr. Diane M. McKnight, Dr. Noah P. Molotch, Dr. Holly R. Barnard, and Dr. Robert L. Runkel, whom contributed invaluable suggestions for improving the methodology of this research and writing of this dissertation. Also many thanks go to Holly Hughes and the staff of the Kiowa laboratory for sample analysis and to Jen Morse and staff at the Niwot Ridge LTER for tireless fieldwork and collection of water samples used in this research. Funding assistance was provided by the National Science Foundation grants DEB 1027341 and 0724960.

A final thank you goes to Mike Wireman, the U.S. EPA Region 8, and the Colorado Department of Public Health and Environment for the opportunity to conduct research at two abandoned mine sites in Colorado.

TABLE OF CONTENTS

List of Tables	x
List of Figures	xi
CHAPTER	
1. Introduction	1
Statement of Problems	1
1.1. Climate drivers of hydrological processes in mountain catchments	1
1.2 Hydrologic impacts of abandoned hardrock mines in mountain catchments	4
1.3 Research Objectives and Experimental Design	7
Previous Work	9
1.4 Natural Tracers and Hydrograph Separation	9
1.5 Applied Tracers in Hydrology	10
1.6 Age Dating with Radioactive Isotopes	11
2. Hydrological Processes Controlling Streamflow Generation in Headwater Catchments Across and Elevational Gradient in Boulder Creek Watershed, CO	14
Abstract	14
2.1 Introduction	15
2.2 Study Area	21
2.3 Data and Methods	30
2.3.1 Climate: Air Temperature and Precipitation	30
2.3.2 Discharge	32
2.3.3 Snow and Snowmelt	34
2.3.4 Surface water, Groundwater, Talus and Soil water sampling	35
2.3.5 Laboratory Analysis	36

2.3.6 Hydrograph Separation with End Member Mixing Analysis	37
2.3.7 Diagnostic Tools of Mixing Models	38
2.4 Results	40
2.4.1 Climate	40
2.4.2 Spatial Distribution of Precipitation in Como Creek	43
2.4.3 Snowpack	45
2.4.2 Discharge	46
2.4.5 Runoff Efficiency	48
2.4.6 Stream Water Chemistry	50
2.4.7 End Member Mixing Analysis	51
2.5 Discussion	66
2.5.1 Temperature and Precipitation	66
2.5.2 Snowpack and Snowmelt	69
2.5.3 Discharge and Runoff Efficiency	71
2.5.4 Surface-Groundwater Interactions	74
2.5.5 Conceptual Models of Catchment Hydrologic Processes	79
3. Use of Natural and Applied Tracers to Guide Targeted Remediation Efforts in an Acid Mine Drainage System, Colorado Rockies, USA	84
Abstract	84
3.1 Introduction	85
3.2 Methods	89
3.2.1 Site Description	89
3.2.2 Study Design	92
3.2.3 Natural Tracers and Synoptic Sampling	96
3.2.4 Applied Tracers	98
3.2.5 Tracer Selection and Application	99
3.2.6 Tracer Sampling and Analysis	104
3.2.7 Measuring Streamflow and Mine Discharge	107
3.3 Results and Discussion	109
3.3.1 Silver Creek: Streamflow and Hydrologic Connectivity	

to the Argentine Mine	109
3.3.2 Water Quality	112
3.3.3 Isotopes	116
3.3.4 Applied Tracers: Blaine Tunnel to 517 Shaft	121
3.3.5 Applied Tracers: 517 Shaft to St. Louis Tunnel Portal	125
3.3.6 The St. Louis Tunnel Portal Discharge	130
3.3.7 Targeted Remediation	133
3.4 Conclusions	135
4. Isotopic and Geochemical Approaches to Characterizing Water Movement Through Abandoned Mine Workings, Nelson-Wooster-Humphrey Tunnel Creede, Colorado	137
Abstract	137
4.1 Introduction	138
4.2 Study Area and Background	143
4.2.1 Hydrologic Setting – Watershed	145
4.2.2 Hydrologic Setting – Mine	147
4.2.3 Paleo-hydrogeology	149
4.2.4 Geologic Setting	151
4.2.5 Background: Water Chemistry Techniques	156
4.3 Methods	161
4.3.1 Sampling Locations	161
4.3.2 Nelson Tunnel Tracer Studies	164
4.3.3 Water Chemistry Analytical Parameters	165
4.4 Results and Discussion	171
4.4.1 Water Temperatures	171
4.4.2 Tracer Tests	175
4.4.3 Discharge and Water Balance	176
4.4.4 Groundwater Elevations	180
4.4.5 Water Chemistry	182
4.4.6 Stable Water Isotopes (^{18}O , ^2H)	184

4.4.7 Tritium	187
4.4.8 Radiocarbon analysis (DIC and DOC)	189
4.4.9 Fluorescence Analysis of DOC	196
4.4.9 Strontium	201
4.4.10 Conceptual Flow Path Development	205
4.4.11 Recharge Zone	209
4.4.12 Localized Recharge Areas and Shallow Flow Paths	210
4.5 Remediation Options	211
5. Synthesis of Results and Implications for Future Research	214
5.1 Introduction	214
5.2 Boulder Creek Catchment Hydrology	214
5.2.1 Space-For-Time Substitutions	219
5.3 Surface and Groundwater Interactions with Abandoned Mines	220
5.4 Cumulative Conceptual Model	221
5.5 Implications for Future Research	224
5.5.1 Natural Mountain Environments	224
5.5.2 Mining Impacted Mountain Environments	226
References	227
Appendices	249

List of Tables

Table

2.1	Sampling site descriptions with site abbreviation, elevation at the basin outlet (m), catchment area (ha), dominant landscape type with percent of forest cover, mean annual air temperature (°C), and mean annual precipitation (mm). Mean air temperature and precipitation values are long-term averages from each site.	21
2.2	Precipitation totals of four independent precipitation collectors at C-1, totals at Saddle and D-1, and the distributed precipitation total for CC f or the water years 2010-2012.	44
2.3	Runoff efficiency for GL4 (2010-2012), CC (2010-2012), and GG (2011-2012).	49
3.1	Summary of natural and applied tracers including the amount of tracer used and the application method. Silver Creek locations are marked in figure 3.1b. Detection limits for stable isotopes reported as twice the precision. [TU, tritium units]	94

List of Figures

Figure

2.1	Boulder Creek Watershed Map	22
2.2	Green Lakes Valley Site map	23
2.3	Como Creek Site Map	26
2.4	Gordon Gulch Site Map	28
2.5	Daily Mean Air Temperature Boulder Creek watershed	41
2.6	Precipitation Totals and Type by Elevation 2010-2012	42
2.7	Weekly Snow Depths by Elevation 2010-2012	46
2.8	Specific Daily Discharge by Catchment 2010-2012	48
2.9	Stream Solute and Isotopic Chemistry 2010-2012	51
2.10	Distribution of Residuals from EMMA for Green Lake 4	53
2.11	Distribution of Residuals from EMMA for Como Creek	54
2.12	Distribution of Residuals from EMMA for Gordon Gulch	55
2.13	Relative Root Mean Square Error for all tracers used in EMMA	56
2.14	Mixing Diagram with all Potential End-members for Green Lake 4	58
2.15	Mixing Diagram with Selected Bounding End-members for Green Lake 4	59
2.16	Mixing Diagram with all Potential End-members for Como Creek	60
2.17	Mixing Diagram with Selected Bounding End-members for Como Creek	61
2.18	Mixing Diagram with all Potential End-members for Gordon Gulch	62
2.19	Hydrograph Separation for Green Lake 4, 2010-2012	63
2.20	Hydrograph Separation for Como Creek, 2010-2012	65

2.21	Hydrograph Separation for Gordon Gulch, 2011-2012	66
2.22	Conceptual Diagrams of Hydrologic Cycling in each Catchment	83
3.1	Site Map for Rico-Argentine Mine Complex	97
3.2	Box Plot of pH in mine workings and surface waters	112
3.3	Dissolved zinc and Total Dissolved Aluminum	113
3.4	Sulfate and Dissolved Zinc in Silver Creek	114
3.5	Plot of $\delta^{18}\text{O}$ vs. δD for precipitation, surface waters, and mine waters	119
3.6	Tritium Concentrations in Mine Waters, Surface Waters, Precipitation	121
3.7	Fluoride (F^-) concentrations measured in the 517 Shaft	124
3.8	Tracer Break Through Curves at St. Louis Tunnel Portal	126
3.9	Discharge from the St. Louis Tunnel portal and from Silver Creek	132
4.1	Site Map of Willow Creek Watershed and Nelson Tunnel	144
4.2	Mine sampling locations along the Nelson Tunnel	149
4.3	Central San Juan Caldera Complex and Creede Mining District	155
4.4	Mean Water Temperatures from Different Locations in the Nelson Mine	174
4.5	$\delta^{18}\text{O}$ vs. δD for precipitation, Surface and Groundwater, and Mine water	186
4.6	Tritium Concentrations from Surface Waters, Springs, and Wells	188
4.7	Tritium Concentrations in Mine Waters	189
4.8	$^3\text{H}/^{14}\text{C}$ Diagram for Water Samples with both DIC ^{14}C and Tritium	190
4.9	Radiocarbon results for DIC and DOC of Mine Waters	193
4.10	Radiocarbon Results for DIC and DOC Outside of Mine	196
4.11	Excitation-Emission Matrices for DOC of Mine Waters	200
4.12	Measured vs. Modeled Excitation-Emission Matrices	201
4.13	Box Plots of Strontium Concentrations	203

4.14	Relationship Between $^{87}\text{Sr}/^{86}\text{Sr}$ ratios and $1/\text{Sr}$ Concentrations	205
4.15	Plan View Conceptual Diagram of Water Sources for Mine Discharge	208
4.16	Cross Sectional view of Amethyst Fault and Potential Flow Paths	209
5.1	Conceptual Diagram of Surface Groundwater Interactions	224

Chapter 1

1.0 Introduction

Statement of Problems

1.1 Climate Drivers of Hydrological Processes in Mountain Catchments

The hydrology of the western United States and many other semi-arid regions of the world are dominated by snowmelt runoff (Serreze *et al.*, 1999). Snowmelt-dominated watersheds serve as important landscape features for year-round water retention, supply long term storage, and provide freshwater, energy generation and other ecosystem services to downstream users (Viviroli *et al.*, 2003). Decrease in snow accumulation (Mote *et al.*, 2005; Pederson *et al.*, 2011a,b) and earlier snow melt (Stewart, 2009; Pederson *et al.*, 2011a,b) over the second half of the 20th century in the United States have been linked to increasing winter and spring temperatures and an increasing fraction of precipitation falling as rain instead of snow (Knowles *et al.*, 2006; McCabe & Wolock, 2010). Earlier and decreased snow melt will reduce stream flow during the summer growing season when demand is largest, thus increasing water scarcity in semi-arid areas (Barnett *et al.*, 2005, Cayan *et al.*, 2010; Seager & Vecchi, 2010). In addition, across the western United States a positive feedback loop has been observed in which rising aridity increases the dust load on mountain snowpack, decreasing snow albedo and shifting peak snowmelt earlier leading to even more intensified dryness (Painter *et al.*, 2010; Seager & Vecchi, 2010). For the arid and semi-arid mid-latitude regions worldwide, snowpack is a major component of water storage and source of runoff (Schlaepfer *et al.*, 2012). Specific to Western North America, snow melt contributes up to 50-80% of annual streamflow (Stewart *et al.*, 2005)

and in the Colorado River Basin upwards of 90% of the year-round water supply for municipal and agricultural water is derived from snowmelt-dominated catchments (Viviroli *et al.*, 2003).

The potential impacts of global change on surface water, especially related to projected regional climate patterns and trends, have been studied in some detail (Green *et al.*, 2011). However, much less is known about how subsurface (i.e. soil water and groundwater) will respond to climate change coupled with changes in human activities on the landscape (Holman, 2006; Bovolo *et al.*, 2009; Green *et al.* 2007).

Snowmelt in mountain catchments can be a dominant control on recharge of soil moisture at depth and establishment of hydraulic connectivity in the subsurface (Williams *et al.*, 2009; Hinckley *et al.*, 2012) and therefore exerts important influence on hydrologic partitioning of surface and subsurface waters. However, an outstanding question for snowmelt-dominated watersheds of the western US is how changes in the timing and magnitude of melt will impact the role groundwater plays in streamflow generation. There is evidence that suggests groundwater reservoirs in snowmelt-dominated catchments can be directly impacted by climatological changes through hydrological inputs (e.g. Molotch *et al.*, 2009; Teague & Grant, 2009; Green *et al.*, 2011), particularly headwater catchments with ephemeral discharge (Gleeson & Manning, 2008), with implications for surface water hydrochemistry (e.g. Williams *et al.*, 2006). The challenges of understanding climate-change effect on groundwater are unprecedented because climate change may affect hydrogeological processes and groundwater resources through both direct and indirect ways that have not been sufficiently explored (Dettinger and Earman, 2007).

We know little about mountain aquifers because they commonly involve structurally complicated rocks, extreme head gradients (ground slope angles 10-40°), and dramatically

fluctuating recharge driven by seasonal snowmelt (Liu *et al.*, 2004; Manning & Caine, 2007). Groundwater flow occurs primarily through fractures in these crystalline catchments, reducing the effectiveness of the classic porous medium approach for understanding surface-groundwater interactions (Hazen *et al.*, 2002). Recent studies of alpine areas (Williams *et al.*, 1996; Sueker *et al.*, 2000; Liu *et al.*, 2004) have established that subsurface waters are contributing to streamflow, even in alpine settings. Additional studies in forested mountain headwater catchments have also shown that old water (pre-event/baseflow/groundwater) composes the majority of the surface water outflow (Clow *et al.*, 2003, Manning and Caine, 2007; Liu *et al.*, 2008; Tague & Grant, 2009). Laudon and Slaymaker (1997) compared the runoff sources in a nested alpine and sub-alpine catchment spanning a 400-m elevational gradient in British Columbia, Canada and found a significant difference in the water sources at each location with considerable increase in the amount of pre-event water in the sub-alpine area. The results therefore show the importance of the landscape structure on hydrograph components since the two sub-catchments differed in their soil development and topographic gradients.

However, there has been a lack of research sites spanning large elevation gradients from alpine to the montane, which investigate both seasonally snow-packed and intermittently snow covered catchments within the same watershed. Indeed Burns (2002) made a plea to the catchment hydrology community to apply hydrograph separation studies to catchments with different climates and land use types to gain a better insight into runoff generation processes. An improved understanding of the magnitude and timing of groundwater contributions to streamflow in headwater catchments that span a large elevational gradient will enhance our ability to predict runoff and streamflow generation in response to changes in climate. Additionally, identification of water pathways gives an understanding of the magnitude and

timing of solute fluxes from different hydrological reservoirs in the landscape (Slaymaker, 1988; Williams *et al.*, 2006) and is, therefore essential for the understanding of variations of the stream water chemistry at the catchment scale (Laudon and Slaymaker, 1997). Recent work by Williams *et al.* (2011) addressed changes in stream water chemistry along a large elevational gradient in the Boulder Creek drainage in Colorado and suggested that a space-for-time substitution along the elevational gradient is warranted for at least some biogeochemical processes when there is a switch from the snow to rain transition in annual precipitation. However, the study suggested that steep gradients in air temperature and precipitation resulted in stratification of ecosystem type along the elevational gradient, which translated into a non-continuum in hydrological processes such as water yield from different catchments. Addressing processes such as groundwater storage and the role of groundwater in streamflow generation may provide further insight on the processes that create the non-continuum and if understood may enable revisiting the use of an elevational gradient as a space-for-time substitution to predict how changes in climate will impact water resources in mountain areas. Ultimately, more research is needed to provide greater understanding and predictive capabilities of mountain hydrology (Bates *et al.*, 2008) and the implications of climate change on high-elevation hydrologic partitioning and streamflow generation in the arid mountain west (e.g. Jepsen *et al.*, 2012).

1.2 Hydrologic Impacts of Abandoned Hardrock Mines in Mountain Catchments

The legacy of past hard-rock mining in the United States includes more than 200,000 abandoned or inactive mines (US EPA, 1997) and is a common problem at thousands of abandoned mine sites in the Rocky Mountains (Riebsame, 1997). At the time the mining operations were at their highest levels, environmental controls were limited or non-existent,

leading to a range of environmental impacts. The environmental problems are wide-ranging and include movement of sediments, discharge of acidic waters, and the release and transport of trace metals and other contaminants (e.g. Davis *et al.*, 1991; McKnight *et al.*, 2001; Runkel and Kimball, 2002; Kimball *et al.*, 1994,2002,2007; Bryne *et al.*, 2012). The release of hazardous substances at abandoned mine sites is a result of the extraction and separation of minerals or metals from the host rock material. In addition to waste rock, the underground workings (tunnels, shafts, stopes, etc.) can also generate the release of hazardous substances. The most common type is the release of acid mine drainage (AMD) from mines where sulfide-bearing rocks are present. Streams that drain mineralized areas or catchments impacted by mining activities typically carry substantial loads of dissolved metals and other products of mineral weathering (Nordstrom and Alpers, 1999). Minerals like pyrite (FeS_2), the most abundant of all sulfide minerals, are both chemically and biologically stable when both oxygen and water are excluded from interactions (Johnson & Hallberg, 2003). However, when these minerals are exposed to air and water (i.e. through mining and milling of sulfide-containing ores) the sulfide minerals will oxidize spontaneously with either oxygen or ferric iron acting as the oxidizer. This reaction is abiotic but the rate of reaction can be much greater if lithotrophic prokaryotes are present (Johnson & Hallberg, 2003).

Acidic, metal-rich drainage from abandoned hard-rock mines can produce both acute and chronic environmental problems (McKnight and Feder, 1984; August *et al.*, 2002; Wireman and Stover, 2011; Todd *et al.*, 2012). For example, mine drainage exerts chemical stress (i.e. low pH, dissolved metals) and physical stress (i.e habitat degradation via deposition of metal precipitates) on stream biota (Niyogi *et. al.*, 2002).

From a hydrologic prospective, most hard rock mine settings are located in areas of high mineralization that are commonly associated with fracturing and faulting of geologic materials. The result is high secondary porosity, which combined with the un-uniformity of man-made mining excavations, creates a highly complex hydrogeologic setting. Mines are often located in mountains where the aquifers exist in highly fractured bedrock settings. The mine workings can provide a rapid pathway for groundwater to move to the surface while aiding in the production and transport of AMD along the way.

Given the importance of water resources in mountains, the implementation of successful hydraulic remedies to AMD, and management to prevent remedies from causing additional damage, depends on the ability to properly identify sources of groundwater (or surface water) to the mine workings (Walton-Day and Poeter, 2009). Limited safe access to abandoned mines and associated subsurface waters generating AMD often prevents direct identification and quantification of those sources. An alternative is to use applied tracers to understand water movement within and out of abandoned mines. This can then be coupled with comparison of natural tracer content (stable and reactive isotopes, geochemical constituents) of the mine waters and the surrounding hydrologic environment. The multiple methods of hydrologic investigation improve the conceptual understanding of the interactions of mines with surface water and groundwater in mountain environments. Application of groundwater dating techniques can also be used to improve understanding of flow paths and mean residence times of water contributing to mine discharge, further enhancing the understanding of how surface waters interact with subsurface flows encountered in mine environments.

1.3 Research Objectives and Experimental Design

To address hydrologic processes in natural mountain environment data collection was performed using multiple existing long-term climate stations to first characterize the amount and type of precipitation occurring in three headwater catchments that span an elevational gradient from the rain/snow transition in the montane forest to the snow dominated alpine in the Boulder Creek drainage located in the Colorado Front Range. Continuously recording temperature and precipitation data was analyzed for the 2010-2012 water years and precipitation was characterized as snow/rain or mixed precipitation to provide seasonal context. Streamflow discharge was quantified in each catchment using stage-discharge relationships to develop empirical rating curves. The runoff efficiency was calculated as the amount of annual discharge relative to annual precipitation in each catchment. Next the annual discharge was separated into sources and relative contributions using End Member Mixing Analysis (EMMA) (Christophersen & Hooper, 1992; Christophersen *et al.*, 1990). The identified hydrologic processes were then incorporated into conceptual models of the individual catchments. The models were designed to provide a framework to address spatial and temporal variability of the drivers (inputs) and resulting responses (streamflow generation) in each catchment. The results of the study were then used to address the variability of catchment scale hydrologic response to climate variability along a large elevational gradient and re-visit the predictive capabilities of “space-for-time” substitutions (Williams *et al.*, 2011).

The hydrologic processes controlling mine drainage were investigated in two specific abandoned mine sites in the San Juan Mountains of Colorado. The investigations were designed to provide the information necessary to develop remediation strategies for controlling AMD and minimizing long-term environmental impacts. The first study at the Rico-Argentine mine in

Rico, Co addressed the need to define hydrologic connections between surface water, groundwater, and mine workings to understand the source of both water and contaminants in the drainage tunnel discharge. To identify hydrologic connections the study utilized a combination of natural and applied tracers including water isotopes, ionic tracers, and fluorescent dyes. The study specifically focused on using multiple combinations of applied tracers that would identify unique sources and flow paths in a complex mixing environment. Tracer application and recovery was also designed to account for potential analytical complications associated with interactions with low pH, high metal content waters.

The second study at the Nelson Tunnel in Creede, CO was also designed to identify the sources and pathways of water contributing to mine tunnel drainage. The study utilized multiple techniques including physical hydrologic parameters, hydrogeologic information, solute chemistry, applied tracers, and a suite of isotopic analysis. Preliminary results from this study indicated that the mine discharge water had longer residence times than seen in Rico and other mine systems in Colorado (Hazen *et al.*, 2002; Wireman *et al.*, 2006; Walton-Day and Poeter, 2009). Therefore, this study included additional analysis of the $\delta^{14}\text{C}$ of dissolved inorganic carbon (DIC) and dissolved organic carbon (DOC) and strontium ($^{87}\text{Sr}/^{86}\text{Sr}$) to gain insight on subsurface residence times and flowpaths of groundwater that could not be identified with the shorter-lived tritium isotopes or identified by temporal variability in stable water isotopes.

Although both applied studies were at mine sites in the volcanic San Juan Mountains of Colorado, they differed in groundwater residence times driven by local hydrogeologic setting. The two mine studies thus provided a unique opportunity to address the applicability of using similar isotopic, geochemical, and applied tracer techniques to understand hydrologic processes controlling mine discharge in different settings.

Previous Work

1.4 Natural Tracers and Hydrograph Separation

Understanding streamflow generation using natural tracers in semi-arid, seasonally snow-covered mountain streams is an essential tool for water resources management, water quality study and evaluation of impacts from climate change (Jin *et al.*, 2012). Graphical, hydrometric-based separation of storm hydrographs dates back over 50 years with early approaches equating to defining fast and slow components equated to storm runoff and groundwater (Klaus & McDonnell, 2013). Development of hydrograph separation using water isotopes was a major development first introduced by Hubert *et al.* (1969) using tritium (^3H). Since that time, over 200 published journal articles have used the naturally occurring stable isotopes in water (^{18}O and ^2H (deuterium)) to separate event and pre-event water flow in a variety of climates, landscapes, and land use conditions (Klaus & McDonnell, 2013). Early recognition that soil water can contribute to streamflow (Kennedy *et al.* 1986) and can have different isotopic composition than groundwater (DeWalle *et al.* 1988) provided evidence that two-component hydrograph separation was incomplete leading to early use of three-component hydrograph separation using both an isotope and a geochemical tracer (e.g. DeWalle *et al.* 1988, Swistock *et al.* 1989, Wels *et al.* 1991). More recent research has gone beyond the original two time-source components to define other geographic sources such as snow, rain, and subsurface water (e.g. Seuker *et al.*, 2000), and specific geomorphical units (Hoeg *et al.*, 2000). Recently others (e.g. Liu *et al.*, 2004; Williams *et al.*, 2006) have combined isotopes with several geochemical tracers in end-member mixing analysis (EMMA) technique developed by Hooper *et al.* (1990). The application of EMMA operates under an assumption that the solute and isotope tracers are conservative and the

chemical reactions, mixing, and transport processes of different contributing sources in ground and surface waters generate unique signatures for each end member. If distinct end members can be identified then the application of EMMA across space (different catchments) and time (multiple years) can help improve our understanding of how varying geoclimatic conditions influence hydrologic partitioning and streamflow generation in mountains.

1.5 Applied Tracers in Hydrology

Conservative tracers used in hydrologic studies include naturally occurring natural cations, anions, and isotopes as well as applied artificial tracers (Kendall and Caldwell, 1998; Herczeg and Edmonds, 2000). Artificial tracers commonly include fluorescent dyes and inorganic salts and tracer injections are commonly used to estimate discharge, particularly in streams where conventional measurements are not really possible or practical (Kilpatrick and Cobb, 1985; Zellweger, 1994; Kimball *et al.* 2002). Fluorescent dyes have been widely used as tracers in both surface and ground water systems (Sabatini and Austin 1991; Smart and Laidlaw 1977). Today, the most common water tracers are Rhodamine WT (an orange fluorescent dye) and fluorescein (a Green fluorescent dye). Fluorescein is often chosen as a suitable tracer in groundwater applications because it is visible detectable in low concentrations but undergoes photochemical decay in sunlight while Rhodamine WT is less photochemically active and more commonly used in surface water studies (Smart and Laidlaw, 1977). Salts such as chloride, bromide, lithium, and fluoride are good alternative tracers to fluorescent dyes for both surface and groundwater tracing because they are very soluble, relatively inexpensive, conservative, and nontoxic at typical tracer concentrations while also being easily detectable at low concentrations. Continuous injections of salt tracers such as sodium bromide (NaBr) can be used to quantify

streamflow estimates via the tracer dilution method (Kilpatrick and Cobb, 1985) and enables researchers to identify potential areas of flow loss. Conservative tracer injections have been successfully used to estimate discharge, particularly in streams where conventional measurements (i.e. current meters) are not possible or practical (Kilpatrick and Cobb, 1985; Zellweger, 1994, Kimball *et al.*, 2002; Schemel *et al.*, 2006). When salt tracer injection techniques are combined with solute-transport calculations, multiple scale metals loading and attenuation processes can be assessed when studying streams affected by AMD (i.e. Kimball *et al.*, 2002; Runkel and Kimball, 2002; Schemel *et al.*, 2006). Injection studies can also be used for travel time studies in natural surface water settings (i.e. Williams *et al.*, 1993) and in subsurface water movement in abandoned mines (i.e. Davies, 2002, Cowie *et al.*, 2014). In recent years, surface and groundwater tracing techniques have been used in a variety of complex hydrogeologic settings to aid in characterizing groundwater flow systems (e.g. Alvarado *et al.*, 2007; Trolldberg *et al.*, 2008; Lavastre *et al.*, 2010, Cowie *et al.* 2014). Tracing techniques have been demonstrated to be useful in karst and fractured rock hydrogeologic settings (Moore *et al.*, 2012) especially when traditional Darcy's Law approach to define hydrologic conditions cannot be easily applied to these settings. The coupling of both natural and applied tracers can further enhance the understanding of hydrologic partitioning in mountains.

1.6 Age Dating with Radioactive Isotopes

Radioactive isotopes, such as ^3H and ^{14}C , provide a method of obtaining information on physical parameters of water sources that are not easily obtained by other approaches. Tritium has a half-life of 12.43 years (Maloszewski *et al.*, 1983) and is the only conservative tracer that can be used to determine the age of water older than one year. Kaufman and Libby (1954) were

the first scientists to recognize the potential for dating groundwater with cosmogenic tritium, and coincidentally generation ^3H from thermonuclear bombs was in 1951. As a result, for several decades after nuclear weapons testing the presence of thermonuclear tritium in groundwater was used as clear evidence for active recharge (Clark and Fritz, 1997). As of the late 1990's most levels of tritium in precipitation had returned to near background (i.e. 5-10 TU's) so now it is used primarily for identifying "modern" groundwater. Qualitatively, measurable ^3H in ground waters generally signifies modern recharge. If levels are above background (i.e. > 10 TU in Colorado) "bomb spike" water is decades old water, and if levels are near detection (i.e. 1-2 TU) the water was recharged prior to the 1950's and is considered sub-modern. Therefore, tritium's useful timescale is on a decadal level with a maximum range of about 50 years.

There are three principal isotopes of carbon, which occur naturally: ^{12}C , ^{13}C (both stable) and ^{14}C (unstable or radioactive). The radiocarbon method is based on the rate of decay of the radioactive or unstable ^{14}C isotope, which has a half-life of 5730 years (Clark and Fritz, 1997). ^{14}C is a useful tracer for aiding in estimating the age of ground waters that were recharged in the late Quaternary or later. ^{14}C is one of the leading tools in estimating the age of paleo and fossil groundwaters. The method is based upon incorporation of atmospherically derived ^{14}C from the decay of photosynthetically-fixed carbon in the soil. ^{14}C in the soil can be incorporated into solution as dissolved inorganic carbon ($\text{DIC} = \text{CO}_2 + \text{HCO}_3^- + \text{CO}_3^{2-}$) or as dissolved organic carbon (DOC).

Groundwater age is based on measuring the loss of parent ^{14}C by radioactive decay and assumes that the initial concentration of the parent ^{14}C is known and that radioactive decay is the only process that changes the concentration of the parent ^{14}C (or other processes are corrected for). For example the reaction and evolution of carbonate systems can dilute the initial ^{14}C

activity in DIC and DOC (Clark and Fritz, 1997). Anthropogenic activities over the past century have also resulted in further dilution of initial ^{14}C activity. These problems are not simple and result in a complicated analytical methodology that requires corrections to account for the dilution. In this research age estimates of groundwater will be made using ^{14}C measurements from both DOC and DIC with application of a tritium correction technique (Verhagen *et al.*, 1974) to try and account for age uncertainties.

Chapter 2

Hydrologic Processes Controlling Streamflow Generation in Headwater Catchments Across an Elevational Gradient in Boulder Creek Watershed, Colorado

Abstract

Isotopic ($\delta^{18}\text{O}$ and $\delta^2\text{H}$) and geochemical (Na , K^+ , Si , Ca^+ , Mg^+ , Cl^- , ANC) tracers were used to identify temporal changes in relative contributions of source waters to streamflow generation in three headwater catchments along an elevational gradient (2446 m to 4084 m) within the Boulder Creek Watershed in the Front Range of Colorado. The three catchments represent the rain-snow transition zone in the montane forest, the seasonally snow covered sub-alpine to alpine transition zone, and a snow dominate high elevation alpine zone near the continental divide. During the three-year study (2010-2012) the catchments experienced precipitation inputs that were average (2010), above average (2011) and below average (2012) relative to long-term records. In 2012 all catchments experienced peak discharge associated with summer rain as opposed to traditional snowmelt dominated hydrographs observed in the other years. Precipitation regimes varied from 512 ± 43 mm (39 \pm 10% snow) at the lowest elevation catchment to 1439 ± 289 mm (84 \pm 10% snow) in the alpine. Runoff efficiency (Q/P) increased with elevation, averaging 10% in the montane, 24% in the sub-alpine, and 88% in the alpine.

Diagnostic tools of mixing models were used to identify the conservative tracers necessary to perform End Member Mixing Analysis (EMMA) and identify appropriate end-members (source waters) contributing to streamflow. All catchments were identified as three end-member systems with contributions from groundwater, rain, and snow in the montane and sub-alpine catchments and from groundwater, talus water, and snow in the alpine catchment. On average annual streamflow in the montane was 43% groundwater, 41% snowmelt water, and 16% rain while in the subalpine streamflow was 36% groundwater, 54% snowmelt water, and 10% rain. Alpine streamflow was 21% groundwater, 58% snowmelt water, and 21% talus water. During average and above average snowfall years snowmelt was the dominant contributor to streamflow in all catchments. However in 2012 snowmelt water contribution was reduced to 30%, 42%, and 50% from low to high elevation with earlier and smaller peak contributions in all catchments. Interestingly, groundwater contributions were greatest in 2012 for the montane and sub-alpine catchments but were lower in the alpine catchment. Talus water contributions doubled in the alpine in 2012 while rain contributions increased in the lower elevation catchments, with peak contributions occurring after significant (>100 mm) July rainfall. Results indicate that, under current conditions, surface water and groundwater interaction controlling streamflow generation at different elevations are influenced by non-linear variations in temperature and precipitation. Results also suggest that subsurface contributions (groundwater and talus water) are influenced by both the timing and magnitude of recharge and by the storage capabilities of the subsurface. An improved understanding of the current geoclimatic framework controlling streamflow

generation at different elevations provides key insight on the applicability of a space for time hypothesis to predict future hydrologic scenarios in light of a changing climate.

2.1 Introduction

The hydrology of the western United States and many other semi-arid regions of the world is dominated by snowmelt runoff (Serreze *et al.* 1999). In general, the western United States is predicted to face warmer temperatures, more frequent and prolonged droughts, and more precipitation falling in intense storms (Doherty *et al.*, 2009). When these factors combine we can expect to see a decrease in annual snow pack, earlier onset of snowmelt, and increased evaporation (Hamlet *et al.*, 2005; Stewart *et al.*, 2005; Clow, 2010; Pielke *et al.*, 2005). These studies agree that the most pronounced changes are detected for lower altitudes, which is consistent with the explanation that temperature trends are most visible at those elevations where change in temperature leads to increased rain versus snow precipitation (change in snow line) (Bavay *et al.* 2009). Observed snow reductions are most pronounced at temperatures near freezing, i.e. those that tend to occur more often at lower elevations and in fall or spring (Knowles *et al.*, 2006), whereas colder areas (higher elevations) are less sensitive or may experience increased snowfall due to higher moisture availability (Adam *et al.*, 2009; Stewart, 2009; Ramussen *et al.*, 2011). Therefore the current temperature and precipitation regimes in lower elevation mountain catchments provide insight into what may be received by higher elevation catchments in the future. The combination of shifts in seasonality and changes in total runoff are likely to have consequences for future water availability, increasing the challenges for management of water resources originating in mountains (Viviroli *et al.* 2011). Understanding changes in streamflow generation, and surface groundwater interactions, under these changing

climatic conditions will become increasingly important as water availability becomes limiting for domestic, municipal, and agricultural uses.

An outstanding question for snowmelt-dominated watersheds of the western US is the role groundwater plays in streamflow generation. We know little about mountain aquifers because they commonly involve structurally complicated rocks, extreme head gradients (ground slope angles 10-40°), and dramatically fluctuating recharge driven by seasonal snow melt (Liu *et al.*, 2004; Manning & Caine, 2007). Groundwater flow occurs primarily through fractures in these crystalline catchments, reducing the effectiveness of the classic porous medium approach for understanding surface-groundwater interactions (Hazen *et al.*, 2002). The coarse-grained nature of the surface geological material and steep slopes in alpine catchments has led to the common assumption that these basins have little water-storage capacity resulting in rapid movement of water through the subsurface (Clow, 2003).

Recent studies of alpine areas (Williams *et al.*, 1997; Sueker *et al.*, 2000; Liu *et al.*, 2004; Jepsen *et al.*, 2012; Spencer *et al.*, 2014) have dispelled the myth of a “teflon” basin and established that subsurface waters are contributing to streamflow, even in alpine settings. Recognizing the importance of groundwater derived in mountain watersheds (i.e. Manning and Solomon, 2005; Tague *et al.*, 2008; Ali *et al.*, 2010; Ajami *et al.*, 2011) has also come with the awareness that little effort has been focused on groundwater recharge dynamics in mountainous catchments in relation to precipitation seasonality and catchment storage dynamics (Ajami *et al.*, 2011). In addition, there is evidence to suggest groundwater reservoirs in snowmelt-dominated catchments can be directly impacted by climatological changes through hydrologic inputs (e.g. Molotch *et al.*, 2009; Tague & Grant, 2009; Green *et al.* 2011).

One way to address the interactions between climate drivers (temperature and precipitation) and landscape controls on hydrologic processes in mountain regions is to observe catchment scale processes occurring over large elevational gradients. High elevation watersheds above tree line have seen considerable research on surface-groundwater interaction (e.g. Liu *et al.*, 2004; Manning & Caine, 2007; Williams *et al.*, 2006; Caine, 2010) as have forested watersheds (e.g. Liu *et al.*, 2008; Molotch *et al.*, 2009; Nayak *et al.*, 2010; Bales *et al.*, 2011; Jin *et al.*, 2012; Hinckley *et al.*, 2012). However, there has been less research exploring surface-groundwater interaction in instrumented watersheds that span alpine and forested ecosystems and encompass the rain-snow transition. There appears to be a gap in watershed research that spans large elevational gradients (> 1000 m) and that investigate seasonally snow-packed alpine and forested catchments and lower elevation intermittently snow covered forested catchments within the same watershed. An improved understanding of the magnitude and timing of groundwater contributions to streamflow in headwater catchments that span a large elevational gradient will enhance our ability to predict runoff and streamflow generation in response to changes in climate. Additionally, detailed understanding of the amount and type of precipitation occurring across an elevational gradient under current climactic conditions will aid in modeling and predicting future hydrologic conditions created by perturbations like climate change, wildfire, and the mountain pine beetle epidemic. Current analysis of the effects of climate change on water-limited ecosystems is commonly based on empirical investigations of existing climate gradients. For example, Nayak *et al.* (2010) measured temperature, precipitation, snow, and streamflow data for valley bottom, mid-elevation, and high-elevation sites within the Reynolds Creek Experimental Watershed, Idaho, to evaluate the extent and magnitude of the impact of climate warming on the hydrology and related resources in the interior northwestern United

States. They report that there is a significant elevation gradient in either timing or magnitude in the length of the seasonally snow-covered season and the amount of snowfall. However, such purely descriptive approaches alone do not provide sufficient information to enable accurate modeling of the effects of altered water availability caused by climate change. The greatest uncertainty stems from the assumption that climatic differences are the main single determinant of streamflow variation along a gradient. Therefore care must be taken when extrapolating physical processes from lower elevations to higher elevations along an altitudinal gradient. In terms of local hydrological cycling there are two categories of environmental changes with altitude: those physically tied to elevation, such as atmospheric pressure, temperature and incoming solar radiations; and those that are not generally altitude specific, such as the underlying geology and even human land use changes. The confounding of the first category by the latter has introduced confusion in the scientific literature on the altitude phenomena (Korner, 2007). Therefore, in addition to the altitude driven climate variables it is also important to recognize that the condition of the land surface such as vegetation structure, catchment shape, and directional orientation (i.e. aspect ratios), which can significantly alter hydrologic processes at hillslope scales (Hinckley *et al.*, 2012). The structure of the subsurface may also play a significant role in the above-mentioned surface and groundwater interactions at the catchment scale (Jin *et al.*, 2012). As suggested by Tague and Grant (2009), a geoclimatic framework is therefore necessary for assessing climate change impacts to mountain watersheds. The first step is to identify the differences in sub-surface architecture, which are likely to occur across the elevational gradient of a mountain watershed (Anderson *et al.*, 2007), and then recognize how the various conditions are influencing the current state of water movement through the subsurface. Fortunately there have been recent efforts to characterize the subsurface in mountain

catchments with geophysical techniques (Befus, 2010; Leopold *et al.*, 2013a; Leopold *et al.*, 2013b). Secondly, due to difficult and often limited access, high elevation catchment hydrology studies often lack the necessary infrastructure (i.e. wells) to adequately access, sample, and/or quantify groundwater resources (Manning and Caine, 2007). Combining increased knowledge of subsurface architecture and continued efforts to access groundwater with installation of wells and piezometers in mountain research watersheds (i.e. Zeliff, 2012) will therefore enhance the ability to understand surface water and groundwater interactions in mountain catchments. Knowing that changes to the structure of the subsurface occur on much longer geologic time scales than current rates of climactic change, the subsurface (once characterized) can be treated as in relatively steady state when predicting hydrologic changes on the decade to century scale. If all the physical variations in catchment structure (not related to climate) along a gradient can be accounted for, then a Space-For-Time approach (e.g. Sternberg *et al.*, 2011) enables use of existing hydrologic conditions at lower elevations as proxies for future conditions at higher elevations. The result is the potential to apply the Space-For-Time concept to changes in temperature and precipitation and then use those projected changes to infer how surface and groundwater interactions will respond at the catchment scale across entire watersheds. The results from catchment scale studies may then be applied to larger mountain range scale assessments if subsurface structure is understood and climactic conditions driving hydrologic processes can be linked to elevation.

This study first characterizes the amount and type of precipitation occurring in three headwater catchments that span an elevational gradient in Boulder Creek Watershed. The study then calculates the runoff efficiency (Q/P) of each catchment for 2010-2012. Relative to long-term (30-yr) precipitation records the three years represent average (2010), above average

(2011), and below average (2012) precipitation regimes. Additionally, the isotopic ($\delta^{18}\text{O}$, δD) and geochemical (Na , K^+ , Si , Ca^+ , Mg^+ , Cl^- , ANC) signatures occurring in surface waters and potential source waters of the three headwater catchments will be analyzed using End Member Mixing Analysis (EMMA) to calculate the relative contributions of source waters to streamflow. The EMMA procedure has been previously performed in the highest elevation catchment (Liu *et al.*, 2004, Williams *et al.*, 2006) while recent hydrologic instrumentation of the lower two catchments now allows for application of EMMA across three headwater catchments spanning both the rain-snow transition and the forest-alpine transition in the Boulder Creek Watershed.

An improved understanding of the current catchment scale surface and groundwater interactions across the elevational gradient will then allow for application of the space for time hypothesis to predict future hydrologic conditions in the Boulder Creek Watershed.

The specific research questions are:

1. What are the variations in orographic lapse rates of annual precipitation relative to the amount of precipitation occurring as snow across a large (>1000 m) elevational gradient?
2. How does runoff efficiency vary within and across three headwater catchments spanning an elevational gradient from the montane to alpine?
3. What are the sources and relative contributions of water to streamflow generation in three different headwater catchments that span both rain-snow and forest-alpine transitions?
4. How do source water contributions vary in response to different precipitation regimes (high and low snowfall years)?
5. Does conceptualization of the geoclimatic framework of headwater catchments improve our understanding of surface and groundwater interactions across large elevational gradients in mountain watersheds?

2.2 Study Area

The Boulder Creek catchment (BCC) is about 1160 km² in area and drains the Colorado Front Range from the Continental Divide (4120m) to the eastern plains (1480m) (Figure 2.1). Here we focus on three headwater catchments of the Boulder Creek Watershed: Green Lake 4 (GL4), Como Creek (CC), and Gordon Gulch (GG). Long-term data has been collected by the NWT LTER program in the GL4 and CC catchments, while the GG catchment was instrumented in 2009 as part of the Boulder Creek Critical Zone Observatory (BC-CZO). The three study areas encompass three climatic zones: alpine (GL4), sub-alpine (CC), and montane (GG) (Table 2.1). The underlying bedrock is similar among the four catchments, Precambrian crystalline rock that is primarily granodirite, with nearly equal percentages of gneiss and schist in the alpine and becoming predominantly gneiss in the montane (Braddock and Cole, 1990).

Table 2.1: Sampling site descriptions with site abbreviation, elevation at the basin outlet (m), catchment area (ha), dominant landscape type with percent of forest cover, mean annual air temperature (°C), and mean annual precipitation (mm). Mean air temperature and precipitation values are long-term averages from each site.

Site	Elevation (m)	Catchment Area (ha)	Landscape Type/ (% Vegetation Cover)	Mean Annual Air Temperature (°C)	Mean Annual Precipitation (mm)
GL4	3515-4084	225	Alpine (0.09%)	-3.8	1200
CC	2900-3660	536	Sub-alpine (70%)	4.0	803
GG	2446-2737	263	Montane (68%)	5.9	536

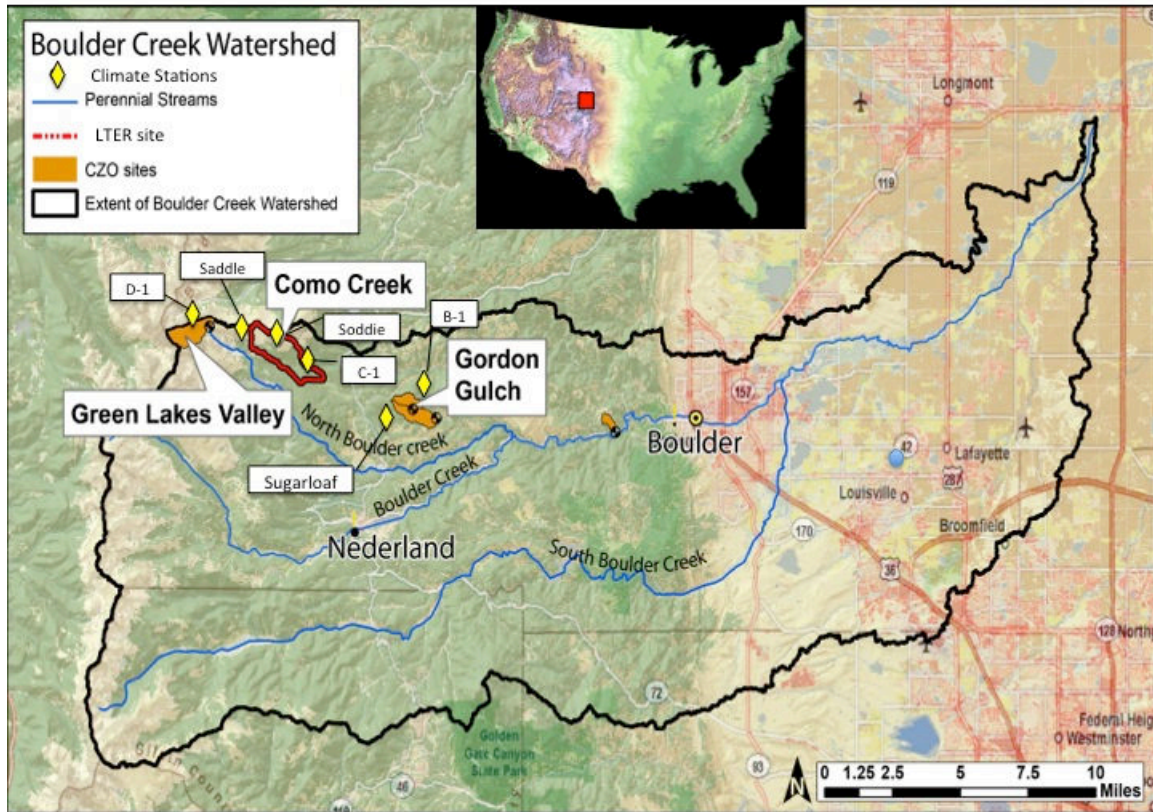


Figure 2.1: Boulder Creek watershed showing locations of each of the four headwater catchments along with the locations of climate and precipitation measurement stations. All snow pack and snow melt sampling occurred adjacent to the precipitation stations except Gordon Gulch where sampling occurred within the catchment near the gauging station rather than at the Sugarloaf precipitation station. The elevation of the watershed ranges from a high of 4120 m along the western boundary to a low of 1420 m in the eastern plains.

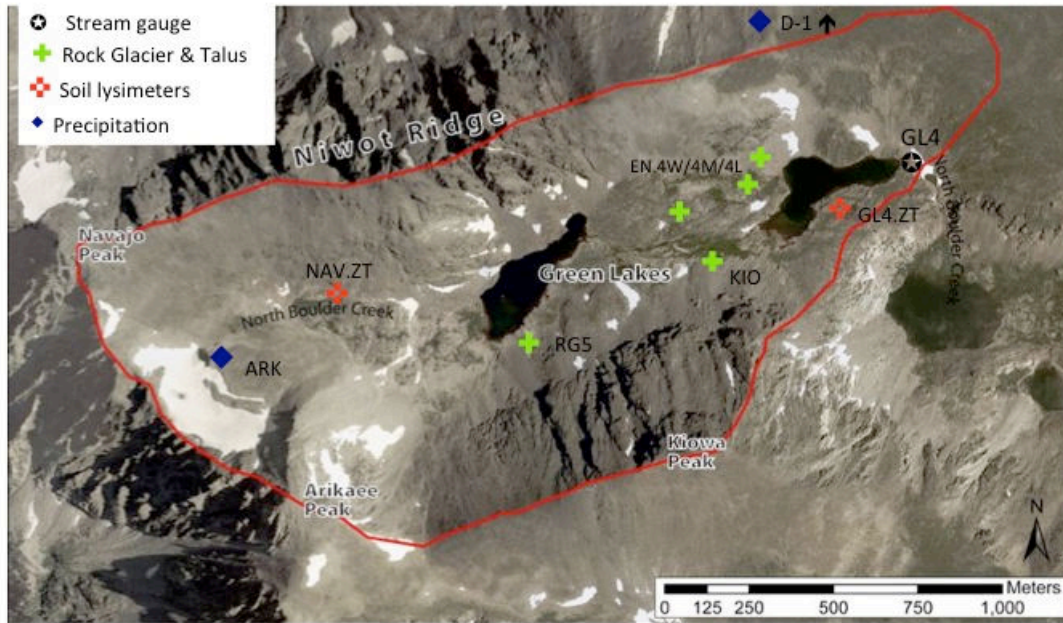


Figure 2.2. Green Lakes Valley with the Green Lake 4 catchment outlined in red. Surface water samples were collected weekly at GL4 and Rock Glacier outflow (RG5) while talus runoff was collected weekly at KIO, and EN.4W/M/L sites. Soil water samples were collected in zero tension lysimeters when there was adequate soil moisture at Navajo Bench (NAV.ZT) and GL4 (GL4.ZT). Precipitation was measured at Arikaree (ARK) and at D-1 located on Niwot ridge just to the north of the catchment.

The upper Green Lakes Valley is an east-facing glacial valley, headed on the Continental Divide in the Colorado Front Range ($40^{\circ}03'0''N$, $105^{\circ}35'0''W$) (Figures 2.1,2.2). Named for a series of shallow paternoster lakes, the Green Lakes Valley is the headwaters of North Boulder Creek and lies within the City of Boulder Watershed. The upper valley is approximately 225 ha in area, and the elevation ranges from 4084 m at the Continental Divide to 3515 m at the outlet of Green Lakes 4 (GL4) (Figure 2.1) (Table 2.1). The catchment consists of steep rock walls above talus slopes and rock glaciers with a valley floor of glacially scoured bedrock. Exposed bedrock makes up 29% of the basin area, talus 33%, vegetated soils 29%, the Arikaree glacier 4%, and the two lakes (Green lake 4 and Green Lake 5) make up the final 5% (Erickson *et al.*, 2005). GL4 is a typical alpine headwater catchment in the Colorado Front Range where active and inactive rock glaciers are indicative of underlying permafrost (Janke, 2005). The rock glacier

adjacent to Green Lake 5 (RG5) is a lobate rock glacier, approximately 8 ha in area at the talus foot zone of Kiowa Peak (Caine, 2001) and has an outflow stream (Williams *et al.*, 2006).

Patterned ground and active solifluction lobes are also common in parts of Niwot Ridge and Green Lakes Valley, especially on ridgelines (Benedict, 1970). Permafrost has been verified above 3500 m on Niwot Ridge (Ives and Fahey, 1971) and more recently by geophysical methods near Green Lake 5 (Leopold *et al.*, 2008).

Geophysical and drilling data collected on the slopes of Niwot Ridge, the northeastern border of the catchment, show that the depth to bedrock ranges from 4 to greater than 10 m, with the top 1 to 2 m consisting of soils and unconsolidated materials overlaying either bedrock or periglacial slope deposits that vary in thickness from 1 to 8 m (Leopold *et al.*, 2008). The subsurface can be summarized as either blockfields or glacial deposits on top of bedrock and where the block layer is thick enough, a frost table (i.e. persisting ice-rich permafrost) exists at 3.9 ± 1.6 m above and elevation of about 3400-3600 m on shaded north-facing slopes (Leopold *et al.*, 2013b), a depth that is supported by ground penetrating radar data measured at Green Lake Valley and nearby Niwot Ridge (Leopold *et al.*, 2008, 2011, 2013a). The ridges defining upper Green Lake Valley consist of bedrock or blockfield-covered, narrow ridges between glaciated cirques (White, 1976).

Below these ridges the alpine slopes fit the cliff-talus-sub-talus model that describes a rock-dominated system, the coarse debris system (Caine, 1974; Thorn and Loewenherz, 1987). Additionally, the Green Lakes Valley is located on the western edge of the Lake Albion mining district that contains a series of well-developed faults (Williams *et al.*, 2006), indicating the potential for additional faults providing considerable secondary porosity within the catchment.

The alpine vegetation is growing on moderately well developed soils, exhibiting Oe, A, and 2Bw horizons, most of which are located in the valley bottom (Litaor, 1993).

Climate in Green Lakes Valley is characterized by long, cool winters and a short growing season (1-3 months). Since 1951, mean annual temperature is -3.8°C , and annual precipitation is 1000 mm (Williams *et al.*, 1996). Precipitation and temperature is measured at the D-1 alpine tundra site ($40^{\circ} 03' 34'' \text{N}$; $105 37' 0'' \text{W}$; 3739 m) (Figure 2.1), which is located on the northern edge of Green Lakes Valley, 2.6 km from the Continental divide. Additional precipitation data has been collected since 1982 at the base of the Arikaree Glacier ($40^{\circ} 02' 56'' \text{N}$; $105 38' 24'' \text{W}$; 3814 m) in the valley floor at the head of the Green Lakes Valley approximately 0.5 km east of the Continental Divide (Figure 2.2). About 80% of the annual precipitation occurs as snow (Caine, 1996). Stream flows are markedly seasonal, varying from $< 0.05 \text{ m}^3 \text{ s}^{-1}$ during the winter months to $> 3.0 \text{ m}^3 \text{ s}^{-1}$ at maximum discharge during snowmelt. Surface waters are dilute, with acid neutralizing capacities (ANC) generally $< 200 \mu\text{eq/L}$ at all sampling sites (Williams *et al.* 2001).

The Saddle site ($40^{\circ} 03' 17'' \text{N}$; $105^{\circ} 35' 21'' \text{W}$; 3528 m) is located in alpine tundra on the northern ridge of Green Lakes Valley, 5.6 km from the Continental Divide. The site includes hydrologic infrastructure including snow and soil lysimeters, a subnivean laboratory, and an aerometrics wet-chemistry precipitation collector, which is part of the National Atmospheric Deposition Program (NADP) (site CO02) (Figure 2.1). Groundwater wells were installed at the Saddle site in the fall of 2005. Wells were drilled to a depth of 9 m, cased, and screened at the bottom 1.6 m. The Green Lakes Valley is a drinking water source for the City of Boulder and has limited access and minimal infrastructure, therefore the Saddle and D1 sites contains the majority of instrumentation used to collect meteorological data for the valley.

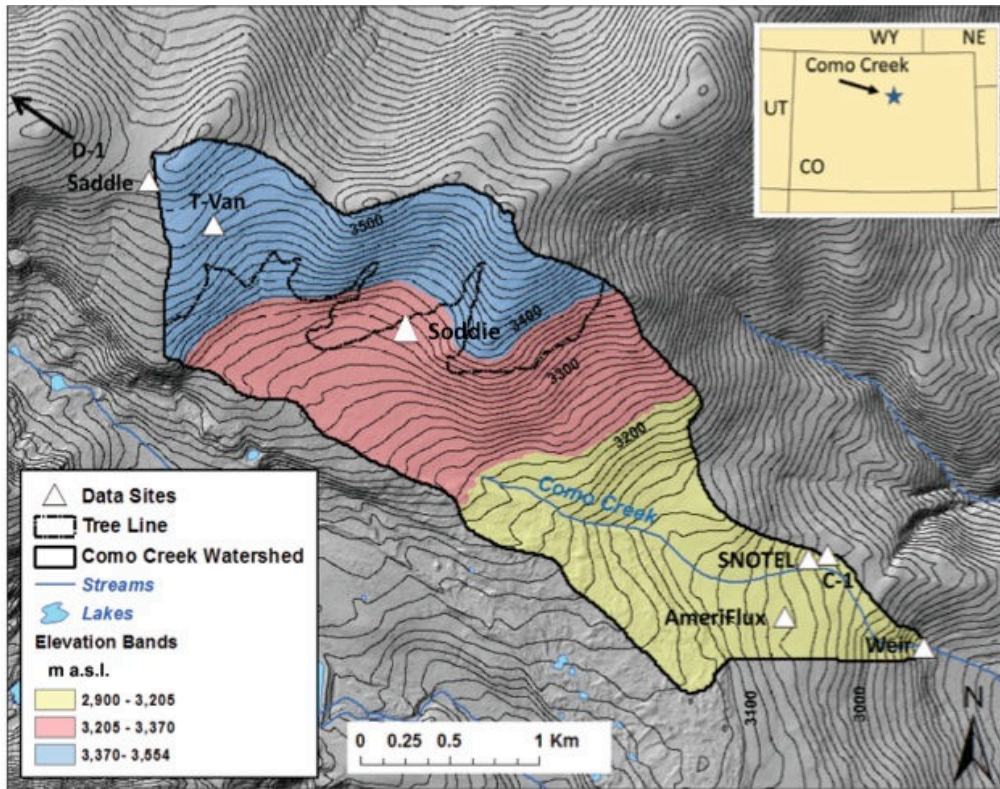


Figure 2.3: Map of the Como Creek catchment showing all sampling locations. The catchment has an area of 5.36 km² with approximately 31% and 69% of the catchment above and below treeline, respectively. Three distinct elevation bands were generated by the Jenks Natural Breaks classification method to spatially distribute *P* across the catchment.

CC originates just to the north and east of Green Lakes Valley on the southeast flank of Niwot Ridge, approximately 8 km east of the Continental Divide (Figures 2.1, 2.3). The catchment falls within the Niwot Ridge Biosphere Reserve, has an area of 536 ha, and ranges in elevation from 2900 m to 3560 m (Table 2.1). The CC catchment differs from the nearby GL4 catchment in two important respects: 1) There are no lakes, and 2) there is no talus, exposed bedrock, steep cliffs, or periglacial features such as rock glaciers.

The area was glaciated during the Pleistocene and the lower half of the CC catchment resides primarily on the Arapaho moraine (USGS Ward quadrangle). Soil development varies throughout the catchment with a mean of 60 cm and a maximum of about 200 cm, but is deeper

in areas composed of glacial till (Lewis and Grant, 1978). Neither the spatial extent nor thickness of glacially deposited materials have been directly measured within the CC catchment, though the USGS Ward quadrangle estimates the moraine thickness at about 10 m. A recently installed sampling well near the C-1 site was drilled to a depth of 33 m and did not encounter bedrock, further indicating significant depths of glacial deposits within the CC catchment.

Approximately 70% of the catchment is below tree line and consists of primarily coniferous forest that was last deforested nearly a century ago, but has seen minimal human disturbance since that time (Lewis & Grant, 1979). The forest has a mixture of trees dominated by Engelmann spruce (*Picea engelmannii*), sub-alpine fir (*Abies lasiocarpa*), limber pine (*Pinus flexilis*) and lodgepole pine (*Pinus contorta*), with some aspen (*Populus tremuloides*).

The Soddie site (40° 02' 52" N; 105° 34' 15" W; 3345 m) is located near the upper extent of CC catchment just below the treeline ecotone. This site has an underground laboratory 10'x30'x8' in size, line power, with an array of snow lysimeters and zero-tension soil lysimeters. Adjacent to the soil lysimeters is a suite of meteorological instruments sufficient to close the energy balance (Williams *et al.* 2009). Snow pits were sampled about weekly from January 1 until the end of snowmelt for physical and chemical parameters. NWTLTER also operates an unofficial NADP wet chemistry collector at the Soddie site, using the same instruments and protocols that the NADP program uses.

The C-1 site (40° 02' 09" N; 105° 32' 09" W; 3021 m) within the lower part of the CC catchment is part of a long-term meteorological study that has recorded continuous climate measurements since the 1950's (Williams *et al.*, 1996). The mean annual temperature is 4°C and mean annual precipitation is 800 mm (Monson *et al.* 2002). There are three additional climate programs operating at the C-1 area, which collected

precipitation data. The C-1 site contains an NADP site (CO90) that was established in 2006 and data can be found at <http://nadp.isws.illinois.edu/data/sites/siteDetails.aspx?id=CO90&net=NTN>). There is also participation in the AmeriFlux program (Monson *et al.*, 2002) and data from the Niwot Ridge AmeriFlux tower are available at <http://ameriflux.ornl.gov>. The SnoTel network operates the NIWOT 663 site here <http://www.wcc.nrcs.usda.gov/snotel/snotel.pl?sitenum=663&state=co>).

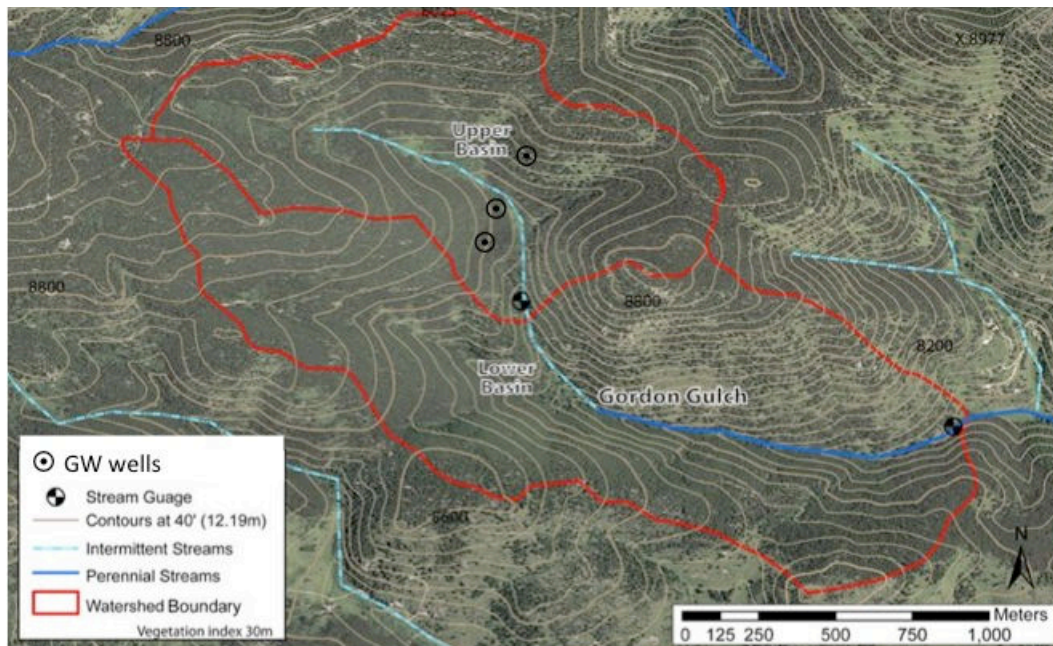


Figure 2.4: The Gordon Gulch catchment divided into an upper and lower sub-catchment. Locations of groundwater wells and the stream gauges are included for reference.

GG is a 266-ha catchment in a mixed conifer montane ecosystem with a mean elevation of 2627 m (Figure 2.4, Table 2.1). The catchment is divided into upper and lower sub-catchments and the upper catchment (defined by upper stream gauge location) will be analyzed in this study. The upper catchment is 94.66 ha and spans from 2588 m to 2737 m elevation. The GG Stream joins North Boulder Creek about 16 km downstream from the headwaters in Green

Lakes Valley and lies within the low-relief post-Laramide surface that was not affected by the Pleistocene Glaciers (Bradley, 1987).

GG is a predominantly west to east drainage resulting in distinct north and south facing slopes representing distinctly different vegetation communities. The north aspect slopes are dominated by Lodgepole pine (*Pinus contorta*) stands of nearly uniform size and age characteristics, along with the more shade tolerant Rocky Mountain Douglas-fir (*Psuedotsuga menziesii* var. *glauca*) and Colorado Blue Spruce (*Picea pungens*). The south aspect slopes have a more open and mosaic patchwork of Ponderosa pine (*Pinus ponderosa*), interspersed with Rocky Mountain Juniper (*Juniperus scopulorum*) and common shrubs including mountain mahogany (*Cercocarpus spp.*) and hawthorn (*Crataegus spp.*). Apparently inconsistent for this type of rolling upland surface, GG contains steep topography with many bedrock exposures of Precambrian granites, gneisses and schists. Geophysical characterization of the subsurface using shallow seismic refraction shows that slow velocity materials (taken to be unconsolidated materials) are generally less than one m thick, while weathered bedrock profiles extend to depths of 11 to 15 m (Befus, 2010). Additional electrical resistive tomography measurements indicated that the boundary between overlying stratified slope deposits and saprolite were identified at mean depths of 3.0 ± 2.2 m while depth to the bedrock surface was 4.3 ± 3.0 m (Leopold *et al.*, 2013b). Soil pits dug on north and south facing slopes ($n = 6$) show that soil development was generally 30 cm to 60 cm thick on the north and south facing slopes and marginally deeper in soil pits ($n = 3$) located in riparian areas at the bottom of the catchment near the stream channel.

The Sugarloaf NADP site (CO94) (39.9939 N; -105.48 W; 2524 m) is located about 3 km to the northeast of GG and was used to collect precipitation chemistry data for GG (Figure 2.1).

Air temperature for GG was measured at the B-1 station (40° 01' 20" N; 105° 25' 45" W; 2621 m) located 2 km east of GG at the same elevation (Figure 2.1).

2.3 Data and Methods

2.3.1 Climate: Air Temperature and Precipitation

Air temperature records at D-1, C-1, and B-1 stations were used to calculate long-term averages (50-year) and daily temperature record during the study. Data from these sites can be downloaded through the Niwot Ridge LTER database (<http://culter.colorado.edu/NWT>). The air temperature record at B-1 was unavailable from January 2011 to June 2012 so no annual record was calculated for GG during that period.

Daily precipitation for GG was measured at NADP Sugarloaf CO94 station located in an Upper Montane Forest at an elevation of 2621 m, 22.5 km east of the Continental Divide and within 3 km of the GG catchment (Figure 2.1). Daily precipitation for GL4 was measured at the D-1 climate station. Additional precipitation measurements for GL4 catchment have been recorded since 1982 at the base of the Arikaree Glacier (3814 m), on a small moraine, in the valley floor at the head of the catchment approximately 0.5 km east of the Continental Divide (Figure 2.2). Based on a 30-year record of winter (October to June) precipitation totals at D-1 and Arikaree, the Arikaree site receives an average of 136% ($r^2 = 0.78$) of the total precipitation recorded at D-1 (N. Caine, personal communication, July 20, 2014). Due to inherent spatial variability of winter precipitation received across the GL4 catchment, a correction factor of 1.18 (half the difference) was applied to the D-1 winter precipitation totals to more accurately represent GL4 inputs. Summer precipitation at D-1 is used uncorrected to represent GL4 summer precipitation.

Due to extensive instrumentation located within and adjacent to the CC catchment more detailed precipitation calculations were performed to more accurately quantify the precipitation inputs across the catchment. Additionally, the CC catchment is unique to the other catchments because it spans across both forested and alpine ecosystems. Precipitation measurements were collected from four independent collectors in the lower, forested part of the catchment (NADP CO90, C-1 LTER, Niwot SNOTEL, and Niwot Ridge AmeriFlux) and two alpine sites (Saddle, D-1) above the upper part of the catchment (Figure 2.3). The NADP CO90, C-1 LTER, Saddle, and D-1 collectors are all shielded Belfort 5-780 type collectors mounted ~2 m above the ground while the SNOTEL is also a shielded 12” diameter collector located at a height of ~4 m and the AmeriFlux is an unshielded Met One Model 385 heated rain gauge located in the forest canopy 10 m above the ground. Precipitation measurements were collected at the four locations near C-1 and then averaged on an annual basis to determine representative precipitation for the C-1 elevation and provide insight on the variability between different types of collectors. Alpine precipitation was measured at the Saddle and D-1, and Saddle precipitation was corrected for over-catch due to blowing snow following the method of Williams *et al.* (1998).

Following Dingman (2002) a hypsometric method was applied to spatially distribute precipitation across the entire catchment, using data from the C-1, Saddle, and D-1 stations across a range of 718 vertical meters. Precipitation was calculated by summing daily data to generate an annual total by water year (1 October to 30 September) for each site. A unique hypsometric curve was established for each water year by linear regression of summed precipitation against station elevation:

$$p(z) = az + b \quad \text{(Equation 2.1)}$$

where the dependent variable p is a function of elevation (z) in meters asl, a is the slope, and b is

the y-intercept. To calculate z , the total drainage area was divided into three elevation bands by application of the Jenks Natural Breaks classification method (Jenks, 1967) to a catchment DEM using ArcMap. The Jenks Natural Breaks method separates the topography of the catchment into distinct classes (elevation bands) by minimizing the variance within classes, while maximizing the variance among classes. We calculated the mean z and the area of each band relative to the total area of the catchment (a_h), and then total precipitation for each band was determined using Equation 1 and multiplied by the corresponding a_h and summed to generate a value for the entire catchment:

$$\hat{P} = \sum_{h=1}^H p(z) \cdot a_h \quad (\text{Equation 2.2})$$

where h is elevation band, H is the number of elevation bands, and \hat{P}_n is total catchment precipitation.

For all precipitation data the daily precipitation totals were classified as either snow, mixed, or rain based on temperature records during precipitation events. If the local air temperature was greater than 2°C then the precipitation was classified as rain. If the temperatures during the precipitation event crossed the 2°C point in either direction, or if there were multiple events during one day where at least one event is in the opposite of all the others for that day then the precipitation was classified as mixed. If the air temperature was less than 2°C then the precipitation was classified as snow.

2.3.2 Discharge

Water level was measured with a continuously recording pressure transducer and converted to volumetric discharges by empirical rating curves at the outlets of the three

catchments. The empirical rating curves were unique to each water year to account for any physical changes to the stream channel above the weirs, which may change the stage discharge relationship. The discharge was calculated as a power function:

$$Q = aX^b \quad \text{(Equation 2.3)}$$

where Q is discharge in L s^{-1} , X is the stage height in cm, and a and b are constants derived from a power curve fitted to the plot of stage height versus discharge. Weekly measurements of stage and velocity were used to create the empirical rating curves for each water year. The flow records for GL4 have been collected since 1982 and are part of the Niwot Long-Term Ecological Research (LTER) program and the records are available at <http://niwot.colorado.edu/exec/extracttoolA?gl4disch.nc>. Starting in 2009 the pressure transducer was left in the stream at GL4 throughout the winter so that annual cumulative discharge could be more accurately quantified.

At the CC and GG catchments the transducers were installed and removed annually due to the possibility of freezing in the stilling well, which resulted in variations in the start and end dates of discharge measurements across the catchments. However, the discharge not measured by the transducers was primarily during winter baseflow conditions and thus assumed to represent an insignificant amount of total annual discharge (e.g. Liu *et al.* 2004). In CC a baseflow value of 3 L s^{-1} was applied during the winter months (\sim day of year (DOY) 315 to DOY 115), which amounted an average of 4% of the total annual flow in CC. This value was chosen based on late season (baseflow) transducer values, occasional hand measurements during winter months, and earlier work that reported winter flow of 3 L s^{-1} using a flume at a nearby location on CC (Lewis and Grant, 1979). When the transducer record began after DOY 115 or ended prior to DOY 315, daily discharge values were linearly interpolated to baseflow values at

the beginning or end of the year. All other gaps in discharge were interpolated using a five-day running mean discharge so that annual water year (Oct-Sept) discharge volumes could be calculated. The flow records for GG have been collected since 2010 as part of the Boulder Creek Critical Zone Observatory (CZO) and are available at <http://criticcalzone.org/boulder/data/dataset/2919/>.

Volumetric discharge was divided by catchment area to convert to specific discharge, and then reported as a depth of water (in mm) over the entire catchment.

To provide an analysis on the relationship between water entering a catchment as precipitation and leaving the catchment as surface waters, the runoff efficiency was calculated. Runoff efficiency (K) for each catchment was calculated as:

$$K = Q \text{ (mm)} / P \text{ (mm)} \quad \text{(Equation 2.4)}$$

Where Q is measured as the annual specific discharge for the catchment and P is the annual water entering the catchment as rain and snow.

2.3.3 Snow and Snowmelt

The snowpack was sampled approximately weekly at the Saddle, Soddie, C1, and GG locations for chemical content, physical properties, and oxygen isotopes of water following the protocols of Williams *et al.* (1999; 2009). Annual snow surveys were conducted in the GL4 catchment each year at maximum accumulation following protocols of Erickson *et al.* (2005), which included snowpack chemical and physical analysis from five snow pits spatially distributed across the catchment (see GL4, GL5, Navajo, and Arikaree sites in Figure 2.2). Weekly snow depths are reported for the Saddle, Soddie, C1, and GG locations. Chemical and isotopic content of snowpack reported for all locations at maximum accumulation and prior to

snowmelt, when maximum loading of solutes stored in the seasonal snowpack occurs (Williams *et al.* 2009). The depth-integrated concentrations of solutes (and water isotopes) in the snowpack for each duplicate core were determined by calculating the volume-weighted mean concentrations (VWM) as in Williams and Melack (1991a,b) and Williams *et al.* (1996, 1999). The snowpack at GG is intermittent and does not necessarily reach a maximum accumulation at the end of season, therefore the winter snowpack value was more appropriately generated by calculating the volume weighted mean concentration of all winter precipitation collected at the Sugarloaf NADP site.

At the Saddle, Soddie, and GG sites snow melt was also collected and analyzed following the protocols of Williams *et al.* (2009). Snowmelt water was collected in 1-m² snow lysimeters before contact with the ground (Williams *et al.*, 1996). Snowmelt water flowed by gravity from the snow lysimeters into bottles collected as grab samples approximately daily during the melt season.

2.3.4 Surface, Groundwater, Talus and Soil Water Sampling

Stream samples were collected as grab samples following the protocol of Williams *et al.* (2009). Samples were collected on a weekly basis at the outlets of the GL4, CC, and GG catchments (Figure 2.1). In the GL4 catchment additional surface flows were collected from the outflow of a rock glacier (RG5) while sub-talus water was collected as grab samples when water was available from KIO, EN.4L, EN.4W, and EN.4N sites (Figure 2.2). Soil water was collected in the GL4 catchment from zero tension lysimeters located at GL4, NAV, KIO, and GL5 sites (figure 2.2). Soil water was also collected in CC catchment from zero tension lysimeters located

at the Soddie site and from tension lysimeters at three sites co-located with groundwater wells near C-1.

Groundwater was sampled weekly during ice-free months and monthly during the winter at the alpine Saddle site from four observation wells located on Niwot ridge between the CC and GL4 catchments. The wells are piezometers screened at the bottom 1.5 m and have total depths of 6.3-8.4 m. Additional groundwater wells were installed in 2010 near the C-1 sites in CC, of which three medium depth (6-8 m) and one deep (18m) were sampled for the study. Six groundwater wells were installed in the upper GG catchment in fall 2010, and the water chemistry from three of the wells (Figure 2.4) are included in this study. The sampled wells in GG included two deep wells (screened from ~ 8 to 18 m) located on the North and South facing slopes of the upper catchment and one shallow well (screened from 1.4 to 4.5 m) located in a meadow adjacent to the stream channel. Sampling of all wells was performed with a 1-m teflon bailer to minimize chemical contamination after purging three well volumes, and then followed the protocol for surface water collection.

2.3.5 Laboratory Analyses

All precipitation and water samples were analyzed for pH, acid-neutralizing capacity (ANC), specific conductance, NH_4^+ , Ca^{2+} , Na^+ , Mg^{2+} , K^+ , Cl^- , NO_3^- , SO_4^{2-} , Si, DOC, dissolved organic nitrogen (DON) and total dissolved nitrogen (TDN) at the Kiowa Environmental Chemistry Laboratory in Boulder, CO. Detection limits and instrumentation are as presented in Williams *et al.* (2009); in general detection limits for all solutes were less than $1 \mu\text{eq L}^{-1}$.

Samples were also analyzed for deuterium (D) and ^{18}O using an L1102-i Isotopic Liquid Water Analyzer, developed by Picarro Incorporated. The analyzer is based on Picarro's unique

Wavelength- Scanned Cavity Ring Down Spectroscopy (WS-CRDS), which is a time-based measurement using near-infrared laser to quantify spectral features of molecules in a gas contained in an optical measurement cavity. Isotopic compositions are expressed as a δ (per mil) ratio of the sample to the Vienna Standard Mean Ocean Water (V-SMOW), as shown for ^{18}O :

$$\delta^{18}\text{O} = \frac{(^{18}\text{O}/^{16}\text{O})_{\text{sample}} - (^{18}\text{O}/^{16}\text{O})_{\text{VSMOW}}}{(^{18}\text{O}/^{16}\text{O})_{\text{VSMOW}}} \times 1000 \quad (\text{Equation 2.5})$$

The precision for $\delta^{18}\text{O}$ was $\pm 0.05\%$ and for D was $\pm 0.1\%$.

2.3.6 Hydrograph Separation with End Member Mixing Analysis

End-member mixing analysis (EMMA) uses a statistically unbiased technique to identify the most important end members contributing to streamflow (Christophersen & Hooper, (1992) and Christophersen *et al.* (1990)). A principal component analysis (PCA) was performed to extract eigenvectors using a correlation matrix of conservative tracers, as previously demonstrated for the Green Lakes Valley by Liu *et al.* (2004) and Williams *et al.* (2006). Streamflow data were orthogonally projected using the eigenvectors identified by

$$U = X * V^T \quad (\text{Equation 2.6})$$

where X is the data matrix of stream water and V T is the matrix of eigenvectors (Christophersen & Hooper, 1992). Using the PCA, we take the product of the data matrix and its transpose XT X, which gives us eigenvectors that form the geometrical coordinates of the U-space. The corresponding eigenvalues equal the variance in the data and give us the amount of variance explained by each end member. While this method does not specifically and quantitatively relate a given end member to a particular variance, it does qualitatively suggest both the total number and type of end members needed to explain a certain amount of variance in the data. End

members are chosen based on their Euclidean distance from the U-space projection. This distance is given by:

$$d_j = \| b_j - b_j^* \| \quad (\text{Equation 2.7})$$

where b_j is the end member data point and b_j^* is the orthogonal projection of b_j in U space (Christophersen & Hooper, 1992). Christophersen and Hooper suggest comparing b_j^* and b_j solute by solute by using the projection itself:

$$b_j^* = b_j V^T (V V^T)^{-1} V \quad (\text{Equation 2.8})$$

The orthogonal (Euclidean or U-Space) projections of stream flow samples and end members were used to solve for proportions of end members contributions to stream flow using traditional mixing model mass balance techniques. Thus, U-space projections (U_n) are substituted for tracer concentrations in hydrologic mixing models.

2.3.7 Diagnostic Tools of Mixing Models

Following the methods of Liu *et al.* (2008) the diagnostic tools developed by Hooper (2003) were used to determine the number of end-members and conservative tracers used in EMMA by assessing the “fit” of stream flow chemistry to a lower dimensional mixing subspace (Euclidean U-space). To initiate this analysis, stream flow chemistry was projected using eigenvectors extracted from stream flow chemical data:

$$X^{\wedge*} = X^* V^T (V V^T)^{-1} V \quad (\text{Equation 2.9})$$

Where X^* is the Standardized streamflow data, $X^{\wedge*}$ is the projection of the standardized data using eigenvectors (V , $n \times n$, where n is the number of solutes) extracted from the correlation coefficients of streamflow chemistry data including all available solutes without using any information from end-members.

Following the methods established in Hooper (2003), diagnostics from PCA, including plots of measured solute concentrations vs. regression residuals of the projected vs. measured concentrations and relative root-mean square error (RRMSE) of the projected concentrations, were used to evaluate the appropriate number of potential end-members as well as identify potential tracers that do not violate the assumptions of standard mixing models. Two main criteria were used to select tracers and choose the dimension of the mixing subspace. First, tracers were considered acceptable if the measured vs. residual plots displayed a random pattern, indicated by a linear model with low R^2 (≤ 0.2). Alternatively, the absolute values of the residuals were evaluated with RRMSE, with smaller RRMSE ($< 5\%$) being used to indicate more appropriate tracers (Hooper, 2003). For example, if the distribution is a random pattern using two-dimensional (2-D) eigenvectors, which are the first two rows of the eigenvector matrix, three end-members are needed and the solutes that show a random pattern for their residual distributions are conservative (e.g. Liu *et al.*, 2008). If the distribution of residuals shows any structure there is a lack of fit in the model, which indicates a potential violation of any of the assumptions inherent in the mixing model (Hooper, 2003, Liu *et al.*, 2008). To measure the fit of the residuals the relative root-mean-square error (RRMSE) was calculated. The RRMSE for solute q is

$$R_q = \sqrt{\frac{\sum_{i=1}^n (x_{iq}^{\wedge} - x_{iq})^2}{n * x_{-q}}} \quad (\text{Equation 2.10})$$

Where i is the i th sample, x^{\wedge} is the predicted solute concentration, x is the measured solute concentration, and x_{-} is the mean of the measured solute concentration from all samples. The RRMSE indicates the “thickness” of the data cloud beyond the lower dimensional subspace. The dimension of the mixing subspace (m) should be simply the rank of X , which is one less than the number of end-member (Hooper, 2003).

2.4 Results

2.4.1 Climate

Air temperature

Daily mean air temperature during the study is plotted for the B-1, C-1, and D-1 climate stations (Figure 2.5). The annual mean air temperature for Green Lakes Valley measured at the D-1 climate station was -2.4°C in 2010, and decreased to -4.6 in 2011 and -6.0 in 2012, fluctuating both above and below the 50-year mean of -3.7°C . At the D-1 site, winter temperatures were consistently below freezing at about -10°C to -20°C , with daily mean air temperature rising above 0°C in mid-May and averaged 9°C in July and August, before decreasing below freezing in October. The annual mean air temperature of CC measured at the C-1 climate station was 4.3°C in 2010, decreased to 2.5°C in 2011 and increased to 3.8°C in 2012. The air temperatures were similar to the 50-year mean of 4.0°C . At C-1 daily mean air temperatures drop below freezing in November and average about -5°C through the winter until rising above freezing in April and averaging about 15°C in July and August. The annual mean air temperature of GG, measured at the B-1 climate station, was 6.6°C in 2010, slightly warmer than the 50-year mean of 5.9°C . Unfortunately air temperature was not recorded at the B-1 station in 2011 and part of 2012 so annual calculations are not available. From the available record at B-1 the daily mean air temperature is not consistently below freezing until mid-December and then fluctuates above and below freezing throughout the winter with a winter average of only about -2°C . Air temperature at B-1 remains consistently above freezing starting in March and reaches a summer maximum of about 20°C in July and August. The air temperature records therefore suggest that at GG snowmelt can occur throughout the winter

while the snow accumulation period increases to approximately five months in the CC catchment and seven months in the GL4 catchment.

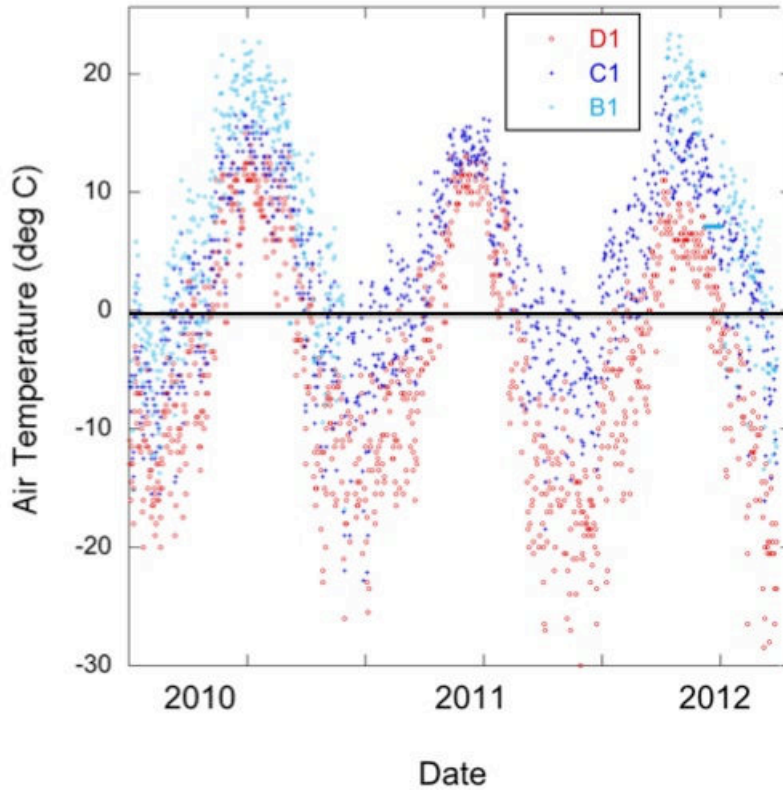


Figure 2.5: Daily mean air temperatures at the B1 (2621 m), C-1 (3021) and D-1 (3739 m) climate stations for 2010 to 2012.

Precipitation

The annual precipitation (measured by water year) and the amount of annual precipitation falling as snow generally increased with increasing elevation across the Boulder Creek watershed (Figure 2.6). From 2010 to 2012 the mean annual precipitation was 512 ± 43 mm at Sugarloaf (2524 m), 772 ± 91 mm at C-1 (3012 m), 1122 ± 346 mm at Saddle (3258 m), and 1439 ± 289 mm at D-1 (3739 m).

There was large variation in annual precipitation among the three years. 2011 was one of the largest on record with the alpine totals being 50% greater than the long-term average of 1000

mm (Caine, 1996) and 2012 being below average.

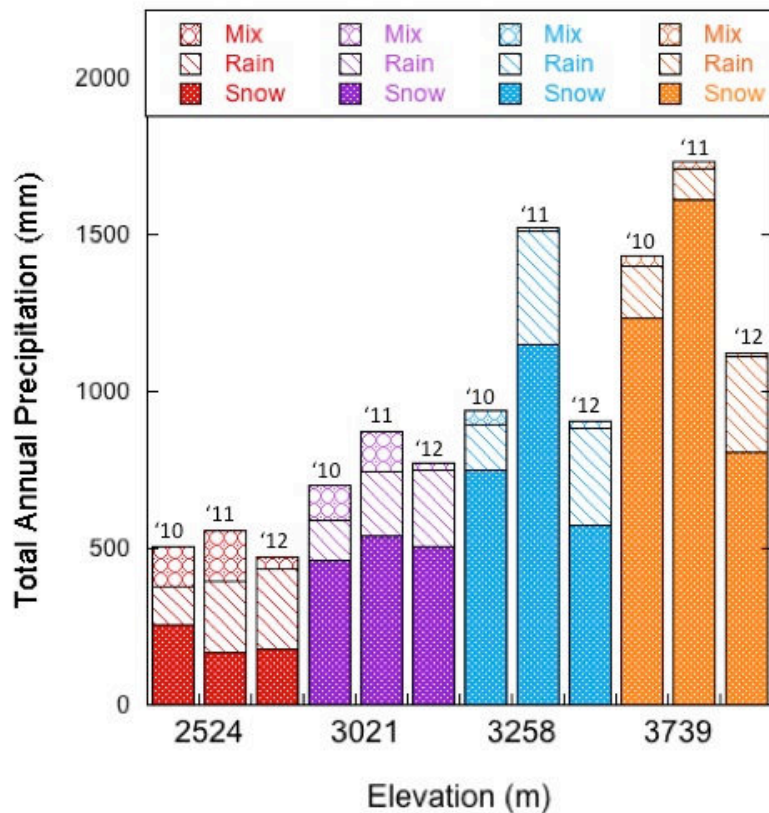


Figure 2.6: 2010 to 2012 annual (water year) precipitation classified as snow, rain and mixed precipitation for climate stations at different elevations in the Boulder Creek watershed. The data for the C-1 location (3021 m) is from the CO90 NADP station.

Based on the difference in total precipitation between the lowest elevation (Sugarloaf; 2525 m) and the highest elevation (D-1; 3739 m) the orographic lapse rate was 76 mm per 100 m elevation gain in 2010, 97 mm per 100 m elevation gain in 2011, and only 53 mm per 100 m elevation gain in 2012. The amount of precipitation falling as snow also increased with elevation with similar lapse rates of 80 mm per 100 m elevation in 2010 and 52 mm per 100 m elevation in 2012. Interestingly, in 2011 there was a greater lapse rate of 119 mm per 100 m elevation gain in 2011 due to proportionately higher snowfall at D-1 and lower snowfall at Sugarloaf. In 2011, the Sugarloaf station only received 30% of precipitation as snow, less than the 51% as snow in 2010 and 38% as snow in 2012. The amount of precipitation falling as snow at the C-1 station

was consistent between years at 65% in 2010, 62% in 2011, and 66% in 2012. The Saddle station recorded slightly greater total precipitation than C-1 and more snow with 80% snow in 2010, 76% snow in 2011, and 68% snow in 2012. Interestingly, the D-1 station received 93% of precipitation as snow in 2011 compared to 86% in 2010 and just 72% in 2012.

At the lowest elevation (Sugarloaf) rain was a greater contributor to total precipitation at 23% in 2010, 41% in 2011, and as the majority of precipitation as 54% in 2012. Moving up in elevation, the Saddle station recorded nearly the same amount of precipitation as rain (15%, 24%, 30%) as C-1 (18%, 23%, 31%) for 2010, 2011, and 2012 respectively. At the highest elevation (D-1) rain represented just 12% of precipitation in 2010 and 6% in 2011 but increased to 27% in 2012 due to lower snowfall that year and a large single precipitation event (~140 mm) in July of 2012.

2.4.2 Spatial Distribution of Precipitation in Como Creek

To apply the hypsometric method the Mean Annual Precipitation (*MAP*) for the C-1 site was first calculated by averaging results from the four independent precipitation collectors available at C-1 (Table 2.2). The C-1 AmeriFlux gauge consistently recorded the highest amount of precipitation while the Niwot LTER gauge was consistently lower than the other gauges. The SnoTel and NADP totals were bracketed by the other two stations and were most similar from year to year. The *MAP* for C-1 (772 ± 91 mm) was lower than the 1981 to 2013 SnoTel average (820 mm), but greater than the C-1 Niwot LTER 30-year record from 1951 to 1980 (692 mm; Greenland, 1989).

Table 2.2: Precipitation totals of four independent precipitation collectors at C-1, totals at Saddle and D-1, and the distributed precipitation total for CC for the water years 2010-2012.

Water year	C-1 Ameri-Flux (mm)	C-1 NADP CO90 (mm)	C-1 Niwot LTER (mm)	C-1 SnoTel (mm)	Mean C-1 (mm)	Saddle (mm)	D-1 (mm)	Distributed Catchment P (mm)
2010	748	747	592	721	702 ±74	937	1431	867
2011	974	882	748	894	874 ±94	1522	1732	1186
2012	965	721	691	719	774 ±128	908	1155	833
Mean	896	739	677	778	772 ±91			962 ±195

To calculate catchment-wide *MAP* the *MAP* for C-1 along with annual precipitation totals from the Saddle and D-1 generated a unique hypsometric curve for each year. The Jenks Natural Breaks method then generated three distinct elevation bands with mean elevations of 3108 m, 3286 m, and 3443 m, which represented 33%, 36%, and 31% of the total catchment area, respectively (see Figure 2.3). The hypsometric curve was then applied to each of the three elevation bands to estimate a unique precipitation total for each elevation band. Summation of the estimated precipitation from each elevation band produced a *MAP* for the entire CC catchment between 2010 and 2012 (Table 2.2). The spatially distributed catchment *MAP* was 962 ± 195 mm and ranged from a low of 833 mm in 2012 to a high of 1186 mm in 2011 (Table 2.2). Application of the hypsometric method to distribute the precipitation across the entire CC catchment resulted in catchment precipitation being greater than precipitation totals at C-1 by 165 mm in 2010, 312 mm in 2011, and just 59 mm in 2012.

2.4.3 Snowpack

Total depth of the snow pack was measured weekly from January until spring melt out on the north-facing slope of upper GG, at the C-1 and Soddie sites in CC catchment, and at the alpine saddle site (Figure 2.7). Due to limited access to GL4 in the winter, snowpack is only analyzed once per year at maximum accumulation. In general snowpack depth and duration increases with elevation. The snowpack depth peaks at about 0.5 m in GG and can decrease to zero in March, prior to the final snowfall events of the year as seen in 2010 and 2011. In GG the peak snowpack occurred on February 23, 9, and 14 in 2010, 2011, and 2012 respectively. At the C-1, Soddie, and Saddle sites the snow pack tends to accumulate throughout the winter season with consistent depths of 1-1.5 m at C-1 and ~ 2.5 m at the Soddie site. However the timing of peak snow at C-1 was variable, occurring on March 24, 2010, May 3, 2011, and February 29, 2012. Timing of peak snowpack depth at the Soddie was May 14, 2010, May 6, 2011, and then on March 16, in 2012. The Saddle site has the most variable snowpack depths ranging from over 3.5 m in 2011 to just 1 m in 2012. The peak snowpack at the Saddle occurred on May 11, 2010, April 22, 2011, and then on March 2, in 2012.

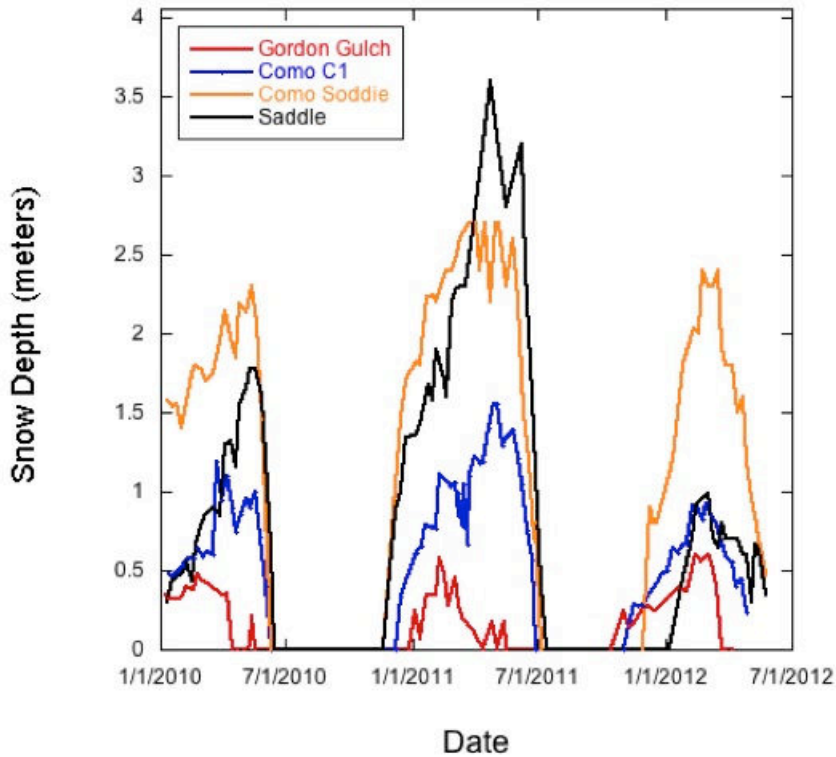


Figure 2.7: Weekly snow depth measurements collected in GG, CC at C-1 and Soddie, and at the alpine Saddle site from 2010 to 2012.

2.4.4 Discharge

For water years 2010 and 2011 the specific discharge hydrographs in all catchments are characteristic of snowmelt-dominated watersheds with steep rising limb driven by snowmelt runoff in April, May and June (Figure 2.8). Conversely, in 2012 the peak discharge in all catchments was associated with rainfall occurring in early July when 100+ mm of precipitation occurred in just a few days. In 2012 GG showed almost no increase in discharge associated with spring melt while the other two catchments had earlier and much less intense increases in discharge from snowmelt in 2012 relative to the previous years. The 2012 peak in snowmelt discharge occurred on 2 April in CC and on 3 June in GL4. During the large snowfall year of

2011, peak discharge occurred on May 22 in GG, then on June 19 in CC, and on July 9 in GL4. The lag time of 48 days between GG and GL4 indicates a lag time of approximately four days per 100 m change in elevation across the Boulder Creek watershed. In addition to later peak discharge with elevation the Como and GL4 catchments also exhibited longer and more gradual recession limbs compared to the GG hydrograph.

Interestingly, there was a very sharp but short-lived peak in discharge on June 5, 2010 in GL4 that is believed to be the result of an ice dam release upstream of the gauge from Green Lake 5 and thus is not considered to be the true peak in the spring runoff. The unnatural spike in discharge at GL4 also coincides with the hydrograph peak at the sub-alpine CC catchment, indicating that the climactic drivers of melt in the sub-alpine also may be a trigger for the release of this water in the alpine, but not the peak discharge in the alpine.

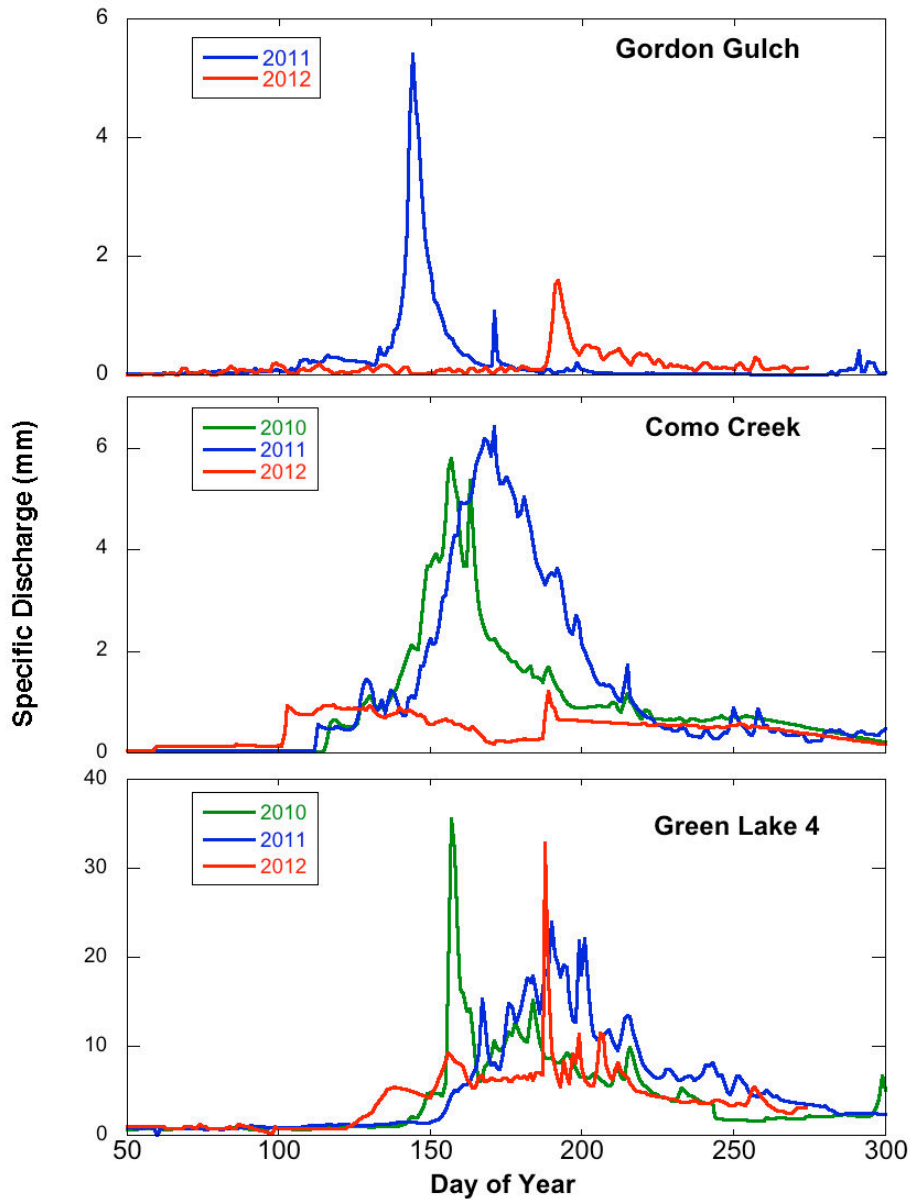


Figure 2.8: Specific daily discharges (mm) for GG, CC and GL4 for 2010 to 2012. A complete discharge record was not available for GG in 2010 and was excluded.

2.4.5 Runoff Efficiency

Runoff efficiency was calculated for each catchment using the cumulative precipitation and cumulative discharge from each water year (Table 2.3). The cumulative precipitation for GG is from the Sugarloaf precipitation record and the cumulative precipitation for GL4 is from

the D-1 precipitation record. Meanwhile, the cumulative precipitation for CC was calculated using the spatially distributed values presented in section 2.4.2. Runoff efficiency increased with elevation in all years, averaging just 10% in GG, 24% in CC, and 88% in the GL4. In GG there was almost no change in efficiency between 2011 and 2012 while in CC the runoff efficiency decreased 12% from the high snowfall year of 2011 to the low snowfall year of 2012.

Interestingly in the alpine GL4 catchment the runoff efficiency was highest in 2012 when snowfall was lowest and rain was greatest.

Table 2.3: Runoff efficiency for GL4 (2010-2012), CC (2010-2012), and GG (2011-2012). Due to a limited discharged record for GG in 2010 a cumulative specific discharge could not be calculated.

	Specific Precipitation (mm)	Specific Discharge (mm)	Runoff Efficiency (%)
2010			
CC	867	238	27
GL4	1431	1120	78
2011			
GG	557	64	11
CC	1186	327	28
GL4	1732	1503	87
2012			
GG	471	43	9
CC	833	131	16
GL4	1155	1132	98

2.4.6 Stream Water Chemistry

Changes of solute and isotopic concentrations over time in all catchments followed a similar pattern (Figure 2.9). Solute concentrations become diluted during snowmelt and then increase on the recession limb of the hydrograph with total solute concentrations decreasing with elevation. At GL4, ANC, Ca^{2+} , and SO_4^{2-} concentrations have the largest seasonal variations while ANC, Ca^{2+} , and Si have large seasonal variations in CC. At GG, the seasonal variation in ANC is much larger than other locations and other solutes at CC, with Ca^{2+} showing the second largest seasonal variation. At GG there is a spike in Cl^- and SO_4^{2-} concentrations in the fall, which is not associated with any large change in discharge. This trend is also apparent in CC with Cl^- concentrations spiking in September and October. The isotopic ($\delta^{18}\text{O}$) values in all streams become more depleted during snowmelt followed by enrichment throughout the summer. Seasonal variations in $\delta^{18}\text{O}$ are on the order of 2-3 ‰ across all catchments with seasonal variations being largest at GL4. In 2012 both GL4 and CC showed less depletion in $\delta^{18}\text{O}$ with spring snowmelt followed by summer enrichment that was greater than observed over the previous two years.

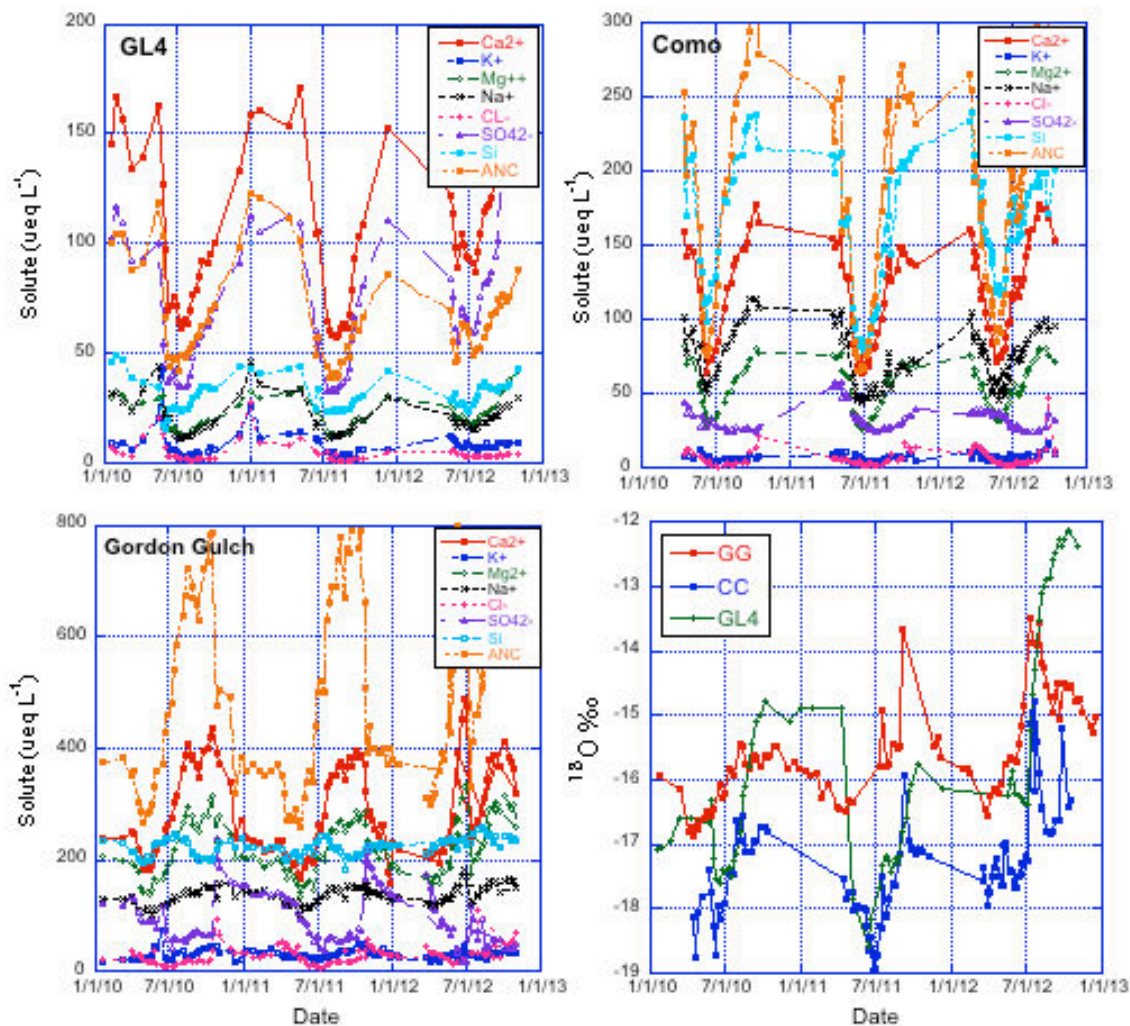


Figure 2.9: Time series from 2010 to 2012 of solute and isotopic concentrations in stream chemistry from GL4, CC, and GG. Streams samples were collected approximately weekly throughout the study with some longer periods between samples during winter months when access was limited in GL4 and CC.

2.4.6 End Member Mixing Analysis

Conservative Tracers and Number of End-Members

At GL4 the distribution of residuals of Ca^{2+} , Mg^{2+} , Cl^- , SO_4^{2-} , ANC, and $\delta^{18}\text{O}$ were near a random pattern ($R^2 < 0.12$) in 2-D mixing space (Figure 2.10). The R^2 for all these tracers

changed significantly from 1-D to 2-D mixing space (data in 1-D not presented), particularly for SO_4^{2-} , Cl^- , and $\delta^{18}\text{O}$. The R^2 values in 1-D were 0.14, 0.64, and 0.64, respectively. Na^+ and Si do not seem to be conservative as their residual distributions in 2-D were not random pattern ($R^2 = 0.16$ and 0.25). Thus, 2-D mixing space (three end-members) was defined for the conservative tracers Ca^{2+} , Mg^{2+} , Cl^- , SO_4^{2-} , ANC, and $\delta^{18}\text{O}$. Five of the conservative tracers selected (Ca^{2+} , Mg^{2+} , SO_4^{2-} , ANC, and $\delta^{18}\text{O}$) were the same as previously used in EMMA for GL4 by Liu *et al.*, (2004). However, the inclusion of Cl^- and exclusion of Na^+ and Si was opposite of tracer selection made by Liu *et al.* (2004) whom did not utilize diagnostic tools (Hooper, 2003) in their study.

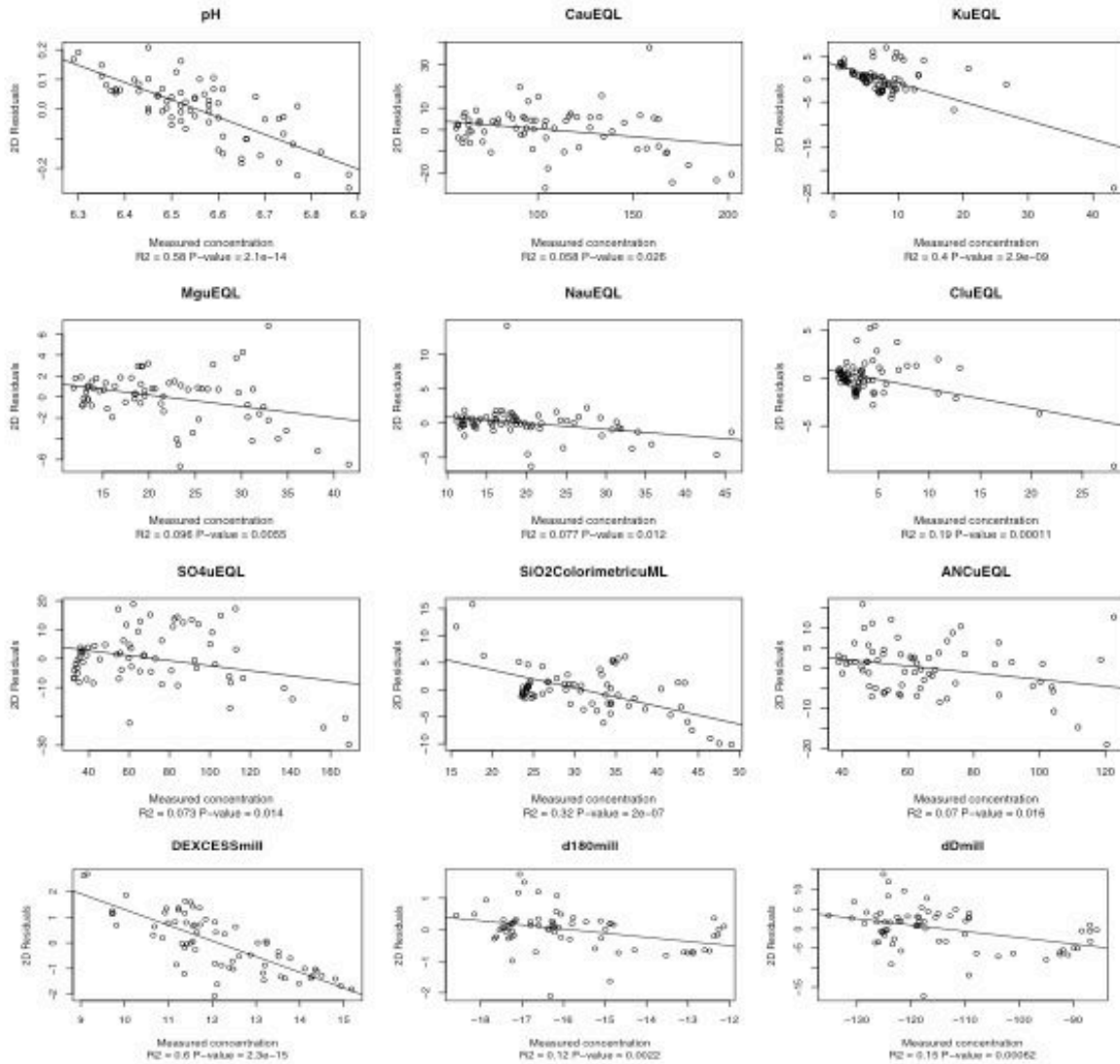


Figure 2.10: Distribution of residuals against measured tracer concentrations in streamflow under 2-D mixing space for Green Lake 4. R² values are shown for fitted lines.

Similar to GL4, the distribution of residuals in 2-D at CC was a near random pattern for Ca²⁺, Mg²⁺, ANC, and ¹⁸O with R² < 0.12 (Figure 2.11). In addition, the distribution of residuals was near random pattern for Na⁺ and Si (R² < 0.17). The R² for all tracers improved from 1-D to 2-D mixing space (1-D not shown), especially for ¹⁸O where R² improved from 0.64 to 0.11. However Cl⁻ and SO₄²⁻ were not conservative in CC as their residual distributions in 2-D were

not random pattern ($R^2 = 0.8$ and 0.4 respectively). Thus, 2-D mixing space (three end-members) was needed for mixing of conservative tracers Ca^{2+} , Mg^{2+} , ANC, Na^+ , Si, and ^{18}O in CC.

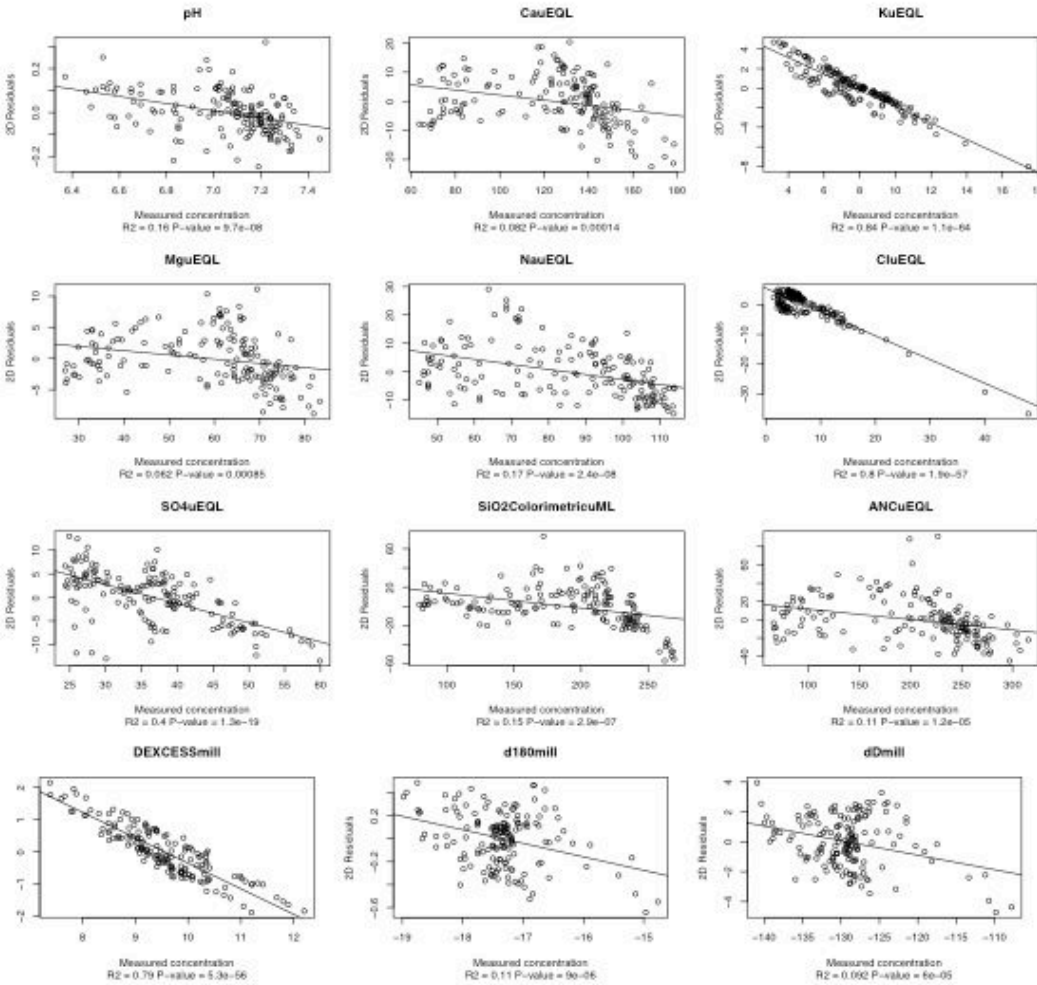


Figure 2.11: Distribution of residuals against measured tracer concentrations in streamflow under 2-D mixing space for Como Creek. R^2 values are shown for fitted lines.

In GG, the distribution of residuals in 2-D was near random pattern for Ca^{2+} , Mg^{2+} , and ANC with $R^2 < 0.06$ (Figure 2.12). The Na^+ also expressed near random pattern with an acceptable R^2 of 0.14 in 2-D mixing space. The ^{18}O exhibited a less random pattern in GG ($R^2 = 0.31$), which was likely influenced by a few outliers that had unexpectedly enriched values. However, the ^{18}O was retained as a conservative tracer as it is needed to differentiate between

the potential end members of rain and snow since the other conservative solute tracers have very low values in both forms of precipitation. The R^2 for all tracers improved from 1-D to 2-D mixing space (1-D not shown), especially for ^{18}O where R^2 improved from 0.54 to 0.31. Similar to CC the Cl^- and SO_4^{2-} were not conservative in GG as their residuals in 2-D were not random pattern ($R^2 = 0.79$ and $.061$ respectively). Thus, 2-D mixing space (three end-members) was needed for mixing of conservative tracers Ca^{2+} , Mg^{2+} , ANC, Na^+ , and ^{18}O in GG.

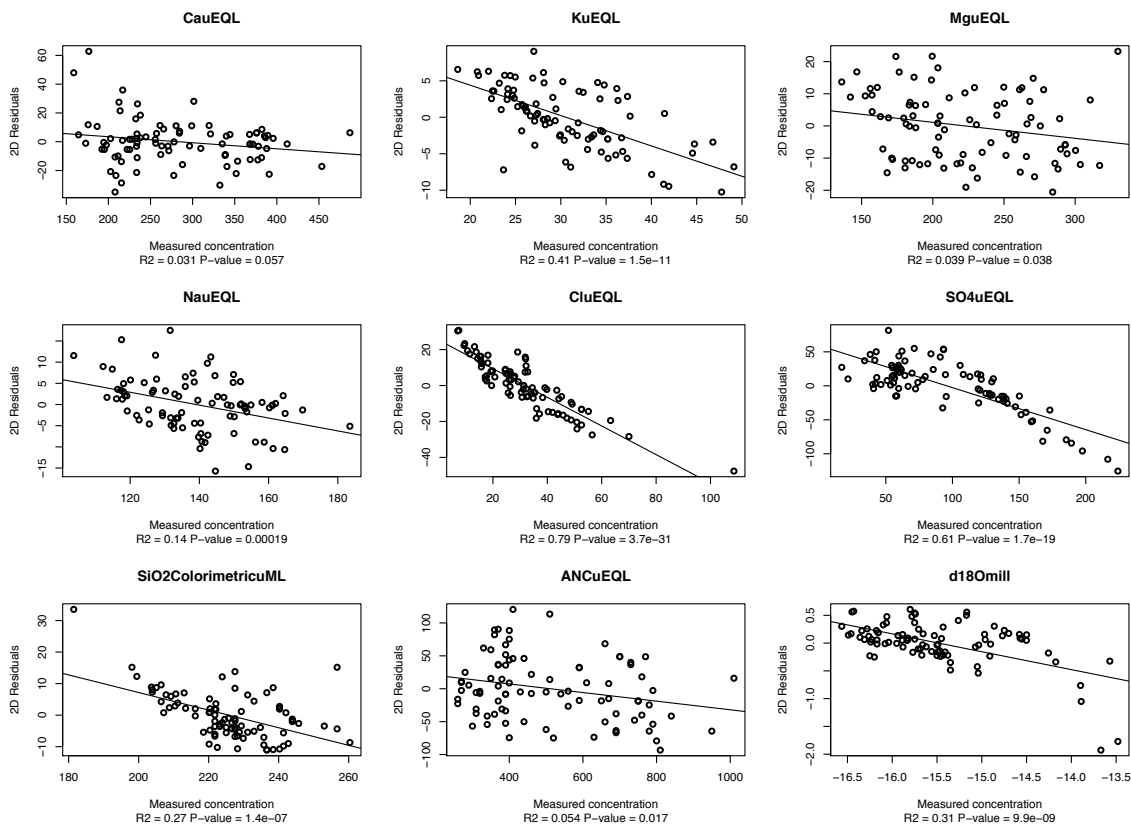


Figure 2.12: Distribution of residuals against measured tracer concentrations in streamflow under 2-D mixing space for Gordon Gulch. R^2 values are shown for fitted lines.

The fit between observed stream water chemistry concentrations and their orthogonal projections was also evaluated by measuring the relative root-mean-square error (RRMSE) for each solute. The RRMSE indicates how “noisy” the data cloud is in the reference mixing space (Ali *et al.* 2010) therefore the greater the RRMSE the lesser the ability of the reference mixing

model to explain the variability in stream water chemistry. The RRMSE for the selected tracers were generally < 2% for all catchments with the exception of ANC in GG (RRMSE = 5%) (Figure 2.13). Therefore all the previously selected tracers were considered acceptable to use for explaining the variability in observed stream water chemistry.

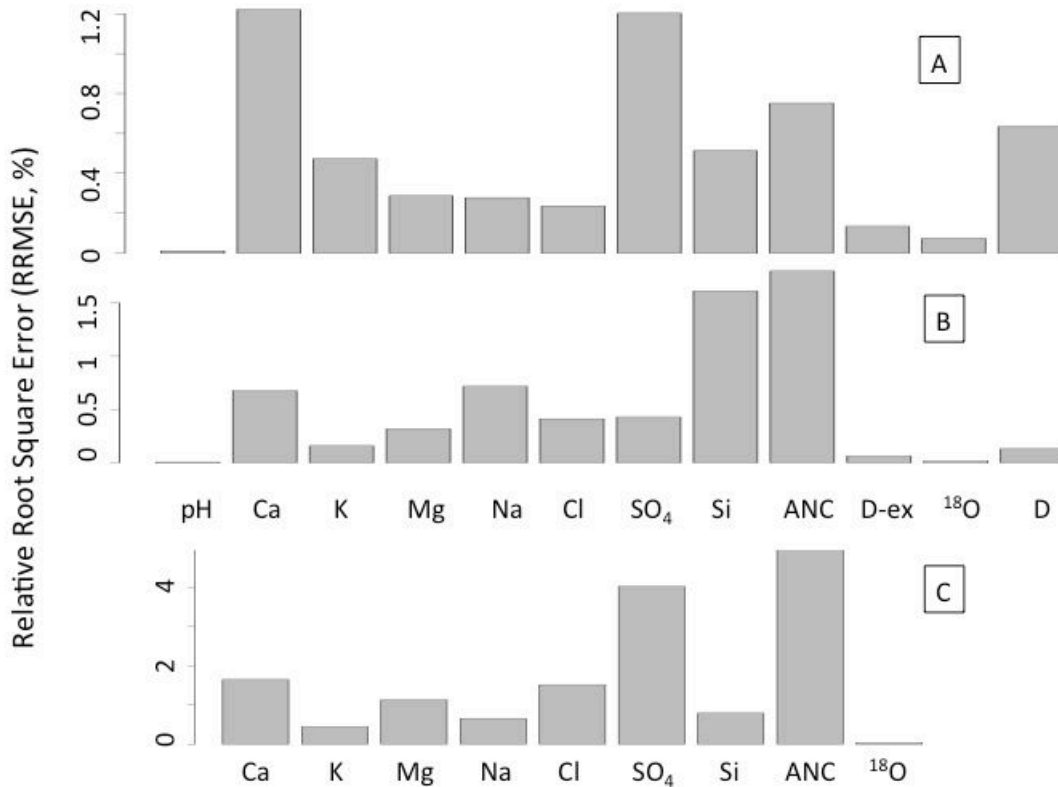


Figure 2.13: Relative Root Mean Square Error (RRMSE, %) for all potential tracers in; A) Green Lake 4, B) Como Creek, and C) Gordon Gulch. The same set of tracers were tested in Green Lake 4 and Como Creek so the x-axis labels in B also apply to A.

Since the stream chemistry of all three catchments could be explained by 2-D (three-end-member) systems, a principle component analysis (PCA) was performed using the correlation matrix of streamflow data to extract eigenvalues and eigenvectors. The first two PCA components explain 94%, 93%, and 95% of the total variance of the streamflow data at the GL4, CC, and GG catchments respectively.

Mixing Diagrams

Since 2-D (three end-members) was needed for end member mixing in all three catchments, the first two U-space projections (U1 and U2) were used in mixing diagrams to screen end-members and determine end-members that contribute to stream flow. In GL4 a total of 18 potential end-members were plotted in the mixing diagram to screen for the ones contributing to streamflow (Figure 2.14). The potential end members included samples from multiple groundwater wells, soil lysimeters, snowmelt lysimeters, snowpack, precipitation (separated into rain and snow), and subsurface flows emerging from talus slopes and a rock glacier. In general samples of the same type tending to plot in the same region of the mixing space. For example the snowpack and snowmelt samples are grouped to the right of stream samples and the groundwater samples all plot in the lower portion of the mixing space. In addition, the rock glacier sample plots in the same direction as one of the talus (Kiowa Talus) suggesting that water from both of these locations is of similar tracer composition but that the Euclidean distance is less between stream samples and the Kiowa Talus making that end-member superior to the rock glacier end-member. In contrast, the soil water samples do not group in plotting space indicative of non-conservative nature of soil water spatially across the catchment, eliminating its selection as a consistent end-member.

To identify three end-members among all the potential ones, eligible end-members must be vertices of a triangle to bound most, if not all, streamflow samples. At GL4, three vertices appear to be the Kiowa talus site, snow from Arikaree snow pit, and groundwater from well 3 (Saddle deep well 3). To better observe the mixing space most of the non-contributing end-members were removed and the triangle of chosen end-members is included (Figure 2.15). End-members are shown by their medians with lines drawn to their 10% and 90% quartiles to give an

indication of total variability in end-members through time. The stream samples falling outside the triangle are geometrically forced to zero and become a two-component contribution.

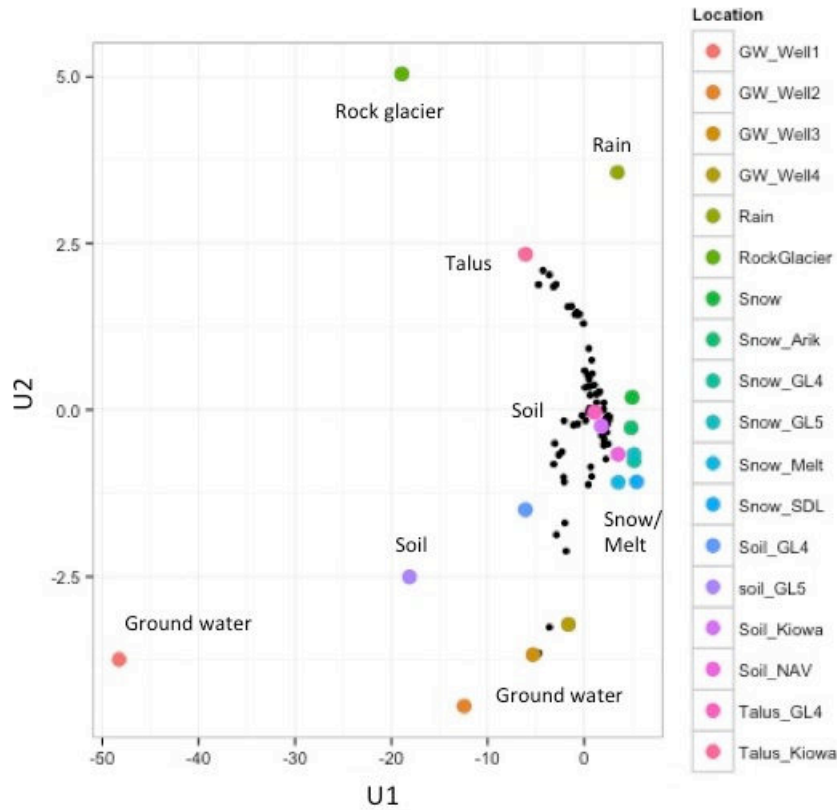


Figure 2.14: Mixing diagram (in U space) for Green Lake 4 including all stream samples from 2010 to 2012 (black) along with 18 potential end-members plotted as the location for the projection of the median value of all selected tracers. The general location of different end-member types is indicated by labels on plot.

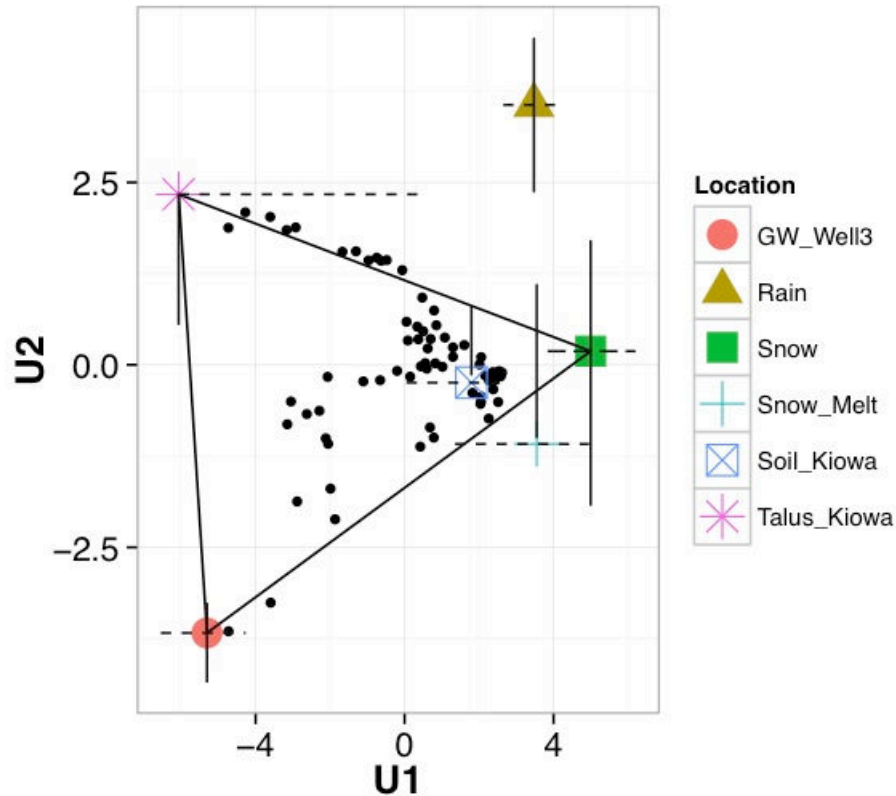


Figure 2.15: Mixing diagram (in U space) for Green Lake 4 including all stream samples from 2010 to 2012 (black) and select end-members plotted as medians with lines drawn to their 10% and 90% quartiles. The 90% quartiles of the talus end-member are excluded to improve plot clarity.

The CC catchment has the most extensive hydrological instrumentation, which resulted in analysis of 22 potential end-members that were plotted in the mixing diagram to screen for streamflow contributors (Figure 2.16). Similar to GL4, snow/melt samples and the groundwater well samples are grouped and represent two of the end-members. Although rain plots further away than soil from stream samples, the location of rain is best suited for the third vertices. Again, there were wide variations in soil waters in the plotting space. The end-members chosen for mixing analysis were groundwater from the C-1 deep well, rain from C-1, and snowmelt from the Soddie (Figure 2.17). The chosen end-members bound 100% of the stream samples and exhibited fairly low temporal variability (as demonstrated by the 10% and 90% quartiles) relative to other potential end-members.

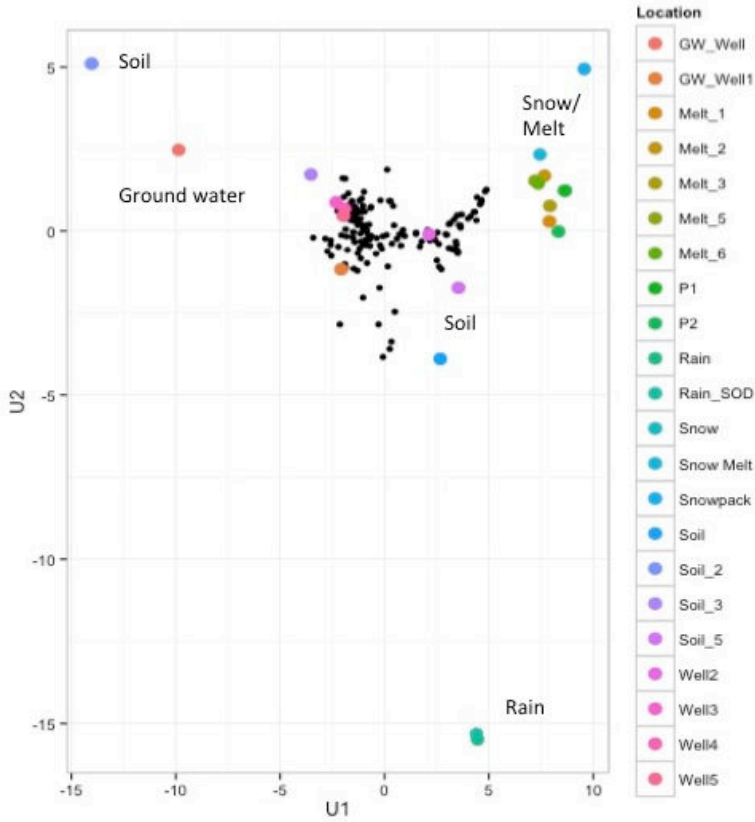


Figure 2.16: Mixing diagram (in U space) for Como Creek including all stream samples from 2010 to 2012 (black) along with 18 potential end-members plotted as the location for the projection of the median value of all selected tracers. The general location of different end-member types is indicated by labels on plot.

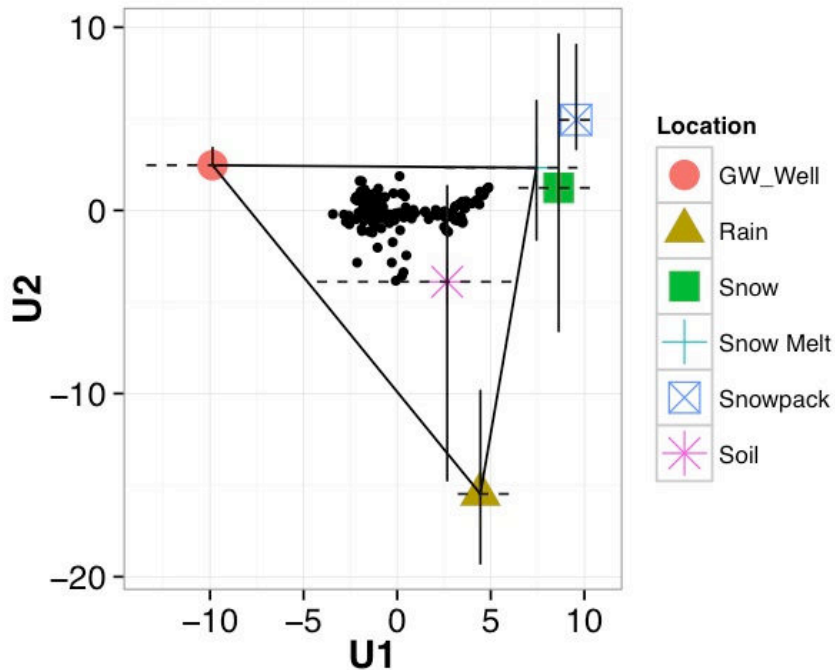


Figure 2.17: Mixing diagram (in U space) for Como Creek including all stream samples from 2010 to 2012 (black) and select end-members plotted as median medians with lines drawn to their 10% and 90% quartiles (shown as lines).

In GG potential end-members included rain and snow as measured at the Sugarloaf CO94 NADP station along with three groundwater wells (Figure 2.18). The wells represented groundwater from the north-facing slope (well 1), the south-facing slope (well 6) and closer to the middle of the catchment (well 2). The groundwater on the north-facing slope has the closest projection to stream chemistry and was chosen as one vertices along with the rain and snow. The location of well 6 suggests that the groundwater from the south-facing slope is dissimilar to that found in the stream. The endmembers constrain 100% of the stream samples.

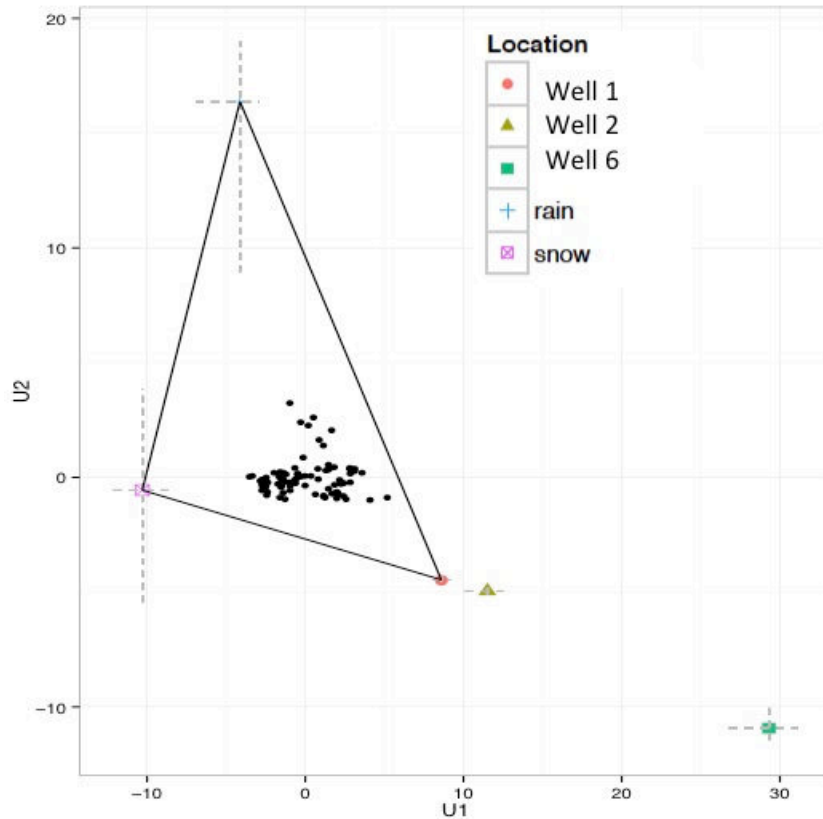


Figure 2.18: Mixing diagram (in U space) for Gordon Gulch including all stream samples from 2011 and 2012 (black) and select end-members plotted as median medians with lines drawn to their 10% and 90% quartiles (shown as dashed lines).

At GL4 streamflow was composed of on average 21% groundwater, 58% snowmelt water, and 21% talus water (Figure 2.19). In 2010 and 2011 the three source contributions were very consistent with groundwater being 24% and 26%, snow was 62% both years, and talus contributed 14% and 12% respectively. The groundwater contribution peaked at 86% on 20 May 2010 on the rising limb of the hydrograph with a similarly timed (but lower magnitude) peak occurring at that time in 2011 suggesting that the snowmelt pulse is first pushing groundwater to the stream before becoming the major contributor. The groundwater peak in 2011 was measured at 96% on 3 January, which may have been true in all years but only in 2011 was a sample collected in January when we would expect the minimum inputs from other sources due to

freezing conditions. In 2012 there was a very different result in which groundwater only contributed 14% of discharge with the peak being a much smaller 38% on 8 April. Interestingly, in 2012 the groundwater contribution was reduced to 0 in mid summer at which time the talus contribution was at it's greatest (78% on 30 September 2012) over the entire study period. The talus water contributed just 14% and 12% in 2010 and 2011 but increased to 36% of total discharge in 2012, likely as a combined result of a decreased groundwater contribution to summer streamflow and from greater flushing of talus water with large rain events that occurred in July of that year. Rain was not chosen as one of the three primary end-members, so direct quantification of rain contribution to streamflow was not available for GL4. In all years the talus water peaked in fall, on the receding limb of the hydrograph. As expected snowmelt water was the greatest contributor to discharge in all years but was reduced from 62% in 2010/2011 to 50% in 2012. The peak contribution from snow was 76% on 8 July 2010, 78% on 9 August 2011, and then much earlier at 63% on 5 June 2012.

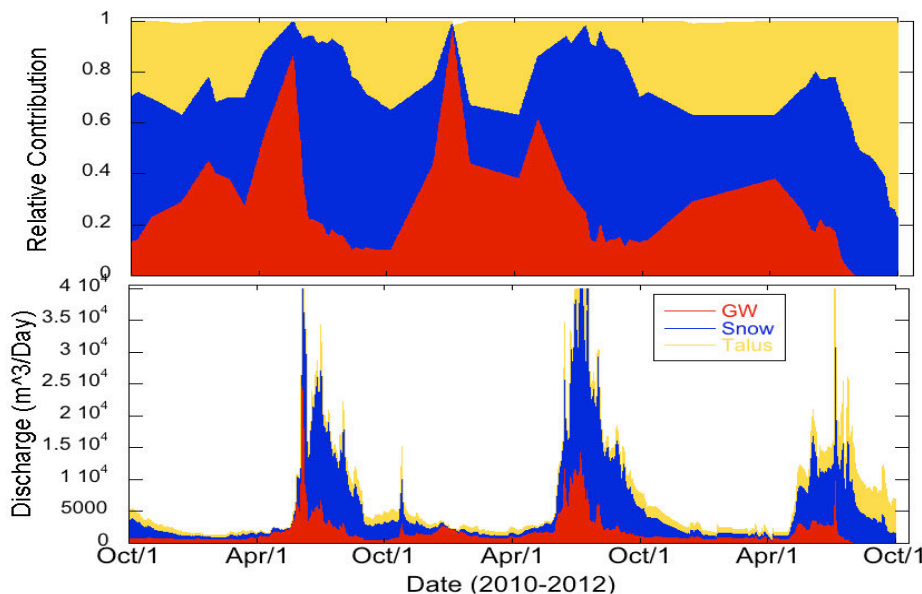


Figure 2.19: Time series of three-component mixing models using EMMA for Green Lake 4. Daily discharge was measured while daily contributions are linearly interpolated based on the observed samples.

At CC streamflow was composed of on average 36% groundwater, 54% snowmelt water, and 10% rain (Figure 2.20). Similar to GL4, in 2010 and 2011 the three source contributions were very consistent with groundwater at 36% and 29%, snow at 56% and 65%, and rain contributing 8% and 6% respectively. The timing and magnitude of contributions was also very consistent between these two years with groundwater peaking at 60% on 30 September 2012 and 62% on 8 October 2011. The snowmelt water contributions peaked at 75% on 10 June 2010 and 79% on 27 June 2011 while the rain water contribution peaked at 16% on 10 August 2010 and then 25% on 7 September 2011. The results suggest that during these years CC discharge is a snowmelt dominated in the spring with an increase in rain contributions in the summer before becoming a groundwater dominated system in the fall and winter months. In 2012, snowmelt contribution still peaked in summer (67% on 1 June) but fell below half of the total contribution as 42%, while groundwater and rain contributions both increased. Interestingly, groundwater had similar timing and magnitude of peak contribution at 58% on 16 September 2012 suggesting that the increase in overall contribution was likely directly related to the decrease in a dominate snowmelt pulse. Additionally, the rain contribution increased to 15% in 2012 peaking at 33% on 24 July likely as a direct result of large precipitation events in July of that year.

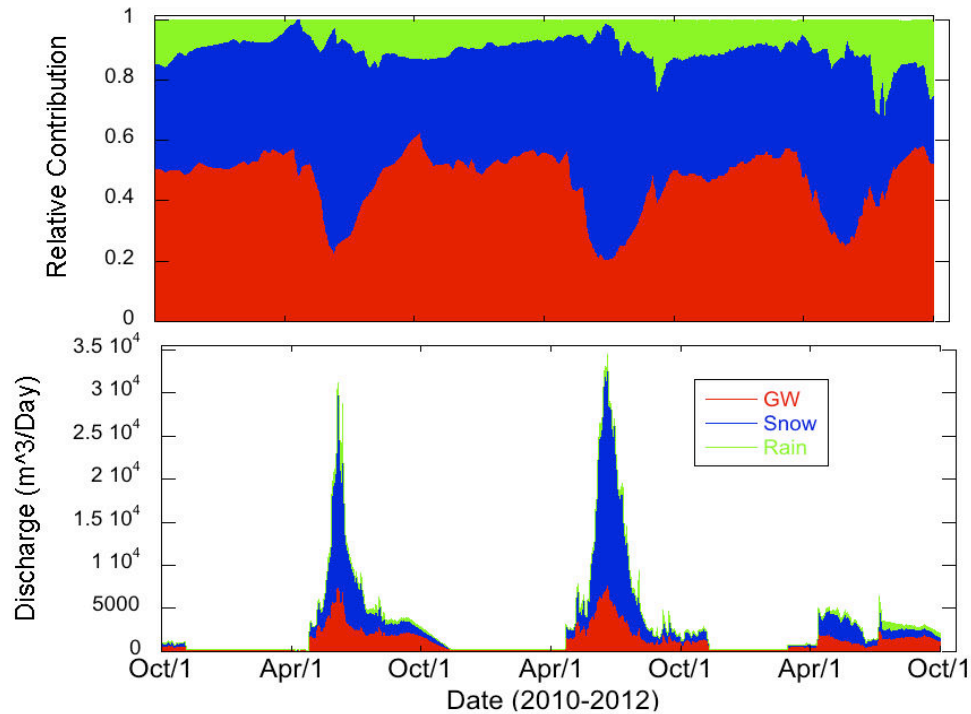


Figure 2.20: Time series of three-component mixing models using EMMA for Como Creek. Daily discharge was measured while daily contributions are linearly interpolated based on the observed samples.

At GG mixing models were only performed for 2011 and 2012 during which time streamflow consisted of 43% groundwater, 41% snowmelt water, and 16% rain (Figure 2.21). In 2011 snow was the dominant contributor to streamflow (52%) and peak contribution (57% on 23 May) coincided with peak discharge. In 2011 groundwater represented 37% of streamflow peaking at 63% on 1 October, while rain contributed 11% and peaked at 28% on 6 September. In 2012 there was a switch with groundwater becoming the dominant contributor to streamflow (49%) peaking at 77% on 27 June while snow was reduced to 30% contribution and peaked at 53% much earlier on 27 March. Rain contribution increased to 21% in 2012 peaking at 32% on 10 July following several days of heavy rain.

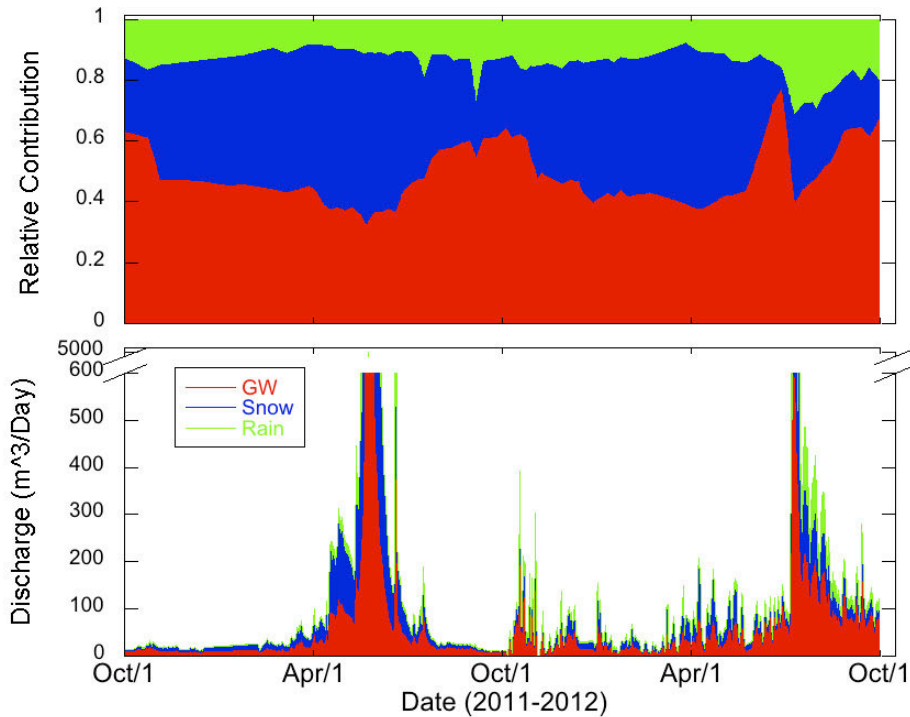


Figure 2.21: Time series of three-component mixing models using EMMA for Gordon Gulch. Daily discharge was measured while daily contributions are linearly interpolated based on the observed samples.

2.5 Discussion

2.5.1 Temperature and Precipitation

During the study daily mean air temperatures in GG were consistently below freezing for two months (~Jan-Feb) while that period was extended to five months (Nov-April) in CC catchment and then seven months (October-May) in GL4. The shorter period of below freezing temperatures at GG translated into nearly 50% of precipitation falling as rain ($39 \pm 10\%$). Meanwhile at C-1 (3012 m) the amount of precipitation as snow was most consistent of all elevations at $64 \pm 2\%$ with that number increasing to $84 \pm 10\%$ at D-1 (3739 m). Total precipitation increased almost three-fold with elevation as *MAP* was 512 ± 43 mm at GG increasing to 962 ± 195 mm at CC and $1,439 \pm 289$ mm at GL4. The *MAP* measured at GL4 was higher than the 1,186 mm measured in 1996 by Liu *et al.* (2004) and the fifty-year average

of 1,000 mm (Williams *et al.*, 1996). Importantly, previous studies did not use the Arikaree/D-1 precipitation correction, which increased total winter precipitation by 18%. The winter correction of D-1 precipitation does not fully address spatial variation across the catchment but it is likely a better representation of the catchment as a whole because D-1 is along the windy ridge while the Arikaree precipitation collector resides closer to the center of the upper basin. The winter correction is supported by Rasmussen *et al.* (2012) who estimate that measurement errors for solid precipitation frequently range from 20% to 50% due to under-catch in windy conditions.

Spatial variability of precipitation was further addressed in CC by averaging multiple collectors at C-1 and by applying a lapse rate to different elevation bands in the catchment. The annual variability between the four independent precipitation collectors at C-1 alone was ($12 \pm 3\%$) and somewhat surprisingly the greatest annual variation between collectors (274 mm) or 32% difference between the Niwot LTER and AmeriFlux gauges) was during the low snow and high rain year of 2012 (Table 2.2). The C-1 MAP of 772 ± 91 mm over the study was slightly lower than a 10-year average of 800 mm reported by Monson *et al.* (2002) from AmeriFlux measurements. The annual totals from the AmeriFlux precipitation collector were consistently higher than the other three gauges (Table 2.2), which further suggests that there may be systematic errors associated with the different collectors used in this study. The differences in net precipitation may be attributed to the AmeriFlux collector being the only collector that was 1) heated, 2) completely unshielded from wind, and 3) located at 10 m above the ground in the forest canopy as opposed to the 2 m height of other collectors. Additional over and under catch associated with differences in collector type, spacing from vegetation, degree of wind sheltering, and interplay of nearby canopy interception and re-distribution of precipitation are all likely contributors but it is beyond the scope of this paper to further analyze the observed variability.

Additionally, distribution of precipitation into three distinct elevation bands increased the catchment *MAP* by 17 ± 9 % relative to the *MAP* at C-1 alone, further demonstrating that extrapolating point measurements of precipitation to catchment scale may considerably over or under estimate catchment inputs.

The observed increase in precipitation with elevation was also associated with a greater year-to-year variability in total precipitation with elevation (Figure 2.6). When analyzing changes in precipitation with elevation between C-1 and D-1, Knowles *et al.*, (2014) found that during the period 2008-2012 there was a significant relationship ($p = 0.08$) between precipitation and elevation only during the winter (snowfall) with no relationship in the summer. Expanding the elevational gradient down to GG also showed no relationship in summer precipitation with elevation because in 2011 GG received more rain than GL4 but the opposite was true in both 2010 and 2012. This result is likely attributed to summer precipitation typically occurring as afternoon convective storms, which can bring intense but spatially and temporally sporadic rainfall (Greenland and Losleben, 2001). Results therefore indicate that increasing annual precipitation with elevation in Boulder Creek watershed is primarily controlled by winter precipitation, which translates into more variable year-to-year precipitation totals in the snow-dominated higher elevation catchments (CC and GL4). In these catchments winter temperatures are persistently below freezing and sufficient to maintain snowpack accumulation throughout the winter. Meanwhile, GG experienced relatively small change in year-to-year total precipitation but greater amount and inter-annual variability of “mixed” precipitation (7-30%). The “mixed” precipitation was 3-16% at C-1 narrowing to 1-4% at the SDL and 1-2% at D-1. Greater “mixed” precipitation indicates a greater percentage of annual precipitation that is vulnerable to predicted warming temperatures. The result will be an increase in the rain to snow ratio, which

suggests GG is more hydrologically sensitive to climate changes in temperature than precipitation.

To summarize, catchments like GG that reside in the rain/snow transition zone (i.e S/P <0.5) appear to be experiencing less hydrologic variability caused by inter-annual changes in total precipitation, but rather in changes in temperature which drive other factors like changes in water storage, infiltration, and runoff. In the context of the elevational gradient in Boulder Creek watershed, it appears that in catchments in the rain/snow transition currently experience temperature controls on the type of precipitation inputs throughout all parts of the years while in snow-dominated catchments winter precipitation accumulation is the primary driver of precipitation inputs while temperature is less of a factor during the accumulation season.

2.5.2 Snowpack and Snowmelt

At the sub-continental scale, most studies concur that recent snowpack losses are associated with late winter/early spring (February-March) warming that decreased snow accumulation while advancing the timing of snowmelt, primarily at elevations near the freezing level (Hamlet *et al.*, 2005, 2007; Kapick and Hall, 2010; Minder, 2010; Nolin and Daly, 2006; Regonda *et al.*, 2005). These losses have been attributed to increased temperatures (Mote *et al.*, 2005; Hamlet *et al.*, 2005), which lead to snow loss via some combination of increased frequency of rain vs. snow (Knowles *et al.*, 2006) and increased wintertime melting (Mote *et al.*, 2005). Complicating the picture is large year-to-year variability in snowfall (Minder, 2009) with inter-annual variability of springtime snowpack resulting largely from variability of wintertime precipitation (Cayan, 1996; Hamlet *et al.*, 2005).

Hinckley *et al.*, (2012) found that in GG the snowpack dynamics are strongly affected by aspect with north-facing slopes developing a seasonal snowpack, and south-facing slopes experience more intermittent snow accumulation throughout the winter and spring. Therefore at the elevations where air temperature is near freezing during winter precipitation events the accumulation and storage of the precipitation is sensitive to changes in energy balance controlled by aspect which can be observed at the hillslope scale. The changes in energy balance (i.e. incoming solar radiation) with aspect will translate into aspect specific differences in water storage and delivery via snowpack and snowmelt and losses associated with evapotranspiration of the stored water (Molotch *et al.*, 2009; Tague and Grant, 2009; Tague *et al.*, 2009). The Rocky Mountains run north and south and are drained by east-west trending valleys in the Colorado Front Range, resulting in predominantly north-south aspect hillslopes (Hinckley *et al.*, 2012). Therefore, from a regional context, the role of aspect may be of particular importance in controlling catchment hydrologic processes at elevations near the rain-snow transition.

In this study the GL4 and CC catchments experienced noticeable differences in the timing of both maximum snow accumulation and the resulting peak in discharge associated with snowmelt runoff between years. When compared to long-term LTER climate records at Niwot Ridge, 2012 was anomalously warm and dry during the winter and spring (Knowles *et al.* 2014). Peak snow depths at C-1, Soddie, and SDL, occurred three months earlier in 2012 than in 2011 which translated into peak discharge (from snowmelt) occurring six weeks earlier in CC in 2012 and five weeks earlier in GL4 in 2012. The dramatic difference in the size of the winter snowpack from 2011 to 2012 was similar to relationships previously observed at the SDL site by Cline (1996) who reported a 300% difference in snowpack between 1994 and 1995. However, in that study the difference in timing of maximum snow accumulation (inferred as start of melt)

was < 1 month at the SDL (5 May to 1 June) whereas in this study max accumulation at the SDL occurred on 6 June 2011 and on 3 March 2012. From 30-year SNOTEL records from 1978-2007 Clow (2010) documented a shift in snowmelt timing of 2-3 weeks (4.8 days per decade) in Colorado. The inter-annual variability of melt timing in this study suggest that in addition to long-term trends in change in snowmelt timing, the magnitude of year-to-year variability is also important to consider from a water resource perspective. Equally important is recognition that variability in timing of snow accumulation and melt is currently occurring at all elevations in Boulder Creek watershed and not just near the rain-snow transition, negating assumptions that spatial separation from the rain/snow transition provides a temporal buffer to the effects of changing climate on high elevation snow-dominated catchments.

2.5.3 Discharge and Runoff Efficiency

In 2010 (CC & GL4) and 2011 (GG, CC, GL4) catchments represent snowmelt dominated hydrographs with low winter baseflow followed by a steep rising limb during spring snowmelt and a slightly more gradual receding limb returning to baseflow by late summer (Figure 2.8). The duration of the recession in these years was greater in GL4 and CC than GG, driven by more snow and slower melt at higher elevations. In 2012 all three catchments expressed a peak snowmelt discharge that was only about 30% of the magnitude of the other years and all three catchments had a peak annual discharge that was associated with summer rain, which was shorter lived than the traditional snowmelt peak having both steep rising and recession limbs. In GL4, the 2012 peak discharge occurred at the same time as in the lower catchments but came from talus waters that had been flushed by rain events rather than direct contributions from rain to streamflow.

The specific discharge (Q , mm) is similar in magnitude for GG and CC, but is about three times the magnitude for GL4. Potential explanations include the greater amount of total precipitation, cooler temperatures, and less vegetation to drive ET in the alpine catchment. Additionally, the alpine has less developed and shallower soils than lower elevations, resulting in less water being held in the near surface (i.e. unsaturated soils) reducing near-surface ET processes. CC has similar discharge magnitude to GG but a longer duration of snowmelt discharge therefore a greater total yield, consistent with greater total precipitation and lower potential ET at the higher elevation catchment.

The runoff efficiency (Q/P) showed consistent increase with elevation over the study but the year-to-year variations between catchments was not consistent. In GL4 the efficiency (K) actually increased from 78% in 2010 to 87% in 2011 and 98% in 2012 despite 67% less precipitation and 20% lower S/P ratio. In light of potential error associated with calculation of catchment *MAP* from two point measurements (36% difference between Arikaree/D-1), the absolute changes in K are likely within the range of error and may not be significant. At CC, K was steady at 27% and 28% in 2010 and 2011 but decreased to 16% in 2012. At GG, although there was only two years of record, K was most consistent at 11% and 9%. Again the absolute values of K are presented without error analysis associated with measuring both P and Q at the catchment scale. Previous efforts to assess measurement uncertainty associated with quantifying water balance components suggest that uncertainty can be up to 20% of total component flux (Graham *et al.* 2010). Therefore inter-annual changes in K at each site may not be significant, but still provide a first-order qualitative comparison of spatial and temporal changes over the full elevation gradient under investigation. During the study alpine K was 80-100% and decreased to 15-25% in the partially forested CC catchment and just 10% in the rain-snow transition GG

catchment. The dramatic decrease in K from alpine to forested ecosystems was influenced by some combination in the forested portion of CC of snow sublimation in winter (Claassen & Downey, 1995; Molotch *et al.* 2007), and evapotranspiration (ET) (Barnett *et al.* 2005; Christensen *et al.* 2008). Changes in storage or groundwater recharge not observed at the catchment outlet (e.g. Graham *et al.* 2010, Knowles *et al.*, 2014) could impact inter-annual changes in K at the catchment scale but are likely small relative to the changes observed between catchments.

It is known that global changes in temperatures directly affect the hydrology of the land surface through changes in the accumulation and ablation of snow, as well as in ET (Nijssen *et al.*, 2001). Unfortunately, there is little agreement on the direction and magnitude of historical and future ET trends (Barnett *et al.*, 2005). Barnett *et al.* (2005) states that earlier snowmelt drives a timing and magnitude shift on ET due to greater soil moisture earlier in the season when potential ET is low but then less soil moisture later in the fall (because melt supply is gone). The result may be reductions in annual ET if initial melt water infiltrates past the root zone prior to increases in vegetative uptake. However, recent research in CC by Molotch *et al.* (2009) shows that commencement of the growing season was coincident with melt-water input to the soil. This suggests that with earlier snowmelt the vegetation will “turn on” earlier in the year ultimately lengthening the summer growing season. Additionally, Hu *et al.* (2010) found that in the spruce-fir forests of CC are highly dependent on snow water uptake from the soil even into late summer with 57-68% of water in the xylem in mid August coming from the previous winters snow. Reynolds and Knight (1973) report that in subalpine forests rain events of < 10 mm were mostly intercepted by the canopy or absorbed by forest liter and rarely penetrated into deeper soil layers. During the three-year study in CC, Hu *et al.* (2010) found that rain events occurred

approximately every 3.3 days but <11% of all rain events were > 10 mm. In the absence of large rain events the earlier onset of increased ET, caused by earlier melt out of snowpack, could be offset by a decrease in ET later in the growing season due to limits in water availability, thereby not being solely responsible for observed decreases in runoff efficiency. Conversely, in the case of this study the low snow and early melt in 2012 was followed by large (>100 mm) rainfall over a few days in early July. As a result, the ET losses likely began earlier in 2012 relative to other years but instead of diminishing due to drying soils in the summer the large input of rain would have increased water availability in mid-summer allowing ET rates to remain elevated over a longer period in 2012. The result is then a greater portion of input (P) being lost to ET, providing an explanation for reduced K in 2012.

In GG from 2011 to 2012 the decrease in P was nearly equivalent to the total decrease in Q resulting in only a 2% decrease in K. Overall there was less variability in P at GG between the two years and even though the timing of peak Q was correlated with spring melt in 2011 and summer rain in 2012 the catchment showed little change in the efficiency of converting P into Q.

2.5.4 Surface-Groundwater Interactions

Results from this study indicate that groundwater is an important contributor to streamflow in all catchments and inclusion of a groundwater end-member was necessary to adequately bound all stream samples and perform EMMA. Previous use of EMMA for source water identification in GL4 (Liu *et al.* 2004) did not have a distinct groundwater end-member (study was prior to well installation) thus was forced to chose a baseflow value in late fall to represent the subsurface contribution. Addition of a groundwater end-member helped bound all stream samples (Figure 14) and enabled the inclusion of winter stream samples that had been

excluded by Liu *et al.* (2004). Although there were a limited number of winter stream samples collected in GL4, all winter samples plotted towards the groundwater end-member. By mid-winter surface inputs (snow) and shallow subsurface waters (talus) are frozen promoting groundwater to be the dominant source. Inclusion of a groundwater end-member also improved EMMA for GL4 because it highlighted more distinct differences between the timing of groundwater and talus contributions by eliminating the assumption that fall baseflow was distinct from talus water. The separation was particularly important in 2012 when talus water contributions peaked following the low snow spring and high rainfall summer.

Talus water is essentially a second (shallower) subsurface reservoir that contributes to streamflow primarily in the late summer when the snowmelt inputs have decreased. The connection of talus water to stream discharge appears to be particularly influenced by the magnitude and timing of new water (rain) inputs to the system. In 2012 the low snowpack translated into increased areas of snow free talus slopes at the time of heavy rains in early July. The combination of a large influx of new water increased the hydrologic connectivity and movement of water in the talus blockfields to the stream channel, greatly increasing the contribution of this source to stream discharge. To summarize, both the bedrock groundwater and the talus/glacial deposit pore waters are important to streamflow and the magnitude of those contributions is dependent on the magnitude of new water inputs, with snowmelt recharging groundwater and rain recharging talus water reservoir particularly in low snow years. If future climate shifts the inputs to more rain and less snow we are likely to see an overall decrease in groundwater and a potential increase in talus water contributions to streamflow. However, the magnitude of rain events may be a large control on the talus water contributions because a threshold volume and intensity may be necessary to achieve the hydrologic connectivity between

subsurface reservoirs and the stream discharge. In the absence of threshold rain events, there will likely be an overall decrease in runoff efficiency under projected climate scenarios for alpine catchments like GL4 as small and isolated rain events may not sufficiently contribute to stream discharge. Also as indicated by Caine (2010) a warmer climate may initially increase stream discharge in the fall due to accelerated loss of additional stored water in the form of permafrost and or rock glacier ice (Williams *et al.*, 2006) in the upper portions of the catchment (Leopold *et al.*, 2011, 2013). However, the absolute volume of this stored water resource is difficult to quantify (Clow *et al.*, 2003), thus the duration of its contribution is unknown.

The CC and GG catchments fall below the extent of all talus fields or rock glaciers reducing potential sub-surface end-members to soil water and/or groundwater. Soil water was too spatially and temporally variable to constrain end members in all catchments. The recent installation of groundwater wells in both CC and GG catchments enabled a groundwater end-member to be identified in both catchments. In CC the most representative groundwater end-member was from the deepest well at C-1, which sampled water from 14-16 m depth in glacial deposits residing on top of local bedrock (Figure 2.16). The groundwater at this location was more similar to streamflow than the bedrock groundwater from the deep wells at SDL (wells 1 & 2 in Figure 2.16), suggesting that streamflow is primarily receiving groundwater that has resided in the glacial deposits and is not dominated from flow paths in the deeper bedrock that are sampled by the SDL wells.

Meanwhile in GG there was a clear difference between the groundwater encountered in the wells on north-facing (well 1) and south-facing (well 6) slopes (Figure 2.18) with both the meadow groundwater (well 2) and the stream water being most similar to the groundwater on the north-facing slope. This suggests that more water that infiltrates the north-facing slope is recharging to

depth and then contributing to both groundwater in the meadow and stream discharge. The ability of EMMA to identify greater groundwater contributions from the north-facing hillslope agrees well with Hinckley *et al.* (2012) whom found that in GG north-facing slope snowmelt had connected vertical flow through the soil matrix to depth while the south-facing slopes expressed less consistent hydrologic connectivity through the soil matrix reducing the potential for groundwater recharge on south-facing slopes. Therefore aspect in GG controls the accumulation and storage of winter precipitation, which translates into influencing streamflow via larger groundwater contributions from north-facing slopes.

Overall the contribution of groundwater to streamflow was inversely related to elevation, decreasing from 45% contribution in GG to 36% in CC and 21% at GL4. Interestingly, during the low snow year of 2012 total groundwater contributions increased in both GG and CC but decreased considerable in GL4. The inverse trend between the alpine and forested catchments can be explained by two mechanisms. First, the actively contributing groundwater in GL4 is likely confined primarily to fracture flow in the bedrock. The extent of groundwater reservoirs in alpine watersheds is controlled by the depth of the fracture system (comprising the active layer) which can be hundreds of meters thick (Snow, 1973; Gleason & Manning, 2008) and seasonal water table fluctuations in these types of aquifers have been observed to be up to 50 m in the upper part of an alpine watershed in Colorado (Manning & Caine, 2007). In crystalline and other lower-permeability regions, existing data (though limited) also suggests that the water tables are often relatively close to the land surface, even below high ridges (Bossong *et al.*, 2003; Caine *et al.*, 2006). Therefore without ability to directly measure head gradients in the upper GL4 catchment (sample wells were located on flat portion of Niwot ridge away from the steep catchment headwalls) it is assumed that the elevation of the groundwater table can dramatically

fluctuate in response to variability in seasonal snowmelt recharge. A large decrease in magnitude of snowmelt in the alpine in 2012 would translate into less recharge and a more rapid decrease in groundwater elevation. If the elevation of the potentiometric surface of the bedrock groundwater was sufficiently lowered in 2012, it may have become disconnected from stream discharge at and above the elevation of the catchment outlet and thus become a non-contributor to streamflow in late summer.

The >100mm rain that fell on GL4 over just 10 days in July 2012 likely flushed the talus pore waters, increasing connectivity between talus reservoir and the stream thus increasing the talus contribution. In all catchments there was a short spike in discharge associated with the rain event where rain may have been the primary source but without event stream chemistry (EMMA performed with weekly samples only) it was not possible to calculate the direct contribution of rain at event resolution. However, EMMA was able to demonstrate that the rain served to recharge the subsurface storage in CC and GG. The recharge was evident because there was an increase in snow water contribution to streamflow following the rain event, only explained by infiltrating rain pushing out some snow water that had been held in the subsurface since the previous winter.

To summarize the low snow but high rainfall in 2012 helped to demonstrate that in GL4 the bedrock groundwater contribution to streamflow is sensitive to magnitude of snowmelt recharge while the talus water source can have increased hydrologic connectivity to stream when high magnitude rain events occur following low snow inputs. In CC and GG the groundwater reservoirs appear to be sufficiently large (or long enough transit times) to not become disconnected from the stream in summer following a low snow year. In CC the groundwater contributing to streamflow appears to be residing in the glacial deposit materials above the

bedrock. The recharge of this reservoir is likely from infiltrating snowmelt in the upper catchment where snowpack accumulation is greatest and not coming from mountain block recharge of bedrock groundwater residing at elevations above the catchment (i.e. SDL wells). In the rain/snow transition elevation of GG the groundwater contributing to streamflow comes from the north-facing slopes where snowpack and resulting recharge is greatest.

2.5.5 Conceptual Models of Catchment Hydrologic Processes

Conceptual models were generated for each catchment to provide physical context to the hydrologic partitioning identified in this study (Figure 2.22). Development of conceptual diagrams for each catchment also provides a visual representation of how the specific geoclimatic conditions influence source water production, storage, and streamflow generation. Although sub-surface transit times and storage capacity were not directly measured, the current knowledge of subsurface composition was included to show generalized pathways for groundwater (or talus water) contributing to streamflow.

At GL4 (Figure 2.22 A) precipitation is snow dominated and runoff efficiency is high, indicating that annual water losses (ET) are low. Seasonally, ET may be higher in the winter than summer due to sublimation of blowing snow and limited vegetative transpiration in summer (i.e. Knowles *et al.*, 2014). Wind re-distribution of snow creates uneven distribution of snowpack and melt leading to spatially variable infiltration and subsequent recharge. Groundwater is likely recharged from areas of deeper snow accumulation and may also be spatially variable depending on preferential flow through overlying talus and into a complex bedrock fracture system. Groundwater contributes to streamflow throughout the year becoming the dominant source during winter when other sources are primarily frozen. The amount of groundwater contributing

to streamflow also increases when discharge increases from spring snowmelt, indicating that some of the initial melt is infiltrating the sub-surface and pushing stored water to the stream. In low snow years the reduction in groundwater recharge has potential to limit and/or disconnect the dominant groundwater flow from the stream. Snowmelt is the dominant source to streamflow annually with maximum contributions occurring during summer. The talus water is recharged from snowmelt with potential recharge from summer rain when event intensity is sufficient as seen in 2012. The talus water is stored in the near surface materials resulting in shorter flowpaths to stream than deeper groundwater.

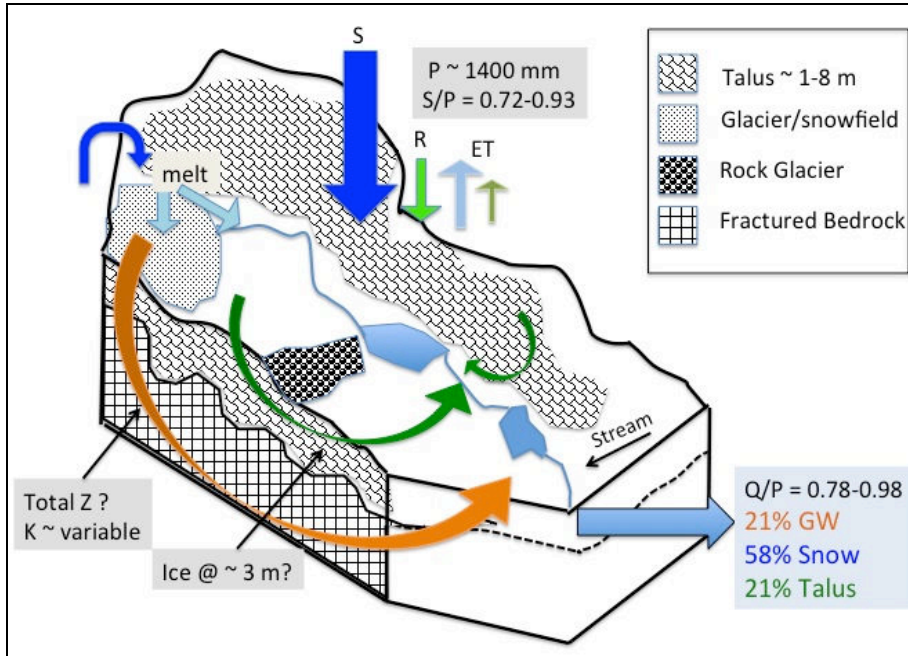
At CC (Figure 2.22 B) precipitation is snow dominated with the orographic lapse rate greater in the winter. Greater snow accumulation at and above treeline likely generates greater melt water contribution to both streamflow and groundwater recharge from the upper portion of the catchment. The ET is lower in the alpine than in the forest during melt and summer season further influencing recharge/discharge control by the upper catchment. Lower snowpack and greater water use (ET) in the forest likely reduces recharge/discharge contributions from the lower portion of the catchment. The direct snowmelt recharge in the forest is used throughout the summer by trees and likely does not contribute significantly to streamflow. Greater total catchment ET than alpine reduces runoff efficiency by an additional 50-65%. Based on the C-1 deep well end-member selection for EMMA, the groundwater contributing to streamflow appears to be recharged up high and stored within the deeper portions of the glacial deposits rather than being derived directly from bedrock flowpaths as would have been represented by the SDL well water. Due to low degree of stream incision in the catchment, the shallow sub-surface near the stream channel in the lower catchment may act as a seasonal sponge with the stream losing water to the subsurface during rising limb of hydrograph and then potentially draining back to stream

during hydrograph recession. The resulting annual streamflow is dominated by snowmelt with greater and more temporally consistent groundwater contributions than observed in the alpine, explained by greater potential storage and more uniform flow within the glacial deposits than in the alpine bedrock. Overall rain contributions remain small with occasional short duration increases to streamflow following precipitation events.

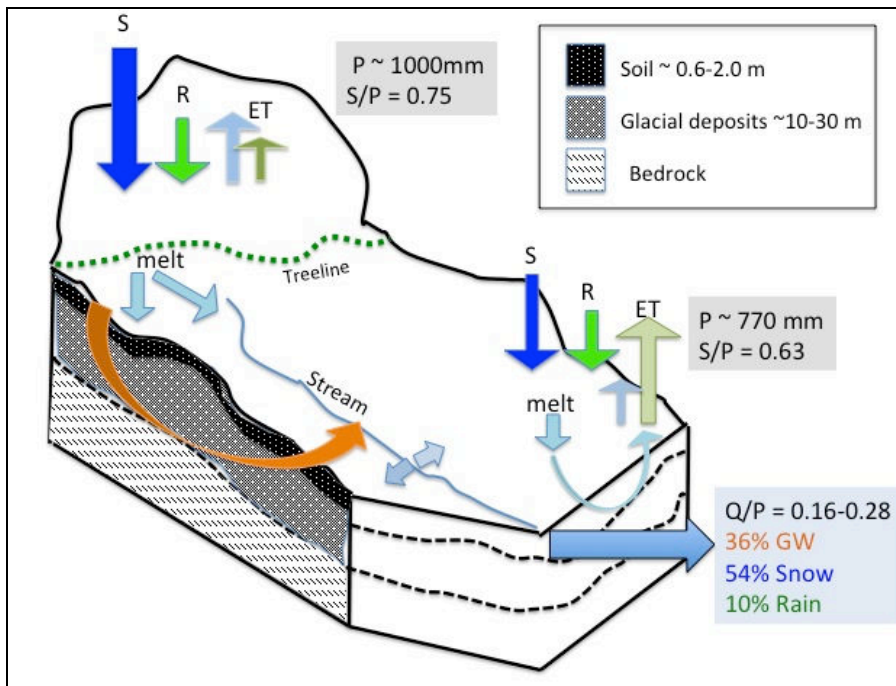
At GG (Figure 2.22 C) annual precipitation is only about half of that at treeline and is a near even distribution of rain and snow. However snow is a larger contributor to streamflow than rain indicating that snowmelt still plays a dominant role at the catchment scale. Air temperatures remain near freezing throughout the winter at this elevation, with aspect differences being sufficient to promote large differences in hydrologic partitioning by aspect. Snowpack is intermittent on south-facing slopes with small periodic melt events throughout the winter leading to limited hydrologic connectivity in the soil and minimal groundwater recharge. Conversely snowpack is more seasonally persistent on north-facing slopes resulting in a greater sustained snowmelt pulse sufficient to provide hydrologic connectivity through the soil and enable groundwater recharge. The weathered bedrock on the north-facing slope is capable of storing, and consistently delivering, groundwater to streamflow throughout the year making groundwater the dominant source of annual streamflow. Snowmelt contributions to streamflow are also likely derived predominantly from the north-facing slopes. Although rain is ~50% of precipitation only about 2% of that rain contributes to streamflow. The runoff efficiency is lowest at this elevation indicating that losses (ET) are greater than at the higher elevation catchments. Seasonally, ET is likely larger on the south-facing slopes in winter due to periodic melting creating more water availability in the near surface and because lack of hydrologic connectivity immobilizes soil water for longer periods of time. On north-facing slopes sustained snowmelt provides greater

water availability into the summer, which translates into higher tree density on north-facing slopes and thus higher summer ET.

A)



B)



C)

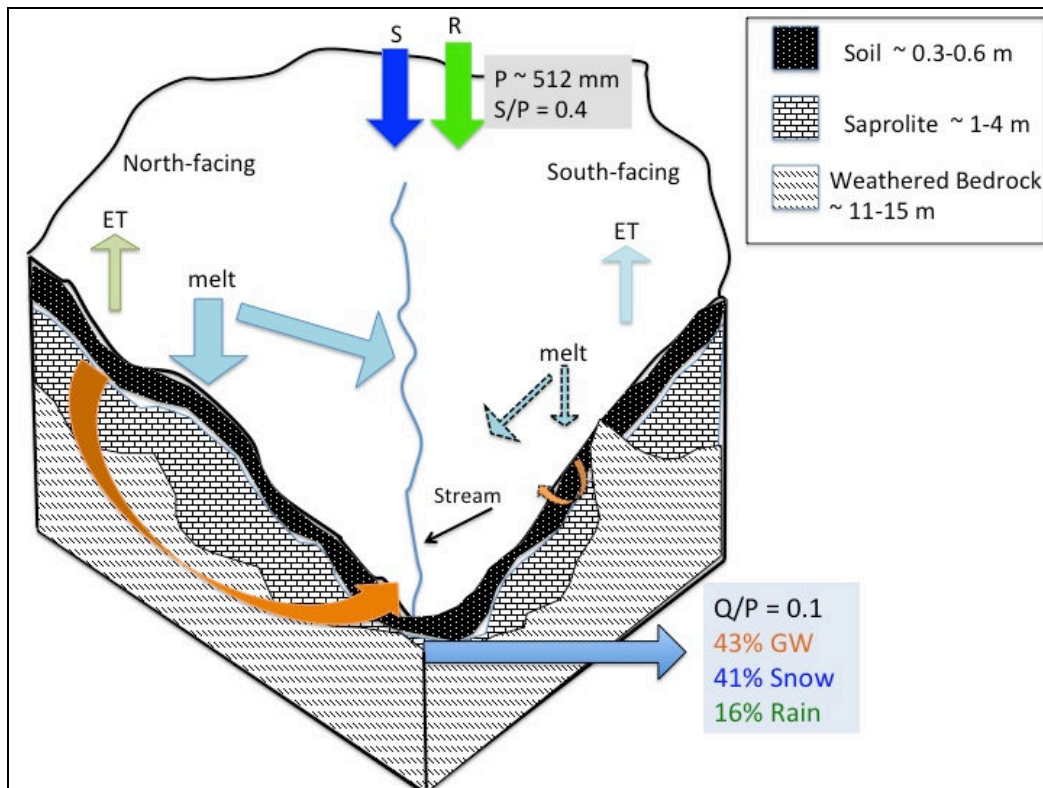


Figure 2.22: Conceptual diagram of hydrologic cycling: A) Green lake 4, B) Como Creek, C) Gordon Gulch. Arrows represent direction, magnitude, and type of water movement through the catchments. Terms: Q, discharge; P, precipitation; S, snow; R, rain; ET, Evapotranspiration; GW, groundwater; Q/P, runoff efficiency; K, hydraulic conductivity.

Chapter 3

Use of Natural and Applied Tracers to Guide Targeted Remediation Efforts in an Acid Mine Drainage System, Colorado Rockies, USA

Abstract

Stream water quality in areas of the western United States continues to be degraded by acid mine drainage (AMD), a legacy of hard-rock mining. The Rico-Argentine Mine in southwestern Colorado consists of complex multiple-level mine workings connected to a drainage tunnel discharging AMD to passive treatment ponds that discharge to the Dolores River. The mine workings are excavated into the hillslope on either side of a tributary stream with workings passing directly under the stream channel. There is a need to define hydrologic connections between surface water, groundwater, and mine workings to understand the source of both water and contaminants in the drainage tunnel discharge. Source identification will allow targeted remediation strategies to be developed. To identify hydrologic connections we employed a combination of natural and applied tracers including isotopes, ionic tracers, and fluorescent dyes. Stable water isotopes ($\delta^{18}\text{O}/\delta\text{D}$) show a well-mixed hydrological system, while tritium levels in mine waters indicate a fast flow-through system with mean residence times of years not decades or longer. Addition of multiple independent tracers indicated that water is traveling through mine workings with minimal obstructions. The results from a simultaneous salt and dye tracer application demonstrated that both tracer types can be successfully used in acidic mine water conditions.

3.1. Introduction

Acidic, metal-rich drainage from abandoned hard-rock mines can produce both acute and chronic environmental problems (Wireman & Stover, 2011). The legacy of past hard-rock mining in the United States includes more than 200,000 abandoned or inactive mines (US EPA, 1997) with thousands of abandoned mines located near headwater regions of the Rocky Mountains of Colorado (Riebsame, 1997). Watersheds in mineralized regions often receive drainage from a complex distribution of mine systems (Kimball *et al.*, 2002), which are gravity driven and often discharge at low points adjacent to surface waters. The combination of low pH and high concentrations of metals associated with the acid mine drainage (AMD) can then create severe toxicological effects on local and downstream aquatic ecosystems (Jarvis & Younger, 1997). Traditionally, an end of the pipe (e.g. at the mine discharge point) treatment strategy has been employed to handle AMD prior to mixing with local surface waters. However, this strategy is very expensive and treatment must occur in perpetuity, which does not represent a permanent solution to the problem. A more recent approach to controlling AMD involves developing targeted remediation strategies that address the feasibility of actually reducing or shutting off the AMD at its source (Wiremen & Stover, 2011). Targeted remediation can be thought of as a source and pathway control measure and may refer to the source of the acid producing minerals themselves, the source of the water that mobilizes contaminants, or both. In most mine settings it is impractical to isolate or remove the mineralized rock itself. Therefore, remediation efforts may be most successful when the source of water producing the AMD can be targeted and separated, isolated, or removed from the area of a mine most prone to AMD production.

A major challenge in using a targeted remediation approach to control AMD is that many hard-rock mine settings are located in mountainous areas of high mineralization that are commonly associated with fracturing and structurally deformed rocks. The result is high secondary porosity, which combined with the diverse spatial scales of man-made mining excavations, creates a highly complex hydrogeologic setting where water flow paths are particularly difficult to quantify (Nordstrom, 2009). Steep slopes and large amounts of snowfall add to the complexity of understanding the hydrology of these sites. In addition, many of the hard-rock mining sites in the Western U.S. have been abandoned for many decades leading to varying degrees of degradation to the originally engineered designs for mine drainage control. Information on the mine sites is often incomplete because mine maps may be unavailable, incomplete, or inaccurate. Therefore, the hydrologic connectivity of abandoned mines is often unknown or poorly understood. The complexities of flow paths in flooded mines are often comparable to flow paths found in karstic aquifers (Wolkersdorfer, 2002), where flow may be concentrated in subsurface conduits, making Darcy's law approach inapplicable for evaluation of subsurface flow regimes in flooded mines (Field *et al.*, 1995). A reasonable approach to understanding the hydrology of these systems involves applying ground-water tracing techniques to abandoned mine sites that generate empirical data while measuring properties *in-situ* to minimize assumptions about hydrogeological conditions (Wolkersdorfer, 2008).

In recent years, surface water and groundwater tracing techniques have been used in a variety of complex hydrogeologic settings to aid in characterizing groundwater flow systems (Alvarado *et al.*, 2007; Troldborg *et al.*, 2008; Lavastre *et al.*, 2010). Tracers have been used in various combinations of natural tracers, injected tracers, and chemical perturbations to identify and quantify transport processes in mountain streams impacted by AMD (McKnight & Bencala,

1990; Kimball *et al.*, 2002; Runkel *et al.*, 2013). Fluorescent dyes are often used as an applied tracer (Smart & Laidlaw, 1977; Smart, 1985; Käß, 1994) with the use of fluorescent dye to trace groundwater dating back to at least 1877 when sodium fluorescein (uranine) was used to evaluate the connection between the Danube River and the Aach spring (Knop, 1878). Fluorescent dyes are commonly chosen as applied tracers for groundwater studies in areas with low clay content, and recent studies have found dye tracers to work well in both karst and fractured crystalline rock settings (Field *et al.*, 1995). However, the use of such dyes is problematic in AMD waters, because below a pH of 6 the sorptivity of uranine increases and its fluorescence intensity diminishes (Käß, 1994); Smart and Laidlaw (1977) demonstrated that the fluorescence of uranine can be reduced by as much as 50% below a pH of 5. An additional difficulty in dye tracer application in groundwater and mine systems is accurately quantifying the mixing reservoir. The reservoir represents all waters (mine pools and inflows of surface or groundwater) that the tracer could mix with between the injection point and the sampling point and will influence the mass of tracer applied in order to produce appropriate dye concentrations in collected samples (Wolkersdorfer, 2008). If the mixing reservoir is overestimated then resulting dye concentrations may become toxic or exceed the dynamic range of the instruments, whereas an underestimated reservoir will result in low dye concentrations, possibly below analytical detection. Therefore, a multiple tracer approach is often recommended for complex hydrologic settings with limited access points and unknown flow-through times, especially when field-work time and logistical support are limited ((Wolkersdorfer, 2008; Geyer *et al.*, 2007).

The Rico-Argentine Mine Site near Rico, Colorado (USA) provides an opportunity for the use of natural and applied tracers to understand the hydrological connectivity of a perturbed system where AMD is produced. The mine consists of multiple levels of underground workings

that are interconnected by a series of tunnels that pass directly underneath a tributary creek, resulting in potential pathways for hydrologic connections between the mine and surface waters. Additionally, the mine complex is connected to a series of long drainage tunnels, which transport AMD from the mine to a discharge point adjacent to the Dolores River, a relatively pristine headwater ecosystem. At present, the AMD passively flows through a series of degraded water treatment ponds before entering the river.

The objective of this paper is to use multiple natural and applied tracers to quantitatively and qualitatively address the hydrologic connections between local inputs from precipitation, surface waters, and groundwater to interior mine workings, and resultant mine discharges. As recommended by Wolkersdorfer (2008), the paper first highlights the use of synoptic and time-series analyses of naturally-occurring isotopic and geochemical tracers to develop a conceptual understanding of the hydrogeology of the mine system. Secondly, applied tracers (salts and fluorescent dyes) were introduced, either simultaneously or at separate discrete locations, to provide a comparative analysis of tracer approaches in an AMD setting. To expand on previous research by Naurath *et al.* (2011), this study aims to further investigate the effectiveness of uranine as a tracer in acid mine waters by performing a dual tracer application with uranine and lithium salt.

The results of this study will help determine the feasibility of reducing the volume of water and/or the load of contaminants that discharge from the Rico-Argentine mine. Reducing the flow of water into and through the mine workings, reducing the mobilization of contaminants within the mine, and/or isolating high-concentration contaminant source water for limited smaller-scale treatment, may create alternative targeted remediation strategies for managing the AMD discharge that are not currently available.

3.2. Methods

3.2.1 Site Description

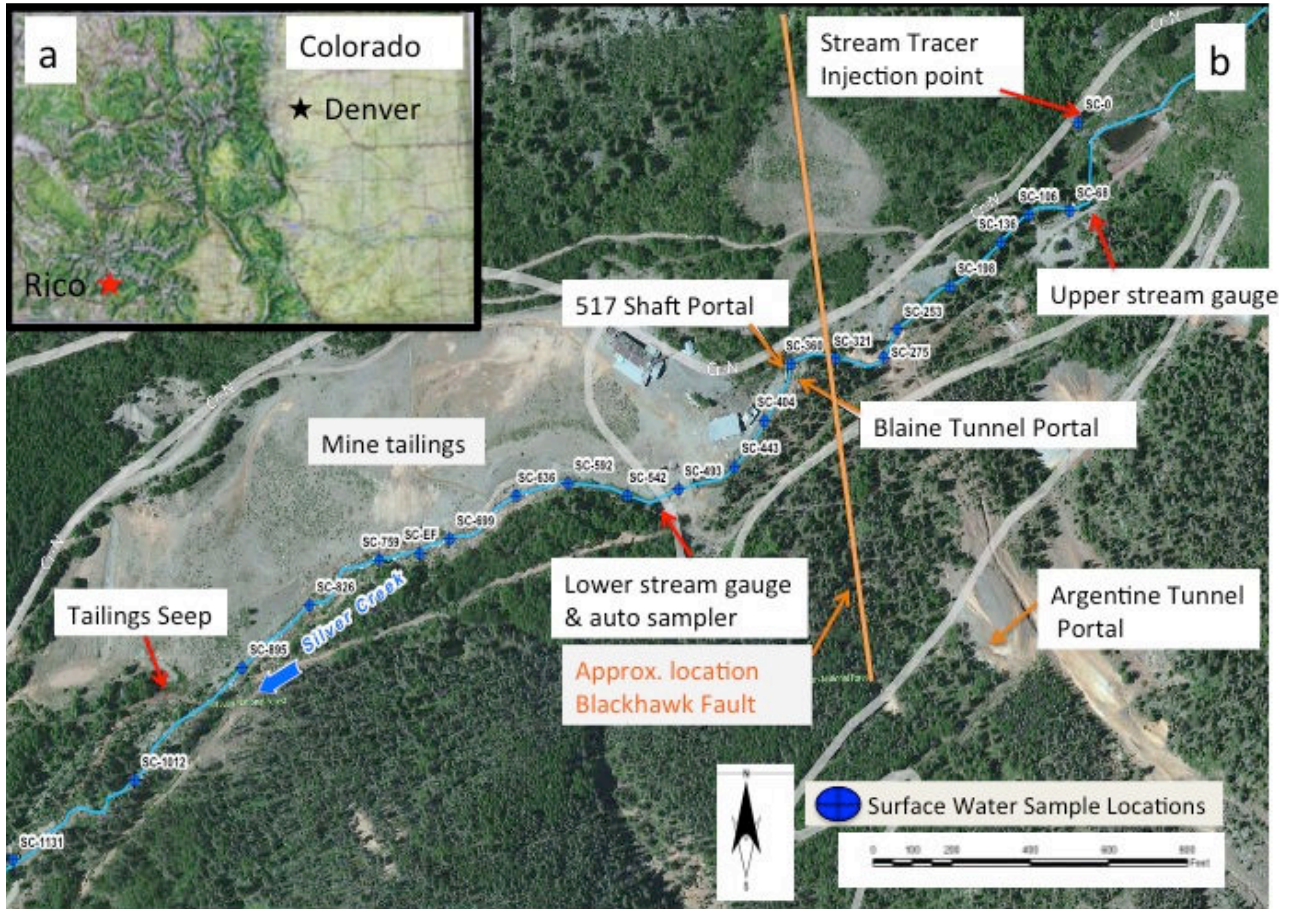
The historic Rico-Argentine mines are located in the San Juan Mountains of southwestern Colorado, USA (Figure 3.1a) and are situated along Silver Creek (Figure 3.1b), about 2.5 kilometers (km) northeast of the Town of Rico (Figure 3.1c). The mines were built to access sulfide replacement deposits associated with hydrothermal mineralization of faults in the Pennsylvania-age Hermosa formation. The mines were active from the 1860's until the 1970's with silver, zinc, and lead as the primary mining products. The mines consist of extensive underground mine workings in the ridge southeast of Silver Creek that were historically accessed by a number of entrances at and above the elevation of Silver Creek. There are also at least 7 levels (30 m of vertical separation between each) below the surface elevation of Silver Creek with historical maps indicating several levels of the mine tunnels pass directly under Silver Creek and connect to mine workings on the northwest of Silver Creek. The proximity of the mine workings adjacent to, and below, Silver Creek was hypothesized as supporting a possible hydrologic pathway (in either direction) between surface waters in the creek and the subsurface mine workings. The mine workings on the northwest side of Silver Creek are connected to the SE crosscut, which connects to the St. Louis Tunnel (Figure 3.1c). The crosscut and the St. Louis Tunnel extend approximately 2,500 m from the mine workings to the portal adjacent to the Dolores River. The SE crosscut and the St. Louis Tunnel connect to the Rico-Argentine mine at the 500 Level (name is a reference to being about 500 ft (152 m) below Silver Creek) and were built primarily to de-water or drain the upper mine workings using gravity flow. Water with

elevated levels of metals including zinc and cadmium currently discharge from the St. Louis Tunnel and flow through a series of passive treatment ponds, eventually entering the Dolores River from the pond system outfall (Figure 3.1b).

For safety reasons, mine access at the time of study was limited to just a few locations in the vicinity of Silver Creek. The first accessible tunnel on the southeast side of the creek was the Argentine Tunnel, located a few hundred feet upslope of the Blaine Tunnel (Figure 3.1b). The Argentine Tunnel was accessible for 183 m before becoming unsafe to access, at which point samples were collected from a stagnant mine pool. The mine pool was believed to have drained to lower level mine workings, as the water was not flowing out the tunnel to the surface. The second access point was the Blaine Tunnel, with a portal just 12 m from Silver Creek on the Southeast side. At the time of the study, water was flowing into the back of the Blaine tunnel, presumable as drainage from above workings (i.e. those accessed by the Argentine Tunnel), resulting in about 1 m of water on the tunnel floor behind a cofferdam located 244 m back from the tunnel portal. Water levels behind the cofferdam were relatively stable (fluctuated < 5 cm over a 6 week period) suggesting that inflows were proportionate to water movement out of the tunnel towards the lower level workings that went under Silver Creek. Samples were collected in the Blaine tunnel from both the inflow and the pooled water behind the cofferdam.

The third access point was a short tunnel on the northwest side of Silver Creek, directly across Silver Creek from the Blaine portal, which accessed the vertical 517 Shaft approximately 50 m from the portal along Silver Creek. Historical mine maps indicated that the 517 Shaft extended vertically to at least the 500 level and that several of the tunnels under Silver Creek intersected the shaft at multiple levels (Figure 3.1d). The water level in the 517 Shaft was approximately 146 m below the elevation of the shaft collar, which corresponds to the elevation

of the SE Crosscut and St. Louis Tunnel. Water samples were collected from the shaft using a bailer and mechanical pulley system located at the collar. The final access point to sample mine water was the St. Louis Tunnel portal. The portal had collapsed preventing underground access so samples were collected at first emergence from the collapse.



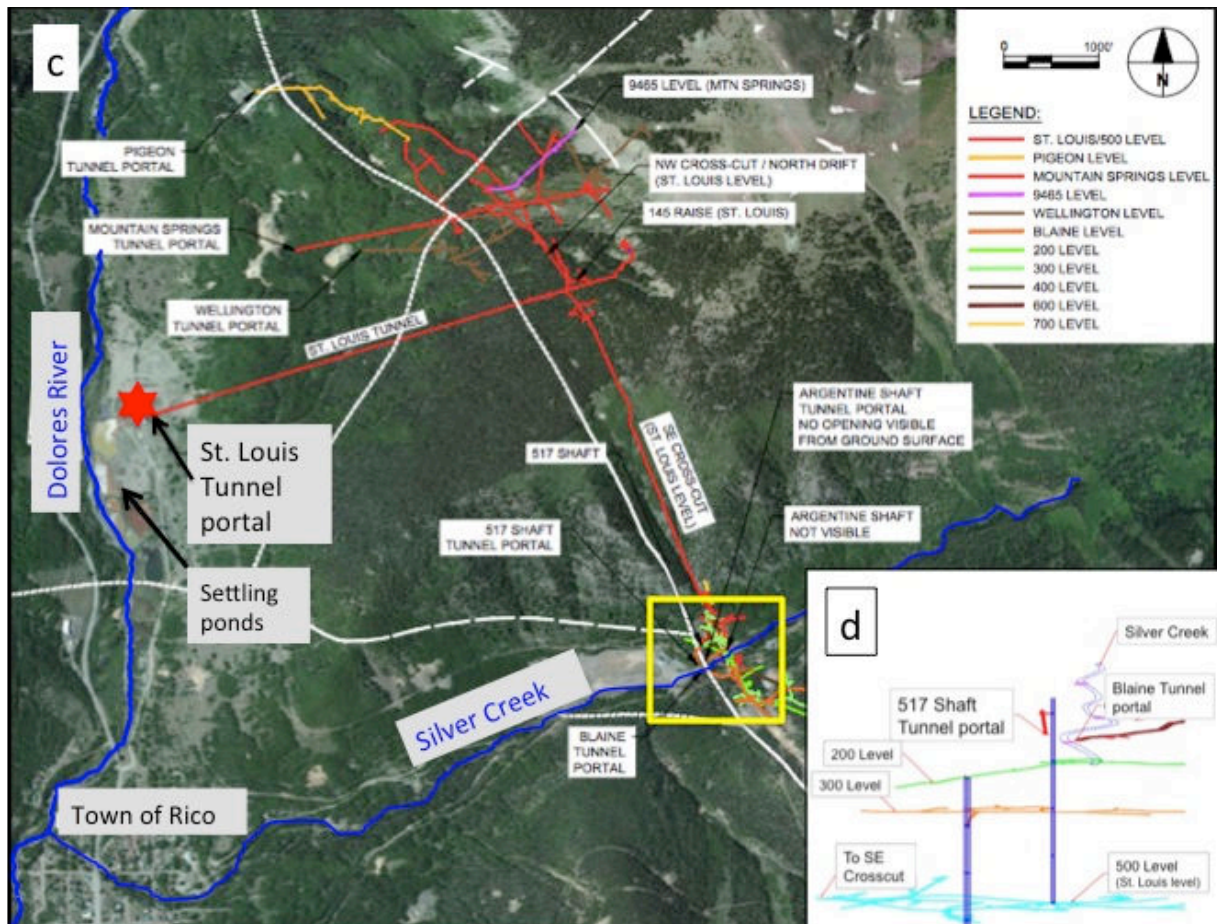


Figure 3.1. (a) Map of State of Colorado with location of Town of Rico located in the San Juan Mountains of southwestern Colorado. (b) Site map of Rico-Argentine mine complex and Silver Creek. Silver Creek sampling location numbers refer to the distance downstream (m) from the tracer injection point. (c) Overview map of entire Rico-Argentine mine complex in relation to the Town of Rico and the Dolores River. Yellow box shows location of mine complex and represents extent of figure 1b. Location and extent of the subsurface workings are overlain on top of aerial imagery to demonstrate how mine workings near Silver Creek are connected to the St. Louis Portal. (d) Vertical view of mine workings in relation to Silver Creek and access points. The 200 and 300 levels pass directly under Silver creek.

3.2.2 Study Design

The study was designed to understand the hydrologic connections between surface water, groundwater, and mine water associated with the Rico-Argentine mine. The tracer study was performed in October 2011, when surface water flows were at low-flow conditions, to try and minimize event based influences (rain and snowmelt) on the prevailing hydrologic conditions.

Much of the southwestern USA, including the San Juan Mountains, can be characterized by bimodal precipitation patterns, i.e. spring snowmelt and summer monsoon rains (Bales & Cline, 2003). Previous mine drainage studies in the region have demonstrated that consistent low-flow conditions are most attainable in late summer (August-October) after monsoon rains have subsided and prior to freezing conditions during the winter months (Runkel *et al.*, 2013). To quantitatively and qualitatively assess individual components of the hydrologic system, a series of independent environmental and applied tracers were applied and/or sampled at discrete locations within the study area. All tracers used in the study are summarized in Table 3.1.

Table 3.1: Summary of natural and applied tracers including the amount of tracer used and the application method. Silver Creek locations are marked in figure 3.1b. Detection limits for stable isotopes reported as twice the precision. [TU, tritium units].

Tracer	Amount of tracer applied	Detection Limit (mg/L)	Type of Application; Location; Date	Sampling Location; Date	Objective
Oxygen (^{18}O)	NA	0.056 (‰)	Natural, Local Precipitation, 2011	All	Source water identification
Deuterium (^2H)	NA	0.296 (‰)	Natural, Local Precipitation, 2011	All	Source water identification
Tritium (^3H)	NA	0.3 (TU)	Natural, Local Precipitation, 2011	All	Source water identification; water apparent age
Sulfate (SO_4^-)	NA	0.0022	Naturally occurring in mine impacted waters	Silver Creek (0 to 1131)	Hydrologic connectivity; mine water \Leftrightarrow surface water
Sodium Bromide (NaBr)	75 kg NaBr	0.0031	Constant injection (from 189 L reservoir); Silver Creek (0); 10/5 to 10/7/11	Silver Creek (0 to 1131)	Identify changes in streamflow
Lithium (LiOH)	9 kg LiOH	0.0108	Slug injection (227 L); 517 Shaft; 10/4/11	St. Louis Tunnel portal; 10/4 to 11/16/11	Hydrologic connectivity; mine \Rightarrow drainage tunnel
Sodium Fluoride (NaF)	6 kg NaF	0.0057	Slug injection (30 L); Blaine Tunnel; 10/5/11	517 Shaft; 10/5 to 11/6/11	Hydrologic connectivity; mine \Leftrightarrow mine
Sodium Chloride (NaCl)	1400 g NaCl per slug	0.0017	Slug injections (8 L); Silver Creek (0,198,220, 384, 493,530);	Silver Creek (106,321,493 ,636); 10/3 to	Estimate streamflow above and below mine workings

			10/3 to 10/7/11	10/7/11	
Rhodamine WT (liquid)	1.2 L	0.000006	Constant injection (from 189 L reservoir); Silver Creek (0; 10/5 to 10/7/11	Silver Creek (443), Tailings Seep, 517 Shaft; 10/4 to 11/6/11	Hydrologic connectivity; Silver Creek ⇔ mine, tailings seep
Uranine (Sodium Fluorescein)	13.63 kg	0.000002 (0.002 ppb)	Slug injection (227 L); 517 Shaft; 10/4/11	St. Louis Tunnel Portal; 10/4 to 11/16	Hydrologic connectivity; mine ⇒ drainage tunnel

To broadly understand how inputs to the system (precipitation) contribute to the surface and mine waters, the naturally occurring stable ($\delta^{18}\text{O}/\delta\text{D}$) and radioactive (^3H) water isotopes were measured in precipitation and at all other sampling locations. The stable isotopes provide information on source water contributions whereas the radioactive isotopes provide insight on mean residence time of waters in the mine system. The second objective of the study was to determine if Silver Creek is losing water to the mine workings. Silver Creek flow was measured using several different measurement techniques to evaluate the presence, magnitude, and timing of stream flows on Silver Creek around the area of the Rico-Argentine mine. Additionally, the mine waters (517 Shaft and St. Louis Tunnel) and mine tailings seep were analyzed for detection of tracers used in Silver Creek to look for direct hydrologic connections between the creek and the mine waters. The third objective was to determine the hydrologic connection between the Blaine tunnel mine water and mine water in the 517 Shaft. The approach was a slug injection (Table 3.1) into the Blaine tunnel mine pool and sampling for the breakthrough of that tracer in the 517 Shaft. The surface water in Silver Creek was concurrently monitored for Blaine tunnel tracer to check for movement of Blaine mine water towards surface flows. Finally, the study addressed the hydrologic connection between the mine water in the 517 Shaft and mine water

discharging from the St. Louis Tunnel. The approach involved simultaneous slug additions of two independent tracers (Lithium salt and uranine dye; Table 3.1) in the 517 Shaft, which were analyzed for in samples continuously collected at the St. Louis Tunnel portal. A dual tracer approach was chosen at this location to have unique data sets to compare tracer functionality in an AMD setting.

3.2.3 Natural Tracers and Synoptic Sampling

Representative water samples were collected from along the study reach on Silver Creek, from the St. Louis Tunnel portal, and from the Dolores River above and below the mine treatment ponds. Prior to any disturbance from tracer applications, additional samples were collected from all mine locations described above and from a seep below the mine tailings pile along Silver Creek to establish background conditions (Figure 3.1b). Local snow and rain precipitation were analyzed for isotopes to characterize sources and timing of inputs to local surface water, groundwater, and mine water. The snow was a depth integrated sample collected adjacent to the mine complex in April 2011 to represent maximum snow accumulation prior to the study while rain samples were collected as weekly composites from five rain gauges located in the San Juan Mountains (within 50 km radius). Surface water and mine water samples were collected at several different times between April and October 2011 to examine both short-term (i.e. daily) and seasonal variations at different locations. All samples were analyzed for isotopes including oxygen-18 (^{18}O), deuterium (^2H), and tritium (^3H). Water samples were also analyzed for total and dissolved metals and solute chemistry to identify and distinguish the many contributions to metal load in Silver Creek and the St. Louis tunnel.

Water samples for ^2H (D) and ^{18}O analysis were collected unfiltered in clean 25-mL borosilicate bottles with no-headspace lids to avoid any evaporation or fractionation. The D and ^{18}O analyses were performed at the Kiowa Environmental Chemistry Laboratory in Boulder, Colorado, using an Picarro L1102-i Isotopic Liquid Wavelength- Scanned Cavity Ring Down Spectroscopy (WS-CRDS), a time-based measurement using near-infrared laser to quantify spectral features of molecules in a gas ratio of the sample to the Vienna Standard Mean Ocean Water (V-SMOW) standard, as shown for ^{18}O :

$$\delta^{18}\text{O} = \frac{\left(\frac{^{18}\text{O}}{^{16}\text{O}}\right)_{\text{sample}} - \left(\frac{^{18}\text{O}}{^{16}\text{O}}\right)_{\text{VSMOW}}}{\left(\frac{^{18}\text{O}}{^{16}\text{O}}\right)_{\text{VSMOW}}} \times 1000 \text{‰} \quad (\text{Equation 3.1})$$

The 1- σ precision of $\delta^{18}\text{O}$ was $\pm 0.028 \text{‰}$ and of D was $\pm 0.148 \text{‰}$ (per mil) based on replicate samples.

Water samples to be analyzed for tritium 1- σ were collected as grab samples in high-density polyethylene (HDPE) bottles and kept at 4°C. The tritium samples were analyzed at the USGS Tritium Laboratory in Menlo Park, California, by electrolytic enrichment and Liquid Scintillation Counting. Distilled sample water was reduced electrolytically in electrolysis cells to 10 mL from an initial 200 mL in a cooling bath. The detection limit is reported as twice the precision. Tritium results reported in tritium units (TU) where 1 TU = 1 tritium atom per 10^{18} hydrogen atoms.

Water samples collected during synoptic sampling from along the study reach on Silver Creek, within the mine workings, and at the St. Louis Tunnel portal were analyzed for total and dissolved metals, select anions, and hardness. Onsite processing included filtration and measurement of pH. Filtration was completed using 0.45 μm capsule filters. Aliquots for cation

analysis were acidified to $\text{pH} < 2.5$ with ultrapure nitric acid. Total recoverable and dissolved cation concentrations were determined from unfiltered and filtered samples, respectively (dissolved is used herein as an operational definition that refers to the concentration of the water after filtration; some colloidal material may pass through the $0.45 \mu\text{m}$ filter). Samples were analyzed at the U.S. EPA Region 8 Laboratory operated by the Environmental Sampling Assistance Team (ESAT) contractor for total and dissolved metals analysis using EPA 200 Series methods, for anions using EPA Method 300, and hardness was calculated using EPA method 2340B.

During synoptic sampling a subset of each unfiltered sample was also sent for chemical analysis to the Kiowa Environmental Chemistry Laboratory in Boulder, Colorado, where samples were immediately filtered through pre-combusted glass fiber filters with a nominal pore size of $0.7 \mu\text{m}$ and stored in the dark at 4°C prior to analyses. Samples were analyzed for chloride (Cl^-), nitrate (NO_3^-), sulfate (SO_4^{2-}), bromide (Br^-), and fluoride (F^-), using a Metrohm 761 Compact Ion Chromatograph. The within run precision (%RSD) was $< 1.1\%$ for all solutes. Lithium (Li^+) was analyzed on a Perkin Elmer AAnalyst 200 Atomic Absorption Spectrometer with a within run precision of 1.06% .

3.2.4 Applied Tracers

The usefulness of applied tracer test results is highly dependent on proper test design (particularly determination of injection and sampling locations), the nature of the tracer, the ability to detect the tracer at low concentrations, and correct interpretation of recovery data (Wolkersdorfer, 2002; Käß, 1994; Field, 2002; Field, 2003). Results from initial synoptic sampling (in May and June 2011), along with background information on the mine complex

design and local geology, were used to develop a basic understanding of the hydrogeologic setting allowing for design of the applied tracer study which was performed in October 2011. Additionally, due to the hypothesis that the entire system under investigation was hydrologically connected the study was designed to ensure that all applied tracers were distinctly and independently measureable from each other in the event that mixing of tracers occurred. A previous dye tracer study was conducted by Davis (1994) at a separate mine site (the Atlantic Cable mine) in Rico, Colorado, at the confluence of Silver Creek and the Dolores River, approximately 2.5 km downstream from the Rico-Argentine mine complex (Figure 3.1). The results of the Davis (1994) study indicated that water chemistry (metals analysis) alone was inconclusive with respect to identifying and separating mine waters from local surface waters. The study was also unsuccessful at identifying surface water and mine water interactions using Sulpho-Rhodamine B dye tracer (no dye was observed at any of the sampling points around the mine site) and suggested that Rhodamine WT (RWT) may be a more effective tracer for future mine water studies in the area. These results further support the use of a multiple natural and applied tracer approach to better understand surface water and mine water interactions in the current study of the Rico-Argentine Mine.

3.2.5 Tracer Selection and Application

In the state of Colorado, the use of surface water or groundwater tracers at permitted mining sites must be approved by the state mining regulatory agency, which is the Division of Reclamation, Mining, and Safety (DRMS) (Wolkersdorfer *et al.*, 2012). The study was performed under the authority of the U.S. EPA Superfund Technical Assessment and Response Team and the DRMS, whom both approved the experimental design and provided technical

assistance and oversight throughout the course of the study. All applied tracers were chosen based on suggestions from literature reviews and based on analytical capabilities and on the ability to safely use at concentrations that are distinguishable above background signals. Tracer amounts were determined following guidelines presented in Wolkersdorfer (2008). For all applied tracers the minimum detection limit (Table 3.1) was considered along with measured background concentrations and estimated mixing reservoir size (anticipated dilution) to ensure the tracer concentrations would be clearly identifiable at the sampling point.

There were six tracers used in the study (Table 3.1) including four salts and two fluorescent dyes. Tracers applied to surface waters (Silver Creek) included sodium bromide (NaBr) and sodium chloride (NaCl), which were applied to quantify streamflow and are described in further detail in section 3.2.6. Additionally, the fluorescent dye Rhodamine WT (RWT; CI Acid Red 388; CAS 37299-86-8; Keystone Analine Corporation # 703-010-27) was applied to Silver Creek concurrently with the continuous injection of NaBr to provide a dye that could be sampled for concurrently with the NaBr at several mine sampling points. The RWT was used because it is one of the most commonly recommended dye tracers for surface water application (Käb, 1998) and was recommended for future use by a previous study performed at a nearby mine interacting with Silver Creek (Davis, 1994). Although RWT has been reported to have some genotoxic properties (Smart & Laidlaw, 1977; Käb, 1998; Behrens *et al.*, 2001), the dye was found to exhibit ecological toxicity at concentrations greater than 1 milligram per liter (mg/L; 1000 parts per billion (ppb)) and human toxicity at concentrations greater than 100 mg/L (100,000 ppb) (Field *et al.*, 2008). Therefore, the RWT was applied to the stream at low concentrations (<30 ppb) that were detectable but created minimal visible disturbance and remained well below concentrations of concern. The continuous injection ran from October 5 to

October 8 with two rounds of synoptic sampling for bromide occurring on October 5 and 7. Samples were also collected from the mine tailings seep and 517 Shaft and analyzed for bromide and RWT to test for presence of Silver Creek water in the in mine workings or associated tailings pile.

The remaining three tracers were applied as slugs directly into mine waters with sodium fluoride (NaF) applied to the Blaine tunnel mine pool whereas lithium (as LiOH) and uranine (Uranine; C.I. Acid Yellow 73; CAS 6417-85-2; Keystone Analine Corporation 801-073042) were applied concurrently to the mine pool at the bottom of the 517 shaft. The ability to easily sample and accurately quantify discharge at the St. Louis Tunnel portal motivated the application of multiple tracers at this location. By calculating the mass recovery of independent tracers the effectiveness of each tracer could be addressed. The lithium tracer was chosen because of low background signal in the mine water and because several of the other most common salt tracers (NaCl, NaBr, and NaF) had been used in the study. Uranine was chosen as the second tracer because it has long been used as a subsurface tracer due to low sorptive properties (Smart & Laidlaw, 1977; Flury & Wai, 2003; Davis *et al.*, 1980; Sabatini & Austin, 1991; Kasnavia *et al.*, 1999) and for being safe in terms of human or ecological toxicity [8,18,31]. Uranine also readily undergoes photo-degradation (Smart & Laidlaw, 1977), but has shown long-term stability when not affected by sunlight (Wolkersdorfer *et al.*, 2012), making it most suited for subsurface tracing. Uranine has only negative functional groups, and sorbs least onto negatively-charged media and most onto positively charged surfaces (Kasnavia *et al.*, 1999). Mine waters often contain metal cations, especially iron (Fe), which can precipitate as hydroxides at higher pH values (Aldous & Smart, 1988). Uranine may therefore undergo adsorption onto iron hydroxides and be removed from the sample through filtration (Aldous & Smart, 1988). Conversely, if the

collected mine samples are not filtered then fluorescence intensity may be overestimated due to scattering effects caused by increased sample turbidity. Results from the dual tracer application will therefore enable this potential complication to be addressed.

On October 4 at 12:00, a 189-L slug containing 9 kg of LiOH and 13.63 kg of uranine was injected into the 517 Shaft. The size of the mine pool (mixing reservoir) at the bottom of the 517 Shaft was unknown due to inaccessibility to the flooded lower levels of the mine. Therefore, the necessary mass of tracer was estimated using the flow rate at the St. Louis Tunnel portal (assumed mine pool discharge point), the distance between injection and sampling location, and by assuming a reasonable estimated mine water flow velocity. Additionally, background concentrations of lithium were low (0.025 mg/L) and background fluorescence in the wavelengths used to detect uranine were below detection (<0.002 ppb) at the St. Louis Tunnel portal confirming minimal background interference with tracer detection. The estimated velocity (and mass) was verified based on the authors' experience with a similar tracer test at another mine site drainage tunnel with similar distance between injection and sampling points [37]. Additionally, the mine outflow at the St. Louis Tunnel portal flowed directly into a series of passive settling ponds and not into natural waters, which eliminated concerns for high concentrations of tracers (from over estimating tracer mass) rapidly entering local surface waters in the event of incomplete mixing of the tracer slug. The slug was mixed using acidic water (pH 2.7) from the Blaine Tunnel to simulate the water found at the bottom of the 517 Shaft (pH 2.5). The slug was mixed in two new, clean 115-L plastic tubs located adjacent to the top of the shaft and then siphoned from the tubs into the shaft using 137 m of new, clean garden hose. To avoid tracer contamination all materials used to transport and mix the tracers (including applicators clothing) were left at the injection site. The slug injection took approximately 45 minutes to

complete and was then chased by approximately 189,000 L of water from Silver Creek delivered by a high capacity water pump over a 30-minute period.

On October 5 at 14:15, a slug containing 6 kg of NaF was added to the Blaine Tunnel mine pool behind the cofferdam. The tracer mass was estimated based on the size of the mixing reservoir at injection and sampling points (Blaine tunnel mine pool and 517 Shaft mine pool), and information on background levels of fluoride at the injection point. The tracer mass was sufficient to increase F⁻ concentrations to approximately three times background (from 50.2 to 143.1 mg/L) in the Blaine Tunnel. The tracer recovery point (517 Shaft) had F⁻ background of only 1.95 mg/L. Dissolving NaF powder into 30 L of Blaine Tunnel water using two 20-L buckets and a stirring rod made the slug. The NaF solution was slowly poured in the mine pool about 8 m behind the cofferdam. The mine pool had an estimated minimum volume of 42,500 L, but the inflow/outflow rates were not quantifiable. After the slug injection, a 7.6 cm diaphragm water pump was used to move water from the mine pool over a visible tunnel collapse (pile of rock and debris) and toward a drainage stope that extended to the lower mine levels that intersect with the 517 Shaft. The pump was able to move between 22,700 and 36,300 liters of water past the initial visible collapse in the first 2 hours after injection. However, during that period no reduction in water level was observed in the mine pool and pumping was then terminated due to freezing of equipment and unsteady pump rates, so it was not possible to calculate the rate at which the entire mine pool (containing the fluoride slug) was moved past the initial blockage.

The exact pathway of the water (and tracer) leaving the Blaine Tunnel pool is unknown, but based on existing maps it was expected that water flows down a complex series of interconnected inclines, raises, winzes, stopes, tunnels, and shafts before reaching the 500 level via the 517 Shaft. Given the myriad of potential pathways, all in varying states of structural

integrity, it was difficult to determine the actual distance the water and tracers would travel. Using all available information it was estimated that the shortest possible pathway from the Blaine Tunnel mine pool to the bottom of the 517 Shaft was 200 m.

3.2.6 Tracer Sampling and Analysis

Automated samplers were placed at 3 locations; SC-493, the mine tailings seep, and the St. Louis Tunnel portal (Figure 3.1). The samplers in Silver Creek and at the mine tailings seep collected samples at 1-hour intervals for the duration of the constant injection of tracers in Silver Creek and then at 4-hour intervals for 3 weeks following tracer application. At the St. Louis Tunnel portal water samples were collected at 1-hour intervals for the first 40 hours, starting 2 hours before the 517 Shaft tracer injections. A Cyclops 7 field fluorometer from Turner Designs, Inc., confirmed that the peak of the uranine slug occurred within the first 36 hours, so sample collection was reduced to 4-hour intervals on October 7 and continued for 6 weeks.

At the 517 Shaft, water samples were collected at a depth of 7.6 m below the water surface, which was 137 m below the collar of the shaft. Samples were collected manually using a stainless steel bailer lowered to the same depth for each sample using a calibrated cable reel and motorized pulley system. Samples were collected at 1-hour intervals for the first 36 hours after tracer injections were made in the Blaine Tunnel and then daily for 2 weeks. The last sample was collected in the 517 Shaft 690 hours after tracer was injected in the Blaine Tunnel.

To provide real time confirmation of tracer emergence, the Cyclops-7 field fluorometer from Turner Designs Inc. was used to make *in-situ* field measurements for the presence of the two fluorescent dyes, RWT and uranine. The field fluorometer was calibrated for both dyes using a 4-point calibration with standards of 0, 1, 100, and 400 ppb solutions. The standards were

prepared in the laboratory by diluting the purchased dye concentrates using water collected directly from the mine site at locations where the dyes were to be applied or measured. The RWT was mixed using water from Silver Creek (pH 8.2) and the uranine was mixed using water from the St. Louis Tunnel portal (pH 7.4). The manufacturer stated that the instrument's dynamic range for detection of uranine dye was 0 to 500 ppb so calibration from 0 to 400 ppb was considered sufficient for the intended use of the field fluorometer. The field fluorometer was used to qualitatively provide a rapid assessment of samples for presence/absence of the dye of interest to constrain the number of field samples that would be sent to the laboratory for analysis. At the Kiowa Laboratory, a Fluoromax 2 (F2) spectrophotometer was used to analyze water samples for the concentrations of the two fluorescent dyes. The presence of each dye was analyzed using a single excitation and a single emission value and a record of the spectrum for a 100 ppb standard for both dyes was created to determine the appropriate excitation/emission values to use for analyzing the dye tracers. The RWT dye was run with 550/580 nm excitation/emission and the uranine was run with 492/512 nm excitation/emission. The excitation and emission values for both dyes were within the expected variability (Naurath *et al.*, 2011) of values previously reported for fluorescence analysis of these dyes (Field *et al.*, 1995; Käß, 1998; Naurath *et al.*, 2011). For RWT, a 5-point calibration curve was developed using standards between 1 and 400 ppb concentration. For uranine, a 12-point calibration curve was developed with concentrations ranging from 1 to 1000 ppb. Dye concentrations were plotted against emissions values to generate calibration curves. Interestingly, for the uranine, F2 emissions peaked with the 500 ppb standard and then became inversely related to concentrations over 500 ppb. As reported in Käss (1998) the intensity of the fluorescence likely decreased as a consequence of its individual light absorption and due to retrograde dissociation. To compensate

for the decrease in emissions for high concentration samples, the standard power calibration curve (dye concentration in ppb (C) = $10^{-13} \times E^{2.1558}$; where E = measured emission (nm); $R^2 = 0.99$, N = 6) was used to calculate dye concentrations in samples with concentrations <500 ppb and a second linear equation (dye concentration in ppb (C) = $-10^{-4} \times E + 2948$; where E = measured emission (nm); $R^2 = 0.9$, N = 6) was used to estimate dye concentrations in samples with concentrations >500 ppb. The inflection point of 500 ppb was chosen from visual interpretation of emission/concentration plot. Additionally, when the standard curve was applied to all F2 emission results there was a false double peak in calculated uranine concentrations in the St. Louis Tunnel samples. Fortunately, the sample with the lowest uranine concentration (between the 2 false peaks) had the highest measured concentration of lithium (the second concurrently applied tracer) confirming a simultaneous arrival of the peak concentration of both tracers. The two false peaks were also at concentrations just below 500 ppb, further confirming that at concentrations over 500 ppb the F2 was unable to accurately quantify the amount of fluorescing compounds in the sample.

The fluorescence intensity of dyes is known to have a variable response to changes in pH (Smart & Laidlaw, 1977; Käss, 1998; Käss, 1994; Lyons, 1993; Naurath *et al.*, 2011; Davis, 1994; Sabatini & Austin, 1991; Kasnavia *et al.*, 1999). To test for the effects of acidification on fluorescence, high concentration (400 ppb) standards of both uranine and RWT were acidified to a pH of 2.5 for 24 hours and then filtered. The result was a 77% reduction in uranine emissions and an 11% reduction in RWT emissions. The reduction in uranine fluorescence agrees with previous research documenting considerable decrease in fluorescence intensity (up to 90% at pH 3) due to reversible ion exchange reactions caused by the acidic conditions (Smart & Laidlaw, 1977; Käss, 1998; Lyons, 1993). However, as reported by Käss (1998), the pH effects were

reversible; when the standards were re-neutralized to the slightly alkaline conditions of the original standards (pH 8.2 and 7.4 for RWT and uranine, respectively) there was full recovery of the dye fluorescence emissions for both uranine and RWT. Although the uranine dye reaches maximum fluorescence under alkaline conditions ($\text{pH} \geq 9$) (Smart & Laidlaw, 1977; Käss, 1998; Naurath *et al.*, 2011), the dye standards (for calibration and pH response measurements) were made with the actual mine water at the sampling location, so the above mentioned results should be representative of the range of pH the dye will be exposed to in the study.

3.2.7 Measuring Streamflow and Mine Discharge

There are many challenges to measuring streamflow in mountains including bed surface roughness, difficult to constrain channel dimensions, and steep stream gradients with varying degrees of hyporheic zone storage (Bencala *et al.*, 1990; Jarrett, 1990). Furthermore, Marchand *et al.* (1984) suggest that conventional current meter measurements of discharge do not properly account for hydraulic conditions commonly found in high-gradient, shallow streams of mountain catchments. Therefore a number of streamflow measurement techniques were used to determine the magnitude and timing of flows in Silver Creek, and to evaluate potential flow losses from Silver Creek to mine workings underlying and on either side of the creek. The measurements would also identify any major inflows to Silver Creek in the vicinity of the mine. Quantification of streamflow was performed during both high flow (spring snowmelt) and low flow (fall base flow) to understand stream dynamics across the full range of the hydrograph. For this paper, only the low flow discharge will be discussed in detail, as applied tracer studies were performed during base flow.

Silver Creek flow was measured at two locations: an existing rectangular concrete weir structure with attached gauge house located upstream of the Blackhawk fault and mine workings (SC-68; Figure 3.1b), and at the downstream side of a road culvert just below the mine workings (SC-493; Figure 3.1b). Stage-discharge relationships (rating curves) were developed by correlating data from pressure transducers (stage) with discharge measurements made using an electromagnetic flow meter. Pressure transducers recorded stage every 15 minutes from June to August and October to November and discharge measurements were collected periodically to capture the full range of the stream hydrograph. Pressure transducers were removed in August to prevent vandalism and were re-installed in the same locations prior to the start of tracer tests in October.

Slug additions of sodium chloride (NaCl) were made to develop point estimates of streamflow at select locations above and below the mine workings along Silver Creek. Transport of the slug to a downstream observation point was monitored by portable sonde that recorded specific conductance at 4-second intervals. Several grab samples were collected from the stream during slug tests and analyzed for Cl⁻ concentrations, which were matched with corresponding observations of specific conductance to develop a chloride-specific conductance relationship. The relationship was then used to convert the observed increases in specific conductance to chloride concentrations with the resultant profiles integrated to provide estimates of streamflow (Q, L/s) (1) following Kilpatrick and Cobb (1985):

$$Q = \frac{C}{V} \quad (\text{Equation 3.2})$$

Where C is the mass of Cl added (in kg) ($C = 0.59 \times \text{mass of NaCl}$) and V is the time integral of the Cl concentration (above background) at the monitoring site. The units of V are (mg/L) per second. The third approach for quantifying streamflow in Silver Creek consisted of a continuous

sodium bromide (NaBr) injection to provide streamflow estimates via the tracer dilution method (Kilpatrick & Cobb, 1985) and document any potential areas of flow loss. Once the bromide tracer concentration reached a plateau, synoptic sampling provided a spatial snapshot of bromide concentration and was used to determine a flow regime. In gaining streams, dilution of bromide with respect to distance is indicative of increased streamflow. Losing or constant flow streams, in contrast, will exhibit steady bromide concentrations with distance, as water leaving the stream does not affect the in-stream concentration.

Discharge was also measured at the St. Louis tunnel portal. Flow was directed through a 9-inch (22.86 cm) Parshall flume and stage heights were measured at 3 mm resolution at 15-minute intervals with an ultrasonic automated water level detector that was installed on May 12, 2011. Flow estimates (L/s) were then determined using the flume's standardized stage-discharge relationship. Due to limited access to the interior portions of the mine, flow could not be directly measured along tracer flow paths in the mine workings.

3.3 Results and Discussion

3.3.1 Silver Creek: Streamflow and Hydrologic Connectivity to Mine

The multiple techniques used to quantify Silver Creek streamflow across the study site found that flow varied between 19.8 and 56.6 L/s during the October tracer study. Unfortunately, the high gradient mountain stream combined with unsteady streamflow (caused by two small precipitation events) produced unavoidable challenges in accurately quantifying streamflow. During the study period the discharge records from stage-discharge relationships at SC-68 (above the mine) and SC-493 (below the mine) produced “cross-over” where the largest instantaneous flow was at the upstream location during some periods of the study and at the downstream location at other times. Therefore, the two locations of measured discharge alone

were inconclusive on determining if Silver Creek was only gaining or only losing water as it moved past the mine complex, and suggest that both inflows and outflows may be occurring within the study reach. The slug addition techniques also produced varying results ranging from 7 to 29% loss across the study reach during the sampling event with loss rates being smaller after precipitation events. The precipitation events likely masked some of the streamflow losses by adding small but influential surface water inflows along the study reach. The constantly injected RWT and Br⁻ tracers were analyzed by two separate synoptic sampling events, both following precipitation events, and the Br⁻ profiles on both sweeps suggested a gaining stream at the upstream end of the study reach (above the mine workings) and the potential for flow loss downstream of the mine workings between SC-542 and SC-759. To summarize, Silver Creek likely has some net flow loss along the study reach but high gradient stream channel and the precipitation events made it difficult to accurately quantify streamflow variations during the study period.

Concurrent with the continuous injection of Br⁻ and RWT, the 517 Shaft and the mine tailing seep were sampled for the presence of the injected tracers to identify if water leaving Silver Creek (as identified by discharge calculations) was interacting with the mine system or tailings pile on the northern side of the creek. The Br and RWT tracers injected into Silver Creek were not detected at elevated concentrations in the mine workings or discharges from the tailings seep and St. Louis Tunnel portal. At the seep Br⁻ concentrations remained below detection (<0.003 mg/L) for the duration of the sampling. There was no detectable increase in RWT concentrations, which remained below detection (0.006 ppb) throughout the sampling period. In the 517 Shaft, background concentrations of Br (0.046, $\sigma = 0.037$ mg/L) were detected both before and during the tracer study, but concentrations remained at background levels with no

evidence of an increase or breakthrough slug emerging at the 517 Shaft. There was no detection of RWT before or during the tracer study.

The results fail to confirm a hydrologic connection from Silver Creek to the tailings seep or the mine workings directly connected with the 517 Shaft. However, results prevent positive confirmation or rejection of minor flows from Silver Creek through the mine to the 517 Shaft during low-flow conditions. One logistical constraint in the tracer design was that the RWT concentrations in Silver Creek were maintained at very low concentrations (range 16 to 28 ppb) to avoid any potential negative (toxicological or visual) impacts. Additionally, the in-stream Br^- concentrations were kept at a measureable but conservative concentration (4.73 , $\sigma = 0.7$ mg/L) to ensure that there were no potentially toxic effects to aquatic life. The low concentrations of stream tracers, combined with the large volumes of mine waters, made it unlikely for the tracers to be detected, especially if additional dilutions from ground water were considered. A second challenge to identifying stream tracers in the mine was that the length of the sampling window. Tracer recovery sampling in the mine was limited by personnel availability and seasonal access, which only continued for approximately 30 days after the tracer injections. Therefore tracers may not have arrived at the sampling locations during the sampling window. Third, it is possible that some Silver Creek water (containing the applied tracers) reached the subsurface mine workings but underwent dilution from mixing with other groundwater or mine water prior to arrival at the sampling point, causing dilution to background concentrations. The use of low concentrations of tracers in Silver Creek to minimize adverse environmental impacts was likely the ultimate limiting factor preventing positive confirmation or rejection of hydrologic connection between Silver Creek and the sampled mine water locations.

3.3.2 Water Quality

Water quality varied widely across all sampling sites, with the highest concentration of contaminants generally associated with the mine pools and lowest concentrations in Silver Creek and the St. Louis Tunnel portal. The pH of samples ranged from a high of 8.7 (± 0.19 (1SD), N = 17) in Silver Creek to a low of 2.38 (± 0.06 (1SD), N = 5) in the Blaine Tunnel mine pool (Figure 3.2). Dissolved aluminum and zinc concentrations were highest in the mine workings to the southeast of Silver Creek and decreased prior to exiting the St. Louis Tunnel portal. Aluminum ranged from a high concentration of 654 mg/L in the Argentine Tunnel to less than 0.1 mg/L at the St. Louis Tunnel portal (Figure 3.3). Similarly, zinc concentrations were highest in the Argentine Tunnel pool at 24,600 mg/L and decreased to 3.8 mg/L at the St. Louis Tunnel portal. Solute loading analysis was not performed as flow rates from the Argentine Tunnel, Blaine Tunnel, and 517 Shaft mine sites were not measured during the study.

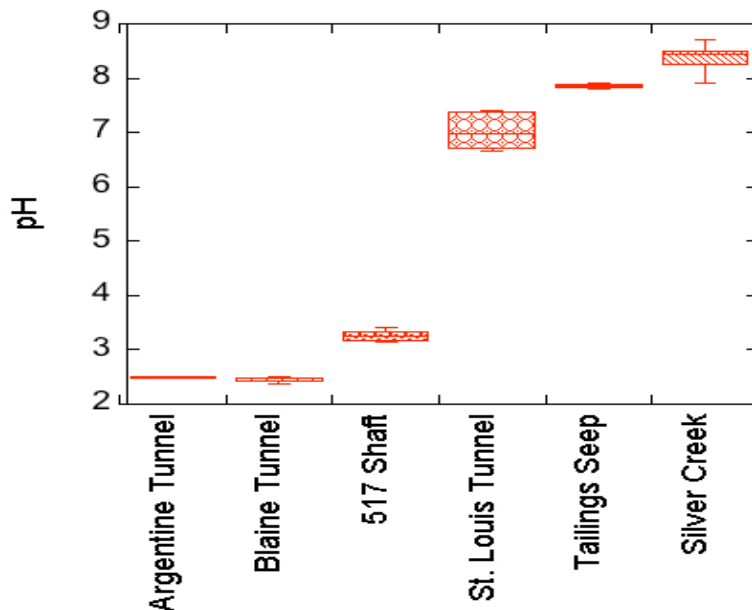


Figure 3.2: Box plot of pH in the mine workings along with that of the St. Louis Tunnel portal and tailings seep discharges and of surface waters in Silver Creek.

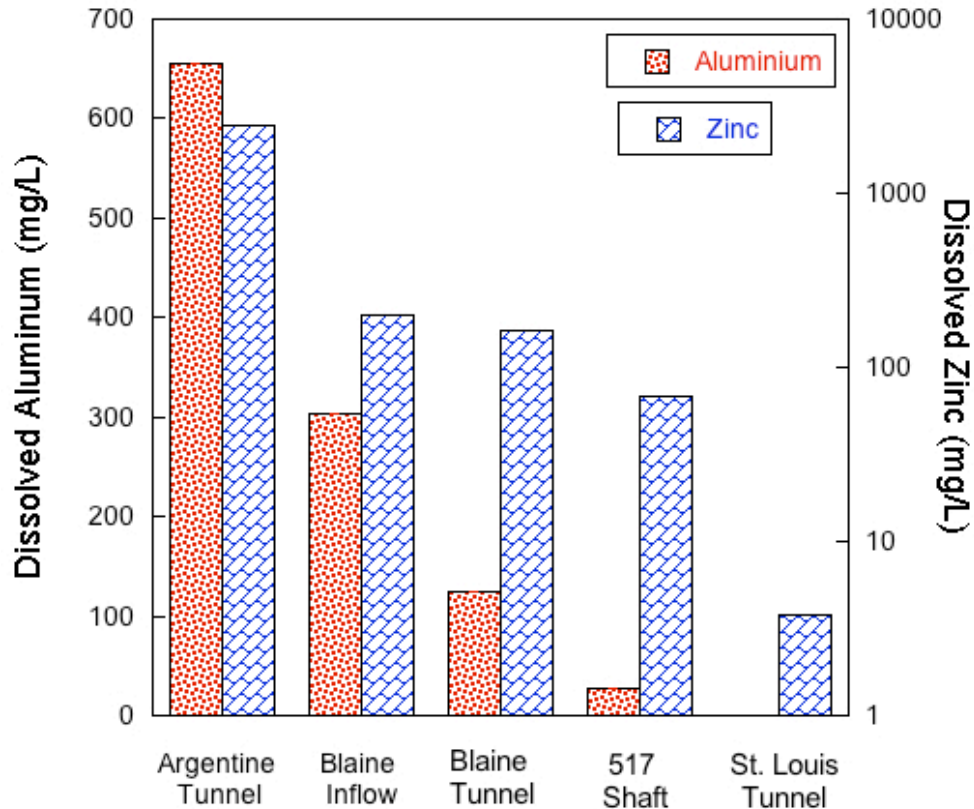


Figure 3.3: Dissolved zinc and total dissolved aluminum concentrations in mine workings. The mine workings are listed from left to right in the direction of hydrologic flow towards the discharge point at the St. Louis Tunnel portal.

During the tracer experiment water quality along Silver Creek was synoptically sampled at the same locations as were used for the stream tracer study (Figure 1b). Sulfate (SO_4^{2-}), generally considered a conservative tracer in AMD settings (Field, 2002), was measured at all sampling points and showed a measureable increase from under 10 mg/L above SC-198 to over 50 mg/L at SC-1131 the furthest downstream sampling point (Figure 3.4). Dissolved zinc concentrations were measured at nine of the sampling points and increased from under 0.005 mg/L upstream of the mines to 570 mg/L at SC-1131. Both sulfate and zinc concentrations had the largest increases in the 200 m upstream of the mine entrances (at approximately 400 m) and then remained relatively constant until increasing again beyond 800 m.

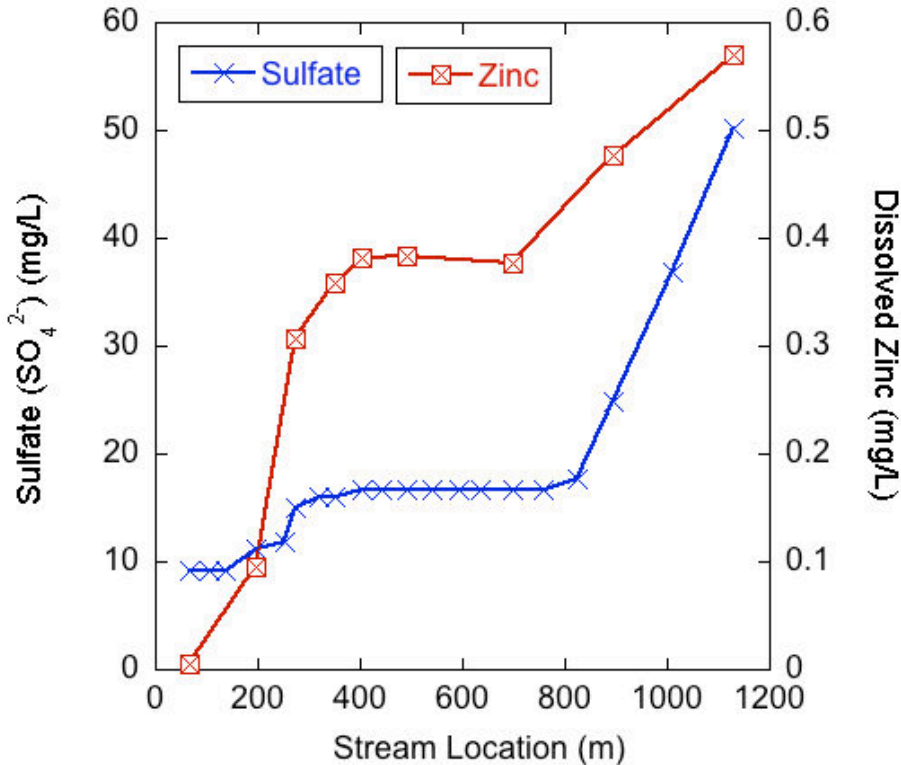


Figure 3.4: Sulfate and dissolved zinc concentrations in Silver Creek from synoptic sampling during base flow conditions on October 7, 2011. Stream locations are in m downstream from the location of the stream tracer injections with the stream crossing the mine workings at approximately 400 m. There are known inflows to Silver Creek from seepage below the mine tailings entering between SC-895 and SC-1131 in Figure 1.

Silver Creek chemistry suggests that mining activities impact Silver Creek and the sources of AMD products (sulfate and zinc) are occurring in similar locations. The sulfate and mining-associated metal concentrations begin to increase in Silver Creek in the vicinity of the Rico-Argentine mines and indicate that even though there is a potential net loss of flow in the reach, there may be small inputs of mine water or other inflows that influence the stream chemistry. The first considerable increases in stream solutes occur between 200-300 m, which is upstream of the primary mine entrances (Figure 3.1b), but within the area of historical mining operations. Due to mining activities, there are considerable amounts of mine debris (mill tailings and mine waste rock) scattered along the banks of the stream channel starting at approximately 100 m (Figure 3.1b). Given the variable discharge (gains and losses) measured along the study

reach it is likely that the Silver Creek waters are undergoing hyporheic zone mixing in areas where solute laden mine wastes are present. As a result, contaminated sediments in the hyporheic zone may be representing a long-lasting supply of contaminants to hyporheic pore water (Palumbo-Roe & Dearden, 2013). A second source of solutes is slow percolation of highly concentrated AMD water in the Blaine Tunnel mine pool into the subsurface and eventual movement towards the stream channel, which would likely occur at or just downstream of the Blaine Tunnel portal between 350 and 400 m. The relatively consistent solute concentrations between 400 and 700 m is likely because previous mine cleanup work at this site included capping the mine tailing pile (Figure 3.1) and reinforcing the bank between the tailings pile and Silver Creek to reduce erosion of the tailings pile into Silver Creek. As a result, the amount of surface water and hyporheic zone mixing may be decreasing along this segment creating less opportunity for mining-associated sulfate and zinc to enter Silver Creek. The increase in AMD contaminants to Silver Creek at locations below the mine entrances (below SC-826) are likely from diffuse inflows from the tailings pile seep which are visually present between SC-895 and SC-1131 in Figure 3.1.

The results in Figure 3.3 and Figure 3.4 therefore suggest that, when excluding the contributions from the large mine tailings pile, the sulfide deposits sourcing the AMD may be most prevalent in the mine workings and shallow subsurface on the southeastern side of Silver Creek between 200 and 400 m. As suggested by Nordstrom (2009) this shallow acidic groundwater can then be mobilized by infiltration of meteoric waters, resulting in movement towards surface waters (or further into the mine complex). To elaborate, the high metals concentrations found in the mine waters to the southeast of Silver Creek may be partially explained by the mines applied lowering of the local water table. The mine drainage tunnels were

built to help dewater the mine workings but as a consequence the mine workings also exposed large amounts of sulfide minerals to air, which increased oxidation reactions. Therefore, the combined exposure to air and water (from seasonal meteoric infiltration and shallow groundwater flow) in the mine workings adjacent to, and above, Silver Creek has created an ideal situation for AMD production that is impacting the water quality in Silver Creek and at the St. Louis Tunnel.

3.3.3 Isotopes

Stable isotope results from all samples including precipitation, surface water, and mine water were plotted as the $\delta D - \delta^{18}O$ relationship (Figure 5a). The $\delta^{18}O$ value for snow of approximately -20‰ and the mean rain value of -5‰ are characteristic values for the Colorado Rocky Mountains for winter and summer precipitation (Liu *et al.*, 2004). Empirical results have shown that $\delta D/\delta^{18}O$ values in precipitation co-vary and are generally described by the relationship:

$$\delta D = 8\delta^{18}O + 10\text{‰} \quad (\text{Equation 3.3})$$

which is defined as the Global Meteoric Water Line (GMWL) (Craig, 1961). The Local Meteoric Water line (LMWL) has a similar slope and y-intercept:

$$\delta D = 7.8\delta^{18}O + 8\text{‰} \quad (\text{Equation 3.4})$$

The similar values in slope between the LMWL (7.8) and the GWML (8.0) suggest an absence of complex kinetic fractionation processes affecting the $\delta D - \delta^{18}O$ relationship of precipitation (inputs) in the local hydrologic system (Craig, 1961). All surface water and mine water samples

fell on a mixing line between the snow and rain inputs, suggesting that they were a mixture of the two precipitation types with $\delta^{18}\text{O}$ values between -14 ‰ and -15.5 ‰.

To better observe the variations in surface waters and subsurface waters (relative to the LMWL) the $\delta\text{D} - \delta^{18}\text{O}$ relationship was examined at a finer resolution (Figure 3.5b). The isotopic concentration of Silver Creek had the greatest seasonal variation with waters more depleted in δD and $\delta^{18}\text{O}$ in June as a result of snow melt and more enriched in δD and $\delta^{18}\text{O}$ in October from summer rains and/or groundwater contributions. All of the samples collected in or near the mine (tailings seep, Blaine Tunnel, 517 Shaft) had an isotopic composition similar to Silver Creek in October, indicating that stream water during baseflow was of similar origin to the water moving through both the upper mine and the seep. Additionally, there was little variation in isotopic signature of the tailings seep, which did not follow variations observed in Silver Creek, indicating that water exiting the tailings seep was coming from a well-mixed source distinct from Silver Creek waters. However, the samples from the tailings seep and the Blaine Tunnel all plot below the LMWL with a decreased slope and y-intercept:

$$\delta\text{D} = 3.1\delta^{18}\text{O} - 60\text{‰} \quad (\text{Equation 3.5})$$

This linear relationship is represented by WL-1 in figure 5b and the decreased slope suggests that an evaporation trend occurred at these locations since recharge (Craig, 1961; Williams *et al.*, 2006). Conversely, samples from the St. Louis Tunnel and Silver Creek express the following $\delta\text{D} - \delta^{18}\text{O}$ relationship:

$$\delta\text{D} = 7.4\delta^{18}\text{O} + 3\text{‰} \quad (\text{Equation 3.6})$$

The linear relationship is represented by WL-2 in figure 3.5b, and the similarity between WL-2 (7.4) and LMWL (7.8) again suggests an absence of fractionation processes affecting those water sources since meteoric recharge. The two samples from the 517 Shaft plot close to, and slightly below, the LWML indicative of a mixture of predominantly unfractionated waters (since recharge) with a lesser amount of fractionated waters (i.e. from the Blaine Tunnel). The Results therefore suggest that the waters with evidence of evaporation (Tailings seep and Blaine Tunnel) are distinct from local precipitation (LMWL), surface water (Silver Creek), and the dominant source of water exiting the mine system (St. Louis Tunnel).

Figure 3.5b also indicates that the water discharging from the St. Louis Tunnel had similar isotopic concentration in May, June, and October, indicating the water was predominantly from a well-mixed groundwater source with limited seasonal variation. The St. Louis Tunnel samples were also consistently more depleted than the samples from the 517 Shaft and Blaine Tunnel, indicating that water flowing downgradient from the 517 Shaft was mixing with water that has a distinctly different isotopic signature (more depleted) before emerging at the portal. The stable isotope analysis provides initial insight into the hydrologic connectivity of the system, but due to the limited range (magnitude) of isotopic variability across all sites, is insufficient as a stand-alone tool for identifying the sources and relative contributions of water contributing to the AMD.

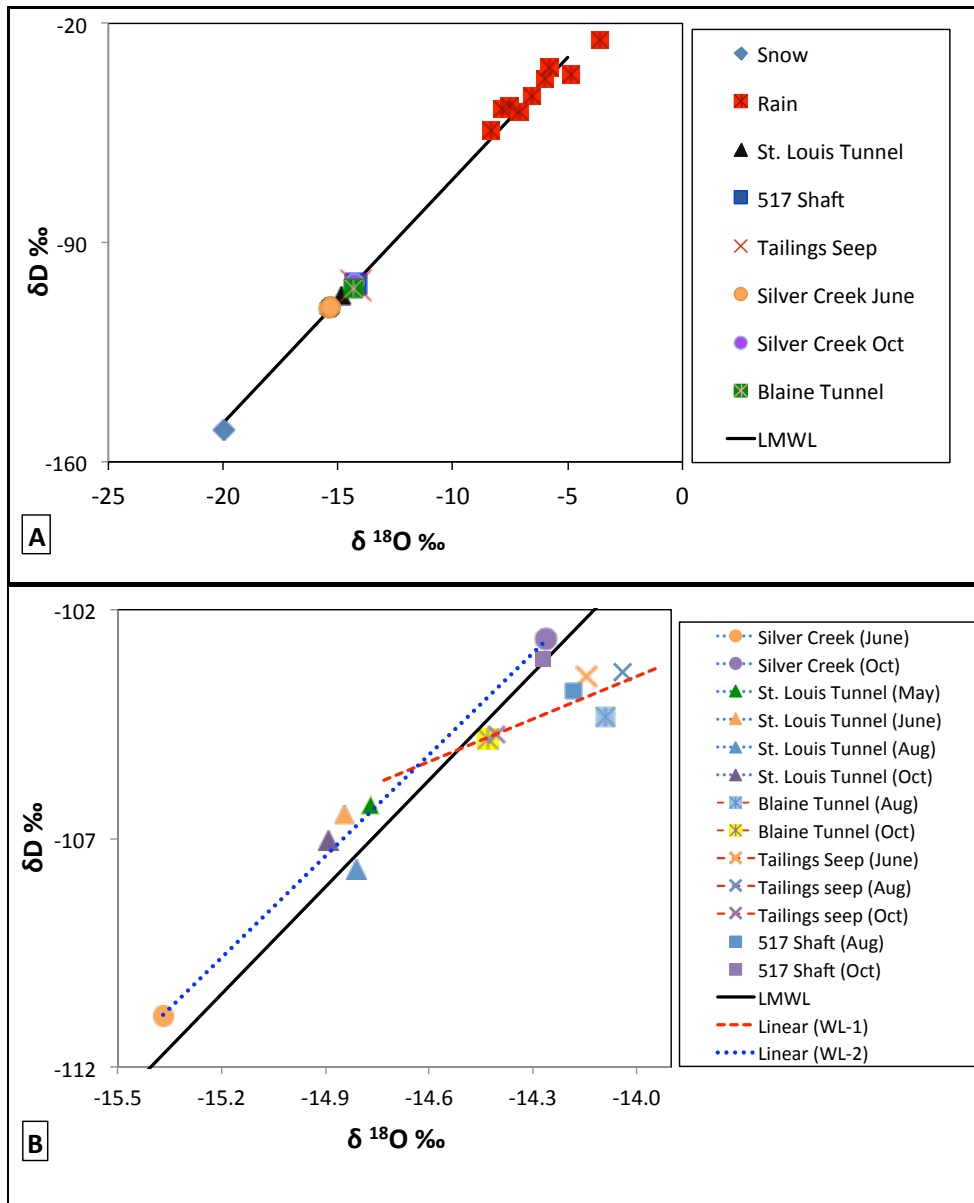


Figure 3.5: (A) Plot of $\delta^{18}\text{O}$ vs. δD for precipitation, surface waters, and mine waters. The St. Louis Tunnel, 517 shaft, Blaine tunnel, tailings seep, and Silver Creek are the arithmetic mean from all samples collected. The Local Meteoric Water Line (LMWL) is plotted in black. (B) Seasonal variations of $\delta^{18}\text{O}$ vs. δD for surface waters and mine waters in 2011. The LMWL is plotted with a second water line (WL1; red dash) representing samples from the Tailings seep and the Blaine Tunnel and a third water line (WL2; blue dot) representing samples from Silver Creek and the St. Louis Tunnel. The symbol shapes correspond to similar sites in 5a and 5b, while colors represent similar dates for different sites in 5b.

Tritium values from 21 rain and snow samples collected in the San Juan Mountain region between January 2010 and October of 2011 had a mean value of 6.2 TU with the 25th and 75th percentiles of samples being 4.6 and 6.5 TU respectively (Figure 3.6). The narrow range of tritium in incoming precipitation provided a strong estimate of the current meteoric inputs of tritium to the local hydrologic system under investigation. For comparison the annual mean tritium concentration in precipitation in Colorado was only 7.5 TU in 1999 (Davies, 2002), suggesting that tritium levels in meteoric waters have only decreased by about 1 TU in the decade preceding the current study. The tritium data provide insight as to the mean residence time of “old” *versus* “new” groundwater in the study. Tritium (^3H ; $t_{1/2} = 12.43$ years) is naturally present only in minute quantities but was produced in large quantities during thermonuclear weapons testing from 1952 to 1963 (Michel, 1989). As a consequence, without consideration for complex mixing scenarios, water with a tritium value <1 TU may be considered “old” water recharged prior to 1952 while higher values would represent “new” water being wholly or partially recharged since 1952. Additionally, if a tritium concentration is greater than the current meteoric recharge it can be considered to have some portion of water that precipitated with a “bomb spike” signal in the decades following weapons testing. No samples had <1 TU while all mine water and surface water tritium concentrations were near or within the range of recent precipitation suggesting that those waters were derived predominantly from recent (within a few years) meteoric recharge. The Argentine Tunnel sample, along with the Silver Creek and the Dolores River samples, had slightly elevated tritium concentrations relative to the current (2010-2011) meteoric inputs, suggesting that the water in those locations may have had slightly longer mean residence times than the waters emerging at the tailings seep and moving through the mine to the St. Louis Tunnel. The tritium results provide only a qualitative estimate of water residence

times, but suggest that the mean residence times of the mine waters are not distinctly different from residence times of the local and regional surface waters.

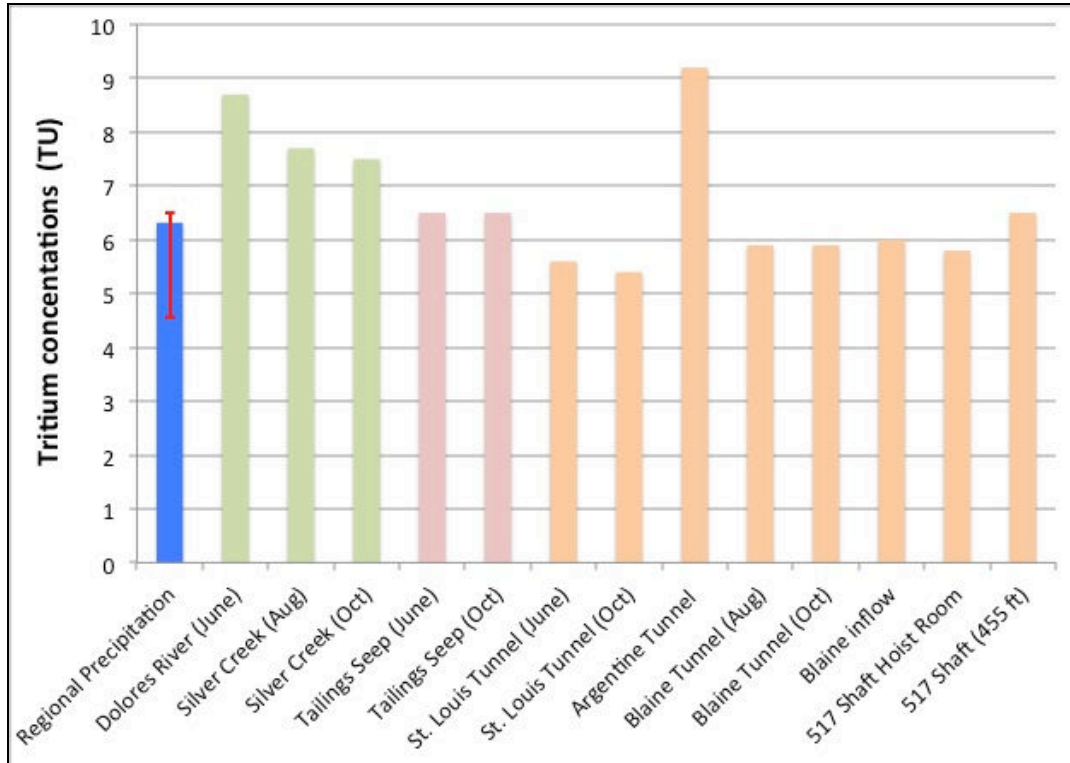


Figure 3.6: Tritium (^3H) values from recent (2010-2011) regional precipitation (blue), surface waters (green and pink), and mine waters (orange). The blue precipitation bar represents the mean value of all samples while the red error bar represents the 25th and 75th percentiles.

3.3.4 Applied Tracers: Blaine Tunnel to 517 Shaft

The first hydrologic connection to be investigated with applied (injected) tracers was the movement of water from the Blaine Tunnel to the 517 Shaft and the interior mine workings. There was no practical way to quantify the volume of water entering the 517 Shaft from the Blaine Tunnel area, thus quantification of tracer mass recovery was not possible. Additionally, it was estimated that only between 50 to 85% of the mine pool water (containing the fluoride tracer slug) was successfully pumped over the first debris blockage towards the drainage stope exiting the Blaine Tunnel making it unclear what percentage of the initial tracer was moved out of the

Blaine Tunnel mine pool via pumping. However, positive detection of the tracer provided a qualitative assessment of hydrologic connectivity between the Blaine Tunnel and the 517 Shaft area of the mine. Figure 3.7 displays a time series plot of fluoride and chloride concentrations in the 517 Shaft starting on October 5 at 14:00 when the fluoride slug was added to the Blaine Tunnel behind the cofferdam. Chloride concentrations remained relatively steady (2.11, $\sigma = 0.08$ mg/L) over the first 48 hours, indicating that the changes in fluoride concentrations were occurring independently from any changes in the mine water chemistry caused by previous hydrological alterations such as the water chase applied to the 517 Shaft during the uranine/lithium tracer application. Interestingly, the chloride concentrations did decrease to a mean of 1.78 ($\sigma = 0.05$) mg/L for approximately 96 hours (approximately hour 48 to 144 in Figure 3.7), which corresponds to the period when the highest fluoride concentrations were measured in the 517 Shaft. Given that background chloride concentration was lower in the Blaine Tunnel (1.54 mg/L) than in the 517 Shaft (2.14 mg/L) it is reasonable to suggest that the Blaine Tunnel water (which was partially moved out of the Blaine Tunnel by pumping) arrived at the 517 Shaft at an increased rate relative to background flow rates creating increases and decreases in fluoride and chloride concentrations respectively.

The initial fluoride concentration in the 517 Shaft (1.95 mg/L) indicated that there was a measureable background presence of fluoride in the system. However, the fluoride concentrations began to show a steady increase above background concentrations beginning 10 hours after injection, and more than doubled to reach a peak concentration of 4.94 (mg/L) 68 hours after the slug injection. The fluoride concentration then began to fall sharply approximately 8 days after the tracer injection. Given an approximate minimum distance from the Blaine Tunnel cofferdam to the base of the 517 Shaft of 200 m, the velocity of the advection

front (maximal velocity) was 0.34 m/min while the average velocity of the peak fluoride concentration was just 0.05 m/min. When compared to results reported by Wolkersdorfer (2008), the average velocity is considerably slower than the range of 0.3 to 1.6 m/min reported as 95% confidence interval of 42 tracer tests. From a qualitative standpoint the results suggest that the hydrologic flow paths between the Blaine Tunnel and 517 Shaft may have major obstructions and/or the water is moving slower than has been most commonly observed in previously studied mine water environments. Additionally, there is diffusion in the system because there was not a distinct breakthrough curve. One anticipated possibility is one or several obstructions at points along the tunnel/stopes that causes the water to interact with rock and sediment. The collapsed portion of the adit over which water was pumped immediately after tracer injection is one likely obstruction. As mentioned in the methods, the tracer recovery at the 517 Shaft was achieved by sampling from a mine pool of unknown volume and flow-through rates. Additionally, the precise volume and rate of water moved out of the Blaine Tunnel mine pool (injection point) was not quantified due to pumping inefficiencies and unsafe access to drainage points. The flow path of the tracer between the Blaine Tunnel and the 517 Shaft was also likely diverse (multiple interconnected tunnels, stopes, and inclines present) making quantification of tracer travel distance difficult. Therefore the tracer breakthrough rates should be considered in a qualitative manner and no quantitative transport model (e.g. Wolkersdorfer, 2008; Käß, 1998; Field, 2002) was used to evaluate solute transport and dispersion.

During the Blaine Tunnel tracer injection, water samples were also collected from SC-493 (about 120 m downstream from the Blaine Tunnel adit, Figure 1b) to determine if a detectable amount of water was flowing from the Blaine Tunnel, through the subsurface, to Silver Creek. The fluoride concentrations at SC-443 after the Blaine tunnel injection remained

relatively steady (0.104 , $\sigma = 0.018$ mg/L) with intermittent but not sustained increases, which neither confirms nor rejects the hypothesis that water contained in the Blaine Tunnel may be directly entering Silver Creek in the vicinity of the portal.

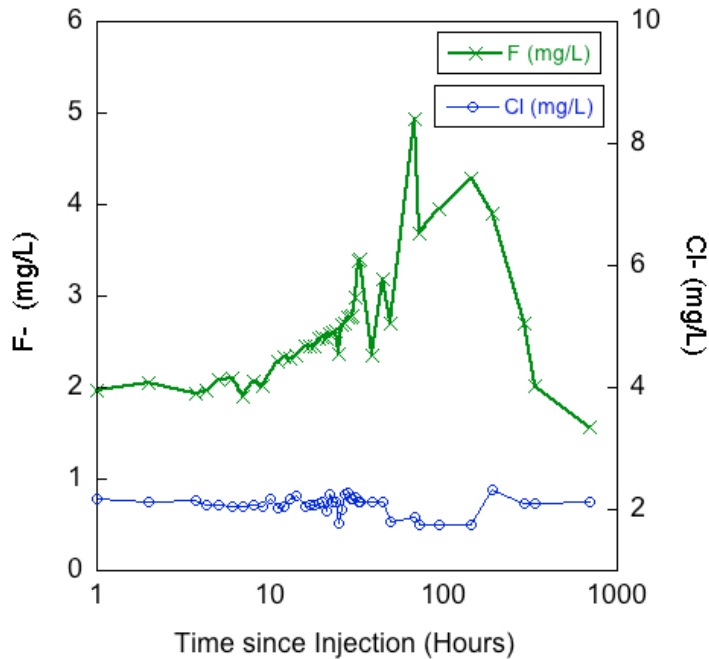


Figure 3.7: Fluoride (F^-) concentrations measured in the 517 Shaft. Background chloride (Cl^-) concentrations are plotted over the same time period. Time (x-axis) plotted as log scale.

The original tracer design included pairing a third fluorescent dye (PTSA; 1,3,6,8-Pyrenetetrasulfonic Acid Tetrasodium salt; CAS # 59592-10-0) with the fluoride salt tracer applied to the Blaine tunnel. This dye tracer has a fluorescence emission peak that is distinct from both uranine and RWT so it could be used in a multiple tracer situation when tracer mixing is possible. Additionally, the Cyclops 7 field fluorometer from Turner Designs has a submersible sensor specifically designed for detection of PTSA. However, knowing that there were potentially multiple blockages (rock collapses in-filled with sediments or AMD derived precipitates) the dye tracer was not used and thus still available for additional future studies. This is important because if a tracer is used and full recovery cannot be confirmed then that tracer would not be desirable for future use in the same location for reasons of cross contamination.

3.3.5 Applied Tracers: 517 Shaft to St. Louis Tunnel Portal

The arrival time for both uranine and lithium at the St. Louis Tunnel portal was at 03:00 on October 5, 15 hours after injection (Figure 3.8). After arrival, the concentration of both tracers increased rapidly with uranine reaching a peak concentration of 2,900 ppb at 08:00, and the lithium tracer reaching a peak concentration of 0.258 mg/L at 09:00 on October 5, representing 20 and 21 hours to peak concentration, respectively. There was no clear increase in discharge as a result of the water chase (189,000 L in 30 minutes \approx 105 L/s) added to the 517 Shaft immediately following tracer injections. The fast times for the advection front of the tracer movement from the 517 Shaft to the St. Louis Tunnel portal suggest that in general the tunnel has few obstructions and water moves through it relatively quickly as channel flow.

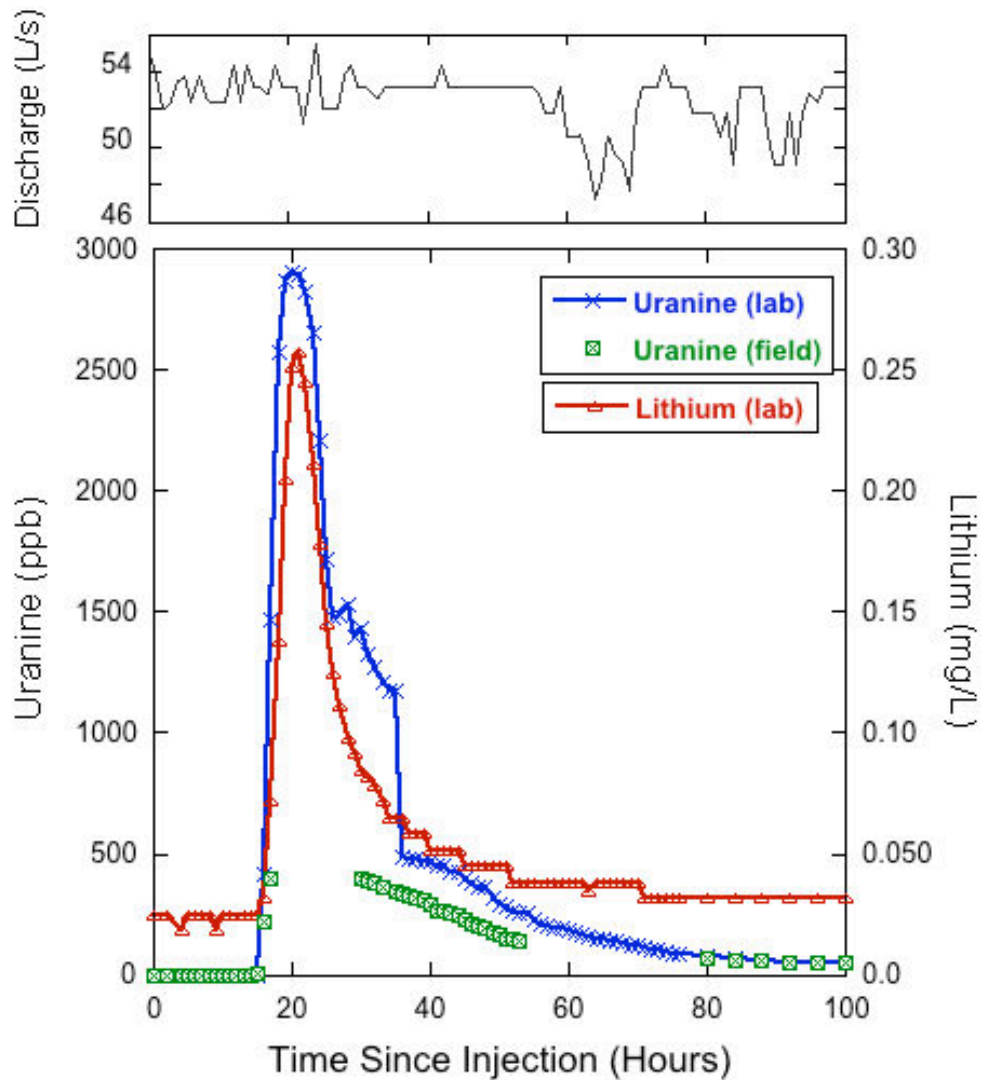


Figure 3.8: Time series of hourly discharge (top) and tracer breakthrough curves (bottom) for lithium and uranine at the St. Louis Tunnel portal. Time 0 represents 12:00 on October 4.

Figure 3.8 also shows the data collected at the St. Louis Tunnel portal by the field fluorometer and confirms the timing of tracer arrival and subsequent rapid increase in uranine concentration. Unfortunately, the upper limit of calibration for the field fluorometer was 400 ppb for this experiment so the instrument was unable to record the peak concentrations of the tracer breakthrough. The field instrument was then able to pick up the recession limb of the uranine slug. The general performance of the instrument was quantified by determining that the

instrument tracked the laboratory analyses well, though with a near linear 45% reduction in concentration ($r^2 = 0.99$, $N = 43$) when sample concentrations were below 400 ppb. According to the information provided by the manufacturer of the field fluorometer, the uranine probe was designed to analyze samples using excitation/emission values of 485/540 nm, which is shifted from the 492/512 nm values used for laboratory analysis. Therefore the field fluorometer may have failed to accurately capture the uranine fluorescence peak, resulting in consistently lower measured concentrations of uranine dye in the St. Louis Tunnel samples.

Given an estimated tunnel distance of 2591 m between the 517 Shaft and the St. Louis Tunnel portal, the average velocity of the advection front (maximal flow velocity) was 2.87 m/min while the mean velocity of the lithium and uranine peaks were 2.16 m/min and 2.06 m/min, respectively. Although time elapsed between tracer injection and passage of maximal-concentration provides a good approximation of the mean velocity, it is recognized that the true effective flow velocity occurs after the passage of maximal-concentration and cannot be calculated from the breakthrough curve alone (Käb, 1998). However, when a steep and narrow breakthrough curve occurs, as observed in Figure 3.8, the correct time for calculating effective flow velocity is only insignificantly larger than the time of passage of maximal-concentration and the difference can be practically neglected (Käb, 1998). Therefore, the approximated effective flow velocity was used, and when qualitatively compared to results presented by Wolkersdorfer (2008) the effective flow velocity is considerably faster than the range of 0.3 to 1.6 m/min reported for 42 documented mine tracer tests. The results suggest this system differs from those reviewed by Wolkersdorfer (2008), or that the water chase applied behind tracer injection may have artificially increased the velocity of tracers as they moved from the 517 Shaft towards the St. Louis Tunnel. Interestingly, the discharge at the St. Louis Tunnel portal did not

show a clear increase or pulse in discharge upon tracer arrival (Figure 3.8). Hourly mean discharges between 01:00 and 24:00 on October 5 (the breakthrough period) fluctuated between 51 L/s and 54 L/s relative to the mean of 52 L/s ($\sigma = 26$ L/s) over the first 100 hours of tracer recovery. As a result, the artificial influence of the water chase on tracer velocity was not directly quantifiable, making the estimated effective flow velocity a qualitative estimate and influencing the decision not to use an established model for solute transport simulation.

The final sample, collected 6 weeks after the tracer injection, showed that lithium concentrations had returned to background levels (approximately 0.025 mg/L) while uranine concentrations were still slightly elevated (≈ 1.8 ppb) relative to background (< 0.002 ppb). The results indicate that 6 weeks after the tracer injection the lithium tracer was no longer moving through the system at concentrations greater than background, while the fluorescent dye tracer was still arriving at the portal in detectable quantities. However, as of the last discharge measurement on November 16, cumulative flow and concentration data were used to calculate 74% and 109% recovery of lithium and uranine respectively. This result conflicts the final instantaneous concentrations by suggesting that all of the uranine was recovered while some of the lithium remained in the mine workings, either through sorption or ending up in an immobile fluid region that was disconnected from the main discharge conduit. Assuming the mine waters flow through a karst-like conduit system, the immobile fluid regions could be conceptually described as resulting from vortices and eddies produced by conduit surface irregularities (Field & Pinsky, 2000).

Given that the St. Louis Tunnel discharge (Figure 3.8) showed considerable albeit irregular fluctuations (min/max hourly discharges were 42.3 and 57.7 L/s) over the 6-week tracer recovery period, it is reasonable to suggest that short-term variations in measured discharge may

have created uncertainty in quantifying tracer recovery. For short projects, such as this study, uncertainties in cumulative flow can be upwards of 14% in a low gradient flow system if conditions are non-ideal (Brigand *et al.*, 2013). The St. Louis tunnel discharge was measured directly downstream from the collapsed adit, with flow emerging through piles of mine timber and debris before being channelized and directed through a flume for quantification. There was no way to completely eliminate turbulence in the flow prior to reaching the flume, which resulted in continuous small scale (\approx 1-2 cm) water surface undulations representing 5-10% variability in total depth of flow at the flume. The variability in depth likely created uncertainties in calculated flow and in the quantification of tracer recovery. Additionally, there is inherent difficulty in calculating mass recovery of a fluorescent dye because the analytical results are an indirect measurement of the dye itself. Variable dye concentrations produce different intensities of fluorescence, which is then converted back to a mass of dye based on calibration curves that do not have perfect fit with standards. Therefore a reasonable degree of error should be expected when calculating mass recovery and results from this experiment are likely within that range. Given that uranine concentrations remained slightly elevated at the end of the study period, it was not possible to have recovered the entire tracer mass. Uranine concentrations on the final day of sampling suggested that discharge from the St. Louis Tunnel portal was only producing approximately 8.16 g of uranine per day, only 0.08% (per day) of the total mass of tracer added.

A second major concern with interpreting fluorescent dye results in a mine tracer study was the effect of low pH waters on the fluorescence properties of the dyes. The results of laboratory acidification tests (described in methods) agreed with previous work (Smart & Laidlaw, 1977; Käß, 1998; Lyons, 1993; Naurath *et al.*, 2011) by showing that the uranine dye had its fluorescence (spectral signature) reduced when exposed to low pH waters. However,

results from the laboratory investigation showed that uranine fluorescence recovered when acidic conditions were re-neutralized to the pH values observed in samples collected at the St. Louis Tunnel portal (pH 7.34), which were likely maintained by reversible ion exchange reactions (Käß, 1998; Naurath *et al.*, 2011). The study results therefore support previous recommendations from Naurath *et al.* (2011) that uranine can be successfully used in mine tracer studies when samples analyzed for tracer recovery are alkaline.

A final consideration for uranine recovery was the influence of mine water iron (Fe) concentrations. The total recoverable Fe was approximately 66 mg/L in the 517 Shaft and only 4 mg/L at the St. Louis Tunnel portal during the study indicating that a significant portion of the iron precipitated as iron hydroxides between the uranine tracer injection and recovery locations. The Fe hydroxides can negatively influence uranine recovery rates due to dye adsorption on the hydroxide surfaces and subsequent loss by filtration (Aldous & Smart, 1988) or settling of precipitates into immobile fluid regions of the conduit. All of the samples were filtered prior to fluorescence analysis to eliminate any fluorescence intensity overestimates due to increased turbidity in the sample. However, Naurath *et al.* (2011) reported that good recovery can be expected in mine waters up to 100 mg/L of Fe, so it is concluded that the Fe levels in the mine waters emerging at the St. Louis Tunnel portal were not high enough to interfere with uranine results, as supported by the high recovery amounts reported previously.

3.3.6 The St. Louis Tunnel Portal Discharge

Mean daily discharge at the St. Louis Tunnel portal from May to November 2011 ranged from 36 to 57 L/s with the peak discharge occurring on September 21 (Figure 3.9). Daily discharge from the St. Louis Tunnel portal is plotted with the daily flows in Silver Creek at the

downstream stream gauge site (SC-493, Figure 3.1). Although the Silver Creek discharge record does not begin until June 17, it is clear that the discharge record depicts a typical snowmelt hydrograph for Silver Creek with discharge peaking in late spring (May or June) and returning to near base flow in August. For comparison, the discharge of the Dolores River at Rico (USGS station 09165000; USGS National Water Information System, <http://waterdata.usgs.gov/nwis>) had a similar snowmelt hydrograph for 2011 with peak discharge occurring on June 7th, just 10 days before the discharge record began on Silver Creek. However, at the St. Louis Tunnel portal, there is no characteristic snowmelt pulse in the discharge. Rather, the hydrograph there has a more consistent flow over time, with peak discharge occurring more than 3 months after peak discharge was recorded in the local surface waters. This observation could be explained by a regional groundwater pulse signal, which suggests that a large portion of the St. Louis Tunnel discharge is coming from or driven by a more regional (i.e. watershed aquifer scale) groundwater reservoir.

The increase in pH and subsequent decrease in dissolved metals concentrations between the mine workings and the St. Louis Tunnel portal also suggest dilution and perhaps titration of acidity by non-AMD groundwater between the locations. The pH and metals concentrations support the notion of increasing dilution as mine waters move downgradient from the Argentine Tunnel (above the Blaine) to the Blaine Tunnel to the 517 Shaft to the St. Louis Tunnel portal, suggesting that the workings to the south of Silver Creek may be the primary source of AMD and that mine water at the 500 level becomes diluted as it moves northeast towards the SE crosscut and the St. Louis Tunnel.

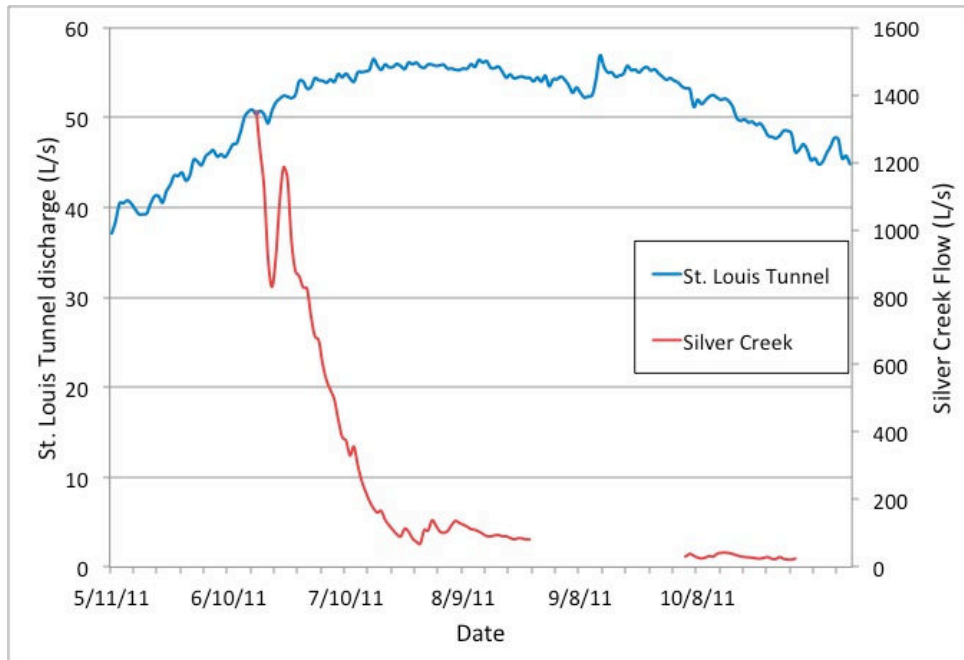


Figure 3.9: Mean daily discharge from the St. Louis Tunnel portal and from Silver Creek. Silver Creek discharge was not measured between August 27 and October 3, 2011 as pressure transducers had been removed from the gauging stations during this period.

Dilution along the drainage tunnels by considerable amounts of well-mixed non-AMD groundwater is further supported by stable isotope results, which indicate a steady, low variability signal at the St. Louis Tunnel portal and greater seasonal variability at the upper mine workings (Blaine Tunnel and 517 Shaft). The potential for considerable amounts of non-AMD water entering the system along the St. Louis Tunnel may also be explained by the regional hydrogeology. The drainage tunnel extends several thousand feet into the Rico dome, which is comprised of a thick series of interbedded sandstone, arkose, shale, limestone and dolomite of the Pennsylvania age Hermosa formation (USGS, 2012). One of units of this formation is the Leadville Limestone, which is locally 75 m thick and the top of the unit exhibits widespread karst and related erosional features (McKnight, 1974). The Leadville Limestone is also overlain by a sequence of clastic and calcareous sedimentary rocks up to 1000 m thick (Larson, 1987). The widespread limestone and sedimentary units may therefore support a large regional aquifer.

As a result, the St. Louis tunnel may likely be intercepting significant amounts of groundwater (with low levels of mineralization relative to mine waters) moving through the regional aquifer, leading to a dilution of the AMD water prior to emergence at the St. Louis Tunnel portal. The delay in peak discharge from the St. Louis Tunnel relative to the local surface waters would then be explained as being driven by the regional groundwater pulse which can lag seasonal surface or near-surface water runoff in mountain watersheds (Hazen *et al.*, 2002)).

3.3.7 Targeted Remediation

Targeted remediation refers to controlling the source of water (i.e. inflow of groundwater or surface water) into underground workings or open pits and/or controlling the outflow of mine drainage from the workings (Wireman & Stover, 2011). From the hydrologic characteristics identified by the multiple tracer approach there are several options for future remediation. Results suggest that there is some degree of hydrologic connectivity between the mine complex and Silver Creek, but it appears that even with the creek being a no-change or losing reach across the mine complex that creek waters are not contributing large amounts of source waters to the underlying mine workings. Therefore, it does not seem necessary to artificially control streamflow in Silver Creek. Conversely, if the study found significant contributions from Silver Creek, then targeted remediation options may have included activities such as lining the stream channel with an impervious membrane or re-routing the stream channel to minimize water exchange in the vicinity of the mine.

The most likely sources of water to the mine are therefore from localized (hillslope scale) meteoric recharge into near surface mine workings to the southeast of Silver Creek. Results suggest that these inputs are seasonally variable with the greatest inputs likely deriving from

snowmelt, which is highly spatially and temporally variable in mountain settings (Williams *et al.*, 1991; Caine, 1996). The variability of input, combined with the highly variable nature of surface or near-surface mine entrance points (i.e. driven by different rates of portal collapses) make it too expensive and difficult to control the most prevalent source waters. Additionally, most of the degraded mine entrance points are on steep slopes with limited access, so additional environmental impact would occur if the entrances were to be adequately shut off.

The study results further suggest that the mine discharge at the St. Louis Tunnel portal is coming from a combination of highly mineralized (and low pH) AMD waters and less mineralized, well-mixed (from stable isotope results) groundwater. The tracers suggest that the highly mineralized waters are moving in a south to north direction, or from the hillslope containing the Argentine/Blaine Tunnels under Silver Creek towards the 517 Shaft area of the mine and along the deep drainage tunnels to the St. Louis Tunnel portal. The remaining question is at what location does the highly mineralized acidic mine water mix with clean, non-mine-impacted groundwater? By untangling the “under-ground plumbing” in these instances, a source-control approach can be used to collect and segregate the mineralized AMD water, before it can mix with and contaminate larger volumes of naturally-occurring groundwater flows (Wireman & Stover, 2011).

A next step would be to perform rehabilitation of the mine workings associated with the Argentine and Blaine Tunnels to increase safe access and provide confirmation and quantification of sources and mixing points. It would also help to know the volume of mineralized AMD water leaving the mine complex via the SE crosscut prior to any additional inflows occurring along the drainage tunnels. If the contaminated water is significantly less than the volume of water exiting the St. Louis Tunnel then active treatment of the lower volume of

water may be the most economically viable option. Currently, *in-situ* treatment to neutralize the acidity (≈ 3 pH) of mine water in the 517 Shaft is being performed. The results of this treatment are pending but if the water quality of the St. Louis Tunnel discharge is improved then smaller scale on-site treatment of mine waters in this area may provide the most feasible targeted remediation option.

Other targeted remediation options may include bulkheads to prevent the flow of contaminated waters from ever reaching the St. Louis Tunnel portal. This requires an in-depth understanding of both the structural integrity of host bedrock and regional groundwater elevations before mining and theoretically after bulkhead installation. Installation of a bulkhead is therefore only acceptable if the compounded waters do not back up and reemerge at unintended or uncontrollable locations.

3.4 Conclusions

Naturally occurring stable- and radio- isotope tracers, applied salt and dye tracers, and synoptic sampling of water quality parameters were utilized to understand the hydrologic connectivity of the Rico-Argentine mine complex. Historical mining activities have led to the production of AMD at this location and accurate hydrological characterization may enable targeted remediation to reduce or eliminate the contaminated discharge. The natural tracer results suggest that the mine hydrology is driven by recharge of recent meteoric waters while the mine discharge appears to be dominated by a well-mixed groundwater signal. The synoptic sampling of water quality suggests that the most highly contaminated mine water resides in the upper mine workings located in the hillside to the southeast of Silver Creek and are diluted prior to discharging at the St. Louis Tunnel. Tracers applied to Silver Creek indicated that the creek may

be losing some water in the vicinity of the mine, but were unable to confirm or reject that Silver Creek was directly contributing water to the mine. Tracers applied directly to the mine workings indicated that mine water was moving in a south to north direction from the workings on the Blaine Tunnel side of Silver Creek to the 517 Shaft area and then draining to the St. Louis Tunnel portal. The concurrent application of a lithium salt and uranine dye tracer to the mine workings produced similar results suggesting that both type of tracers can be successfully used in acidic mine water conditions. However, it was concluded that mass recovery of the uranine dye tracer was more difficult than mass recovery of the lithium tracer because fluorescent dye mass is indirectly measured via fluorescence signal creating greater uncertainty in recovery calculations.

In combination, this suite of natural and applied tracers can provide useful information on complex hydrologic conditions that produce AMD at abandoned hardrock mine sites. The resulting hydrologic characterization of the mine sites may ultimately reduce the impacts of AMD by supporting targeted remediation efforts.

Chapter 4

Isotopic and Geochemical Approaches to Characterizing Water Movement Through Abandoned Mine Workings, Nelson-Wooster-Humphrey Tunnel Creede, Colorado

Abstract

A multiple hydrologic tracer approach is a cost effective way to address water and contaminant movement through complex abandoned mine environments. Long term acid mine drainage (AMD) discharging from the portal of the Nelson Tunnel near Creede, CO impacts water quality in West Willow Creek and the Rio Grande River. Established isotope and geochemical tracer techniques were used to quantitatively determine the sources, ages and pathways of waters in the mine. The study utilized multiple techniques including physical hydrologic parameters, hydrogeologic information, solute chemistry, applied tracers, and a suite of isotopic analyses. Results indicate that waters draining the mine are well mixed and composed to some degree of old groundwater in addition to meteoric inputs. The stable isotope (^{18}O) of the mine water is steady at -14.82 ‰ ($\pm 0.15\text{ ‰}$, $n=25$) throughout the year, suggesting a well-mixed groundwater system composed of equal parts winter snow ($-19.38 \pm 0.37\text{ ‰}$) and summer monsoon rain ($-8.89 \pm 3.13\text{ ‰}$). Tritium (^3H) values within the tunnel are primarily “tritium-dead” indicating water that is at least older than the “bomb-spike” waters of nuclear weapons testing in the 1960s. Additionally, dissolved inorganic carbon (DIC) $\delta^{14}\text{C}$ testing indicates mine water apparent ages of 5,000 to 10,000 years. To provide age verification for the DIC $\delta^{14}\text{C}$ results the mine water samples were also analyzed for the $\delta^{14}\text{C}$ of the fulvic acid fraction of the dissolved organic carbon (DOC) and provided ages similar to the DIC values. Additionally, three-dimensional fluorescence analyses of the final DOC provided characterization of the DOC and helped verify that it represented fulvic acid that was mobilized from the soil zone at the time of source water recharge. Isotopic ratios of strontium ($^{87}\text{Sr}/^{86}\text{Sr}$) were also analyzed to provide an additional geochemical tracer to differentiate between waters flowing along pathways having different host rock geochemistry. Results therefore suggest that mine waters are largely not directly connected to surface waters, or to the shallow groundwater (sampled from springs and domestic wells), but rather are comprised of deeper groundwater likely entering the tunnel via a system of faults associated with the graben structure. The results from this study are used to develop a hydrogeologic conceptual model of the mine complex, which will aid in the development and feasibility analysis of targeted remediation strategies.

4.1 Introduction

Acidic, metal-rich drainage from abandoned hard-rock mines can produce both acute and chronic water quality degradation in many areas where mining occurred (Younger and Wolkersdorfer, 2004). The combination of low pH and high concentrations of metals associated with acid mine drainage (AMD) can have severe toxicological effects on local and downstream aquatic ecosystems (Jarvis *et al.*, 1997). The legacy of past hard-rock mining in the United States includes more than 200,000 abandoned or inactive mines (U.S. EPA, 1997) with thousands of abandoned mines located near headwater regions of the Rocky Mountains of Colorado (Riebsame, 1997). As a result, concentrations of metals associated with mine drainage are exceeding aquatic water quality standards for over 1,300 river miles in Colorado alone (Lewis *et al.*, 1992).

Over the past 30 years there has been considerable research conducted on the fate and transport of AMD in rivers and surface waters (e.g. Bencala *et al.*, 1987; McKnight and Bencala, 1989; Davis *et al.* 1991; Kimball, 1996; Kimball *et al.*, 1994, Runkel *et al.*, 1999; Kimball *et al.*, 2002; Kimball *et al.*, 2007; Canovas *et al.*, 2008; Verplanck *et al.*, 2009; Nordstrom, 2011). While most of these studies provided a one time snapshot of the fate and transport of AMD at various locations, August *et al.* (2002) went a step further to observe the seasonal variability in the way a natural wetland acted as a sink (during summer) or source (winter) of metals transported from mine drainage to a receiving stream. More recently Todd *et al.* (2012) examined 30 years of streamwater chemistry from a mineralized, acidic, metal-rich alpine watershed and showed increasing concentrations of dissolved metals in surface waters during low-flow months, with causal mechanisms driven by rising air temperatures and changing climate. The considerable body of research on mining impacts to surface waters has provided a robust

understanding of the fate of AMD in the surface environment. However, this research has not addressed the subsurface hydrology associated with the production and transport of AMD.

Many of the draining mine tunnels exist in mountainous areas where groundwater occurs in fractured-rock aquifers (Walton-Day and Poeter, 2009). Characterization of groundwater flow in these areas is often challenging due to difficult or limited seasonal access and a lack of water sampling wells. A complete characterization of the hydrology within fractured rock settings requires a multidisciplinary approach using hydrologic, geologic, geophysical, and geochemical techniques (Shapiro *et al.*, 1999; Wireman, 2003). These constraints have limited the extent and type of research associated with the production and transport of AMD in mountainous areas. Additionally, there is often limited or no access to the underground workings of abandoned mines due to structural degradation of the access tunnels and considerable legal constraints. As a result the treatment of AMD has traditionally involved an end-of-the-pipe strategy (Cowie *et al.*, 2014), which is often conducted without a complete understanding of the processes involved in the production and transport of AMD and contaminated water (Lanphear, 1995). The end-of-pipe treatment strategy can be prohibitively expensive (Hazen *et al.*, 2002; Wireman and Stover, 2011) and must be maintained and operated in perpetuity.

In recent years, there has been increasing applied research related to the feasibility of source-control measures to reduce the impacts from AMD and help reduce the need for long term treatment operations (Wireman and Stover, 2011). Source control, which is a targeted remediation approach, involves controlling the inflow of groundwater into underground workings and/or controlling the outflow of mine drainage from underground workings. In order to implement adequate source control measures, the hydrologic conditions within a mine system and the surrounding surface and subsurface environment must be adequately characterized.

Within Colorado there have been a limited number of hydrologic investigations within abandoned hardrock mines including those near Leadville, Colorado (Lanphear, 1995; Hazen *et al.*, 2002; Wireman *et al.*, 2006; Walton-Day and Poeter, 2009) and a recent study conducted in Rico, Colorado (Cowie *et al.*, 2014). These studies used various combinations of data ranging from comprehensive monitoring of water levels within mines, application of artificial tracers, solute chemistry analysis, and analysis of stable isotopes of water (^{18}O and ^2H (deuterium)) to characterize the sources and flowpaths of water into and through underground mines. The results of these studies have been promising for the application of source control measures including stopping or re-routing of clean source waters away from contamination areas within the mines (Hazen *et al.*, 2002; Wireman *et al.*, 2006). Interestingly, in these studies the identified mine water sources are derived primarily from recent (years to decades) meteoric inputs with short flowpaths at seasonal to annual timescales. These relatively short residence times of subsurface water occurred in areas such as the Mary Murphy Mine and the Leadville drainage tunnel, both many hundreds to thousands of feet below the surface (Hazen *et al.*, 2002; Wireman *et al.*, 2006; Walton-Day and Poeter, 2009).

The residence time and nature of the flowpaths is likely related to the rock type and topography associated with the mined ore body, which controls surface water infiltration and groundwater movement in the vicinity of the mine environment. An accurate characterization of the sources and flowpaths is important for choosing source control remediation options. Source waters that have longer residence times and provide steady flows to a mine can be more easily quantified and controlled than recent meteoric sources that are seasonally variable in the timing, magnitude and location of inflow into a mine environment.

This paper presents a recent hydrologic investigation of the sources and pathways of water contributing to AMD discharge from the abandoned Nelson Tunnel in Creede, Colorado. The Creede mining district was formed by epithermal deposits located in a series of graben fault structures formed in conjunction with a series of volcanic calderas in the San Juan volcanic field of southwestern Colorado. The study utilized multiple techniques including physical hydrologic parameters, solute chemistry, applied tracers, and a suite of isotopic analyses. From 2000 to 2013 a series of water samples were collected from sites within the Nelson Tunnel and associated mine workings, from surface waters, natural springs, domestic wells and precipitation collectors in the West Willow Creek watershed. These samples were analyzed for stable isotope content of $\delta^{18}\text{O}$ and deuterium and the radiogenic isotope tritium (^3H). Samples were also analyzed for physical parameters (temperature and pH) along with solute and metal chemistry. Contrary to the previously mentioned Colorado mine studies, the results from the preliminary investigations indicated that the water draining from the Nelson Tunnel was not derived from recent local meteoric recharge. Primarily, injected tracer tests showed that there was rapid discharge of water from the mine but the tritium data indicated that the majority of the discharging water was relatively old – almost certainly predating the early 1960's bomb spike caused by atmospheric testing (Davies, 2002). The initial investigations also found that the water that flows through and out of the Nelson tunnel is warmer than mine waters encountered in mine drainage studies elsewhere, as much as 5 °C above the expected temperature for a standard geothermal gradient at the depth of the Nelson Tunnel level (Byington, 2012). Additionally, over several years of sampling there was minimal observable variation in the stable isotope composition of the Nelson Tunnel waters, suggesting a consistent and well-mixed source.

The recent (2009-2013) mine hydrology investigations related to the Nelson Tunnel have therefore included analyzing samples for the $\delta^{14}\text{C}$ of dissolved inorganic carbon (DIC) and dissolved organic carbon (DOC) and for strontium ($^{87}\text{Sr}/^{86}\text{Sr}$) isotopes. The radiocarbon analysis was used to gain insight on subsurface residence times of groundwater that could not be identified with the shorter-lived tritium isotopes or identified by temporal variability in stable water isotopes.

The initial findings indicated that the mine discharge water has longer residence times than seen in other mine systems studied in Colorado, and that the water may be coming from a deep, long, flowpath(s) allowing for well mixed water with a stronger than anticipated geothermal signal. The following report will discuss the results from a series of hydrologic investigations of the Nelson Tunnel with specific focus on the use of carbon and strontium isotopes to further the understanding of the hydrology producing AMD. The objectives of this paper are:

- Identify the sources and flowpaths of inflow into the mine workings that are drained by the Nelson Tunnel
- Provide a quantitative approach to identify subsurface residence times of > 50 years for water found in the Nelson Tunnel
- Analytically address the hydrologic connectivity between the Amethyst Fault (Nelson Tunnel) and the parallel Bulldog Fault system
- Develop a conceptual model of surface and groundwater hydrology in the local watershed to describe the sources of water contributing to the Nelson Tunnel and address the feasibility of source control techniques to reduce or eliminate the production of AMD in the Nelson Tunnel

4.2 Study Area and Background

Willow Creek, formed by the confluence of East and West Willow Creeks, is a tributary of the Rio Grande River near its headwaters in the San Juan Mountains in Mineral County, Colorado (Figure 4.1a). The Creede mining district, one of the largest silver mining districts in Colorado, occurs within the Willow Creek watershed which spans from the Continental Divide at ~ 3,700 m, to its confluence with the Rio Grande River below the City of Creede at an elevation of 2,682 m (figure 4.1b). During the period from 1890 to 1950 development and operation of numerous silver, gold and base metal mines significantly impaired water quality in the Willow Creek watershed. Concentrations of zinc, cadmium and lead in East Willow, West Willow and the main stem of Willow Creek exceed the water quality standards put in place by the State of Colorado. Zinc is the primary contaminant of concern, with the Nelson Tunnel discharge adding up to 75% (175 kg/day) of the load to West Willow Creek. The State of Colorado has placed the segment of the Rio Grande River below the confluence with Willow Creek on the CWA 303(d) list, which is a formal designation of impairment and requires that concrete actions be taken to restore the water quality to meet applicable standards.

A key mining facility within the Creede mining district is the Nelson / Wooster/ Humphries Tunnel (Nelson Tunnel), which was constructed to access and dewater the underground mines along the highly productive Amethyst vein and to provide a haulage route for ore from mines operating on the Amethyst vein complex (Figure 4.1b). The Nelson Tunnel is a National Priorities List (Superfund) site located in the Creede Mining District in Mineral County, Colorado.

The Nelson Tunnel is approximately 3,350 m long, was constructed between 1893 and 1902, and was operated through the first half of the 20th century (Figure 4.2). The Nelson is the lowest tunnel constructed along the Amethyst vein system and functions as a drain for the

underground workings that are connected via winzes and raises. The collapsed tunnel portal is located on the west side of West Willow Creek about one mile north of Creede. At present, access to the Nelson Tunnel is through the Commodore 5 tunnel, which is approximately 12 m above and to the east of the Nelson tunnel. The Nelson and Commodore Tunnel portals are located 120 m above the City of Creede. The Nelson Tunnel portal currently discharges an annual average of approximately 270 gpm (1.02 m³/min) and is the single largest source of dissolved zinc and cadmium to Willow Creek (WCRC, 2003). Since 2000, the pH of the portal discharge has remained between 4 and 5 and the dissolved zinc concentrations range from 52,600 µg/l to 89,800 µg/l. Dissolved cadmium concentrations range from 114 to 870 µg/l. Based on concentration and flow data collected intermittently since 2000, the Nelson tunnel contributes from 77 to 170 kg of zinc per day to West Willow Creek. These zinc loads comprise from 34% to 74% of the total zinc load to West Willow Creek. The Nelson Tunnel also contributes from 45% to 63% of the total cadmium load to West Willow Creek.

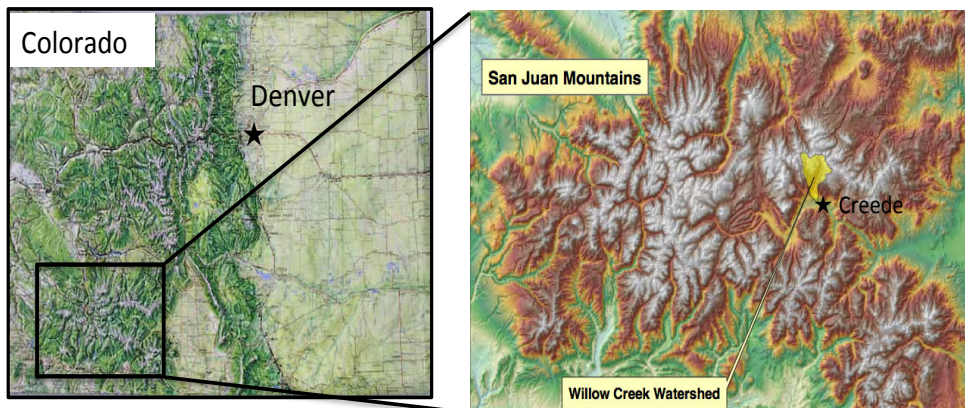


Figure 4.1A: Map of State of Colorado with location of the San Juan Mountains. Detail of the San Juan Mountains includes the location of the Willow Creek watershed located adjacent to the town of Creede, Colorado.

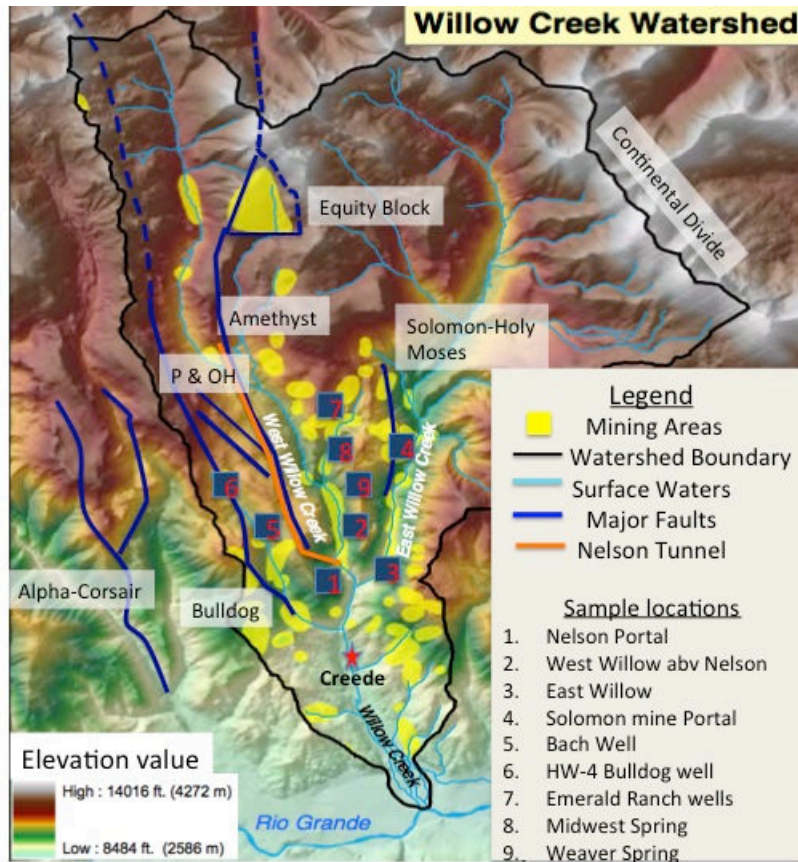


Figure 4.1b: Willow Creek watershed with areas of mining activity highlighted in yellow. The approximate locations of the major graben faults that define the Creede Mining District and the location of the Nelson Tunnel. Water sampling locations are numbered and defined in the legend.

4.2.1 Hydrologic Setting - Watershed

The Willow Creek watershed is currently an un-gauged headwater tributary to the Rio Grande. From June 1951 through September 1982 the U.S. Geological Survey operated a stream gauge (#08216500) on Willow Creek just upstream of the City of Creede. From the available record, Willow Creek at Creede represented a typical headwater stream with low winter baseflow (5 cfs) and variable spring snowmelt driven peak discharge (~70-300 cfs) generally occurring in the month of May. The major mining activity occurred above the town of Creede and to the north of the confluence of east and west Willow Creeks (figure 4.1b). Based on calculations

using the USGS streamstats (<http://streamstats.usgs.gov>) the Willow Creek watershed above the confluence of East and West Willow is 88 km² and ranges in elevation from 2,621 m at the confluence with East Willow Creek to near 4,000 m along the Continental Divide. The large elevational gradient creates considerable variation in precipitation across the catchment and although the Western Regional Climate Center (<http://www.wrcc.dri.edu/cgi-bin/cliMAIN.pl?cocree>) reports a 30-year (1985-2005) mean annual precipitation of just 34 cm for the City of Creede, CO, the USGS streamstats regression analysis predicts that mean annual precipitation for the entire watershed is 80 cm. The Nelson Tunnel drains to West Willow Creek and resides within the western portion of the Willow Creek Watershed.

To accurately quantify the recharge sources compromising the Nelson Tunnel discharge the watershed can be divided into East and West Willow Creeks from their confluence. The East Willow watershed has an area of 54 km² and estimated mean annual precipitation of 78 cm while the West Willow watershed is 34 km² and is estimated to receive 81 cm of precipitation annually. Both watersheds are snowmelt dominated with estimated peak discharges of 94 cfs and 66 cfs occurring in May and low flows of 5 cfs and 3 cfs in January in East and West Willow respectively. Additional limited discharge data is available from previous in-stream chemistry sample collection by the Willow Creek Reclamation Committee (WCRC) and U.S. Environmental Protection Agency (Herman and Wireman, 2005). The sampling included synoptic sampling at multiple locations on both East and West Willow Creeks spanning a distance of 6 km upstream of their confluence (see Herman and Wireman, 2005). The synoptic events provide a brief snapshot of the longitudinal stream profile and help identify gains/losses along the middle and upper reaches of East and West Willow Creek.

4.2.2 Hydrologic Setting - Mine

Testimony from Walter G. Boyle, the superintendent of the Nelson Tunnel during its construction (Moses, 1902), confirmed that the first large amount of water “found in the vein” was encountered at about 7,000 feet (2,134 meters) of advance, or just north of where the Amethyst shaft connects to the Commodore 5 level (Figure 4.2). Superintendent Boyle said: “we had considerable water before that in the tunnel, before we struck that big flow, but nothing to compare with what that was” (Byington, 2012). The discharge was reported to be between 5,000 and 8,600 gpm (18.9 and 32.6 m³/min) in the initial period following tunnel construction, with flow decreasing rapidly in the following years (Byington, 2012) as the groundwater was drained from storage in the fault related structures that were intersected by the tunnel. By 1919 the total flow out the Nelson Tunnel was reported at 1,200 gpm with the majority of the water coming from the hanging wall (northwest side) of the Amethyst fault (Byington, 2012).

By 1920 the vertical exploration had occurred to approximately 100 m below the elevation of the Nelson tunnel via the Commodore shaft (Figure 4.2) and numerous reports by the mine superintendents indicated that much of the water was coming up from depth into the deepest (vertically) portions of the mine (Byington, 2012). As exploration continued further north along the Amethyst fault there was also exploration to 30 m below the Nelson tunnel via the Berkshire shaft and by 1930 drifting to the north off the Berkshire shaft encountered approximately 1,300 gpm (Larson, 1930).

There is limited information on the quantity and temporal variability of discharge from the Nelson Tunnel after 1930. However, there is additional information about events that occurred on the other side of the Creede graben along the Bulldog Mountain fault system (Figure 4.1b) with respect to water encountered there during mining activities in the 1970’s, after closure

of the Nelson Tunnel mines. In 1972 development work was started on the 9,000 Level (referring to 9,000 ft (2,743 m) elevation), which is below the elevation of the Nelson Tunnel (~2,800 m). When the exploration reached the puzzle vein (not shown) the mine was pumping at a rate of 2,400 gpm, and within one year this water flow had decreased to 1,200 gpm (Jackson, 1974). Significantly, by this time outflow from the Nelson Tunnel had slowed to around 25 gpm, which was identified on 19 December 1975 as coming primarily from the Corkscrew Raise (Figure 2) (Ward, 2014). The Bulldog mine was closed and the pumps were shut off on 9 January 1985 and by March of 1986 the water elevation in the Nelson Tunnel had returned to the 2,800 m elevation and flow again increased to near present day conditions (Ward, 2014).

In 1999 a flume was installed just below the collapsed Nelson Tunnel Portal and discharge measurements have been made periodically to date. Since 2001 the discharge has consistently stayed between 250-400 gpm. The flows show some fluctuation, which is likely due to: (a) changes in the mine pool structure caused by mine collapse and blow-outs contributing to periodic surges in discharge and varying mine pool elevations, as documented by Byington (2012) and (b) due to difficult installation and maintenance the flume installed in 1999 does not capture all of the water discharging from the collapsed portal.

The historical accounts suggests that during the early years of dewatering, while active mining was occurring, the mine system was lowering the pre-mining groundwater potentiometric surface (down to the elevation of the Nelson Tunnel), while the relatively consistent current mine discharge indicates that a more steady-state groundwater flow system has been reached. The current groundwater potentiometric surface elevation is controlled by the elevation of the Nelson Tunnel discharge point.

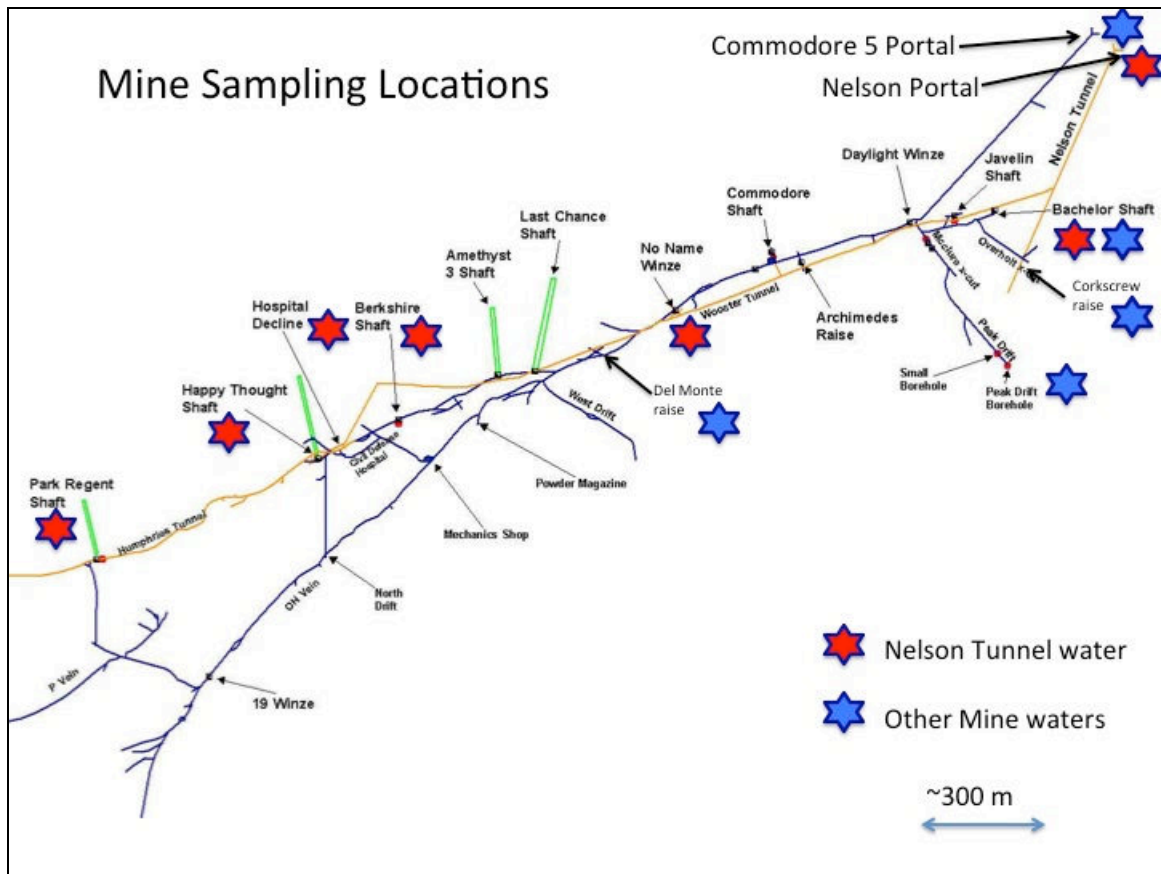


Figure 4.2: Mine sampling locations along the Nelson Tunnel (yellow line) and additional mine waters accessed from the Commodore Tunnel (blue line).

4.2.3 Paleo-Hydrogeology

Within the Willow Creek Watershed, ground water occurs in two types of geologic deposits: (1) unconsolidated surficial deposits including, glacial till, alluvium, and fan deposits and (2) volcanic rocks, including tuffs, flows, and breccias (Steven and Ratte, 1965). Except for the valley fill deposits that underlie the Rio Grande Valley, the unconsolidated deposits within the Willow Creek Watershed are thin, discontinuous and do not yield significant quantities of water to local wells (Herman and Wireman, 2005). The volcanic rocks underlying the unconsolidated deposits have low primary porosity and permeability. The occurrence and flow of ground water within these rocks is controlled by the orientation and distribution of secondary

porosity and permeability features, such as fractures or faults. Ground water intercepted by the mining excavations along the Amethyst fault likely occurs in flow systems dominated by secondary porosity created by faults, fractures and associated structures within the volcanic rocks.

To provide some insight on the present day hydrologic system examination of paleo-system provides a baseline understanding. Steven and Eaton (1975) provided the first conceptual diagram of paleo-fluid flow in the Creede system. Based on geologic observations and augmented by isotopic evidence (Bethke *et al.*, 1973), Steven and Eaton (1975) envisioned a deeply circulating hydrothermal system (~285 °C hydrothermal brine (~ 11.5 wt.% NaCl eq.)) replenished primarily with dilute (160 °C) meteoric waters. They noted that fluid flow was largely confined to fractures in welded tuffs and that the soft, overlying, non-welded tuffs forced the upwelling hydrothermal solutions to flow latterly southward. Barton *et al.* (1977) described the low-permeability horizon as being a highly altered clay cap above the vein that was the direct result of off gassing from hydrothermal fluids. The gases produced weakly acidic solutions upon condensing into the overlying wall rock. As the cap developed, it further decreased the permeability of the non-welded tuffs overlying the veins. The depth of the hydrothermal circulation was 1.6 to ~3 km while fluid inclusion evidence corroborated a 500 m paleodepth of the veins (Barton *et al.*, 1977). Work performed by Hayba (1993) utilized a two-dimensional numerical model to demonstrate that the conceptual meteorically recharged hydrothermal flow model for Creede is a viable representation of the ore-forming system. Within the model parameters included two critical hydrologic elements in the Creede ore forming system, a low-permeability (hydraulic permeability = 10^{-12} cm²) horizon (above the mineralized veins) overlying a permeable (hydraulic permeability = 10^{-9} cm²) fracture system. The recharge, flow,

and pressure head distribution described within the two component paleo-fluid flow model (Hayba, 1993) provides a reasonable characterization of the current ground water flow system in the Creede mining district.

4.2.4 Geologic Setting

Widespread volcanism formed a nearly continuous volcanic field across much of the southern Rocky Mountains in Colorado. The San Juan Mountains constitute the largest erosional remnant of this volcanic activity (Lipman *et al.*, 1970). The first phase of this volcanic activity occurred 35-30 Ma, when numerous scattered volcanoes erupted large volumes of mainly alkali andesite, rhyodacite, and mafic quartz latite lavas and breccias (Hayba, 1993). Lipman *et al.* (1970) refer to these units as the “early intermediate volcanics.” In the central and eastern San Juan Mountains, these volcanics are also known as the Conejos Formation (Steven *et al.*, 1967, Steven and Lipman, 1973). Within the district, the lithologies exposed at the surface, in mine workings, and in well holes are exclusively Tertiary volcanics and volcanoclastic sediments of the central San Juan caldera complex overlying the Conejos formation (Hayba, 1993).

Following the initial volcanic activity, there was formation of six calderas in the central San Juan complex, which erupted and deposited at least seven major ash flows over the brief interval from 28.3-26 Ma (Figure 4.3). The Creede district includes most of the Bachelor caldera (27.4 Ma) and portions of the younger Creede and San Luis calderas. Previous drill cores analyzed by Bethke and Hay (2000) show that the Creede Formation is 85% volcanoclastic sediment and 15% limestone, while the composition of the Bachelor and San Luis calderas have not been fully analyzed due to lack of drill core data. The limestone occurs chiefly as laminae,

which commonly consist of elongated pellets identified by Finkelstein *et al* (1999) as fecal pellets of brine shrimp.

The Bachelor Mountain Member of the Carpenter Ridge Tuff is the primary host for the Creede Ores. Webber (1988) believes the magma body that generated the Carpenter Ridge Tuff was at a depth of about 3-5 km. After erupting, the Creede caldera resurged, and north-to-northwest trending graben faults developed across the elongated dome (Steven and Ratte, 1965). The mineralized veins, that formed later, closely follow the trend of the initial faults (now called the Ancestral Amethyst fault, the Ancestral Bulldog Mountain fault, etc.) (Figure 4.3). There were two main periods of mineralization recognized in the Creede district. Gold-bearing ores, spatially restricted to the north Amethyst and Equity veins, characterize the first period. The second period was comprised of silver and base metal mineralization that extend across the entire district. The historic mining has targeted mineralization from both periods with greater production having come from the silver and base-metal mineralization areas of the Creede district.

The fracture system comprising the Creede graben defines the shape of the district. The Solomon-Holy Moses fault system and the Alpha-Corsair fault system bound the graben (and the district) on the east and west, respectively (Figures 4.1b and 4.3). Production from these outboard faults is small when compared to the amount produced from the silver mineralization of veins filling the interior structures of the graben: the Amethyst, Bulldog Mountain, OH, and P-vein faults. The width of this highly productive portion of the district is about 2 km while lengthwise mineralization related to the silver-rich period extends a distance of approximately 9 km along the Amethyst fault (Hayba, 1993). Mineralization in the clastic facies of the Creede Formation defines the southern limit to the system. From the southern end of the district, near

the Nelson Tunnel portal, the Amethyst vein has been worked northward continuously along strike for more than 3.3 km to the Park Regent shaft (Figure 4.2). North of that point, mineralization of the silver-rich period extends along the Amethyst vein to at least the Equity fault, but apparently not in economic concentration. To date there has been only minor production from the Equity fault and along the Amethyst vein north of the Captive Inca mine (a surface mine near the northern extent of the Nelson Tunnel in Figure 4.1b). Rio Grande Silver Inc. is currently performing exploratory work in both the north end of the Bulldog fault and the Equity Block, but any future mining is dependent on economic viability controlled by the global metals markets (McClure, 2014).

The Amethyst fault appears to die out about 2 km north of the Equity fault, but there is some evidence indicating the paleo-groundwater flow system may have extended another 8 to 10 km north of the Equity mine along the projection of the fault to the Bondholder camp (Hayba, 1993) also referred to as the Spring Creek District located on the western side of the continental divide north of the Creede Mining district. Lipman and Sawyer (1988) suggest that the Amethyst structure may be more continuous than mapped by Steven and Ratte (1973), and lead isotopic and fluid inclusion data imply a genetic link between the Bondholder and Creede Deposits (Hayba, 1993). Thompson (1992) suggests that the Bondholder may have formed from a counter-rotating hydrothermal convection cell that represents the northern complement to the Creede System.

A second important geologic structure closely associated with the Amethyst Fault is the northwest-trending OH-vein, which consists of a conspicuous zone of integrated fractures that extends at least 1,370 m northwest from the Nelson/Commodore tunnel area towards the Bulldog fault (Steven and Ratte, 1965) (Figure 4.1b). The vein is a series of interconnected tension

fractures up to 2 m wide, with a total displacement of a few ten of meters or less (Hayba, 1993). The vein extends for at least 2 km northwest from a swarm of small fractures in the hanging wall of the Amethyst vein. Beneath the vein, the fracture zone becomes an open breccia with minor quartz, chlorite, and sulfide mineralization. The only surface expressions of the OH vein are some prospect pits north of the Bach well site (Figure 4.1b) testing narrow, baron banded quartz veins, 200 m above the top of the ore body. Much of the OH-vein structure was open during mineralization, and large portions are still open as indicated by the occurrence of large crystal-lined cavities (Hayba, 1993). In fact, Barton *et al.* (1977) report an amazing degree of interconnected open space over the entire district as demonstrated by the fact that pumping water from the Bulldog Mountain fault workings lowered the water level in the pre-1920 workings on the Amethyst vein.

The lateral distance between the Bulldog and Amethyst vein systems is about 1.5 km and the nearest probable intersection of the graben faults is 1 km below the lowest mining development (~ 1,830 m elevation) (Steven and Ratte, 1973). Steven and Eaton (1975) noted that soft, poorly welded tuffs (Windy Gulch zone of the Bachelor Mountain Member of the Carpenter Ridge Tuff) overlie the open fractures that host the ore. The tuffs act as a confining layer that precludes infiltration of meteoric water from above and laterally diverts hydrothermal flow coming up from below.

In addition to the poorly welded tuffs, another possible important aquiclude is the local volcanoclastic sediments, informally known as the Bachelor sediments (Hayba, 1993). These sediments, which are predominantly fine-grained mudstone and sandstone with a few matrix-supported conglomerates (Horton, 1985), probable represent early fillings of the Bachelor caldera. The surface exposure of these sediments is very poor, and they were discovered in drill

core in the hanging wall of the Amethyst fault subsequent to Steven and Eaton's (1975) work. Limited drill records hamper the ability to define the western extent of these sediments, but they appear to have covered the entire OH vein. Simpson (1982) notes that the thickness of the sediments ranges up to 55 m, and he estimates that the bottom of the basin that the Bachelor sediments filled was relatively flat at an elevation of 3,127 m.

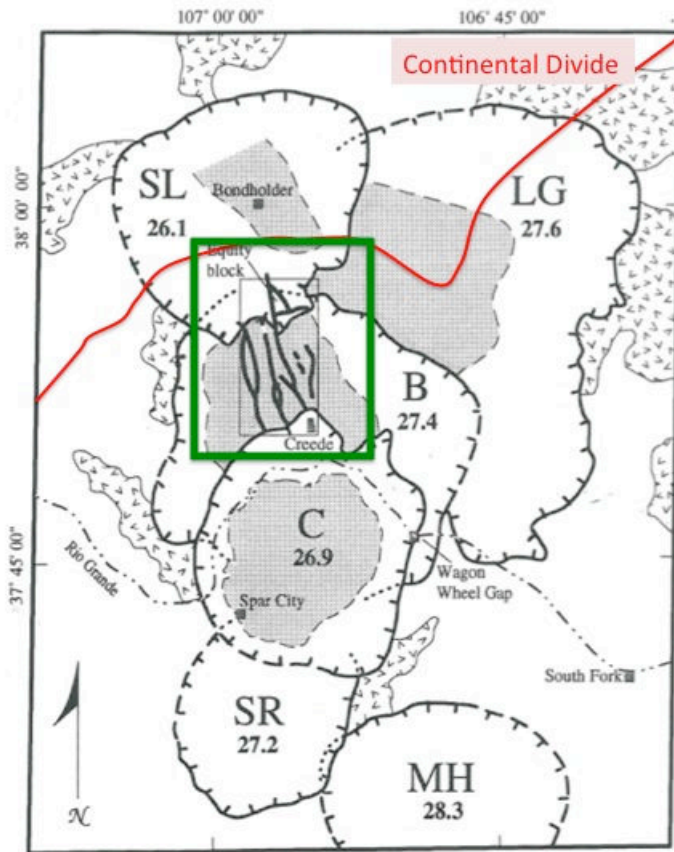


Figure 4.3: Central San Juan Caldera Complex. The Creede Mining District is highlighted by the green box while the present day Continental Divide is highlighted in red for reference. The mining district, located primarily in the Bachelor formation, is bounded to the North by the San Luis Caldera and to the South by the Creede formation. Figure modified from Hayaba (1993), Figure 1.4, p. 15.

4.2.5 Background: Water Chemistry Challenges

Carbon

Radiocarbon (^{14}C) dating of the dissolved inorganic carbonate species (DIC) in ground water has been employed for over 50 years since the early work of Munnich (1957). However, it was soon recognized that carbonate mineral dissolution (Ingerson and Pearson, 1964) and other geochemical processes might result in dilution of radiocarbon content of DIC with very old “radiocarbon dead” inorganic carbon (Wassenaar *et al.*, 1991). Consequently, the great challenge in applied groundwater radiocarbon dating is to resolve and quantify the true age controlled effect of radioactive decay from other possible influences on the measured ^{14}C activity.

There has been extensive development of various geochemical and isotopic models to attempt to quantify a DIC dilution factor, Q , to correct DIC radiocarbon ages from groundwater (Clark and Fritz, 1997; Geyh, 2000). Importantly, creating a dilution factor (Q) from geochemical reactions along the flow path requires knowledge of several factors including major ion chemistry, pH, alkalinity, recharge $P(\text{CO}_2)$, and ^{13}C and ^{14}C isotopic content of the initial DIC at recharge and of the aquifers carbonate minerals (Wassenaar *et al.*, 1991). The first step involves quantification of the hydrochemical reactions contributing to the initial ^{14}C activity of DIC in an open system (recharging groundwater in the unsaturated zone), followed by additional secondary hydrochemical reactions in the saturated zone of the aquifer (Geyh, 2000). Some of the specific geochemical processes that may alter the ^{14}C activity in groundwater include sulfide oxidation, sulfate reduction, lignite oxidation, bacterially mediated methanogenesis, and carbonate mineral precipitation (Clark and Fritz, 1997; Wassenaar *et al.*, 1991). Quantification of all the hydrochemical reactions contributing to the initial ^{14}C activity of DIC that has traveled through both open and closed systems can be quantified as the product of the individual dilution

factors (Clark and Fritz, 1997). However it is important to recognize that the preferred isotopic and hydrochemical initial field parameters employed in the calculation are seldom known precisely (Geyh, 2000). The groundwater flow systems in the Creede district are likely very complex and given the overlapping caldera complex found within the Willow Creek watershed, it was beyond the scope of this paper to determine all the necessary field parameters to constrain any theoretical model.

Aside from modeling, there are many empirical approaches that have been used to estimate ^{14}C activity and directly calculate the calibration factor used to define the assumed age of DIC in groundwater. One approach is to simply use the fixed correction value of 85 pMC (% modern carbon) as originally proposed by Vogel and Ehhalt (1963). A second approach is to reference works such as Geyh (1972), which provide initial ^{14}C activity (and reservoir age correction) for specific geologic setting. Given the structural complexity of the geologic setting for the Central San Juan Caldera complex this approach was not used. Instead, an approach developed by Verhagen *et al.* (1991) can be used which involves the construction of a “ $^3\text{H}/^{14}\text{C}$ ” diagram. This approach is applicable in systems where the groundwater may have incorporated post-nuclear CO_2 (as evidenced by the occurrence of measured ^{14}C activity greater than 100 percent modern carbon (pMC)) and determines an appropriate initial ^{14}C activity based on where the curve intersects the tritium detection limit. The reasoning is that any groundwater sample that does not contain “bomb” tritium will also be free of anthropogenic ^{14}C .

In contrast to DIC, the carbon isotope geochemistry of dissolved organic carbon (DOC) can be viewed as less complex (Wassenaar *et al.*, 1991) and represents a second independent method to calculate subsurface residence times. The DOC in groundwater can only originate from a few sources. The DOC can originate from soluble organic matter from decomposing

organic carbon sources in the soil, which is mobilized as precipitation infiltrates through the unsaturated zone of the subsurface to recharge the groundwater. DOC from these sources consists predominantly of complex carbohydrates, and humic fractions. The humics can be a significant fraction of the DOC and these fractions are produced in soils by microbial degradation of organic detritus and via oxidation of lignite or kerogen. A second source of DOC would come from kerogen or buried organic deposits that are entrained in the aquifer sediments (Thurman, 1985), however kerogen in geologic formations is often highly refractory, insoluble and existing in very small amounts (Degens, 1967). A third potential source is by products of in-situ microbial growth in the groundwater (or mine water) environment. Therefore it is reasonable to hypothesize that the DOC in ground water in most geologic formations would originate as soluble organic matter that is mobilized from the soil zone (Wassenaar *et al.*, 1991). The DOC would then move through the aquifer system at groundwater velocity. The DOC extracted from a groundwater sample at some location down gradient would be representative of carbon that was “fixed” at the time when the meteoric water (recharge) last passed through the soil matrix. The youngest recognized constituent of groundwater DOC is the group of organic compounds classed as fulvic acids (FA) (Geyh, 2000). These are the most promising molecules for dating groundwater DOC (Geyer *et al.* 1993, Aravena *et al.*, 1993). By looking at the ^{14}C isotopic content of the FA portion of DOC a relative “age” or “subsurface residence time” of a particular groundwater sample can be determined. Results can be compared to the ^{14}C results from DIC in the same samples to provide additional support for the age correction procedures discussed above.

The fulvic acid portion of DOC is isolated from water samples using the cation exchange XAD-8 technique described by Thurman and Malcolm (1981). This method involves first

passing an HCl-acidified sample through a column packed with XAD-8 resin to selectively sorb hydrophobic (fulvic) weak acids. Followed by an elution with sodium hydroxide and a rinse with DI water to remove chloride. Salts (i.e. Na⁺) are then removed in the final step using a cation exchange resin-filled column, leaving only these isolated organic carbon constituents.

To better identify the source of the isolated DOC, fluorescence analysis of the dissolved organic matter (DOM) can be performed on aliquots of the samples that are also receiving radiocarbon analysis. Fluorescence spectroscopy has proven to be a robust technique for studying the source and chemical composition of organic matter (Fellman *et al.*, 2010). However, it is important to note that there are spectroscopic difficulties in the application of fluorescence methods associated with fluorescence quenching by metal complexation and pH effects (Gabor *et al.*, 2014). To compensate for high metals content commonly found in mine waters additional steps must be taken when isolating the DOC prior to radiocarbon and spectroscopic analysis.

The most robust fluorescence analyses involve three-dimensional fluorescence scans, referred to as excitation-emission matrices (EEMs), which are acquired for a range of emission wavelengths when excited at multiple wavelengths (Gabor *et al.*, 2014). These fluorescence measurements produce a large amount of spectral data, which require analysis to be interpreted in a meaningful way. The full EEMs indicate differences in humic like and protein like compounds found in the sample. Comparison of measured EEMs with modeled EEMs (i.e. Cory and McKnight, 2005) developed using fluorescence analysis of known organic compounds, further supports identification of the type and abundance of DOC compounds in individual samples. Additionally, spectroscopic fluorescence indices can then be calculated using the EEMs to identify changes in the chemical quality of the DOC in different samples. Interpretation of the

fluorescence analyses can then assist in the interpretation of the character and sourcing of the DOC from which radiocarbon dates are acquired.

Strontium

Strontium has four naturally occurring stable isotopes, variations in the relative proportions of Sr isotopes (expressed as the ratio of ^{87}Sr to ^{86}Sr ($^{87}\text{Sr}/^{86}\text{Sr}$) are due to the formation of radiogenic ^{87}Sr from the natural beta decay of ^{87}Rb (half-life = 48.8 Ga) (Hamel *et al.*, 2010). The extremely long half-life of ^{87}Rb indicates that decay is a very slow process resulting in a slow change in $^{87}\text{Sr}/^{86}\text{Sr}$ ratios. This method is therefore used as a dating tool for rocks, by determining time since crystallization of igneous rocks such as granites (Faure & Powell, 1972).

Strontium is a relatively high-mass element, and therefore fractionation from geologic, biological, and evaporative processes is very small compared to those in the low-mass isotopic systems (e.g., H, C, O). If Rb and Sr are incorporated into a mineral or rock at its formation and the system remains closed with respect to those elements, then the amount of ^{87}Sr increases over time as radioactive ^{87}Rb decays; the amounts of ^{84}Sr , ^{86}Sr , and ^{88}Sr remain constant. Therefore, older rocks will in general have higher $^{87}\text{Sr}/^{86}\text{Sr}$ ratios than younger ones with the same initial Rb/Sr ratio.

Over geologic time, rocks of a given age composed of minerals with a high Rb/Sr ratio (e.g., granites in the continental crust), will develop a higher $^{87}\text{Sr}/^{86}\text{Sr}$ ratio than rocks with a lower Rb/Sr ratio (e.g., oceanic basalt). Thus, $^{87}\text{Sr}/^{86}\text{Sr}$ ratios in geologic materials are indicators of both age and geochemical origin. Therefore, surface and groundwater isotopic composition of strontium is a function of bedrock weathering and atmospheric inputs (Capo *et al.*, 1998). As a result the isotopic ratio of $^{87}\text{Sr}/^{86}\text{Sr}$ has been shown to be quite an effective tracer of water-rock

interactions and has been used to identify and quantify sources of groundwater constituents in areas impacted by human activity (Chapman *et al.*, 2012). Additionally, the isotopic composition of dissolved strontium in groundwater has been extensively applied to study groundwater flow paths (Banner *et al.*, 1996; Frost *et al.*, 2002; Fritz *et al.*, 2006). Strontium isotopes have also proved particularly useful in delineating flow paths and hydraulic connections between different aquifers and between meteoric inputs (rain) and ground water, which have contrasting $^{87}\text{Sr}/^{86}\text{Sr}$ ratios (Raiber *et al.*, 2009). Differences in strontium isotopic signal relative to total strontium concentration in individual water samples may therefore provide an additional independent tracer to differentiate waters that have traveled through unique subsurface environments or flow paths.

4.3 Methods

4.3.1 Sampling Locations

Sampling occurred at multiple underground locations in the Nelson and Commodore 5 tunnels and from surface water locations across the Willow Creek watershed. Additional samples were collected from several domestic wells in the area and from a well accessing mine waters in the Bulldog fault (Figures 4.1b, 4.2).

Mine Sampling

Multiple sampling events occurred in the underground workings between 2000 and 2013 with the majority of replicate samples coming from the most easily accessible locations along the Nelson Tunnel from the portal back to the Berkshire shaft area (Figure 4.2). The 2012-2013 mine investigation focused on four locations within the Nelson Tunnel: Nelson Portal, Nelson Tunnel at Bachelor shaft area, Nelson Tunnel at No Name, and the Berkshire shaft. Samples were collected as grab samples from just below the water surface with the exception of discrete

sampling in the Berkshire shaft and one sample collected from the mine pool in the bottom of the Bachelor shaft. The Berkshire shaft (a winze) descends from the Commodore 5 tunnel at approximately 2,285 m from the portal and extends to approximately 43 m below the Commodore tunnel. The Nelson tunnel is approximately 12 m below the Commodore tunnel, thus the Berkshire shaft extends to approximately 30 m below the Nelson tunnel, into flooded mine workings that extend approximately 190 m to the south and 185 m to the north into the Happy Thought area. In October 2013 samples were collected from 12, 18, and 20 m below the Commodore 5 tunnel level (top of pool was ~ 5m below Commodore 5 level), representing Berkshire water that was at and below the elevation of the Nelson Tunnel. Sampling was limited to these depths due to large amounts of debris entrained in the flooded mineshaft.

Discharge from the Nelson Tunnel has been directed through a flume since 1999 and periodically measured (see appendix 1) The flume is located within the debris of the collapsed portal and is believed to have had variable success in accurately capturing the full volume of discharge exiting the mine due to inadequate installation. Additional flumes have been installed within the Nelson Tunnel at the Bachelor and No Name locations (figure 4.2) where installation was much easier. Flow data from the underground flumes is limited to mine-entry sampling events but the data from the Bachelor flume (closest to the portal) may more accurately quantify Nelson Tunnel outflow. Within the underground workings but external to the Nelson Tunnel there were three additional locations where small (<5 gpm) discharge was observed and estimated at time of sample collection; the Peak Drift Borehole, the Park Regent Shaft, and the Del Monte Raise (Figure 4.2).

Surface Water, Springs, and Wells

Samples were collected from a number of locations outside of mine to better understand

and characterize the local and regional hydrology (Figure 4.1b). Although there were numerous abandoned mine adits and tunnels in the area, there were only two locations, the Nelson Tunnel and Solomon Mine adit, where significant discharge from mine adits could be found contributing to surface waters of Willow Creek. The Solomon Mine adit is the most significant discharge to East Willow Creek while the Nelson Tunnel discharge is the dominant mine discharge into West Willow Creek (WCRC, 2003).

Surface water samples were collected from one location on both East and West Willow Creek (Figure 4.2) at the same time the mine water samples were collected. Springs, including the Midwest and Weaver Springs along West Willow Creek, and a shallow alluvial well on the Emerald Ranch property were also sampled. The shallow well (State of Colorado permit # 197834-A) was installed on the Emerald Ranch property on 4 November 2008 as a domestic / stock well. This well was drilled to a depth of 110 m and was screened from 95 m to 110 m. The drill record suggests that this well was entirely within alluvium. The reported depth to the static water level was 32 m projecting a water table elevation of 3,230 m. The well produced about 7 gpm (0.02 m³/min).

Three additional deep wells were sampled: a domestic well at the Emerald Ranch property; a domestic well (Bach well) located near the Bachelor town site; and a monitoring well owned by Rio Grande Silver Inc. (HW-4 well), which accesses water in the Bulldog mine pool (Figure 4.1b). All wells were purged at least one full well volume followed by triplicate field parameter (DO, pH, T, SC) measurements to ensure stabilization.

The Emerald Ranch well (State of Colorado permit # 197834) was installed on 5 October 1996. The ground surface elevation is 3,262 m and the well was drilled to a depth of 247 m with casing placed from 183 to 247 m. According to the drill record, the well is constructed in

volcanic rock of the Bachelor formation (25 to 180 m) and rhyolite (180 to 247 m). The reported depth to the static water level was 140 m, making the water level elevation 3,122 m.

The Bach well (State of Colorado permit #194882) was drilled in 1996 to a depth of 400 m. The ground surface elevation is 3,161 m, thus the bottom of the well is at 2,761 m. The well maintenance contractor believes that the current depth to water was approximately 350 m suggesting about 46 m of water in the well and a water level elevation of approximately 2,810 m. From the geologic / construction log the entire depth of the well consists of several variable layers of volcanic materials, which are consistent with being part of the Campbell Mountain Rhyolite overlain by some materials from the Creede Formation.

The Homestake Mining Company installed the HW-4 monitoring well into the Bulldog Mine workings in February 1999. The HW-4 well was installed to intercept the deeper mine workings in the Campbell Mountain Rhyolite at an elevation below 2,804 m in order to determine the water level and to characterize the mine pool water. The wellhead is located in Windy Gulch at 3,168 m, between Bachelor and Bulldog Mountains (Figure 4.1b). The water level at the time of well completion was approximately 2,818 m elevation. Water levels only fluctuated between 2,818 m and 2,815 m elevation during the period of February 1999 to September 2002. In September 2012 soundings the water table was measured at 2,816 m elevation, indicating stable conditions over the past decade.

4.3.2 Nelson Tunnel Tracer Studies

In September 2001, Davies (2001) performed a groundwater tracing investigation to investigate flow conditions in the Nelson Tunnel. An injected tracer (4.5 kg of the dye sulphorhodmine [C.I. Acid Red 52]) was added as a slug injection into the water at the Berkshire shaft and an automated sampling machine was used to collect samples at a regular

frequency at the portal. The study was performed to determine travel times of water from the back of the Nelson Tunnel (accessed by the Berkshire Shaft) to the portal.

Subsequent mine investigations determined that there are actually two major mine pools in the Nelson Tunnel. A second tracer investigation was performed in September 2010 to characterize the flow regimes of the individual mine pools and to help determine where water is entering the tunnel and whether it might be exiting the tunnel before reaching the portal. The second tracer investigation used three inorganic salts injected at three discrete locations; Sodium Chloride (14.74 kg) at the Decline, Potassium Sulfate (6 kg) at the Berkshire shaft, and Lithium Bromide (3 kg) at No Name (see figure 4.2). Sampling for tracer recovery was performed using minisipper automated samplers at the No Name, Bachelor, and Nelson Tunnel Portal locations.

4.3.3 Water Chemistry Analytical Parameters

Water samples were analyzed for dissolved and total recoverable metals, and for a suite of isotopes including; ^{18}O , deuterium (^2H), tritium (^3H), strontium isotopes ^{87}Sr and ^{86}Sr , ^{14}C in dissolved inorganic carbon (DIC), and ^{14}C in dissolved organic carbon (DOC). Field parameters (pH, DO, T, SC) were measured at each location using a YSI water quality meter.

Metals Analysis

All samples for total recoverable metals analyses were collected in 250 ml HDPE sample containers that were cleaned in the laboratory. Sample containers and collection devices are rinsed three times with sample water before the sample is collected. Dissolved metals samples were preserved in the field with nitric acid to obtain a pH ~ 3. Dissolved and total recoverable metals samples were analyzed at the EPA Region 8 Laboratory in Golden, Colorado for a full suite of metals using EPA 200 series methods.

Water Isotopic analysis

The stable isotopes of water are oxygen-18 (^{18}O) and deuterium (^2H (D)). These isotopes are used by hydrologists for a variety of applications because they are naturally occurring, do not decay over time to other isotopes, and are considered conservative in reactions with catchment materials (Kendall and Caldwell, 1998).

Water samples for isotopic (D and ^{18}O) analysis were collected unfiltered in cleaned 25-mL borosilicate bottles with no-headspace lids to avoid any evaporation or fractionation. The D and ^{18}O analyses were performed at the Kiowa Environmental Chemistry Laboratory in Boulder, Colorado using an L1102-i Isotopic Liquid Wavelength- Scanned Cavity Ring Down Spectroscopy (WS-CRDS), which is a time-based measurement using near-infrared laser to quantify spectral features of molecules in a gas ratio of the sample to the Vienna Standard Mean Ocean Water (V-SMOW), as shown for ^{18}O :

$$\delta^{18}\text{O} = \frac{(^{18}\text{O}/^{16}\text{O})_{\text{SAMPLE}} - (^{18}\text{O}/^{16}\text{O})_{\text{VSMOW}}}{(^{18}\text{O}/^{16}\text{O})_{\text{VSMOW}}} \times 1000 \quad (\text{Equation 4.1})$$

The precisions of $\delta^{18}\text{O}$ was +/- 0.028.

Tritium (^3H) has a half-life of 12.43 years and is the only conservative tracer that can be used to determine the age of water older than one year. Tritium is produced both by cosmic-ray spallation and by atmospheric nuclear weapons testing. The steady-state level of tritium on the earth from natural processes is about 3.5 kilograms (Lal and Peters, 1967). However, atmospheric testing of nuclear weapons in the 1950s and 1960s produced several hundred kilograms of tritium (Michel, 1976). About 80 kilograms of this isotope are still present on the earth's surface at this time. As a result, the tritium input function is a large spike, with highest concentrations in the early 1960s. Water deposited on the earth's surface prior to nuclear

weapons testing has low tritium concentrations and most of that tritium will have decayed in the intervening years. Thus, if no tritium is present in a water sample, that water can be presumed to be greater than 50 years old. If detectable tritium is present, it is an indication that some fraction of the water has been derived from precipitation since the early 1950s. In 2011 the mean tritium concentrations in precipitation in the San Juan Mountain region of Colorado was 6.2 Tritium Units (TU) (Cowie *et al.*, 2014). Using the historical tritium record, it is possible to use tritium concentrations to put some limits on the ages of water sampled. Tritium's useful timescale is on a decadal level with a maximum range of about 50 years.

Water samples analyzed for tritium were collected as unfiltered grab samples in 1 liter (L) HDPE bottles and kept at 4°C until sent to the USGS Tritium Laboratory in Menlo Park, California for analysis by electrolytic enrichment and liquid scintillation counting. Distilled sample water was reduced electrolytically in electrolysis cells to 10 mL from an initial 200 mL in a cooling bath. This increases the concentration of tritium by a factor of 16. The remaining liquid is mixed with a scintillation cocktail of known tritium concentrations to improve baseline values. The sample is reported in Tritium Units (TU), which are 1 tritium atom per 10^{18} hydrogen atoms. The detection limit is reported as twice the precision.

Dissolved Inorganic Carbon (DIC) Isotopic Analysis

Samples for ^{14}C DIC were collected in 500 ml borosilicate glass bottle with a high-quality ground-glass stopper. The stopper is lubricated prior to collection with Apiezon grease to prevent exchange with the atmosphere. Prior to installation of the stopper, 100 μl of saturated HgCl_2 solution was added to each sample. Samples were shipped to the National Ocean Sciences Accelerator Mass Spectrometry Facility (NOSAMS) at the Wood Hole Oceanographic Institution.

The AMS laboratory performed radiocarbon analysis by stripping of CO₂ gas from water samples. The carbon dioxide is reacted with Fe catalyst to form graphite. Graphite is pressed into targets, which are analyzed by accelerator mass spectrometry along with primary and secondary standards and process blanks. The primary standard NBS Oxalic Acid 1 was used for all ¹⁴C measurements.

The Fraction Modern (Fm) is a measurement of the deviation of the ¹⁴C/C ratio of a sample from “modern”. Modern is defined as 95% of the radiocarbon concentrations (in AD 1950) of NBS Oxalic Acid I normalized to $\delta^{13}\text{C}_{\text{VPDB}} = -19$ per mil (Olsson, 1970). The results are calculated using the internationally accepted modern value of $1.176 \pm 0.010 \times 10^{-12}$ (Karlen, *et al.*, 1964) and a final ¹³C-correction is made to normalize the sample Fm to a $\delta^{13}\text{C}_{\text{VPDB}}$ value of -25 per mil. AMS analyses made on the 500 kilovolt AMS systems were corrected using measured ¹²C/¹³C ratios, but the AMS laboratory does not report the ratios. Reporting of ages and/or activities follows the convention outlined by Stuiver and Polach (1977) and Stuiver (1980). Radiocarbon ages are calculated using 5,568 years as the half-life of radiocarbon and are reported without reservoir corrections. A $\Delta^{14}\text{C}$ activity normalized to 1950 is also reported according to these conventions. Atoms of ¹⁴C contained in a sample are directly counted using the AMS method of radiocarbon analysis, therefore, internal statistical errors are calculated using the number of counts measured from each target in combination with the errors of the standard. An external error is calculated from the reproducibility of individual analyses for a given target. The error reported is the larger of the internal or external errors. Age correction was applied to the radiocarbon dates using a ³H/¹⁴C curve developed by Verhagen *et al.* (1991).

Dissolved Organic Carbon (DOC) Isotopic Analysis

Samples for ^{14}C DOC were collected in cleaned 5-gallon HDPE buckets with lids. Within two hours of sampling the water was filtered using a geopump and in-line 142mm diameter burned 0.45-micron glass fiber filter following filtration protocols from Kiowa Laboratory at the University of Colorado. The filtering prevented Fe^{2+} from oxidizing and precipitating, which would strip out the humic components of the DOM. The filtered water was transferred into 1L brown amber glass bottles and treated with 2M HCL to obtain a sample pH of 3.0. Acidifying samples stabilized the Fe^{2+} . Each sample was a minimum of 4L. Prepared samples were kept at 4 °C and shipped to the Kiowa Laboratory. Before processing the samples for radiocarbon analysis a small aliquot of each sample was run through a Shimadzu Total Organic Carbon Analyzer at the Kiowa Laboratory to measure total DOC concentrations. Within run, and run-to-run precision was 1.33% relative standard deviation of standard duplicates with a detection limit of 0.07 mg CL⁻¹.

In this study several water samples were analyzed for the whole component of the DOM, but due to the high salt content of the mine waters, damage to laboratory equipment prevented whole component DOM analysis on all samples. Instead the fulvic acid portion of DOC was isolated from water samples using the XAD-8 technique described by Thurman and Malcolm (1981). This method involves first passing an HCl-acidified sample through a column packed with XAD-8 resin to selectively sorbs hydrophobic (fulvic) weak acids. Followed by an elution with sodium hydroxide and a rinse with DI water to remove chloride. Salts are then removed in the final step using a cation exchange resin-filled column, leaving only these isolated organic carbon constituents. The DOC samples eluted from the XAD-8 were freeze-dried and stored in sealed glass bottles. Due to high concentrations of iron and other metals in the samples, the samples required multiple runs through the cation exchange column to remove as much of the

metals as possible. The purified humic substances were graphitized (combusted in a pure oxygen atmosphere, and the resulting CO₂ gas was trapped and purified cryogenically for the carbon isotope analysis) at the Laboratory for AMS Radiocarbon Preparation and Research (NSRL) in Boulder, Colorado. The processed samples were analyzed for radiocarbon content by Accelerator Mass Spectrometry (AMS) at the W. M. Keck Laboratory, University of California-Irvine.

Dissolved Organic Carbon (DOC) Fluorescence Analysis

A subset of each eluted water sample was also sent to the McKnight Organic Matter Spectroscopy Laboratory at the Institute of Arctic and Alpine Research to measure the amount and character of the DOC. All humic substances have fluorescent properties, and fluorescence spectroscopy can indicate differences in precursor organic source of humic substances (Klapper *et al.*, 2002). Three-dimensional Fluorescence spectroscopy was performed on an Agilent 8453 spectrophotometer. Excitation emission matrices (EEMs) were created for excitation wavelengths 245- 450 nm at every 10 nm and emission wavelengths 300 to 550 nm at every 2 nm with an integration time of 0.25 s and a slit width of 5 nm. Excitation emission matrices were corrected for variations in lamp intensity by normalizing the sample scan to the reference scan (ratio mode) (Cory *et al.*, 2010). Samples were also corrected for both instrument response and inner-filter effect prior to being Raman-normalized (Lawaetz and Stedmon, 2009).

The EEMs were then modeled by parallel factor analysis (PARAFAC) using the Cory-McKnight model (Cory and McKnight, 2005). PARAFAC statistically resolves EEM data sets of complex mixtures such as DOM into components without making any assumptions on the shapes of the spectra (Stedmon *et al.*, 2003). The model identifies thirteen components, likely

representing groups of similarly fluorescing moieties, which explain the variation of the data (EEM). Of the thirteen components there are seven, which are known as quinone-like. Quinones are a versatile class of biomolecules found in living cells, in extracellular material, and in detrital organic material (produced by oxidation of lignin). There are an additional two components of the Cory-McKnight model, which are identified as amino acid-like based on comparison to tyrosine and tryptophan fluorescence spectra. When the residuals of measured and modeled results show mostly noise, it confirms that the PARAFAC model accounts for all discernable fluorophores and provide confidence that the isolated DOC is derived from precursor sources acquired from the soil during recharge.

Strontium

Strontium samples were collected, unfiltered, in 250 mL HDPE bottles and sent to the G. Lang Farmer Lab at the Cooperative Institute for Research in Environmental Sciences (CIRES) at the University of Colorado, Boulder. Strontium isotopic analyses were obtained using a Finnigan-MAT 261, 6-collector thermal ionization mass spectrometer. $^{87}\text{Sr}/^{86}\text{Sr}$ ratios were analyzed using four-collector static mode measurements and were normalized using an internal laboratory standard. One measurement of the primary standard SRM-987 during study period yielded $^{87}\text{Sr}/^{86}\text{Sr}=0.71029\pm 0.00001$. Total strontium concentrations were also measured as part of the metals analysis described above.

4.4 Results and Discussion

4.4.1 Water Temperatures

There were 26 measurements of water temperature from 7 different locations along the Nelson Tunnel between 2001 and 2013 (Figure 4.4, Appendix 1). Water temperatures were also

taken from seven additional mine locations external to the Nelson Tunnel. Sites within the Nelson Tunnel have a consistent water temperature of 19.4 ± 1.2 °C. The temperature of the water in the Nelson Tunnel decreased by just 3.3 °C from the deepest location (Nelson Tunnel at Decline) to the tunnel portal. Seven additional mine water temperatures were measured at mine locations other than the Nelson Tunnel. The auxiliary mine waters had a larger range of temperatures (11.2 ± 4.0 °C) but were lower than the Nelson Tunnel waters. The highest temperature of auxiliary water was found in the Bachelor Shaft proper (16.1 ± 0.4 °C), which was upwelling from an elevation equal to or below that of the Nelson Tunnel. The lowest temperature mine water was located at the Commodore Tunnel adit (4.4 °C), likely influenced by atmospheric conditions. All of the other auxiliary locations (except the Berkshire Shaft samples) represented low volumes (< 5gpm) of water coming from rock wall seepage or bore hole discharges at elevations above that of the Nelson Tunnel waters. The temperature of the water in the Bulldog mine pool (via HW-4 well) was also elevated at 17.7 °C. Local surface waters were between 2-5 °C during sampling in October 2012 and February 2013 while the groundwater from the nearby domestic Bach well was 7.8 °C. The Solomon adit discharge was sampled outside of the adit portal in February 2013 so the temperature of 11.9 °C is likely lower than the adit discharge prior to discharging from the portal.

The elevation of Nelson Tunnel mine pool water is between 2,804 and 2,816 m (Appendix 1), which is approximately 1 km below the elevation of the upper Willow Creek Watershed along the Continental Divide. If it is assumed that the water was recharged predominantly from snow melt at high elevation (> 3,800 m), then it can be inferred what the approximate water temperature was at recharge, and following a standard geothermal gradient of 25 °C/km, it is reasonable to see 20 °C waters emerging at the Nelson Tunnel portal. In addition,

the Amethyst fault is believed to continue vertically down to an elevation of 1,800 m before intersection with the parallel Bulldog Fault creating a potential significant secondary porosity pathway for some of the meteoric water recharging along the divide to circulate to depths of 2 km before discharging into the mine workings associated with the Nelson Tunnel. Circulation to depths of 2 km would therefore be sufficient to produce >20 °C water in the mine pools, which is in contradiction to Byington (2012) which stated that the Nelson Tunnel water temperatures are as much as 5 °C above the expected temperature for a standard geothermal gradient at the depth of the Nelson Tunnel level. It is therefore assumed that the previous report was simply considering that meteoric recharge was only occurring as vertical flow from directly above the mine workings, which would only generate a 300-400 m gradient for recharge to acquire the elevated geothermal signal. The results therefore suggest the water is traveling along longer and deeper flowpaths that allow contact with host rock that has sufficient geothermal heat to generate water temperatures observed in the Berkshire shaft and the Nelson Tunnel.

Based on the volcanic activity that occurred in the Creede system it is generally assumed that the heat responsible for driving ore formation was derived from magmatic intrusions. The intrusion(s) that provided the heat engine for the main period of mineralization likely also occurs beneath the northern part of the district (Hayba, 1993). Steven and Eaton (1975) suggested the intrusion was located several kilometers beneath the center of the main mining district. District-wide syntheses of fluid inclusion and stable isotope studies have helped clarify the location of the main stage heat source. The fluid inclusion results show a general northward increase in temperature with the hottest fluids found along the Midwest and northern Amethyst veins (Hayba, 1993). The triple junction of the La Garta, Bachelor, and San Luis calderas is a likely site for the emplacement of a pluton (igneous intrusion) capable of driving the ore-forming

system (Bethke and Lipman, 1987). Although the mineralization period was ~20 Ma, the latent heat from this pluton could still be present in the host rock at the depths to which the ground water may be circulating prior to arrival at the Nelson tunnel. Therefore both the potential depth of circulation and the legacy of volcanic activity are reasonable explanations for the high water temperatures found in the Nelson Tunnel waters.

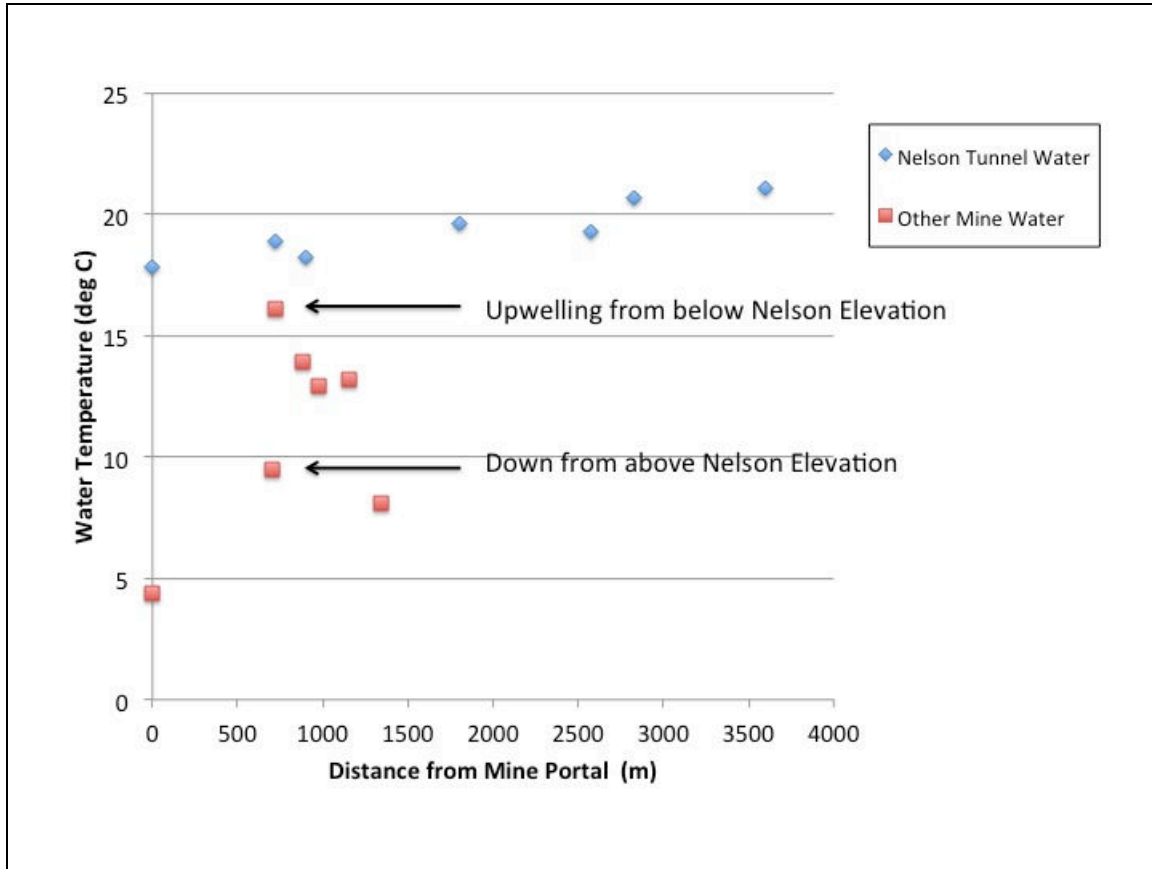


Figure 4.4: Mean water temperatures from different locations in the Nelson Tunnel (blue) and other waters encountered in the mine (red), plotted as distance from the Nelson Tunnel portal. There were between 2 and 8 samples collected at each Nelson Tunnel location and 1 to 2 samples per location away from the Nelson Tunnel. The standard deviation at all locations was $<0.9^{\circ}\text{C}$.

4.4.2 Tracer Tests

The ground water tracing investigation conducted within the Nelson Tunnel in September 2001 produced quantitative results, which revealed hydraulic parameters along the tunnel pathway and demonstrated that there was rapid discharge of water from the mine. Following the slug injection of sulphorhodamine B into the Berkshire shaft, tracer recovery was performed for 1200 hours at the Nelson Portal with 47% of the tracer recovered over that period (Davies, 2001). The tracer test showed a typical breakthrough curve with a mean tracer velocity of 10.9 ± 0.16 m/hr and a maximum tracer velocity of 44.7 m/hr, demonstrating that there is rapid discharge of water along the 4.8 km of Nelson Tunnel from the Berkshire Shaft to the portal. A portion of the tracer was also detected at a seep in the west bank of Willow Creek auxiliary to the Nelson Portal suggesting that not all of the mine discharge is being captured at the portal flume. This result therefore confirms that the discharge calculated at the portal flume is an underestimate of the total mine discharge.

The second ground water tracing investigation in September 2010 defined the flow of water along the Nelson Tunnel floor and demonstrate that there are two main mine pools with varying flow rates. The sodium and potassium tracers were injected simultaneously at the Decline and Berkshire locations, and were detected at the Bachelor location within one hour of each other (170 and 171 hours respectively). The maximum tracer velocity was thus approximately 10 m/hr from both locations to the Bachelor location. The third tracer, lithium, was injected into the Nelson Tunnel flow at No Name with first arrival at the Bachelor location in just 42 hours and then at the Nelson Portal in 52 hours. The maximum tracer velocity was thus 26 m/hr from No Name to Bachelor and 35 m/hr from No Name to the Nelson Tunnel Portal. The results from this test suggest that the upper mine pool, located between the Decline

Shaft and No Name Winze, is the slowest moving portions of the Nelson Tunnel flow and likely has significant lateral exchange due to eddies, tunnel blockages, and dispersion and diffusion with less dominant down-tunnel advection. In contrast to this, the lower mine pool, located between No Name Winze and the tunnel Portal, had much greater flow velocities and produced a well-defined tracer breakthrough curve at both the Bachelor and Nelson Tunnel Portal locations, which indicated advection-dominant channelized flow with likely no additional inflows of water.

The results from the 2010 tracer test therefore suggest that the hypothesized upwelling tunnel inflows are occurring somewhere within the upper mine pool between the Decline Shaft and the No Name location. The inflowing water is generating a well mixed mine pool which allowed both tracers (sodium and potassium) to be mixed into the mine pool before flowing down-gradient at similar velocity and simultaneously arriving at the No Name location. A preliminary underground investigation by the Colorado Division of Reclamation, Mining and Safety on December 5, 2002 revealed an upwelling source of water in the Nelson Tunnel between 335 and 395 m north of the No Name Winze. A tunnel blockage up gradient from No Name currently limits safe access into this portion of the flooded upper mine pool but the combined tracer and physical investigation information further constrain the location of upwelling waters into the Nelson Tunnel to between approximately 2,100 and 2,600 m back from the portal. The exact location of inflowing water cannot be determined, but is constrained to the region of the Nelson Tunnel associated with either the sub-Nelson workings accessed by the Berkshire and/or the complex fracture systems associated with the spiral fracturing associated with the OH vein (Figure 4.2).

4.4.3 Discharge and Water Balance

In the Creede district there are dozens of abandoned mines and adits but only two

significant (acidic) mine discharge points; the Nelson Tunnel and the Solomon Mine adit (Herman and Wireman, 2005). The Solomon mine discharge is quite small (2 to 18 gpm) (WCRC, 2003) and drains to East Willow (Figure 4.1b). There are no continuous data sets for surface water discharge in the upper East and West Willow creek watersheds. However, several discrete synoptic sampling events conducted by the U.S. EPA in conjunction with the U.S. Fish and Wildlife service and the Willow Creek Reclamation Committee provide some information on the character of the surface flows in the upper Willow Creek watershed (see Appendix H in Hermann and Wireman, 2005). Synoptic water quality and flow sampling at 13 locations on East Willow and 14 locations on West Willow in September 1999 (baseflow conditions) documented clear differences in discharge between the two catchments. In West Willow flows nearly doubled from 6.3 cfs to 11.5 cfs along the upper reach from 5.9 to 2.9 km above confluence with East Willow and then remained relatively steady (± 2 cfs) with a small increase to 13.1 cfs directly above the confluence with East Willow. Conversely, flow in East Willow increased from 18.8 cfs to 28.9 cfs along the upper reach from 4.7 to 2.3 km above the confluence with West Willow and then decreased to 18.6 cfs at 1.3 km above the confluence before again increasing to 27.6 cfs at 1.1 km and then decreasing to 22 cfs at the confluence. The results indicate that West Willow, during low flow, has little exchange (i.e. gains or losses in flow) with interflow or groundwater as it passes through the main mining district and flows parallel with the Amethyst fault (Figure 4.1b). Meanwhile East Willow Creek has greater fluctuations in flow along the 5 km reach above the confluence with West Willow, indicating greater exchange with the subsurface and a greater potential for multiple flow paths contributing ground water to the stream within the East Willow portion of the Creede mining district.

Water Balance

A water budget determines how much water is typically delivered to the watershed and its fate by calculating the amount of Water Flow Out (surface water and groundwater—including discharging mine water) + Evapotranspiration (ET) + Recharge (surface and ground) = Water In. Limited discharge and meteorological data in the Willow Creek watershed prevent water budget closure, however using estimated inputs (from USGS streamstats) and the available data for Nelson Tunnel discharge, insight can be gained on the magnitude of Nelson Tunnel waters to the system.

Based on 20 discharge measurements between 1999 and 2012 the mean discharge from the Nelson tunnel was 268.6 ± 40.8 gpm (Appendix 1). During that period there were also nine discharge measurements made in the Nelson Tunnel at Bachelor, indicating a mean discharge of 285.7 ± 6.35 gpm. The slightly higher (and less variable) discharge at the Bachelor location suggests that on average approximately 5% of the discharge from the Nelson Tunnel is not captured at the flume. Detection of Nelson Tunnel applied tracers at above ground locations (seep) external to the portal flume (Davies, 2001) support the loss in flow between the Bachelor location and the portal flume, suggesting that the discharge measured at the Bachelor location more accurately represents Nelson Tunnel discharge. Assuming that the West Willow Creek watershed above the confluence with the Nelson Tunnel (33.9 km^2 , 81 cm annual precipitation) represents a reasonable input, then the Nelson Tunnel discharge represents 2.07% of the annual recharge to the West Willow Creek watershed.

If we consider the ground water intercepted by the Nelson Tunnel to represent some component of mountain block recharge (MBR) in the Willow Creek watershed, then the annual volume of Nelson Tunnel portal discharge is a reasonable quantity but less than that reported in

other studies. For Example, Aishlin and McNamara (2011) estimated that 14% of annual precipitation was partitioned to groundwater recharge in a similarly sized mountain headwater catchment in the Dry Creek Experimental Watershed in southwestern Idaho. At the upper end of deep recharge estimates, Graham *et al.* (2010) attribute as much as 44% of a hillslope irrigation water balance in a forested catchment to deep seepage.

Given that the Nelson Tunnel/Amethyst Fault system is not oriented perpendicular to the watersheds topographic gradient, it is not expected that the workings would be intercepting all deep groundwater flow leaving the catchment. However, given the documented hydrologic connectivity between the Bulldog and Amethyst faults it may be appropriate to consider the areal extent of the Bulldog fault structure when calculating the potential recharge. The Bulldog fault lies below the western boundary of the Willow Creek drainage (Figure 4.1b) and likely extends beyond the northwestern boundary of the West Willow Creek watershed and into the Rat Creek watershed to the west. Additionally, there is mineral emplacement evidence suggesting that the Amethyst and/or Bulldog faults extend beyond the Continental Divide to the north. As a result, the calculated percentage of annual West Willow Creek discharge coming from the Nelson tunnel likely does not represent all of the potential MBR but still represents a measureable amount of the subsurface water in the catchment and may also contain some recharge occurring external to the Willow Creek topographic boundary.

Within the mine complex there were only three locations away from the Nelson Tunnel that had measureable amounts of discharge. The Peak Drift Borehole was measured at 2.7 gpm in June of 2009. Flowing water was also documented and sampled (but not quantified) from the Corkscrew Raise in June 2009. In June of 2003 the Park Regent shaft at the back of the mine also had some minor flow (<5 gpm) at the Commodore tunnel level but the Nelson Tunnel was dry at

this location. The flows at all of these locations were sampled at a location higher than the elevation of the Nelson Tunnel and are likely from more recent meteoric waters directly infiltrating the upper mine workings via surface expressions. The sum of flows from these locations is < 5% of the Nelson Tunnel discharge and therefore suggests that localized direct recharge represents a minor source contribution to mine discharge.

4.4.4 Groundwater Elevations

A preliminary underground investigation on December 5, 2002 identified an upwelling source of water in the Nelson Tunnel between 335 and 395 m north (up gradient) of the No Name Winze. The water elevation at this location was 2,818 m, which was the highest elevation of water in the Nelson Tunnel at that time. Subsequent water level measurements in the Nelson Tunnel upper mine pool (No Name to Berkshire shaft) have indicated a relatively steady water level of $2,816 \pm 2$ m throughout the study period (Appendix 1). In February 2007 a dewatering of the upper mine pool was attempted to try and better characterize the reported inflows to the Nelson Tunnel. The water was pumped from the Nelson Tunnel at the Del Monte Raise and was stored behind bulkheads in the West Drift portion of the Commodore 5 level. The pumping occurred at a rate of 500 gpm, which was estimated to be double the rate of the stable inflow/outflow rate of ~250 gpm. The pump test was able to move 300,000 gallons of water, resulting in a small drawdown of the mine pool, which was recorded as a decrease in the top of water elevation from 2816.2 m to 2814.8 m in the Berkshire Shaft. From the results the upper mine pool has an estimated volume of 19.4 million gallons, and therefore only about 1.4% of the mine pool was moved during the pumping test. From a water balance perspective the volume of water in the upper mine pool would be replaced approximately every 50 days assuming steady

inflow/outflow, and therefore the mine is storing ~14% of the annual Nelson Tunnel discharge. The volume of water stored in the Amethyst fault system is difficult to quantify due to extensive fracture systems beyond the accessible extent of the mine workings and the likely hydrologic connection with the groundwater found in the Bulldog Fault.

At the time of Bulldog HW-4 well sampling in February 2013 the mine pool elevation in the Bulldog fault system was 2,815 m, remarkable close to that in the Nelson Tunnel. The water level in the Bach well, which was sampled on the same day as the HW-4 well, was at 2,816 m. The Bach well is located in the intragraben area between the Bulldog and Amethyst faults, but is down gradient (south) of the fracture systems associated with the P and OH veins (Figures 4.1b, 4.2).

The two wells located on the Emerald Ranch property provide some additional information on water table elevations north of the Nelson Tunnel workings. Both wells are located at 3,262 m but access water at different elevations with the shallow alluvial well intercepting water at 3,230 m and the deeper bedrock well intercepting water at 3,122 m. The Emerald ranch is located to the east of West Willow Creek (Figure 4.1b) while the mine workings are located to the west of West Willow Creek at this location. The shallower well is intercepting ground water that is likely flowing through recent alluvial deposits and unconsolidated layers of volcanoclastic sediments and not interacting with a deeper groundwater system, while the deeper well is certainly accessing a deeper groundwater system that may or may not be associated with the flow system arriving in the Nelson Tunnel. Groundwater in fractured bedrock may have very localized hydrologic gradients so it is difficult to determine if the bedrock groundwater at Emerald Ranch is hydrologically connected to the waters in the mine systems from elevation alone.

4.4.5 Water Chemistry

Metals

Metals results from the current mine sampling investigation (Appendix 2) indicated little change in mine water chemistry from what had been observed in two previous sampling campaigns conducted in 2005 and 2009. The Colorado Department of Public Health and Environment (CDPHE) has identified much of Willow Creek watershed as exceeding the State of Colorado criteria for aluminum, cadmium, copper, lead, and zinc (Herman and Wireman, 2005). Zinc has been identified as the primary contaminant of concern for waters discharging from the Nelson Tunnel (Herman and Wireman, 2005) and will therefore be used to characterize the metals results from the three independent sampling events. From February 2005 to January 2006 there were twelve samples collected from the Nelson tunnel portal in which dissolved zinc had a mean concentration of 59,433 $\mu\text{g/l}$ and ranged from 52,100 $\mu\text{g/l}$ in January 2006 to 67,600 $\mu\text{g/l}$ in August 2005. During this time five samples were collected from the Nelson Tunnel at the Bachelor Shaft access point producing a mean concentration of 61,780 $\mu\text{g/l}$ with a low of 55,500 $\mu\text{g/l}$ in January 2006 and a high of 65,500 $\mu\text{g/l}$ in November 2005. In June of 2009 an additional round of metals samples was taken in conjunction with the first round of sampling for water and carbon isotopes presented in this study. Dissolved zinc at the Nelson Tunnel Portal was 56,000 $\mu\text{g/l}$ and increased to 58,400 $\mu\text{g/l}$ at Bachelor, 62,800 $\mu\text{g/l}$ at No Name, and 60,800 $\mu\text{g/l}$ at Decline. A sample was also collected at the top of the flooded Berkshire shaft (~15 m above Nelson Tunnel elevation), which had a concentration of 32,200 $\mu\text{g/l}$. The lower concentration of dissolved zinc in the Berkshire water at this location was likely a result of incomplete mixing due to stratification of the water column above the actively moving waters at the depth of the Nelson Tunnel.

A third round of samples were collected in October 2012 in conjunction with the second round of sampling for water and carbon isotopes which included the collection of samples from depth in the Berkshire shaft. The Nelson Tunnel Portal dissolved zinc (52,600 µg/l) was similar to previous values as were those at the Bachelor (54,700 µg/l) and No Name (58,100 µg/l) indicating relative steady state conditions for metals contributions to the Nelson Tunnel discharge over the period of record. Interestingly, the samples collected in 2012 from 12, 18, 20 m below the water table in the Berkshire shaft had much higher concentrations of dissolved zinc (95,200 µg/l, 93,300 µg/l, and 95,600 µg/l respectively) than found at the top of the Berkshire shaft in 2009 or at any other locations.

The reduction in dissolved zinc at the top of the Berkshire shaft mine pool as the mine water moves towards the Nelson Tunnel Portal can be partially explained by oxygenation of the mine waters. The dissolved oxygen in the 20 m Berkshire sample (0.7 mg/L) was the lowest measured in the Nelson Tunnel and it steadily increased to 4.3 mg/L at No Name, 5.7 mg/L at Bachelor and 6.3 mg/L at the Nelson Tunnel portal. The shift from anaerobic to aerobic conditions promoted oxidation (likely with the aid of lithotrophic prokaryotes) of soluble ferrous iron (Fe^{2+}) to ferric iron (Fe^{3+}), which readily precipitates, even at low pH (Nordstrom, 2011). Although speciation of iron content was not performed, there was a large decrease in the total dissolved iron content from 11,400 µg/L at 20 m depth in Berkshire to <1,250 µg/L at the Nelson Tunnel Portal. As a result the iron acted as a sorbent for the zinc and other trace metals, leading to coprecipitation of zinc with the insoluble ferric iron (Lee *et al.*, 2002).

Results suggest that the mine water is of lowest quality (highest metals content) at the deepest accessible mine locations, but without complete dewatering of the flooded mine workings (i.e. the sub-Nelson workings) it is unclear whether the degraded water quality has

occurred prior to inflowing into the mine.

4.4.6 Stable Water Isotopes (^{18}O , ^2H)

Sampling of stable water isotopes included precipitation (rain and snow), surface water, groundwater, and mine water. Samples were collected from 2007 to 2013 at multiple different times of the year to characterize seasonal variability (Appendix 3). The $\delta^{18}\text{O}$ value for snow of -19.38‰ and the mean rain value of -8.89‰ are characteristic values for the Colorado Rocky Mountains for winter and summer precipitation (Liu *et al.*, 2004). Results are plotted as the δD - $\delta^{18}\text{O}$ relationship (Figure 4.5a). Empirical results have shown that the $\delta\text{D}/\delta^{18}\text{O}$ values in precipitation co-vary and are generally described by the relationship (Craig, 1961)

$$\delta\text{D} = 8 \delta^{18}\text{O} + 10 \quad (\text{Equation 4.2})$$

which is defined as the Global Meteoric Water Line (GMWL). The Local Meteoric water line (LMWL), based on the δD - $\delta^{18}\text{O}$ relationship for all precipitation samples in our study, has similar slope and y-intercept:

$$\delta\text{D} = 8.1\delta^{18}\text{O} + 9.9 \quad (\text{Equation 4.3})$$

The similar values in slope between the LMWL (8.1) and the GMWL (8.0) suggest an absence of complex kinetic fractionation processes affecting the δD - $\delta^{18}\text{O}$ relationship of precipitation (inputs) in the local hydrologic system. All of the surface water, ground water, and mine water samples fell on a mixing line between the snow and rain inputs, suggesting that they are a mixture of the two precipitation types with $\delta^{18}\text{O}$ values between -14‰ and -16‰ with the exception of one surface water sample collected from Willow Creek during the June 2009 sampling event ($\delta^{18}\text{O} = -19.73\text{‰}$). The observed variation in surface waters ($\sim 5\text{‰}$) is considerable larger than the variation seen in Nelson Tunnel waters either temporally (year to year) or spatially (across all tunnel locations each year). The large seasonal isotopic variability

of surface waters compared to mine waters corresponds to changes in input (rain and snow) and suggests that the water in the streams is not well mixed and has a short (i.e. weeks to months) residence time within the Willow Creek watershed.

To better observe the variations in Nelson Tunnel waters over space and time the δD - $\delta^{18}O$ relationship was examined in finer resolution (Figure 4.5b). Duplicate samples collected from the HW-4 Bulldog well in February 2013 were plotted for reference. The average variability of $\delta^{18}O$ between different Nelson Tunnel samples during individual sampling events was only 0.13 ‰ indicating well mixed waters across all locations with minimal inputs of isotopically unique waters along the flow path from depth in the Berkshire (shown by 2012 samples) to the Nelson Tunnel Portal. The average $\delta^{18}O$ concentration in the Nelson Tunnel water was -14.84 ‰ and varied from the most depleted average of -15.13 ‰ in June 2009 to the most enriched average value of -14.65 ‰ in February of 2007. Results suggest that there is some depletion of $\delta^{18}O$ content following spring snowmelt (June), indicating some small contributions of recent melt (i.e. ~20 ‰) to the flow system at that time. However, this documented change (~0.5‰) is very small compared to the change of ~ 5 ‰ documented for surface flows in West Willow Creek. In conjunction with the June 2009 sampling of the Nelson Tunnel waters isotopic values were obtained for flows encountered at the Peak Drift Borehole and Corkscrew Raise (not shown in Figure 5), which had $\delta^{18}O$ values of -15.48 ‰ and -15.04 ‰ respectively. Although there is no direct line of evidence linking these flows to the Nelson Tunnel waters, they likely represent a recent meteoric signal and support the hypothesis that any additional inflows to the Nelson Tunnel during snowmelt would have a more depleted $\delta^{18}O$ signal and can contribute to slightly depleting the Nelson Tunnel water isotopic compositions in June.

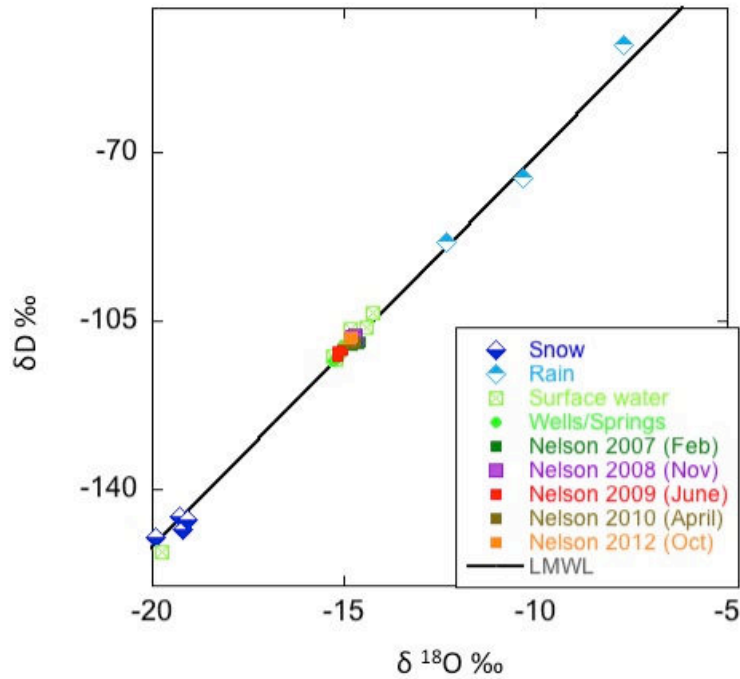


Figure 4.5: (A) Plot of $\delta^{18}\text{O}$ vs. δD for precipitation (partitioned as rain and snow), surface waters, ground water, and mine waters collected in the Nelson Tunnel in different years and different times of the year. The Local Meteoric Water Line (LMWL) is plotted in black.

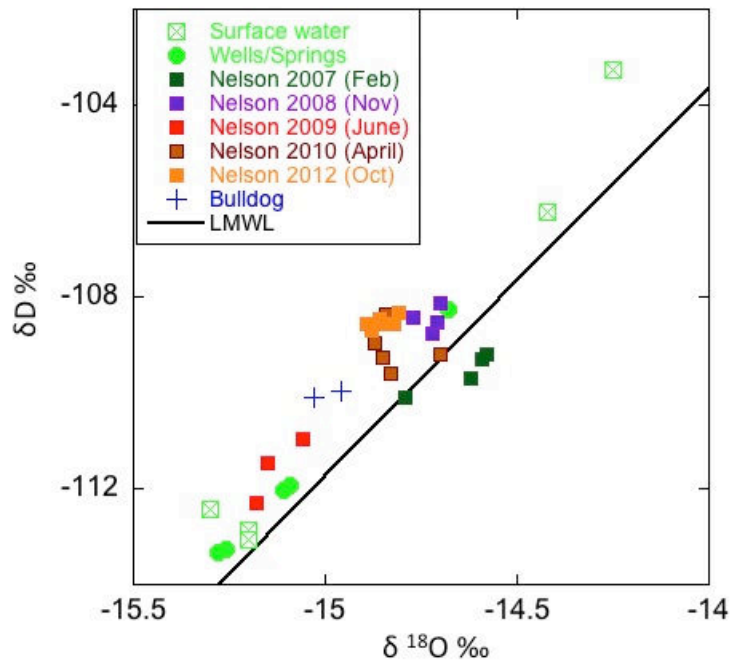


Figure 4.5: (B) Annual and seasonal variations of $\delta^{18}\text{O}$ vs. δD for Nelson Tunnel water. Multiple points from the same date represent different sample locations along the Nelson Tunnel between the portal and the Berkshire Shaft. The Bulldog samples were collected from the HW-4 well in February 2013. The LMWL is plotted for reference

4.4.7 Tritium

The mean tritium concentration in precipitation across the San Juan Mountains of Southwestern Colorado was 6.32 ± 3.0 TU based on 21 samples (including 5 from within the Willow Creek Watershed) collected in 2010 and 2011 (Cowie *et al.*, 2014). Additional samples collected across the Willow Creek watershed demonstrated a range of tritium concentrations that was greater than what was observed in the precipitation (Figure 4.6, Appendix 4). The Nelson Tunnel discharge and the Bulldog mine pool water (HW4 well) had “tritium dead” (<1.5 TU) waters suggesting that the water was at least older than the 1950 bomb spike. The bedrock well at Emerald Ranch had the next lowest tritium concentration (1.34 TU) again indicating predominantly older pre-bomb water. However, the shallow alluvial well at Emerald Ranch showed the most elevated tritium (8.86 TU) indicating recent water with some component of bomb spike waters. The Midwest spring (7.4 TU) and Weaver Spring (7.9 TU) are similar to West Willow Creek (7.9 ± 0.7 TU, $n=3$), and elevated relative to the mean of current precipitation, suggesting that they represent recent (<60 years old) meteoric water containing some bomb spike tritium. The one sample collected on East Willow in February 2013 had concentration of 6.24 TU, which was similar to West Willow but elevated relative to the Solomon Mine Adit (3.1 TU), which drains to East Willow. The tritium value for the Bach Well (4.55 TU) is similar to recent meteoric and suggests that the groundwater at this intragaben location is different than the water encountered in the mines along the flanking graben faults.

Tritium results from mine samples indicate that the water in the Nelson tunnel is primarily tritium dead (< 1.5 TU), suggesting that the water is at least older than 1950 (pre bomb spike) (Figure 4.7). Tritium at the auxiliary mine locations is different than in the Nelson

Tunnel. At the Bachelor shaft proper (-15 feet into water column within shaft) the water is tritium dead (0.02 TU), while water encountered at the Del Monte raise (1.56 TU) and Peak Drift borehole (1.82 TU) have tritium slightly elevated relative to the Nelson Tunnel water, but still below recent meteoric inputs. The Corkscrew raise has the most elevated tritium (mean 4.9 TU) and indicates more recent meteoric waters (or a mixture of pre-bomb and bomb spike waters) entering the mine at this location. At the back of the mine the Park Regent shaft has a small mine pool (not part of the Nelson Tunnel waters because the Nelson Tunnel is dry at this location) with elevated tritium (3.66 TU) relative to the Nelson Tunnel water again suggesting some component of recent meteoric recharge (or some component of bomb spike water mixed with tritium dead water) at this location.

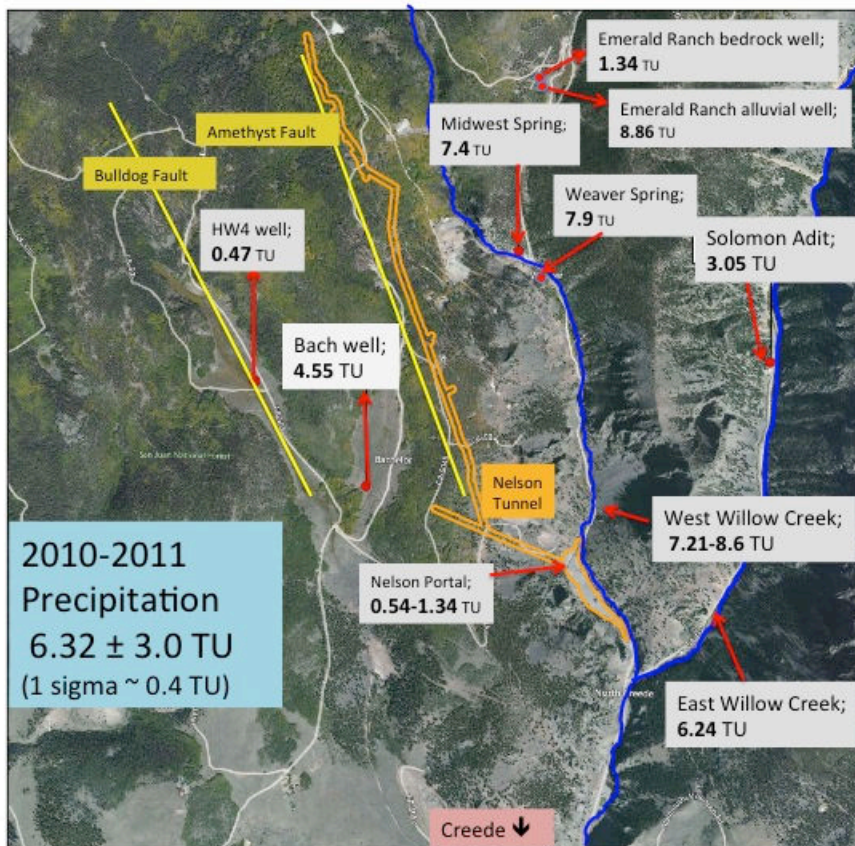


Figure 4.6: Tritium concentrations from surface waters, springs, wells, and mine discharge within the Willow Creek Watershed.

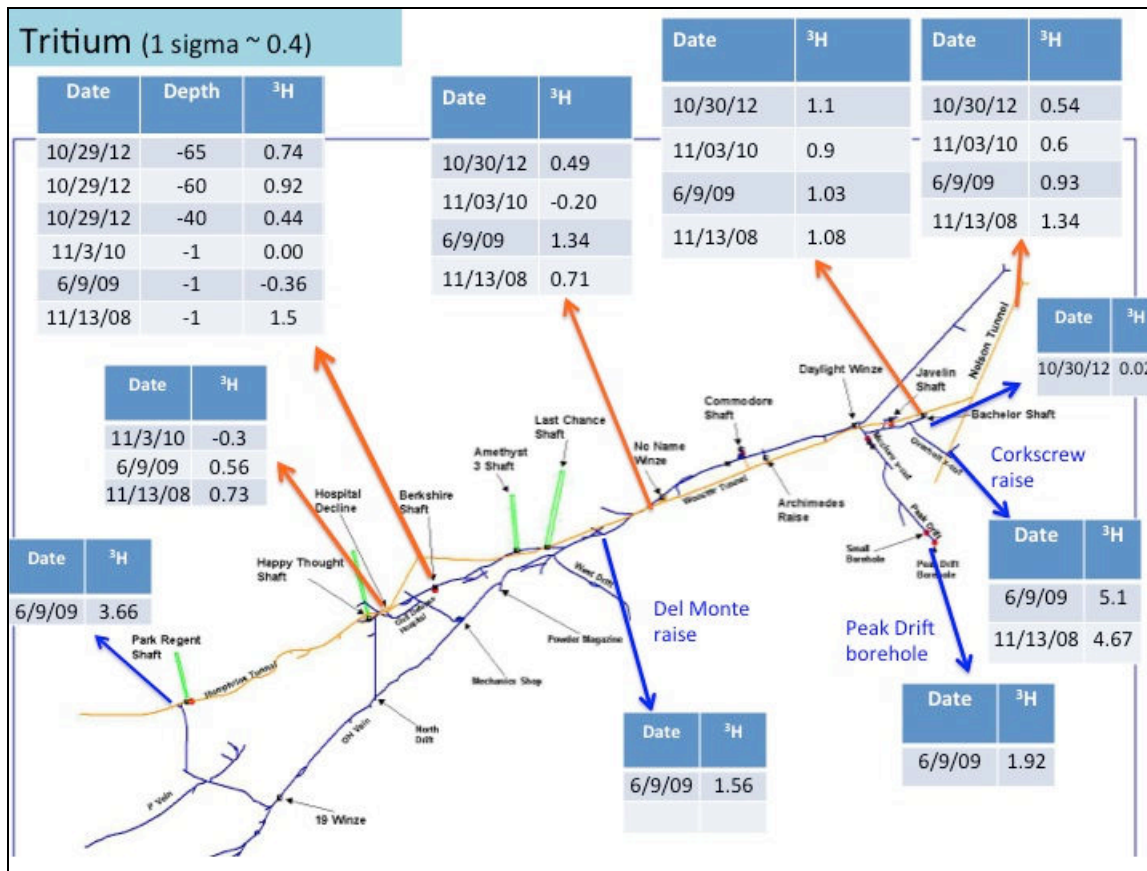


Figure 4.7: Tritium concentrations in mine waters. Orange arrows indicate direct sampling of Nelson Tunnel water, blue arrows are from non-Nelson mine waters. Tritium values are reported in Tritium Units (TU).

4.4.8 Radiocarbon Analysis (DIC and DOC)

To provide an age correction to the DIC $\delta^{14}\text{C}$ data, all uncorrected radiocarbon ages (presented as a percent modern carbon (pMC)) were plotted against the tritium concentrations (Figure 4.8). Assuming a tritium detection limit of 1.5 TU, with all samples < 1.5 TU considered tritium dead and representative of pre bomb spike waters, a curve was drawn to determine an appropriate initial ^{14}C activity based on intersection with the detection limit. The curve therefore suggests that an initial ^{14}C activity of 60 pMC should be used to calculate an appropriate radiocarbon age, based on the assumption that a groundwater (or mine water) sample that does not contain “bomb” tritium will also be free of anthropogenic ^{14}C . In other words the approach

assumes that all samples that are tritium dead must be below the corrected initial activity (60 pMC) while any sample that contains tritium would plot above that initial activity.

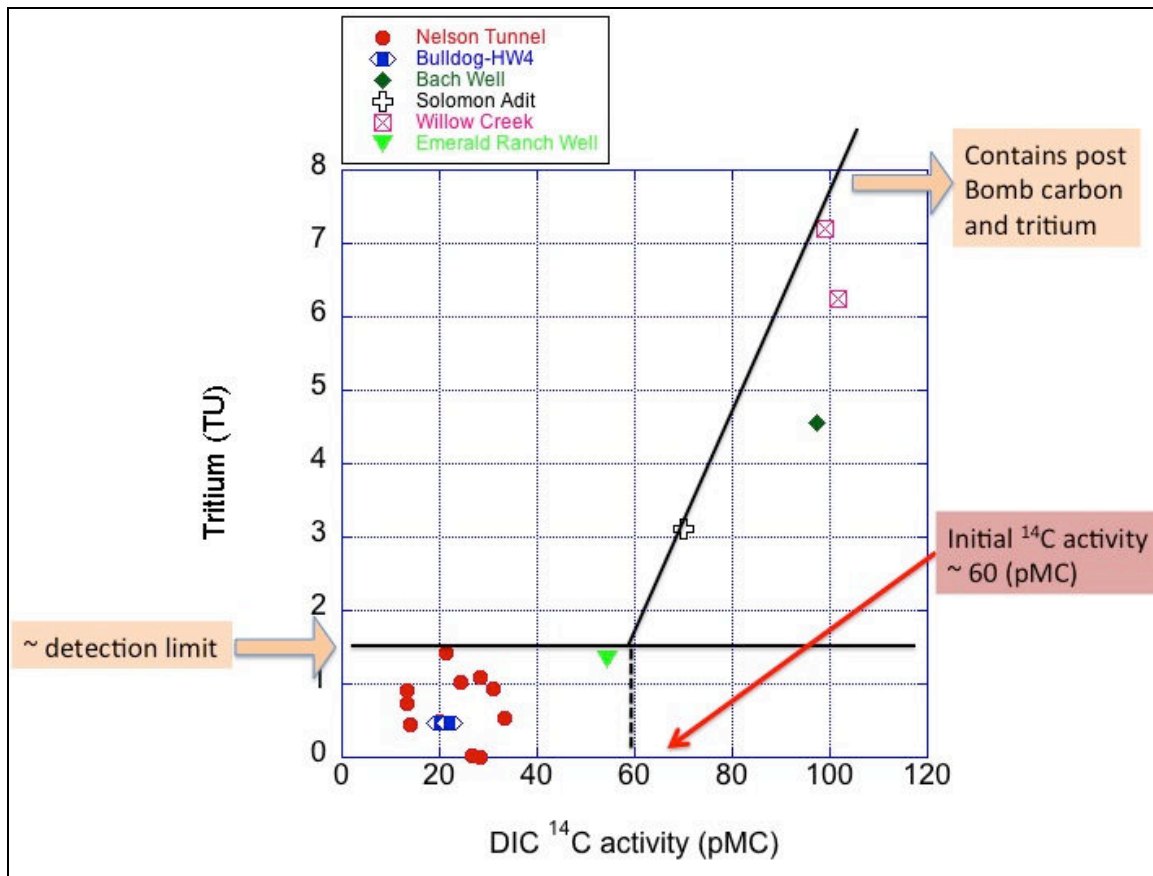


Figure 4.8: A $^3\text{H}/^{14}\text{C}$ diagram for water samples with both DIC ^{14}C and tritium values. The ^{14}C of DIC values are reported as a percent of modern (1950) carbon without reservoir correction. The tritium detection limit is set at 1.5 TU.

The uncorrected DIC $\delta^{14}\text{C}$ results for waters emerging in the Berkshire Shaft below the depth of the Nelson Tunnel are 13-14% modern carbon and therefore have an uncorrected apparent age of over 16,000 years (Figure 4.9, Appendix 5). As the water travels out of the mine towards the Nelson Portal the pMC steadily increases to 20-21% at No Name, 24-28% at Bachelor, and 31-33 % at the Nelson Tunnel Portal. The increase in modern carbon occurs at a rate of approximately 0.66% per meter of distance traveled along the Nelson Tunnel, which can be explained by the incorporation of a modern carbon signal as the water mixes with atmospheric

CO₂. The uncorrected DIC $\delta^{14}\text{C}$ signal therefore appears to become about 50% younger (16,250 to 8,830 years) as it moves from the anoxic conditions in the Berkshire to the oxygenated conditions emerging at the Nelson Tunnel Portal. This result is also supported by the Berkshire - 1 sample, which has double the pMC as the sub-Nelson Berkshire samples. The sample collected at the top of the water column in the Berkshire was exposed to atmospheric conditions and was likely stratified from the waters closer to and within the Nelson Tunnel flow, which would have allowed more time to incorporate modern CO₂ and reduce the apparent age of that specific column of water. Application of the tritium age correction reduces the apparent age of the DIC to 11,400-11,800 years in the Berkshire shaft, which is reduced to 4,380-4,990 years at the Nelson Tunnel Portal. Additionally, the $\delta^{13}\text{C}$ content of the DIC remained consistent (~ -10 ‰, Figure 4.9) from the Berkshire shaft to the Nelson Portal. The consistent values indicate little to no microbial activity occurring along the mine flow path because widely varying $\delta^{13}\text{C}$ content of DIC would indicate introduction of new CO₂ (with different carbon isotope signatures) to the water from microbial activity or abiogenic degradation of available organic carbon sources (Murphy *et al.*, 1989).

The results of DOC $\delta^{14}\text{C}$ analysis are presented alongside the DIC results to provide an independent measure (Figure 4.9). Unique to the DOC $\delta^{14}\text{C}$ results is that the apparent age of the whole component DOC and fulvic acid fraction of DOC tends to bracket the corrected DIC $\delta^{14}\text{C}$ ages with the whole component DOC being older and the fulvic DOC having a younger signature. These results are consistent with a groundwater study by Murphy *et al.* (1989) whom found that the $\delta^{14}\text{C}$ ages of whole component DOC had ages greater than those of fulvic acid fraction of DOC and that the $\delta^{14}\text{C}$ content of the fulvic DOC generally followed that of the DIC. Murphy *et al.* (1989) concluded that although the fulvic acid DOC fractions were also mixtures

of organic molecules of different age, they were thought to originate in the interstitial waters of the soil zone in the area of recharge and probable better suited for radiocarbon dating of groundwater than whole component DOC or the non-fulvic low molecular weight fraction of DOC (Clark and Fritz (1997).

Although replicate samples for both whole component DOC and the fulvic acid portion of the DOC are not available for all locations, some clear differences in these results can be observed. Primarily, the whole component DOC $\delta^{14}\text{C}$ results (Berkshire -1 and Nelson at Bachelor) have 10 to 20 % less modern carbon than the fulvic component DOC $\delta^{14}\text{C}$ results at all other locations. Secondly, the $\delta^{13}\text{C}$ values of the two whole component DOC samples (-39.3 and -36.0 ‰) were considerable more depleted than the $\delta^{13}\text{C}$ values from the fulvic portion of the DOC (-22 to -23.3 ‰). The greater depletion in whole component $\delta^{13}\text{C}$ has been observed by Murphy *et al.* (1989) whom found that the additional low molecular weight DOC in whole component DOC analysis had both more depleted $\delta^{13}\text{C}$ and lower $\delta^{14}\text{C}$ thus producing older apparent ages. Conversely, the remarkably consistent $\delta^{13}\text{C}$ of the fulvic portion DOC from the back of the mine to the portal indicates little to no fractionation or mixing occurring along the Nelson Tunnel flow path. Additionally, the DOC $\delta^{14}\text{C}$ of the fulvic component remains consistent at 38-39 pMC from the Berkshire -40 to the Nelson at No Name and again at the Nelson Tunnel portal, giving a consistent apparent age of ~7,500. The consistent DOC $\delta^{14}\text{C}$ signal further compliments the DIC results in indicating that there is little to no introduction of new or different fulvic acid into the Nelson Tunnel waters from either additional water sources or in-situ sources such as decomposing wooden timbers placed throughout the mine. The DOC $\delta^{14}\text{C}$ results further support the hypothesis that the only significant source of water into the Nelson Tunnel is from a deeper groundwater source, which is entering near the Berkshire shaft.

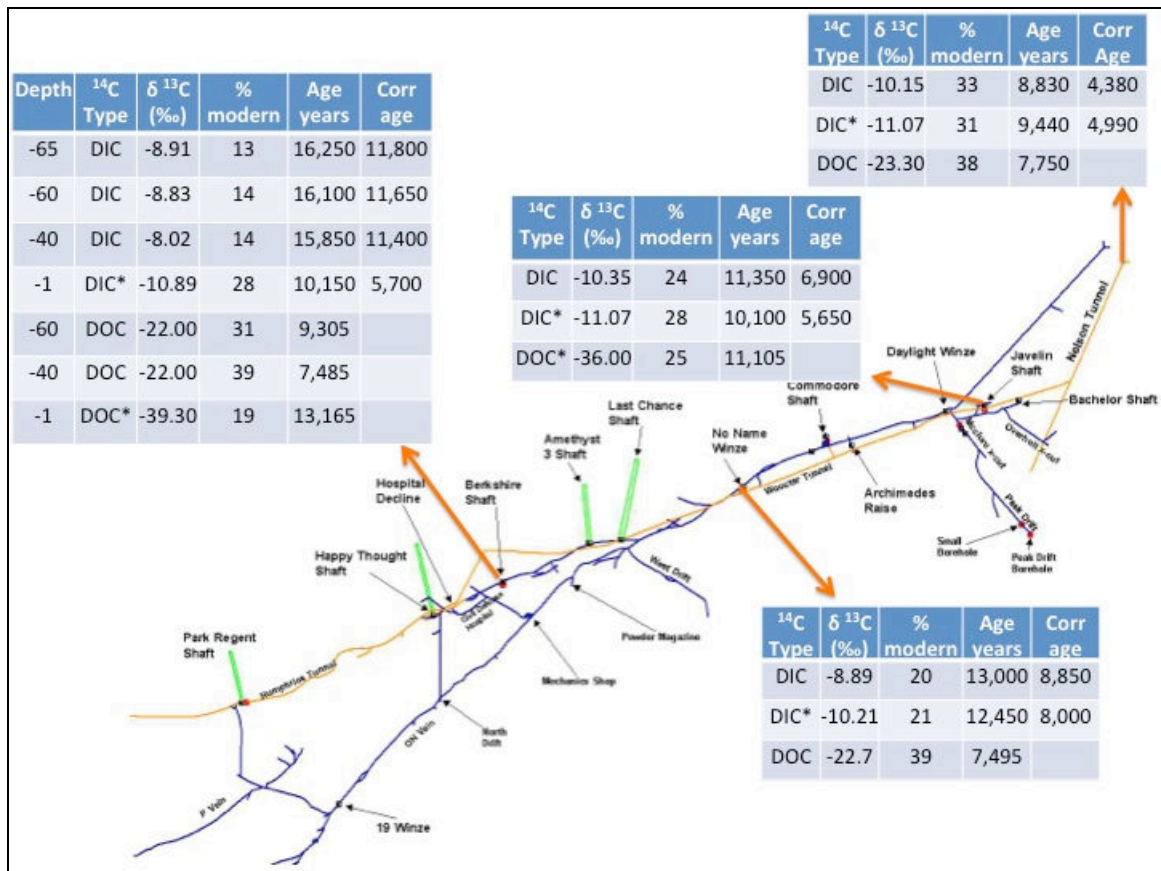


Figure 4.9: Radiocarbon results from dissolved inorganic carbon (DIC) and dissolved organic carbon (DOC) for samples collected in the Berkshire shaft, Nelson Tunnel at No Name and Bachelor, and from the Nelson Tunnel portal. The DIC* results are from 2009 while all others were collected in 2012 with identical analysis techniques. The DOC* results are from 2009 and represent the ¹⁴C from the total DOC while all other DOC results represent ¹⁴C of only the high molecular weight (fulvic acid) portion of the DOC. The corrected ages are based on initial ¹⁴C DIC activity of 60 pMC from figure 8. The depths reported for the Berkshire shaft represent depth sample was collected below the water surface elevation in the shaft a time of sampling.

Radiocarbon analysis of both DOC and DIC was also performed for other waters within the Willow Creek watershed to provide a comparative analysis to the results found for the Nelson Tunnel waters (Figure 4.10). The Bulldog mine water was sampled in duplicate from the HW-4 well and had apparent ages between 6,300 and 8,500, very similar to those encountered in the Nelson Tunnel. The Bulldog mine water was sampled in duplicate from the HW-4 well and had apparent ages between 6,300 and 8,500, very similar to those encountered in the Nelson Tunnel. The DIC δ¹⁴C apparent age of Bulldog waters was younger than those encountered in the Berkshire shaft but very close to the ages reported in the Nelson Tunnel at No

Name. Unfortunately there is no information on the condition of the mine environment within the Bulldog mine pool, but results suggest that there may be some oxygen present at this location which would lower the DIC $\delta^{14}\text{C}$ age as discussed previously.

The DIC $\delta^{14}\text{C}$ of mine discharge, the Emerald Ranch bedrock well, and the Solomon adit along East Willow was 54 and 70 pMC respectively. The water at these locations is therefore likely a mixture of some older groundwater (like that in the other mine waters) mixed with a considerable amount of more recent meteoric waters, suggesting a greater degree of infiltration of rain/snow from the surface in those parts of the watershed relative to what is observed in the Bulldog and Amethyst faults. Interestingly, the Bach well has an even more recent DIC $\delta^{14}\text{C}$ signal of 97 pMC, indicating that even though the groundwater level is at the same elevation (and the well is located between) as the Bulldog and Amethyst faults, it has a different, higher velocity source pathway. At the Bach Well there is some discrepancy with the HMW fulvic DOC $\delta^{14}\text{C}$ of 53 pMC suggesting mixed age water similar to what was observed in the Emerald Ranch Well. The sizeable discrepancy in DIC/DOC apparent ages may be explained by differences in the composition of the HMW DOC that was isolated for radiocarbon analysis, which can be addressed through fluorescence analysis.

The final two samples analyzed for radiocarbon analysis were from surface water flows collected during low flow conditions on East and West Willow Creek (Figure 4.10). As anticipated, the DIC $\delta^{14}\text{C}$ for both creeks indicate modern (< 60 years) waters with East Willow being >100 pMC indicating some post bomb (> 1950s) waters. The results correlate with the tritium results, both indicating recent meteoric source water with relatively short residence times for any sub surface flows contributing to stream discharge even during low flow conditions. The DOC $\delta^{14}\text{C}$ of the West Willow creek was 88 pMC, generating an apparent age of 1,000 years,

which is a good indicator of inherent variability in the age of organic carbon sources within the soil profiles through which the water contributing to low flow surface discharge is flowing. The organic carbon in the soil zone and unsaturated zone typically has radiocarbon ages of zero to at least several thousand years (Plummer and Glynn, 2013). Fierer *et al.* (2005) found that in a grassland ecosystem with deep soil profiles the soil organic carbon ages increased with depth, with mean residence times of 40 to 2,000 years in the upper 60 cm of the profile. For reference, Lawrence *et al.* (2011) found soil profiles formed on volcanic rocks at 3500 m in the San Juan Mountains to range from 0-60 cm, providing a reasonable estimate of the soil profile in the recharge areas of the Willow Creek watershed. This result provides a quantitative estimate of the variability of the input signal for organic carbon and reiterates that the results of HMW fulvic DOC $\delta^{14}\text{C}$ analysis should be interpreted with an understanding that the calculated apparent age can have an associated error of $\sim 1,000$ years in this system.

Overall the DOC $\delta^{14}\text{C}$ results provide age verification for the ^{14}C DIC ages and support the hypothesis that the oldest waters are found in the Berkshire shaft. The independent tracers both indicate subsurface residence times $> 5,000$ years for water in the Berkshire Shaft and along the Nelson Tunnel. The results also suggest that the waters in the Bulldog mine pool have a similar residence time to those in the Berkshire and may therefore be following the same or similarly long and deep (slow moving) flow paths from point of recharge.

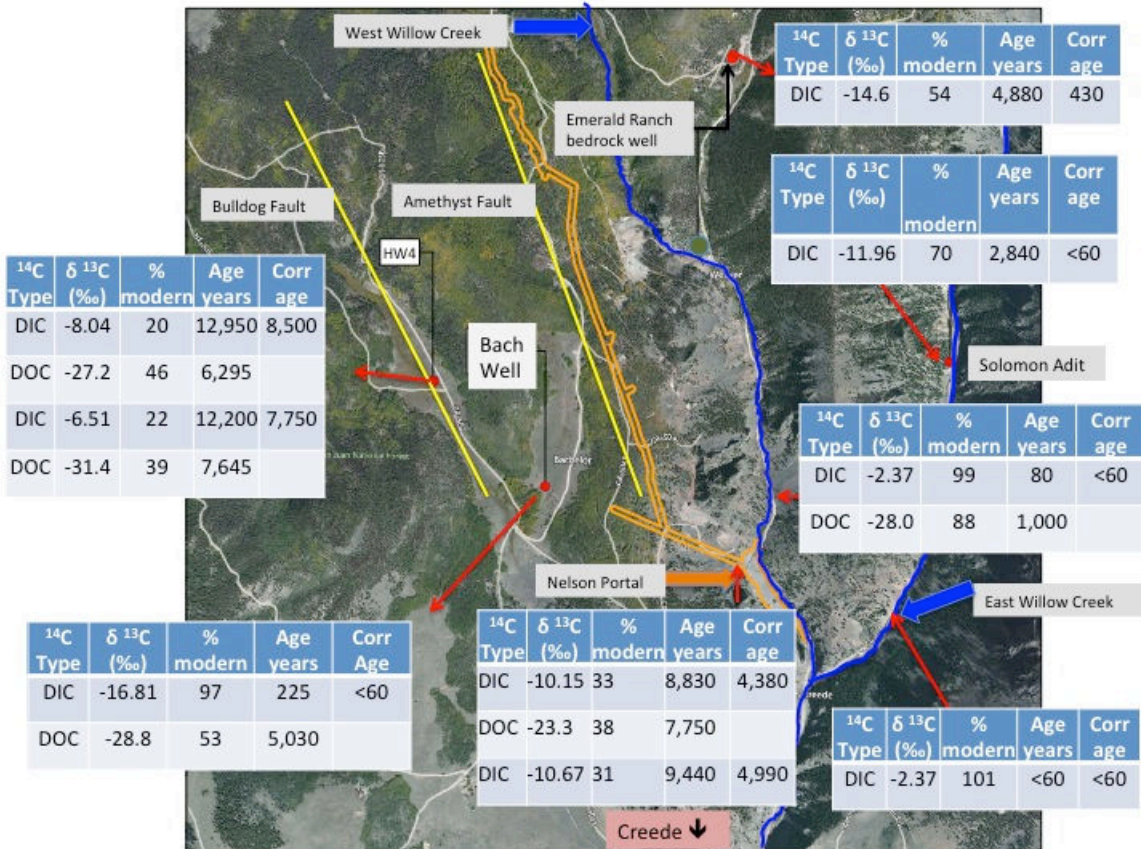


Figure 4.10: Radiocarbon results from dissolved inorganic carbon (DIC) and dissolved organic carbon (DOC) for surface waters, ground waters and mine waters associated with the Bulldog and Solomon mines. The Nelson Tunnel portal data presented in Figure 4.9 is included for easy comparison. All DOC samples represent only the fulvic acid portion.

4.4.9 Fluorescence Analysis of DOC

Fluorescence analysis helped determine whether the DOC in the mine waters was from soil organic matter dissolved into infiltrating snowmelt and rainwater at the time of recharge. If the DOC was acquired at the time of recharge, then the radiocarbon would provide a generally accurate age of water since recharge. The results of fluorescence analysis confirm that the DOC that underwent radiocarbon analysis is from fulvic acids and humic material and was not contaminated during the separation of the fulvic acid fraction of the DOC that was sorbed onto the XAD-8 column. The EEMs from nearly all samples look normal in that they all have humic peaks in the correct places and some samples showing strong amino acid peaks (Figure 4.11). To

further interpret the EEMs there are a number of fluorescence indices, generally defined as the ratio of fluorescence intensity measured at two different points or regions in optical space (Gabor *et al.*, 2014), that were measured. The indices included; specific ultraviolet absorbance (SUVA₂₅₄), fluorescence index (FI), redox index (RI), freshness index (BIX), and humification index (HIX). A detailed analysis of the indices is beyond the scope of this paper but the results are presented in Appendix 6 along with the loading and components values generated from fluorescence analysis. In general, the indices demonstrate that although the EEMs produced reasonable results, the absolute values of the fluorescence spectra appeared to have varying degrees of quenching by metal complexation and pH effects (Cory *et al.*, 2010) associated with high metals content of the mine waters. Further quantification of the amount and speciation of metals (i.e. Fe²⁺/Fe³⁺) that remained in the sample isolates after passing through the cation exchange column would be necessary to better address complexation processes and the effects on resulting fluorescence indices.

When the measured EEMs are compared to EEMs generated by the Cory-McKnight PARAFAC model (Cory and McKnight, 2005) the residuals are very low (Figure 4.12), indicating that the fulvic acid component of the DOC in the mine samples is composed of similarly fluorescing quinone-like moieties used to develop the model and which are commonly found in natural waters with terrestrial (i.e. soil) carbon sources. To interpret Figure 4.12 the residual as a percentage (bottom right) shows that over most of the EEM the measured fluorescence is within 10% of how well the Cory-McKnight model was able to resolve the 13 components of DOM used to build the model.

The EEMs also suggest that two of the samples, the first sample collected at the Nelson portal and the Bach Well sample (Figure 4.11), lack the humic like fluorescence signal. The

original Nelson Portal sample had very low total DOC (0.18 mg C/L), which was likely a result of complexation of the DOC with iron oxides or other metal oxides (McKnight *et al.*, 1992) and then co-precipitation out of solution when the mine waters were exposed to the open air at the portal. The remaining DOC is then subject to further complexation with the remaining dissolved iron which would result in further removal of DOC during XAD-8 column elution with sodium hydroxide and DI rinse to remove chloride. This step raises the pH of solution and causes the iron (and complexed DOC) to precipitate out. A second more likely result was that not all of the iron was removed from the sample through the XAD-8 process, and the remaining iron (or DOC complexed with iron) suppressed the fluorescence signal (Muholland, 2003) in the typical humic like region of the EEM. To test this hypothesis a second larger volume (~ 15L compared to 3L) sample was collected from the Nelson Tunnel Portal and run through the XAD-8 column. The method for analyzing the larger volume sample was as modified by running the sample through the column three times as opposed to just one time to get remove more of the iron but retain enough non-complexed fulvic acid portion of DOC to perform fluorescence analysis. As a result the second attempt at fluorescence for Nelson Portal produced expected results in which the EEM (Nelson Portal 2) looks very similar to the other EEMs from Nelson Tunnel waters (Figure 4.11). The improved fluorescence results demonstrated the importance of sufficient sample size for metal laden waters if the objective is to do both radiocarbon and fluorescence analysis. Since the DOC radiocarbon results for the Nelson Portal, which essentially match those of the other Nelson Tunnel waters (Figure 4.9), came from the first sample (Nelson Portal 1) it can be assumed that the fulvic acid portion of the DOC had been sufficiently isolated by the XAD-8 technique but the additional steps performed on Nelson Portal 2 sample were required to achieve adequate fluorescence analysis.

The modified method mentioned above was not an option for re-analysis of the Bach well as a second larger sample volume was not attainable during the study. However, due to the very strong amino acid peak, the Bach well appears to contain a high concentration of proteinaceous material, specifically tryptophan and tyrosine (Gabor *et al.*, 2014), which are less apparent in the other locations (Figure 4.11). The unique fluorescence signature of the fulvic acid portion of DOC from the Bach well may simply be highlighting that the DOC has come from a unique source. If the Bach well water is from relatively rapid infiltration of direct recharge, as indicated by the young DIC apparent ages and elevated tritium levels, then the recharging water may be leaching organic carbon from a different soil pool than is encountered in other recharge areas contributing to the groundwater observed in the mine pools. One possible explanation is that the Bach well is located within the forested portion of the Willow Creek watershed at 2,761 m. If the well water is recharged locally the water likely passes through a deeper and more well developed soil profile than those recharging in alpine areas of the watershed, resulting in acquisition of older carbon (Fierer *et al.*, 2005) producing a unique spectral signature.

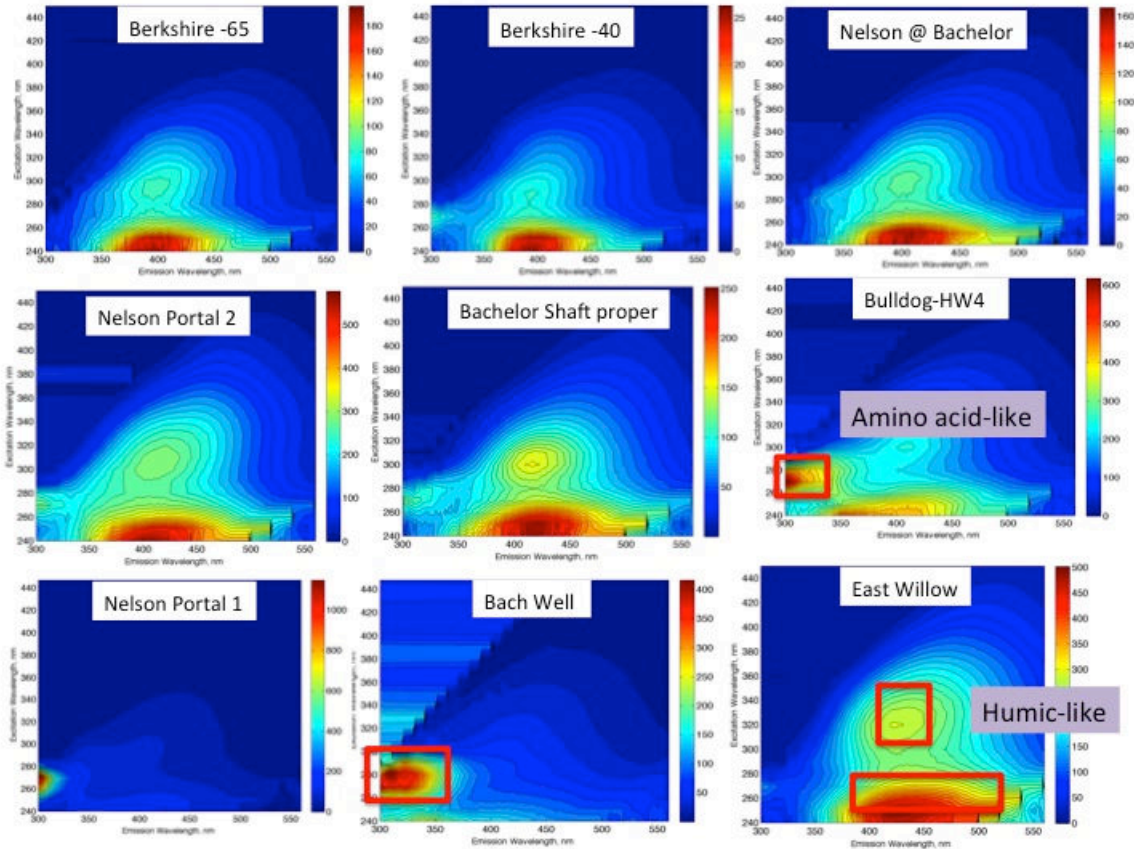


Figure 4.11: The 3-D fluorescence scans, referred to as excitation-emission matrices (EEMs), which are acquired for a range of emission wavelengths when excited at multiple wavelengths. The typical locations for humic-like and amino acid like peaks are highlighted for reference. From left to right, top to bottom, the first four samples represent Nelson Tunnel waters. The Nelson Tunnel Portal 1 sample did not produce sufficient fluorescence results so Nelson Portal 2 is a repeat sample from the same location using 5x more sample volume.

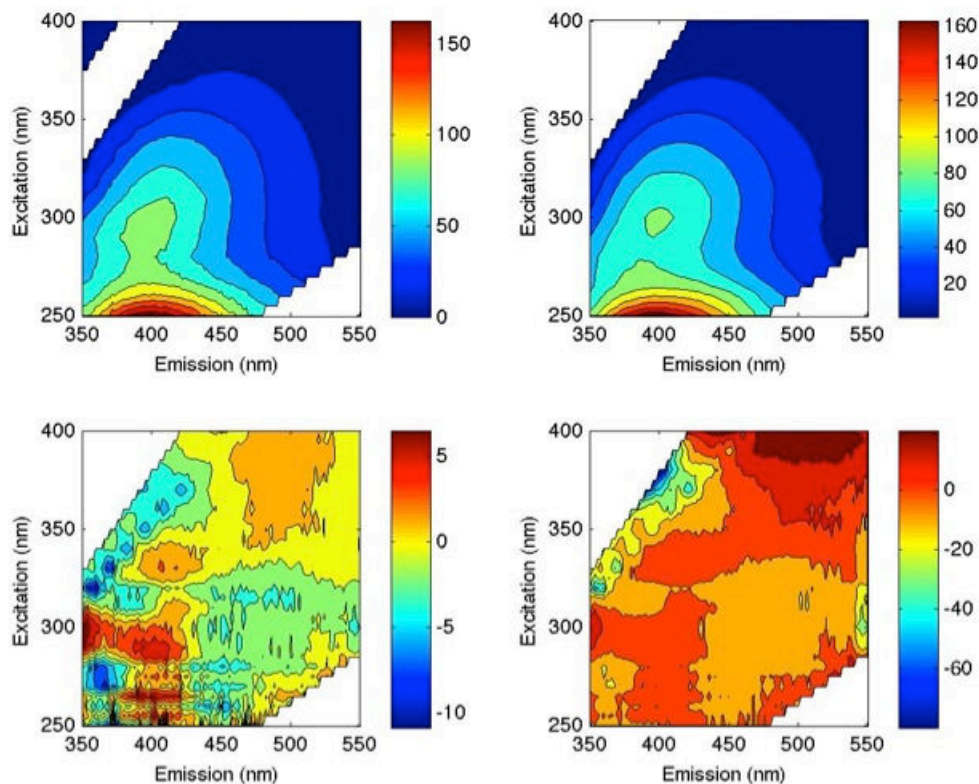


Figure 4.12: Comparison of the measured (top left), modeled (top right), and residual (bottom left, as intensity; bottom right, as percentage) EEMs for the deepest sample collected in the Berkshire shaft (-65'). Intensities are in Raman Units and are a function of the concentration of the prepared fulvic acid solution. Each contour plot was generated in Matlab using 10 contour lines.

4.4.9 Strontium

Strontium concentrations and isotopic ratios provide an independent geochemical tracer to help differentiate groundwater flowpaths. As a first order analysis the strontium concentrations of water samples were compared (Figure 4.13). The strontium concentrations were measured as part of metals analysis for samples collected in the Nelson Tunnel and associated mine workings and across the watershed. Metals analysis was not performed on the local precipitation samples so the authors used results from an independent study conducted for

the U.S. EPA on metals concentrations in the snow pack in the San Juan Mountains near Telluride, CO. In 2012 four depth integrated snowpack samples collected at maximum accumulation produced a mean strontium concentration of 3 $\mu\text{g/l}$, which provides a quantitative estimation of a regional input signal from winter precipitation. Strontium comes from geochemical weathering and the strontium found in the snow in the San Juan Mountains is coming primarily from dust deposition on the snowpack (Lawrence, 2010). Although concentrations in rain were not measured, previous studies indicate that rain concentrations may be slightly higher but within the same magnitude (Capo *et al.*, 1998). For all surface water, shallow groundwater, and mine water not associated with the Nelson Tunnel, strontium concentrations were of similar magnitude ($\sim 100\text{-}200 \mu\text{g/L}$) with the exception of surface waters in East Willow being about one third of those in West Willow (Figure 4.13). The result suggests that there may be different flowpaths with unique geochemical composition just between the East and West Willow Creeks. The strontium concentrations in the Nelson Tunnel waters of $2,082 \pm 173 \mu\text{g/L}$ were an order of magnitude higher than all other waters sampled, indicating much greater accumulation due to either significantly longer residence times or significant variations in host rock geochemistry along the flow path, or both.

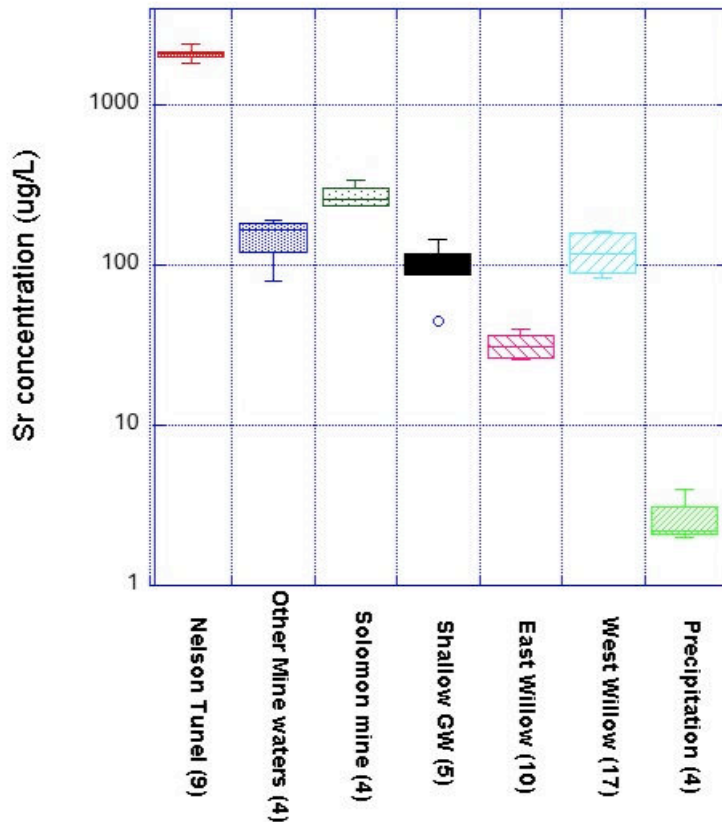


Figure 4.13: Box plot of strontium concentrations found in mine waters, groundwater, surface water and precipitation. Sample size for each sample type is in parenthesis after each location. Note log scale on the y-axis.

To further investigate how the rock-water interactions varied for samples collected in the mine and across the watershed the $^{87}\text{Sr}/^{86}\text{Sr}$ ratios were measured for a number of samples and plotted against the inverse strontium concentration, following the protocol of Bretzler *et al.* (2001) (Figure 4.14). The $^{87}\text{Sr}/^{86}\text{Sr}$ isotopic ratios of the investigated mine water, groundwater, and surface waters samples range from 0.70684 to 0.70777, which fall well within the ranges expected for continental volcanics (Capo *et al.*, 1998). All of the Berkshire shaft and Nelson tunnel samples have remarkable similar $^{87}\text{Sr}/^{86}\text{Sr}$ isotopic ratios with a mean of 0.70702 ± 0.00003 and were very similar to the HW-4 Bulldog sample (0.70712) further suggesting that the mine water in both Nelson Tunnel and Bulldog is derived from a similar flow path and/or source.

The strontium concentration of the HW-4 waters was not available due to the well owners request to not perform metals analysis on waters produced by their well, preventing the plotting of that sample in Figure 4.14. All other groundwater analyzed for strontium isotopes (Solomon adit, Bach well, and the Bachelor shaft proper) had $^{87}\text{Sr}/^{86}\text{Sr}$ ratios greater than 0.70747, again indicating different host rock geochemistry than observed for the Nelson and Bulldog waters. The surface waters in East Willow and West Willow above the Nelson Tunnel portal also had dissimilar $^{87}\text{Sr}/^{86}\text{Sr}$ ratios with West Willow (0.70684) being more similar to the Nelson waters while East Willow (0.70738) being higher and more similar to the other groundwater in the watershed. The results suggest that the Bulldog and Nelson mine waters are traveling through similar host rock, which is consistent with a longer, deeper flow path through the fractured volcanic bedrock that delivers groundwater to both locations. Conversely, waters at other locations (with the exception of West Willow) have distinctly higher isotopic ratios, which would be consistent with contributions from more localized and likely shallower ground water traveling through the volcanoclastic sediments and alluvial deposits overlying the volcanic bedrock. West Willow may be receiving a small portion of water from the Nelson Tunnel flow path, which is sufficient to influence the overall $^{87}\text{Sr}/^{86}\text{Sr}$ ratio at this site.

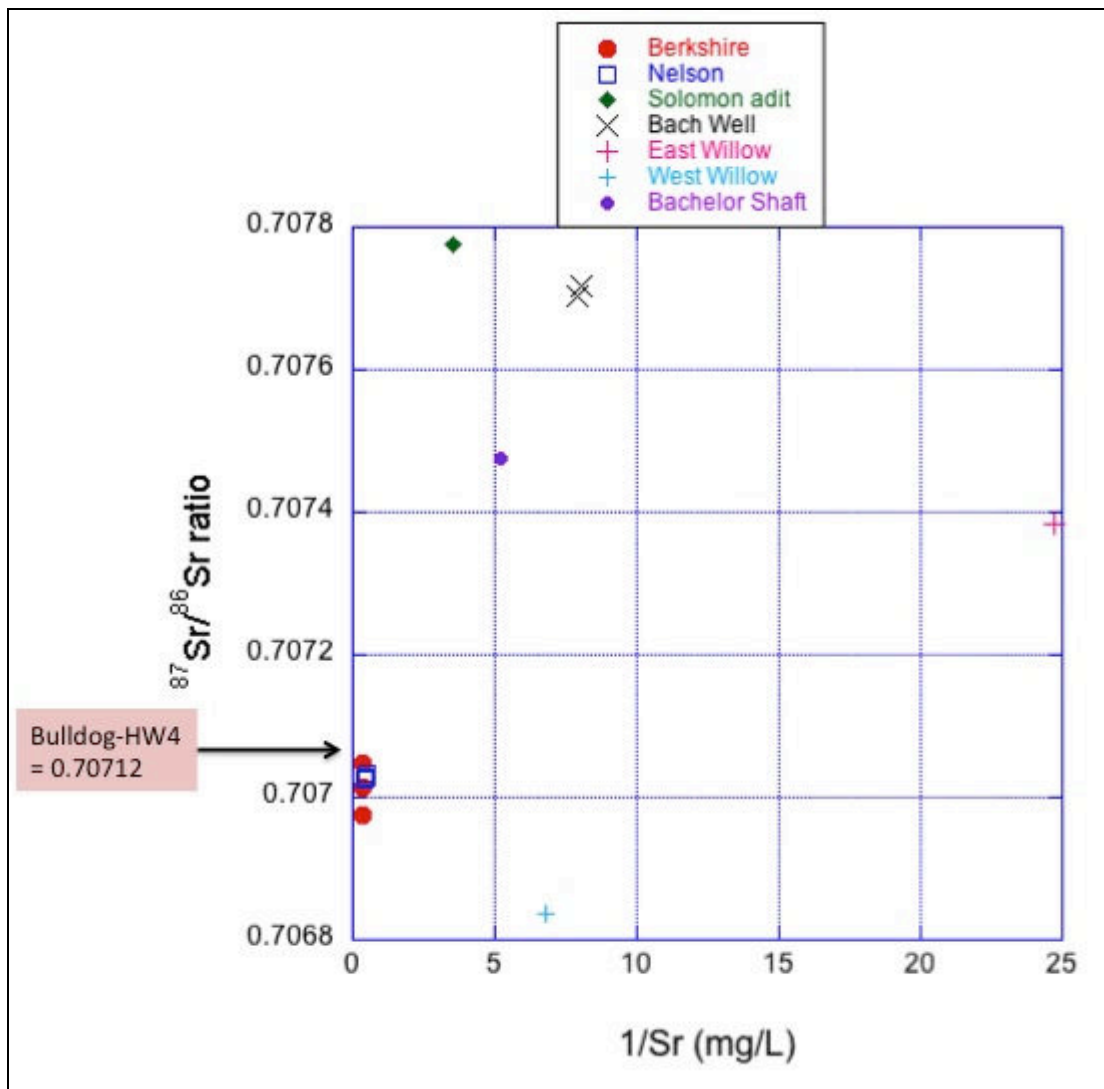


Figure 4.14: Relationship between $^{87}\text{Sr}/^{86}\text{Sr}$ ratios and $1/\text{Sr}$ concentrations of investigated water samples. Different symbols represent different sample locations. The Sr concentration of the Bulldog HW-4 well sample could not be measured (per request of the well owner) so the location of the $^{87}\text{Sr}/^{86}\text{Sr}$ ratio is indicated for reference.

4.4.10 Conceptual Flow Path Development

Drawing from results of the physical and isotopic data presented above, a conceptual model has been developed to help understand the sources and pathways of water contributing to the Nelson Tunnel Discharge (Figure 4.15). The suite of analytical results presented above support the hypothesis that the Nelson Tunnel waters are well mixed (consistent stable isotope

composition) have subsurface residence times of thousands of years (tritium dead and complimentary dual independent radiocarbon analysis) and are likely circulating to depths of 1-2 km below the recharge point within the fractured volcanic bedrock (temperature and strontium). The results also support the hypothesis of strong hydrologic connectivity between the Bulldog and Amethyst fault systems and suggest that water found in both faults has traveled along a similar flow path based on the similarity in isotopic and geochemical compositions found within but not found at any other sampled location within the Willow Creek Watershed.

In further support of the existence of this deep flow path, the recently drilled mining exploration holes on the Amethyst fault at the Equity mine have gone down to approximately 2,622 m elevation with no sign of hitting a local water table within the fault structure (McLure, 2014). This is further supported by current investigations of the Nelson Tunnel at northern extent (Park Regent area, Figure 4.2), which is primarily dry at 2,380 m elevation. The deep apparent groundwater levels in the northern extent of the Creede Mining district suggest that waters recharging the subsurface at the high elevations around the Continental Divide (see Figure 4.1) are finding preferential vertical flowpaths to depths lower than 2,600 m elevation in the northern extents of the Willow Creek watershed. As indicated by Hayba (1993) higher permeability flowpaths in the vertical direction may be due to the ring faults of the San Louis caldera to the north and the Creede Caldera to the south (Figure 4.16). Regionally, the recharging water would be moving down gradient from the Continental Divide to the Rio Grande (north to south) and when it hits the ring faults of the San Louis Caldera (i.e. the Equity fault) it finds preferential flowpaths to greater depths, bypassing the upper elevations of the mineralized areas within the volcanic rock. The variable permeability of the fractured rock associated with the graben structures is likely a significant control on the movement and the elevation of the

groundwater flow system. As the deep groundwater continues to move down gradient towards the Rio Grande it may be flowing at depth along the graben structures, which have a southern terminus associated with the perpendicular ring fracturing of the Creede Caldera. The Creede Caldera then acts as another low-permeability barrier through which some groundwater passes via some highly preferential flow paths while the remaining groundwater moves upwards into a network of variable permeability fractures associated with the intragaben area between the Amethyst and Bulldog graben faults. The discharging pathways to the surface control the potentiometric surface within the intragaben area. Prior to mining the potentiometric surface within the intragaben area was higher than the Nelson Tunnel portal elevation due to the high recharge area elevation. The sub-Nelson mine workings were excavated into a water-bearing zone within the intragaben area and below the pre-mining potentiometric surface. The extensive fracturing described for the intersection of the P and OH veins with the Amethyst fault could provide a pathway for upwelling water in the intragaben area that can easily exit the mine when it reaches the elevation of the Nelson Tunnel (Figure 15). Water within the intragaben area between the Bulldog and Amethyst faults is interconnected, and perturbations of the water level at any point in the area will affect water levels throughout the intragaben area. Since the Nelson Tunnel portal is well below any exits from the Bulldog Mine system, the potentiometric surface in the Bulldog mine pool is therefore controlled by the elevation of the low pressure point of the Nelson Tunnel portal. The exact locations of the inflow(s) to the Nelson Tunnel are unknown as flooded workings prevent current physical access. However, the oldest apparent age of water was encountered in the Berkshire shaft below the elevation of the Nelson Tunnel, supporting an upwelling movement of water into the sub-Nelson workings with subsequent reduction in apparent radiocarbon age occurring due to mixing with the present day atmosphere as waters

move towards the Nelson Tunnel portal. The conceptual flow system suggests that, due to a large regional extent of mineralization associated with the graben fault system, even if Nelson inflows can be intercepted, degraded groundwater quality may still be encountered beyond the extent of the mine environment.

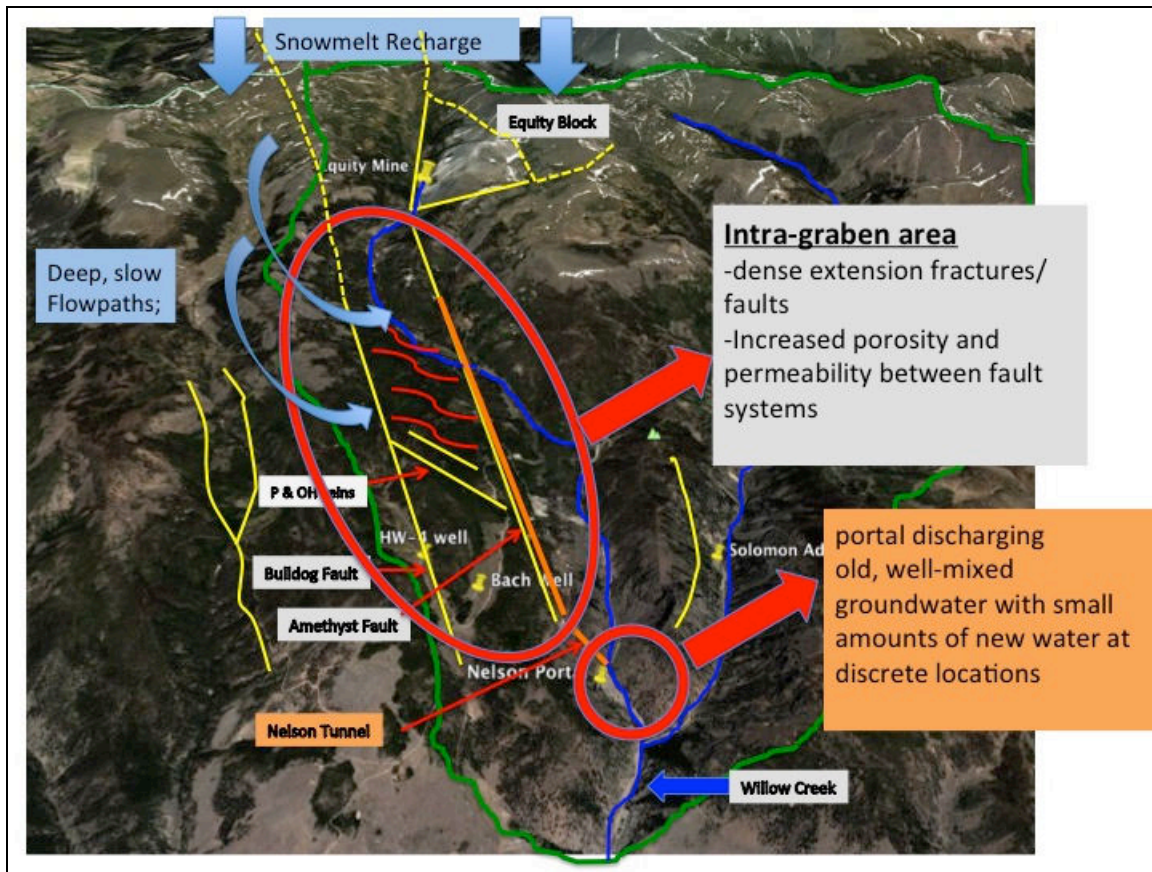


Figure 4.15: Plan view conceptual diagram of the sourcing of water emerging from the Nelson Tunnel Portal.

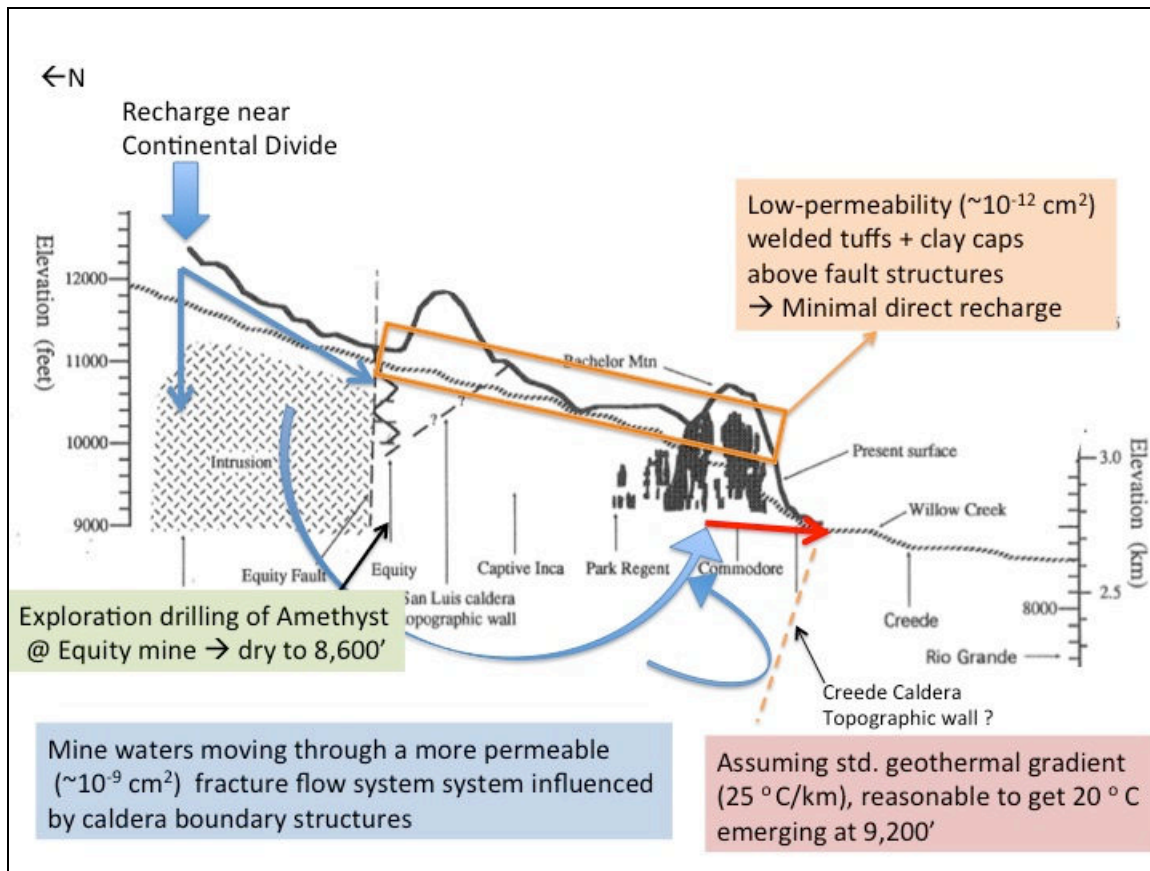


Figure 4.16: Cross sectional view of the Amethyst Fault with potential flow paths highlighted with colored arrows.

4.4.11 Recharge Zone

Given the lack of surface expression of either graben fault in the alpine zone near the Continental Divide it is unclear the lateral extent of the fault systems. However the Bondholder claim/mine has similar mineralization history (Hayba, 1993) suggesting possible trans-watershed subsurface connectivity via a long fault system. The potential continuation of the Amethyst (or Bulldog) fault system beyond the extent of the Willow Creek watershed and spanning the Continental Divide would increase the potential recharge area. The present day topography of the high elevation areas of the Willow Creek watershed masks any surface expression of the fault system, making it difficult to identify locations for meteoric recharge into the fault systems. However the intersection of the Equity and Amethyst faults bounded the uplift of the Equity

block due to localized resurgence of late granitic intrusion (Lipman, 2000). The boundaries of the uplifted block provide another potential focused recharge area for high amounts of meteoric recharge to depth. The Equity block sits near the present day Continental Divide. The high elevation of this region promotes large annual inputs from snow melt and summer monsoon, which even in an alpine environment can significantly contribute to subsurface flow (i.e. Liu *et al.* 2004, Williams *et al.*, 2005) and provide an avenue for recharge to the major fault systems.

4.4.12 Localized Recharge Areas and Shallow Flow Paths

The Bach well is located in the intragraben area between the Bulldog and Amethyst faults and has a water table elevation of 2,810 m, very similar to the water elevation in the Bulldog mine pool (2,815 m) and the Nelson Tunnel upper mine pool (2,816 m). The water has elevated tritium (4.5 TU), which indicates modern water and correlates well with the young DIC age (225 yr.), which could just be a “post modern” carbon signal. The metals levels are an order of magnitude lower in the Bach well than in the mine waters. The combined results suggest that the Bach well is not sourcing the same water as found in the mines even though the water level elevations are similar. This suggests that the elevation of the waters in the mine pools (in both Bulldog and Nelson) is being artificially controlled by the elevation of the discharge point, the Nelson Tunnel portal (2,810 m). The Emerald Ranch bedrock well could be producing from an intermediate flow path based on tritium and radiocarbon results. The Emerald Ranch alluvial well, the springs, and Willow Creek to represent shallower flow paths with shorter residence times that would likely represent groundwater moving through the lower permeability tuffs and volcaniclastic sediments overlying the volcanic bedrock of the Bachelor caldera (see Figures 3 and 15). The Solomon mine adit is also likely intermediate aged water draining the Solomon-

Holy Moses fault system. The extent of this system is much less than the Amethyst and Bulldog and likely does not extend far enough to the north to be significantly influenced by the high elevation recharge.

Willow Creek appears to be recharged at high elevations within the watershed and with little new inputs of groundwater (or losses either) as it flows across the Bachelor caldera, consistent with little local recharge. From the ^{18}O results we see a 5 per mil shift seasonally in the surface waters (reflecting annual meteoric fluxes), again consistent with little groundwater contributions. The springs and surface waters therefore are a good representation of what recent recharge looks like. The springs have intermittent flows which increase with spring snow melt suggesting they are sourced by shallow groundwater flows. The shallow groundwater is likely traveling through near surface unconsolidated sedimentary and alluvial depositions of the Creede and Bachelor formations, which overlie the lower permeability volcanic rocks deposited as welded ignimbrites and lava flows. All of the mine workings through which the Nelson tunnel waters pass are hosted by welded rhyolite tufts with porosity and permeability nearly completely determined by the fractures that penetrate through them (Byington, 2012). Therefore it is believed that the springs are draining water in the overlying unconsolidated layers of the Creede and/or Bachelor formations and that the surface water in East and West Willow Creek has little interaction with the low permeability volcanic rocks.

4.5 Remediation Opportunities

The overarching purpose of this report is to investigate potential hydrologic mediations for mitigating AMD discharging from the Nelson tunnel. Moreover, the control and management of Nelson Tunnel discharge will become more difficult due to the continually degrading mine

tunnel integrity, limited safe access, and unknown spatial extent of inflow areas. Thus, catastrophic discharge from the Nelson tunnel is a possibility, and even likely in the future. The current conceptual understanding is that the Nelson Tunnel discharge is sourced from upwelling deep groundwater into sub-Nelson workings. At this time the lowering of water levels in the Nelson Tunnel and sub-Nelson workings to adequately identify and quantify sources of inflow is cost-prohibitive. Additionally, there is no evidence to support that inflowing water would be of improved water quality relative to the current mine discharge. Based on the large regional extent of mineralization associated with the graben and intragaben fault structures there is reason to believe the groundwater moving along those structures is of poor quality prior to emergence in the mine. Installation of a bulkhead at the Nelson Tunnel will cause the water level behind the Nelson Tunnel portal to rise above the bulkhead (as conceptualized with the higher pre-mining potentiometric surface). The AMD water held behind the bulkhead will then disperse through other existing tunnels associated with the mine, perhaps making the situation worse than its present state. An additional complication to bulkhead options is that the Nelson Tunnel discharge currently represents a surface water right for the City of Creede and any reduction of that source would likely require water court proceedings, which could be uncertain and costly.

There has been some thought given to drilling a well or wells to intercept upwelling water near and up gradient of the Nelson Tunnel inflows. However, the likelihood is very low for a well to intercept preferential flow within the intragaben area sufficient to produce 270 gpm (i.e. equivalent to the current steady state of Nelson Tunnel discharge). Additionally, if sufficient flow was intercepted by wells the water chemistry may still be similar to the AMD currently discharging at the Nelson Tunnel portal and the water would still have to be treated.

The remediation options are therefore likely limited to active treatment of mine water and

a treatment facility at the Nelson Tunnel portal may not be feasible or desirable due to the proximity of the City of Creede. The high degree of hydrologic connectivity between the Bulldog and Amethyst graben faults suggests that you can control water from either location. Therefore, an attractive mitigation strategy is to lower water levels in the non-discharging Bulldog mine. Once the water level in the Bulldog mine decreases below 2,800 m (the elevation of the Nelson Tunnel portal), water will no longer discharge from the Nelson Tunnel. The water pumped from the Bulldog mine could be treated on-site and may be a better and less costly solution than directly treating Nelson Tunnel discharge. The treated water could then be discharged back to Willow Creek via Windy Gulch.

Chapter 5

Synthesis of Results and Implications for Future Research

5.1 Introduction

The primary objective of this research was to characterize surface and groundwater interactions in natural and mining impacted mountain watersheds. To achieve this, physical measurements of hydrological processes were combined with analysis of isotopic and geochemical signatures of various water sources in three undisturbed headwater catchments in Boulder Creek watershed and at two abandoned mine sites in the San Juan Mountains of Colorado. The undisturbed catchments reside across an elevational gradient, which spans from the rain/snow transition in the montane forests to the snow dominated alpine region enabling a comparative analysis of how varying temperature and precipitation regimes influence hydrologic partitioning between surface water and groundwater and the degree to which those changes influence streamflow generation. Tracing techniques were also employed at the abandoned mine sites to quantify the sources, flow paths and residence times of waters contributing to Acid Mine Drainage (AMD). The information obtained from all studies was conceptualized to understand existing hydrologic processes, with the goal of generating a better process-based understanding of how water moves through natural and disturbed mountain areas.

5.2 Boulder Creek Catchment Hydrology

Meteorological data was collected between 2010 and 2012 in each catchment in Boulder Creek watershed to compare and contrast both changes across catchments and inter-annual variability within each catchment. During the study the catchments experienced precipitation

inputs that were average (2010), above average (2011) and below average (2012) relative to long-term records. In 2012 all catchments experienced peak discharge associated with summer rain as opposed to traditional snowmelt dominated hydrographs observed in the other years. Results from 2012 therefore demonstrate that all elevations are currently susceptible to seasonal scale shifts in timing of peak streamflow that are greater than documented shifts in timing attributed to temperature driven changes in snowmelt delivery alone (Clow, 2010). Precipitation regimes varied from 512 ± 43 mm ($39 \pm 10\%$ snow) at the lowest elevation catchment to 1439 ± 289 mm ($84 \pm 10\%$ snow) in the alpine. The orographic lapse rate was greatest in 2011 (97 mm per 100 m elevation), which was attributed to proportionately higher snowfall in the alpine, suggesting that current variability in precipitation is more pronounced in winter. Runoff efficiency (Q/P) increased with elevation, averaging 10% in the montane, 24% in the sub-alpine, and 88% in the alpine. The inter-annual variability in calculated runoff efficiency was greatest in the alpine (20%) and decreased at lower elevations. However measurement errors for solid precipitation frequently range from 20% to 50% due to undercatch in windy conditions (Rasmussen *et al.* 2012), which are common in the alpine environment. Therefore measurement accuracy of precipitation and accounting for orographic lapse rate are particularly important in accurately quantifying runoff efficiency in mountain areas dominated by winter precipitation. This study utilized a 30-year correlation of total winter precipitation measured at two alpine locations (D-1 and Arikaree) to account for the likelihood of undercatch and improve calculations of P. Efforts were also made to improve quantification of Mean Annual Precipitation (MAP) in the mid-elevation CC catchment by averaging measurements from multiple gages at one elevation and accounting for orographic lapse rate. The annual variability between different types of co-located gages at the C-1 site was $13\% \pm 3\%$, which further suggests that the type and

specific location of gages can generate additional uncertainty in quantification of catchment inputs from point measurements even in forested locations. Additionally, distribution of precipitation into three distinct elevation bands increased the catchment MAP by $17 \pm 9\%$ relative to the MAP at C-1 alone, further demonstrating that extrapolating point measurements of precipitation to catchment scale may over or under estimate catchment inputs. When an orographic lapse rate is identified precipitation will be under estimated if measurements are lower in the catchment, especially where catchments span both forested and alpine areas. The identified difficulty in quantifying precipitation at the catchment scale from point measurement suggest that caution should be taken when interpreting the significance of inter-annual changes in runoff efficiency as magnitude of accumulated uncertainty may be as great as the observed change in efficiency calculation. Therefore inter-annual changes in runoff efficiency at each site may not be significant, but still provide a first order qualitative comparison of spatial and temporal changes over the full elevation gradient under investigation. The high runoff efficiency in the alpine, even in during low snowfall years, indicates that at these elevations less snow and early melt does not directly translate into decreased efficiency (i.e. greater ET). However, in the forested CC catchment runoff efficiency was lowest in the low snow year of 2012 (16%), which was more similar to GG (9%) than in 2011 when runoff efficiency was 28% and 11% respectively. A decrease in runoff efficiency in CC could be the result of greater ET losses because less snow and earlier melt promoted a longer growing season (Hu *et al.* 2010). In GG runoff efficiency was only 2% lower in 2012 while there was 15% less total precipitation than in 2011. Interestingly, even though spring snowmelt occurred earlier in all catchments in 2012, GG actually received more snow in 2012 than 2011. This suggests that in the rain-snow transition, where snowmelt can occur throughout the winter, the total amount of snow (and

subsequent snowmelt) may be more important to maintaining runoff efficiency than the timing of the spring snowmelt pulse.

End Member Mixing Analysis (EMMA) in the three catchments was able to examine 45 potential end-members representing all different types of sources that could be sampled including rain, snow, snowpack, snowmelt, soil water, groundwater (various depths), talus flow and rock glacier discharge. Three distinct end-members were able to account for stream variability in each catchment. Streamflow was partitioned into groundwater, rain, and snow in the montane and sub-alpine catchments and from groundwater, talus water, and snow in the alpine catchment. On average annual streamflow in the montane was 43% groundwater, 41% snowmelt water, and 16% rain while in the subalpine streamflow was 36% groundwater, 54% snowmelt water, and 10% rain. Alpine streamflow was 21% groundwater, 58% snowmelt water, and 21% talus water. During average (2010) and above average (2011) snowfall years, snowmelt was the dominant contributor to streamflow in all catchments. However in 2012 snowmelt water contribution was reduced to 30%, 42%, and 50% from low to high elevation with earlier and smaller peak contributions in all catchments. Interestingly, groundwater contributions were greatest in 2012 for the montane and sub-alpine catchments but were lower in the alpine catchment showing that groundwater contributions can be reduced in the alpine when the magnitude of snowmelt is reduced. Subsurface characterization (extent of soil and weathered profile development) indicates that the decrease in groundwater contribution with elevation is at least partly explained by decreasing storage capacity in the subsurface. At GG it appears that potential storage is greater than recharge, as a lack of sustained hydrologic connectivity on south-facing slopes (Hinckley *et al.* 2012) limits groundwater recharge on those slopes. EMMA was able to support this hypothesis by demonstrating that groundwater contributions to

streamflow were most similar to the groundwater collected on the north-facing slopes. In CC groundwater recharge is likely disproportionately supported by recharge from snowmelt derived in the upper portion of the catchment near treeline as snowmelt recharge at lower elevations of the catchment is smaller and is competing against increased water losses (ET) from the forest. Moving to the alpine there are generally limited soil and weathered rock profiles and groundwater storage appears to be constrained by extent of fractured bedrock, which is extremely difficult to quantify. A second subsurface water source is the water stored in talus slopes above the bedrock. The talus water is intermediate in transit time between direct runoff and bedrock groundwater flow and provides an important contribution to streamflow in the late summer and fall. The talus contribution was greatest in 2012 when snowmelt contribution was smallest, which was likely driven by a combination of processes. First there was likely a reduction in groundwater recharge in 2012, which may have lowered the groundwater table to an extent at which it became disconnected from streamflow at the elevation of the catchment outlet. Second, the small snowpack would have exposed many of the talus slopes earlier in the summer allowing greater warming of the subsurface and potential release of additional stored water in the form of melting ice lenses and permafrost (i.e. Caine, 2010). The third confounding factor was above average summer rainfall which was dominated by >100 mm of precipitation in just a few days in early July. The large magnitude rain may have been sufficient to considerable increase hydrologic connectivity in the talus and push more of that water to the stream. Regardless of the mechanism, talus water can be an important source of streamflow in the alpine, and may help to offset limitations in groundwater contributions brought about by reduced snowmelt recharge, but a threshold magnitude of summer rain may be necessary to move the talus water to the stream.

5.2.1 Space-For-Time Substitutions

The results of this study expand upon the applicability of space-for-time substitutions in Boulder Creek watershed first presented by Williams *et al.* (2011). Specifically this study agrees that there is a continuum of decreasing air temperature and increasing precipitation with elevation. However, this study provides evidence that there is a continuum of increasing runoff efficiency with elevation from the rain/snow transition in the montane to the alpine. The results also show that there is a continuum of decreasing sub-surface storage capabilities with elevation that translate into a decrease in groundwater contributions to streamflow with elevation. As a result this study argues that it is the processes governing groundwater recharge that are of greatest importance to understand in order to use space-for-time substitutions to predict how ecosystems at different elevations may respond to changes in climate. Specifically, the alpine is dependent on the overall magnitude of seasonal snowmelt to sustain recharge and groundwater connectivity to stream flow. This trend continues into catchments that span the alpine and sub-alpine with the magnitude of snowfall occurring at and above treeline the dominant control on groundwater recharge. Progressing down from the sub-alpine to montane forests where rain/snow transition occurs, it is still the snowmelt that controls recharge but timing and location of the melt becomes increasingly important as ET losses increase with the warmer temperatures at lower elevations. Specifically the timing of spring melt will influence the length of the growing season and subsequent ET losses. Additionally, in the rain/snow transition of the montane forests catchment orientation dictates aspect controls in which north-facing slopes will have more seasonal snowpack, greater melt and increased hydrologic connectivity in soils promoting proportionately greater groundwater reservoirs and contributions to streamflow from those hill slopes.

5.3 Surface and Groundwater Interactions with Abandoned Mines

The construction of hardrock mines can be analogous with making Swiss cheese out of mountains often resulting in the creation of unnatural increases in surface water and groundwater interactions. Mine tunnels provide direct access to different depths within the flow system, but they can severely perturb natural flow paths and rates, drawing near-surface water to depths well below where it normally circulates (Polyakov *et al.* 1996). Most hardrock mines are specifically targeting mineralization associated with faulting and fracturing of parent bedrock material associated with mountain building processes. For obvious reasons associated with accessibility, the mines are also generally located in areas where there is surface or near-surface expression of the geologic activity associated with mineralization. From an economic standpoint, the mines also generally target mineral reserves that are closest to the surface. As a result the mine environments will frequently interact with surface water and/or groundwater processes that are being actively controlled by present day hydrologic conditions (i.e. timing, magnitude, and type of precipitation). Additionally, mine workings have potential of interaction with deeper groundwater that has traveled along long flow paths associated with the secondary porosity of bedrock fracturing and faulting. The long flow path groundwater is synonymous with what has been described as “mountain block recharge” (Manning and Caine, 2007) in numerous natural mountain settings. This type of groundwater flow is therefore often recharged from high elevation alpine areas where snow-dominated precipitation is greatest and then travels along diverse and non-uniform pathways before being intercepted by the mine. As a result mine environments can interact with both localized and regional scale hydrologic processes demonstrating the need to be able to investigate the surface and subsurface water interactions at a wide range of spatial and temporal scales to gain a process-based understanding of how AMD is

generated. There is also clear implication of the need to understand both the localized and regional geologic setting and sub-surface architecture influencing water movement into and out of mine environments. A strong conceptual understanding of the location and magnitude of both drivers (inputs from precipitation or surface flows) and controls (extent of hydrologic connectivity in the subsurface) is therefore necessary to address remediation opportunities to reduce long-term impacts of mines on water resources in mountains.

The research presented herein has demonstrated that the use of natural tracers (i.e. water isotopes) can successfully discern the variability in source contributions to AMD production even in abandoned mines with limited direct access. The addition of applied tracers to mine hydrology studies can also help locate where surface waters are making direct contributions to mine waters and to help untangle the complex flows and mixing scenarios within the mine workings to ultimately discern where the water is coming from. To elaborate the natural tracers like ^{18}O are good tools for identifying rapid temporal changes in sourcing of AMD when large seasonal fluctuations in inputs (precipitation or surface flows) exist. Furthermore, analysis of naturally occurring radioactive isotopes are particularly useful for understanding the timing of surface water, groundwater, and mine water interactions. Specifically, tritium works well for intermediate time scales (years to decades) while radiocarbon works well for longer time scales (hundreds to thousands of years).

5.4 Cumulative Conceptual Model

A conceptual diagram is presented to compare and contrast the surface and groundwater interactions that were observed in both natural and mine impacted mountain environments (Figure 5.1). The left side of the figure combines the results from each individual catchment in

Boulder Creek watershed to conceptualize the continuum of the hydrologic processes that occur from the rain/snow transition in the montane to the snow dominated alpine. The continuum of increasing precipitation, precipitation falling as snow, and catchment yield or runoff efficiency is shown with the vertical and horizontal arrows while changes in groundwater movement with elevation are shown by the curved arrows. A general representation of the sub-surface architecture is provided to demonstrate that there is similar underlying bedrock geology across the entire elevational gradient that is overlain by variable forms of consolidated and unconsolidated materials. The overall depth of surficial deposits, soils, and weathered rock tends to decrease with elevation, which demonstrates a decrease in potential groundwater storage capacity with elevation. Groundwater flow in the bedrock is primarily limited to fracture flow with direct evidence that some bedrock groundwater has short flow paths discharging to the alpine while indirect evidence from other research in this type of setting (i.e. Manning and Solomon, 2005; Manning and Caine, 2007) suggests that there may be some deeper and longer bedrock groundwater flow paths which are recharged in the alpine and may not discharge until reaching the mountain front. The groundwater flow in sub-alpine catchments is dominated by snowmelt recharge near treeline while in the montane the groundwater contributions to streamflow are coming from snowmelt on the north-facing slope as shown previously in Figure 2.21c. To summarize the recharge in the alpine is driven by the magnitude of seasonal snowmelt while its overall contribution to streamflow is controlled by limited sub-surface storage capacity. Meanwhile the magnitude of recharge from treeline down to the montane is still driven by snowmelt but has increasing sensitivity to the timing of that delivery and landscape controls like aspect because increasing available energy (i.e. warmer temperatures) increases water loss (ET) at lower elevations.

The right side of Figure 5.1 depicts a similar mountain environment with the addition of a complex of mining tunnels commonly found in abandoned hard rock mine settings. The mine tunnels create an artificial flow path for intercepted groundwater to move towards the surface, picking up metals along the way and discharging to the surface as AMD. The shorter flow path (A) depicts mine interception of shallower recharge that occurs near the mine environment and fluctuates on short time scales in response to seasonal meteoric recharge. Meanwhile, the longer flow path (B) depicts mine interception of deep circulating groundwater that has traveled long distances via fracture flow before interacting with the faults that are being mined. The flow path B is recharged at higher elevations where the magnitude of snowmelt is greatest and is similar to the long mountain block recharge flow paths depicted in the natural mountain setting. The flow path A is most similar to the conditions identified as contributing to AMD at the Rico-Argentine mine, while flow path B represents the conditions that are driving AMD production at the Nelson Tunnel in Creede. The conceptual diagram therefore demonstrates that hardrock mines can interact with variable groundwater flow paths generated from unique sources of recharge.

The cumulative results demonstrate the importance of accurate characterization of groundwater flow in both natural and mining impacted mountain environments to fully understand the relationship between inputs (precipitation) and outputs (stream/mine discharge). Improved understanding of the surface and groundwater interactions will ultimately lead to a greater ability to predict how future changes in climate will impact water resources in natural settings while also enhancing the ability improve water quality in mining environments by making informed remediation decision.

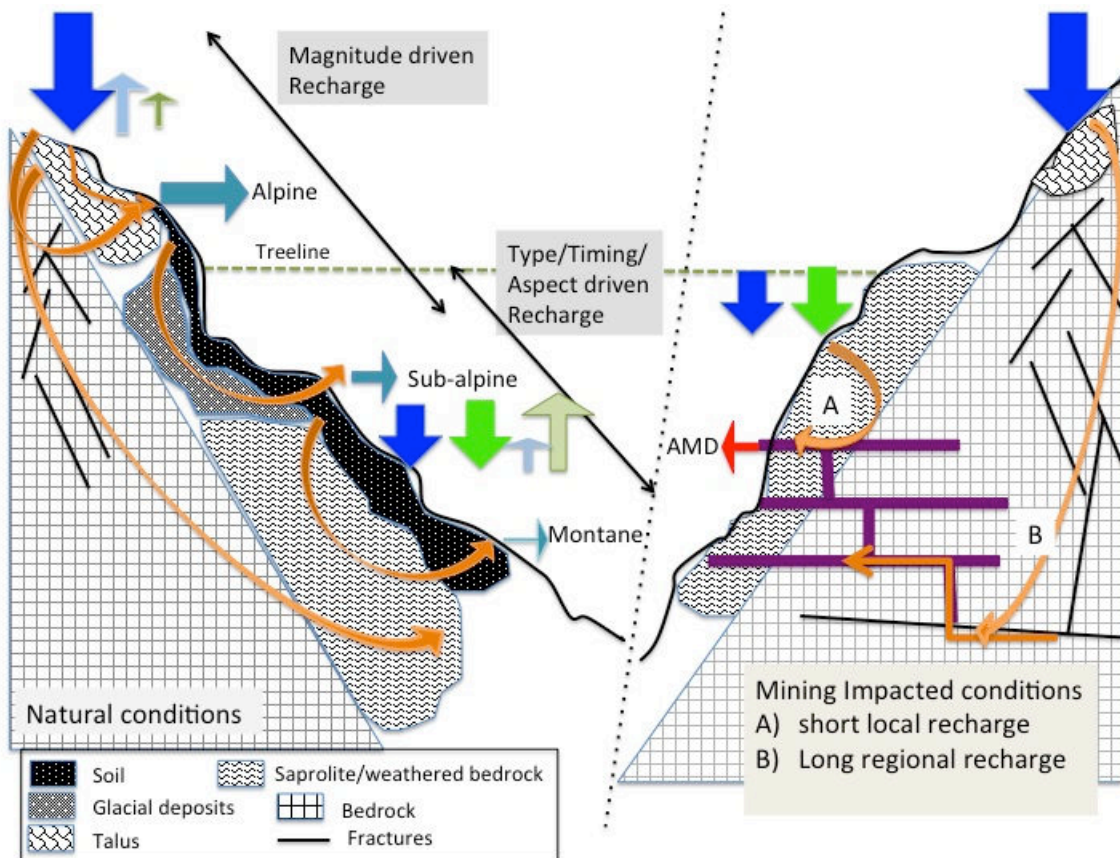


Figure 5.1: Conceptual diagram of surface water and groundwater interactions in natural and mining impacted mountain environments. The arrows depict the direction and magnitude of water movement. Precipitation is separated into snow (blue) and rain (green) with water losses as ET partitioned into summer (light green) and winter (light blue). Natural surface flows are blue/green while mine discharge is red. Groundwater flow is in orange.

5.5 Implications for Future Research

5.5.1 Natural Mountain Environments

The results of this research suggest that there is still a need to improve the quantification and spatial distribution of precipitation in mountain environments. Although there are significant recent advances in remote sensing to quantify the magnitude of snow inputs to mountains, this research demonstrates that even high elevation catchments are experiencing more rain contributions to annual precipitation, which cannot be accounted for with remote sensing. Secondly the current extent of the rain to snow transition zone is under defined, which will

become increasingly important, as this zone is likely to shift higher in elevation with projected climate change. Additionally, this research points to temperature controls on hydrologic partitioning to be strongest in the rain/snow transition zone but are also important to the overall water balance in catchments that span up to and beyond treeline. Warming climate likely to strengthen that temperature control all the way to treeline making the elevation band above rain/snow transition but below the alpine potentially more hydrologically susceptible to change.

In addition, this research further demonstrates the importance of groundwater to streamflow generation and runoff efficiency, thus encouraging greater emphasis on measuring groundwater conditions. Improved understanding of groundwater processes is of particular importance in research catchments where the information can be combined with the large amount of data already collected on hydrologic partition at the surface to comprehensively measure all parts of the hydrologic cycle at the catchment scale.

Meanwhile the alpine hydrologic cycles observed in this research are currently controlled by variability in total precipitation. The direction of future precipitation regimes is less certain than temperature, making predictions harder. However groundwater storage and contribution to streamflow appears lower in the alpine suggesting less stable to future changes in precipitation. Conversely, the lower elevations generally have greater subsurface storage capacity and groundwater contribution to streamflow pointing to the need improve the understanding of groundwater recharge at those elevations. If precipitation shifts towards more rain, recharge may be reduced leading to a decrease in the groundwater portion of streamflow, which may be particularly important with regards to sustaining base flow in headwater streams.

5.5.2 Mining Impacted Mountain Environments

This research has shown that detailed hydrologic investigations in mine settings may present more remediation options than the traditional end-of-pipe treatment strategy that is most commonly employed now. The mine investigations presented here also demonstrate that natural and applied tracer techniques commonly applied in natural settings can be used in mine environments if proper analytical procedures are applied (i.e. removal of iron from mine water samples before attempting fluorescence analysis of dissolved organic matter). Additionally, obtaining a detailed understanding of the sources and pathways of water contributing to AMD and associated surface waters to which it discharges will enable remediation management to account for future climate scenarios. For example, most mines in the western United States are in mountain headwater catchments and adjacent to headwater streams with seasonally variable discharge. Additionally, the level of treatment of AMD is often determined based on adherence to surface water quality standards downstream of where the AMD is discharged with assumption of dilution through mixing with the non-impacted waters. Therefore, with climate driven increased variability in surface flow, and potentially decreased baseflow, it will become harder to determine the level of treatment of AMD to attain in-stream water quality standards. Finally, at mine sites where discharge of AMD is driven by rapid infiltration of meteoric waters there may be an increased variability of timing and magnitude of contaminant load in mine discharge, which makes control more difficult and treatment options more complex.

References

- Aishlin, P., & J. P. McNamara (2011) Bedrock infiltration and mountain block recharge accounting using chloride mass balance, *Hydrological Processes*, 25(12), 1934-1948.
- Ajami, H., Troch, P.A., Maddock III, T., Meixner, T., & C. Eastoe (2011) Quantifying mountain block recharge by means of catchment-scale storage-discharge relationships, *Water Resources Research*, 47, W04504.
- Aldous, P.J., & P. L. Smart (1988) Tracing groundwater movement in abandoned coal mined aquifers using fluorescent dyes. *Ground Water*, 26, 172-178.
- Ali, G. A., Roy, A. G., Turmel, M. C. & F. Courchesne (2010) Source-to-stream connectivity assessment through end-member mixing analysis. *Journal of Hydrology*
- Alvarado, J. A. C., Purtschert, R., Barbecot, F., Chabault, C., Ruedi, J., Schneider, V., Aeschbach-Hertig, W., Kipfer, R., & H. H. Loosli (2007) Constraining the age distribution of highly mixed groundwater using ³⁹Ar: A multiple environmental tracer (H-3/HE-3, Kr-85, AR-39, and C-14) study in the semiconfined Fontainebleau Sands Aquifer (France), *Water Resources Research*, 43, W03427, doi:10.1029/2006WR005096.
- Anderson S.P., von Blanckenburg F., & A. F. White (2007) Physical and chemical controls on the critical zone, *Elements*, 3, 315–319.
- Aravena, R. & L. I. Wassenaar (1993) Dissolved organic carbon and methane in a regional confined aquifer. Evidence for associated subsurface sources. *Applied Geochemistry*, 8, 483-93.
- August, E. E., Mcknight, D. M., & D. C. Hrcir (2002) Seasonal Variability of Metals Transport through a wetland impacted by mine drainage in the Rocky Mountains. *Environmental Science and Technology*, 36(17), 3779-3786.
- Bales, R. C., & D. Cline (2003) Snow hydrology and water resources (Western United States). In *Handbook of Weather, Climate, and Water; Atmospheric Chemistry, Hydrology, and Societal Impacts*; Potter, Bradley, Eds.; John While and Sons: Hoboken, United States; pp. 443-459.
- Bales, R. C., Hopmans, J. W., O'Geen, A. T., Meadows, M., Hartsough, P. C., Kirchner, P., Hunsaker, C. T., & D. Beaudette (2011) Soil moisture response to snowmelt and rainfall in a Sierra Nevada mixed-conifer forest, *Vadose Zone Journal*, 10, 786-799.
- Banner, J. L., Musgrove, M. L., Asmerom, Y., Edwards, R. L., & J. A. Hoff (1996) High-resolution temporal record of Holocene ground-water chemistry: tracing links between climate and hydrology, *Geology*, 24, 1049–1053.

Bates, B., Kundzewicz, Z. W., Wu, S., & J. P. Palutikof (2008) Climate change and water, *Technical paper VI of the Intergovernmental Panel on Climate Change*. Intergovernmental Panel on Climate Change Secretariat, Geneva, Switzerland, 210 pp.

Barnett, T. P., Adam, J. C., & D. P. Lettenmaier (2005) Potential impacts of a warming climate on water availability in snow-dominated regions, *Nature*, 438(17), 303-309.

Barton, P. B. Jr., Bethke, P. M., & E. Roedder (1977) Environment of ore deposition in the Creede Mining District, San Juan Mountains, Colorado: Part III. Progress toward interpretation of the chemistry of the ore-forming fluid for the OH vein, *Econ. Geology*, v. 72, p. 1-24.

Bavay, M., Lehning, M., Jonas, T., & H. Lowe (2009) Simulations of future snow cover and discharge in Alpine headwater catchments, *Hydrological Processes*, 23(1), 95-108.

Befus, K. (2010) Applied geophysical characterization of the shallow subsurface: Towards quantifying recent landscape evolution and current processes in the Boulder Creek watershed, CO, *M.S. Thesis*, Geological Sciences, University of Colorado, Boulder, CO.

Behrens, H., Beims, U., Dieter, H., Dietze, G., Eikmann, T., Grummt, T., Hanisch, H., Henseling, H., Käß, W. A., Kerndorff, H., Leibundgut, C., Muller-Wegener, U., Ronnefahrt, I., Scharenberg, B., Schleyer, R., Schloz, W., & F. Tilkes (2001) Toxicological and ecotoxicological assessment of water tracers, *Hydrogeology Journal*, 9, 321-325.

Bencala, E., McKnight, D. M., & G. W. Zellweger (1987) Evaluation of natural tracers in an acidic and metal-rich stream, *Water Resources Research*, 23, 827-836.

Bencala, K. E., McKnight, D. M., & G. W. Zellweger (1990) Characterization of transport in an acidic and metal-rich mountain stream bed on a lithium tracer injection and simulations of Transient Storage, *Water Resources Research*, 26, 989-1000.

Benedict, J. B. (1970) Downslope soil movement in a Colorado alpine region: rates, processes, and climatic significance, *Arctic and Alpine Research*, 2(3), 165-226.

Bethke, P. M. (1988) The Creede, Colorado ore-forming system: a summary model. U.S. Geol. Survey, Open-File Report 88-403, 29 p.

Bethke, P. M., & R. L. Hay (2000) Ancient Lake Creede: Its volcano-tectonic setting, history of sedimentation and relation to mineralization in the Creede Mining District: Boulder, Colorado, Geological Society of America special paper 346, 326 pp.

Bethke, P. M., & P. W. Lipman (1987) Deep environment of volcanogenic epithermal mineralization: proposed research drilling at Creede, Colorado: EOS (American Geophysical Union Trans.), v. 68, no. 13, p. 177, 187-189.

- Beven, K. J. (2000) Uniqueness of place and process representations in hydrological modeling, *Hydrology Earth System Science*, 4(2), 203-213.
- Bossong, C. R., Caine, J. S., Stannard, D. I., Flynn, J. L., Stevens, M. R., & J. S. Heiny-Dash (2003) Hydrologic conditions and assessment of water resources in the Turkey Creek Watershed, Jefferson County, Colorado, 1998– 2001, *U. S. Geol. Surv. Water Resour. Invest.*, 03– 4034.
- Bovolo, C. I., Parkin, G., & M. Sophocleous (2009) Groundwater resources, climate and vulnerability, *Environmental Research Letters*, 4(3), 035001.
- Bradley, W. C. (1987) Erosion surfaces of the Colorado Front Range: a review. *In: Geomorphic Systems of North America: Graf, W.L. (Ed)*, Boulder, Colorado, Geological Society of America, Centennial Special Volume 2, 215-220.
- Brigand, F. G., Lellouche, G., & T. W. Appelboom (2013) Measuring flow in non-ideal conditions for short-term projects: Uncertainties associated with the use of stage-discharge rating curves, *Journal of Hydrology*, 503, 186-195.
- Bretzler, A., Osenbruck, K., Gloaguen, R., & J. S. Ruprecht (2011) Groundwater origin and flow dynamics in active rift systems – A multi-isotope approach in the Main Ethiopian Rift, *Journal of Hydrology*, 402, 274-289.
- Burns, D. A., (2002) Stormflow-hydrograph separation based on isotopes: the thrill is gone-what's next?, *Hydrological Processes*, 16(7), 1515-1517.
- Byington, C. (2012) Characterization of Water Conduits Related to the Nelson Tunnel Mine Drainage, Creede, Colorado. Report submitted to the U.S. Environmental Protection Agency by Millennium GeoScience.
- Byrne, P., Wood, P. J., & I. Reid (2012) The impairment of river systems by metal mine contamination: A review including remediation options, *Critical Reviews in Environmental Science and Technology*, 42, 2017-2077.
- Caine, J. S., Manning, A. H., Verplanck, P. L., Bove, D. J., Kahn, K. G., & S. Ge (2006) Well construction information, lithologic logs, water level data, and overview of research in Handcart Gulch, Colorado: An alpine watershed affected by metalliferous hydrothermal alteration, *U.S. Geol. Surv. Open File*, 06– 1189.
- Caine, N. (1974) The geomorphic processes of the alpine environment, *In: Arctic and Alpine Environments*, Ives, J. D., & R. G. Barry (eds.), Methuen: London; 721-748.
- Caine, N. (1996) Streamflow patterns in the alpine environment of North Boulder Creek, Colorado Front Range, *Z Geomorphol*, 104, 27-42.

- Caine, N. (2001) Geomorphic systems of Green Lakes Valley, *In: Alpine Dynamics: The structure and function of an alpine ecosystem; Niwot Ridge, Colorado*, Bowman, W., & T. R. Seastedt (eds.), Oxford University Press: Oxford, 45-74.
- Canovas, C. R., Hubbard, C. G., Olias, M., Nieto, J. M., Black, S., & M. L. Coleman (2008) Hydrochemical variations and contaminant load in the Rio Tinto (Spain) during flood events, *Journal of Hydrology*, 350, 25–40.
- Capo, R. C., Stewart, B. W., & O. A. Chadwick (1998) Strontium isotopes as tracers of ecosystem processes: theory and methods, *Geoderma*, 82, 197-225.
- Chapman, E. C., Capo, R. C., Stewart, B. W., Kirby, C. S., Hammack, R. W., Schroeder, K. T. & H. M. Edenborn (2012) Geochemical and Strontium Isotope Characterization of produced waters from Marcellus Shale Natural Gas Extraction, *Environmental Science and Technology*, 46, 3545-3553.
- Christophersen N., & R. P. Hooper (1992) Multivariate analysis of stream flow chemical data: the use of principal components analysis for the endmember mixing problem, *Water Resources Research*, 28(1), 99-107.
- Christophersen, N., C. Neal, R. P. Hooper, R. D. Vogt, & S. Andersen (1990), Modeling stream water chemistry as a mixture of soil water end-members- A step towards second-generation acidification models, *Journal of Hydrology*, 116, 307-320.
- Christensen, L., Tague, C. L., & J. S. Baron (2008) Spatial patterns of simulated transpiration response to climate variability in a snow dominated mountain ecosystem, *Hydrological Processes*, 22, 3576-3588.
- Claassen, H. C. & J. S. Downey (1995) A model for deuterium and oxygen-18 isotope changes during evergreen interception of snowfall, *Water Resources Research*, 31(3), 601-618.
- Clark, I. D. & P. Fritz (1997) *Environmental Isotopes in Hydrogeology*. CRC Press: Boca Raton, FL; 328pp.
- Clow, D. W., Schrott, L., Webb, R., Campbell, D. H., Torizzo, A., & M. Dornblaser (2003) Ground water occurrence and contributions to streamflow in an alpine catchment, Colorado Front Range, *Groundwater*, 41(7), 937-950.
- Clow, D. W. (2010) Changes in the timing of snowmelt and streamflow in Colorado: A response to recent warming, *Journal of Climate*, 23(9), 2293-2306.
- Cory, R., & D. M. McKnight (2005) Fluorescence spectroscopy reveals ubiquitous presence of oxidized and reduced quinones in dissolved organic matter. *Environ. Sci. Technol.*, 39(21), 8142–8149.

Cory , R.M. , Miller , M. P. , McKnight , D.M. , Guerard , J. J. , & P. L. Miller (2010) Effect of instrument-specific response on the analysis of fulvic acid fluorescence spectra, *Limnol. Oceanogr. Meth.*, 8, 67-78.

Cowie, R., Williams, M. W., Wiremen, M., & R. L. Runkel (2014) Use of natural and applied tracers to guide targeted remediation efforts in an acid mine drainage system, Colorado Rockies, USA, *Water*, 6, 745-777, doi:10.3390/w6040745.

Craig, H. (1961) Isotopic variations in meteoric waters, *Science*, 133, 1702-1703.

Davies, G. (2002) Results of Ground-Water Tracing Experiments in the Nelson-Wooster-Humphrey Tunnel; Cambrian Ground Water Co.: Oak Ridge, TN, USA, p. 14.

Davis, S. N., Thompson, G. M., Bentley, H. W., & G. Stiles (1980) Ground-water tracers-A short review, *Ground Water*, 18, 14-23.

Davis, A., Olsen, R. L., & D. R. Walker (1991) Distribution of metals between water and entrained sediment in streams impacted by acid mine discharge, Clear Creek, Colorado, U.S.A., *Applied Geochemistry*, 6, 333-348.

Davis M. W. (1994) The Use of Tracer Dyes for the Identification of a mine Flooding Problem, Rico, Dolores County, Colorado. *Colorado Geological Survey Open File Report 91-2*, 1-20.

Degens, E. T. (1967) Diagenesis of organic matter, in *Diagenesis in Sediments*, Larson, G., & G. V. Chilanger (eds.), pp. 343-390, Elsevier, New York.

Dettinger, M. D., & S. Earman (2007) Western ground water and climate change- pivotal to supply sustainability or vulnerable in its own right?, *Groundwater*, 4(1), 4-5.

DeWalle, D. R., Swistock, B. R., & W. E. Sharpe (1988) Three-component tracer model for stormflow on a small Appalachian forested catchment, *Journal of Hydrology*, 144, 301-310.

Dingman S. L. (2002) *Physical Hydrology (2nd Edition)*. Prentice Hall: Upper Saddle River, New Jersey.

Doherty, S. J., Bojinski, S., Henderson-Sellers, A., Noone, K., Goodrich, D., Bindoff, N. L., Church, J. A., Hibbard, K. A., Karl, T. R., Kajefez-Bogataj, L., Lynch, A. H., Parker, D. E., Prentice, I. C., Ramaswamy, V., Saunders, R. W., Smith, M. S., Steffen, K., Stocker, T. F., Thorne, P. W., Trenberth, K. E., Verstraete, M. M., & F. W. Zwiers (2009) LESSONS LEARNED FROM IPCC AR4 Scientific Developments Needed To Understand, Predict, And Respond To Climate Change, *Bulletin of the American Meteorological Society*, 90, 497-+.

Eastoe, C. J., & R. Rodney (2014) Isotopes as tracers of water origin in and near a regional carbonate aquifer: The Southern Sacramento Mountains, New Mexico, *Water*, 6, 301-323.

- Erickson, T. A., Williams, M. W. & A. Winstral (2005) Persistence of topographic controls on the spatial distribution of snow in rugged mountain terrain, Colorado, United States, *Water Resources Research*, 41, W04014, doi:10.1029/2003WR002973.
- Faure, G., & J. L. Powell (1972) *Strontium Isotope Geology*. Springer-Verlag, New York, 188 pp.
- Faure, G., (1986) *Principles of Isotope Geology*. Wiley, New York, 589 pp.
- Fellman, J.B., Hood, E., & R. G. M. Spencer (2010) Fluorescence spectroscopy opens new windows into dissolved organic matter dynamics in freshwater ecosystems: A review, *Limnology and Oceanography*, 55(6), 2452-2462.
- Field, M. S., & P. F. Pinsky (2000) A two-region nonequilibrium model for solute transport in solution conduits in karstic aquifers, *Journal of Contaminant Hydrology*, 44,329-351.
- Field M. S. (2002) The QTRACER2 Program for the Tracer-Breakthrough Curve Analysis for Tracer Tests in Karstic Aquifers and Other Hydrologic Systems. EPA/600/R-02/001, U.S. Environmental Protection Agency- Office of Research and Development: Washington, United States, pp. 179.
- Field, M. S. (2003) Tracer-Test Planning Using the Efficient Hydrologic Tracer-Test Design (EHTD) Program. EPA/600/R-03/034, U. S. Environmental Protection Agency- Office of Research and Development; National Center for Environmental Assessment: Washington, United States, pp.175.
- Fierer, N., Chadwick, O. A., & S. E. Trumbore (2005) Production of CO₂ in soil profiles of a California Annual Grassland, *Ecosystems*, 8, 412-429.
- Finkelstein, D. B., Hay, R. L., & S. P. Altaner (1999) Origin and diagenesis of lacustrine sediments of the late Oligocene Creede Formation, southwestern Colorado, *Geological Society of America Bulletin*, v. 111, p. 1175-1191.
- Flury, M., & N. N. Wai (2003) Dyes as Tracers For Vadose Zone Hydrology, *Reviews of Geophysics*, 41, 1-33.
- Foley, N. K. (1990) Petrology and geochemistry of precious and base metal mineralization, north Amethyst vein system, Mineral County, Colorado: unpub. PhD thesis, Virginia Polytechnic Institute and State University, Blacksberg, Virginia, 324 p.
- Fritz, D. E., Farmer, G. L., & E. P. Verplanck (2006) Application of Sr isotopes in secondary silicate minerals to paleogroundwater hydrology: An example from K-metasomatized rocks in the western U.S., *Chemical Geology*, 235, 276-285.
- Frost, C. D., Pearson, B. N., Ogle, K. M., Heffern, E. L., & R. M. Lyman (2002) Sr isotope tracing of aquifer interactions in an area of accelerating coal-bed methane production, Powder

River basin, Wyoming, *Geology*, 30, 923–926.

Gabor, R. S., Baker, A., McKnight, D. M., & M. P. Miller (2014) Fluorescence indices and their Interpretation. In *Aquatic Organic Matter Fluorescence*, Coble, P., Lead, J., Baker, A., Reynolds, D., and Spencer, R.G.M. (eds.), Cambridge University Press, in press. ISBN 9780521764612.

Geyer, S., Wolf, M., Wassenaar, L. I., Fritz, P., Buckau, G., & J. I. Kim (1993) Isotope investigations on fractions of dissolved organic carbon for ^{14}C dating. *Isotope techniques in the study of past and current environmental changes in the hydrosphere and atmosphere*. Vienna: IAEA. P 359-80.

Geyer, T., Birk, S., Licha, T., Leidl, R., & M. Sauter (2007) Multitracer Test Approach to Characterize Reactive Transport in Karst Aquifers, *Ground Water*, 45, 36-45.

Geyh, M. A. (2000) An overview of ^{14}C analysis in the study of groundwater, *radiocarbon*, 42, 99-114.

Gleeson, T., & A. H. Manning (2008) Regional groundwater flow in mountainous terrain: Three dimensional simulations of topographic and hydrogeologic controls, *Water Resources Research*, 44, W10403, doi:10.1029/2008WR006848.

Graham, C. B., Verseveld, W. V., Barnard H. R., & J. J. McDonnell (2010) Estimating the deep seepage component of the hillslope and catchment water balance within a measurement uncertainty framework, *Hydrological Processes*, 24, 3631-3647.

Graves, J. (2008) Preliminary Scope of Work - Commodore Mine Investigations, report for U.S. EPA and Colorado Department of Public Health and Environment Division of Reclamation and Mining Safety.

Green, T. R., Taniguchi, M., & H. Kooi (2007) Potential impacts of climate change and human activity on subsurface water resources, *Vadose Zone Journal*, 6(3), 531-532.

Green, T. R., Taniguchi, M., Kooi, H., Gurdak, J. J., Allen, D. M., Hiscock, K. M., ... & A. Aureli (2011) Beneath the surface of global change: Impacts of climate change on groundwater, *Journal of Hydrology*, 405(3-4), 532–560.

Greenland, D. (1989) The climate of Niwot Ridge, Front Range, Colorado, USA, *Arctic and Alpine Research* 21(4): 380-391.

Greenland, D. & M. V. Losleben (2001) Climate. In *Structure and Function of an Alpine Ecosystem: Niwot Ridge, Colorado*, Bowman W.D., Seastedt T.R. (eds.) Oxford University Press: New York; 15-31.

Hamel, B. L., Stewart, B. W., & A. G. Kim (2010) Tracing the interaction of acid mine drainage with coal utilization byproducts in a grouted mine: Strontium isotope study of the inactive Omega Coal Mine, West Virginia (USA), *Applied Geochemistry*, 25(2), 212-223.

Hamlet, A. F., Mote, P. W., Clark, M. P. & D. P. Lettenmaier (2005) Effects of temperature and precipitation variability on snowpack trends in the western United States, *Journal of Climate*, 18(21), 4545–4561, doi:10.1175/JCLI3538.1.

Hamlet, A. F., Mote, P. W., Clark, M. P. & D. P. Lettenmaier (2007) Twentieth-century trends in runoff, evapotranspiration, and soil moisture in the western United States, *Journal of Climate*, 20(8), 1468–1486, doi:10.1175/JCLI3538.1.

Hayba, D. O. (1993) Numerical Hydrologic Modeling of the Creede Epithermal Ore-Forming System, Colorado, PhD dissertation, University of Illinois at Urbana-Champaign, Urbana, Illinois, 186 p.

Hazen, J. M., Williams, M. W., Stover, B. & M. Wireman (2002) Characterization of acid mine drainage using a combination of hydrometric, chemical and isotopic analyses, Mary Murphy Mine, Colorado. *Environmental Geochemistry and Health*, 24, 1-22.

Herczeg, A. L., & W. M. Edmonds (2000) Inorganic Ions as Tracers, *In: Environmental tracers in subsurface hydrology*, Cook, P., & A. L. Herczeg (eds.), Kluwer Academic Publishers, Norwell, Massachusetts, United States, 529 pp.

Hermann, K.A., & M. Wireman (eds.) (2000) Aquatic Resources Assessment of the Willow Creek Watershed, internal report prepared for the Willow Creek Reclamation Committee by the Ecosystems Protection Program, U.S. Environmental Protection Agency, Region 8, Denver, Colorado.

Hinckley, E. S., Ebel, B. A., Barnes, R. T., Anderson, R. S., Williams, M. W., & S. P. Anderson (2012) Aspect control of water movement on hillslopes near the rain-snow transition of the Colorado Front Range, *Hydrological Processes*, doi:10.1002/hyp.9549.

Hinckley, E. S., Barnes, R. T., Anderson, S. P., Williams, M. W., & S. M. Bernasconi (2014) Nitrogen retention and transport differ by hillslope aspect at the rain-snow transition of the Colorado Front Range, *Journal of Geophysical Research: Biogeosciences*, 119, 1281-1296.

Hoeg, S., Uhlenbrook, S., & C. Leibundgut (2000) Hydrograph separation in a mountainous catchment-combining hydrochemical and isotopic tracers, *Hydrological Processes*, 14(7), 1199-1216.

Holman, I. P. (2006) Climate change impacts on groundwater recharge-uncertainty, shortcomings, and the way forward?, *Hydrogeology Journal*, 14(5), 637-647.

Hooper R. P. (2003) Diagnostic tools for mixing models of stream flow chemistry, *Water Resources Research*, 39(3): 1055, doi: 10.1029/2002WR001528.

Horton, D.G. (1985) Mixed-layer illite/smectite as a paleotemperature indicator in the Amethyst vein system, Creede district, Colorado, U.S.A., *Contr. Mineralogy and Petrology*, 91, 171-179.

Hubert, P., Marin, E., Meyback, M. M., Olive, P., & E. Siwertz (1969) Aspects hydrologiques et sedimentologies de la crue exceptionnelle de la Dranse du Chablais du 22 Septembre 1968, *Arch. Sci. Geneve*, 22(3), 581-604.

Jarrett, R. D. (1990) Hydrologic and Hydraulic research in mountain rivers, *Water Resources Bulletin*, 26, 419-429.

Ingerson, E., & F. J. Pearson (1964) Estimation of age and rate of motion of groundwater by the ^{14}C method, In *Recent Researches in the fields of the Hydrosphere, Atmosphere and Nuclear Geochemistry*, pp. 263-283, Maruzen, Tokyo.

Ives, J. D. & B. D. Fahey (1971) Permafrost occurrence in the Front Range, Colorado Rocky Mountains, USA, *Journal of Glaciology*, 10(58), 105-111.

Jackson, D. (1974) Homestake's hard work pays off at Bulldog Mountain mine, *Engineering and Mining Journal*, 175, pp. 65-70.

Janke, J. R. (2005) The occurrence of alpine permafrost in the Front Range of Colorado, *Geomorphology*, 67, 375-389.

Jarvis, A. P., & P. L. Younger (1997) Dominating chemical factors in mine water induced impoverishment of the invertebrate fauna of two streams in the Durham coalfield, UK, *Chemical Ecology*, 13, 249-270.

Jepsen, S. M., Molotch, N. P., Williams, M. W., Rittger, K. E. & J. O. Sickman (2012) Interannual variability of snowmelt in the Sierra Nevada and Rocky Mountains, United States: Examples from two alpine watersheds, *Water Resources Research*, 48, W02529, doi:10.1029/2011WR011006.

Jin, L., Siegel, D. I., Lautz, L. K., & Z. Lu (2012) Identifying streamflow sources during spring snowmelt using water chemistry and isotopic composition in semi-arid mountain streams, *Journal of Hydrology*, 471, 289-301.

Johnson, D. B., & K. B. Hallberg (2003) The microbiology of acidic mine waters, *Research in Microbiology*, 154, 466-473.

Johnson, D. B., & K. B. Hallberg (2005) Acid mine drainage remediation options: a review. *Science of the Total Environment*, 338, 3-14.

Karlen, I., Olsson, I. U., Kallburg, P., & S. Kilici (1964) Absolute determination of the activity of two ^{14}C dating standards, *ArkivGeofysik*, 4:465-471.

Kasnavia, T., Vu, D., & D. A. Sabatini (1999) Fluorescent dye and media properties affecting sorption and tracer selection, *Ground Water*, 37, 376-381.

- Käb, W.A. (1994) Hydrologic tracing practice on underground contaminations, *Environmental Geology*, 23, 23-29.
- Käb, W. (1998) *Tracing Technique in Geohydrology*; Plat: Rotterdam (Balkema), pp. 581.
- Kapnick, S., & A. Hall (2010), Observed climate, snowpack relationships in California and their implications for the future, *Journal of Climate*, 23(13), 3446–3456, doi:10.1175/2010JCLI203.1.
- Kaufman, S. & W. F. Libby (1954) The natural distribution of tritium, *Physical Review*, 93(6), 1337-1344.
- Kendall, C, & E. A. Caldwell (1998) Fundamentals of isotope geochemistry, *In: Isotope Tracers in Catchment Hydrology*, Kendall, C., & J. J. McDonnell (eds.) Elsevier, Amsterdam, The Netherlands.
- Kilpatrick, F.A.; Cobb, E.D. (1985) Chapter A16. Measurement of Discharge Using Tracers. USGS Techniques of Water-Resources Investigations Reports, Book 3; U.S. Geological Survey: Reston, Virginia.
- Kimball, B. A., Broshears, R. E., Bencala, K. E. & D. M. McKnight (1994) Coupling of hydrologic transport and chemical reactions in a stream affected by acid mine drainage, *Environ. Sci. Technol*, 28, 2065–2073.
- Kimball, B. A., Runkel, R. L., Walton-Day, K., & K. E. Bencala (2002) Assessment of metal loads in watersheds affected by acid mine drainage by using tracer injection and synoptic sampling: Cement Creek, Colorado, USA, *Applied Geochemistry*, 17(9), 1183-1207.
- Kimball, B. A., Walton-Day, K., & R. L. Runkel (2007) Quantification of metal loading by tracer injection and synoptic sampling, 1996-2000. *Integrated investigations of environmental effects of historical mining in the Animas River Watershed, San Juan County, Colorado*, USGS professional paper 1651; Church, S. E., von Guerard, P., & S. E. Finger (eds.); U.S. Geological Survey, 417-495.
- Kennedy, V. C., Kendall, C., Zellweger, G. W., Wyerman, T. A., & R. J. Avanzino (1986) Determination of the components of stormflow using water chemistry and environmental isotopes, Mattole River basin, California, *Journal of Hydrology*, 84, 107-140.
- Klapper, L., McKnight, D. M., Fulton, J. R., Blunt-Harris, E. L., Nevin, K. P., Lovley, D. R., & P. G. Hatcher (2002) Fulvic Acid Oxidation State Detection Using Fluorescence Spectroscopy, *Environmental Science & Technology*, 36 (14), 3170-3175.
- Knowles N., Dettinger M. D., & D. R. Cayan (2006) Trends in snowfall versus rainfall in the Western United States, *Journal of Climate* 19(18): 4545-4559.

Knowles, J.F., Harpold, A. A., Cowie, R., Zeff, M., Barnard, H. R., Burns, S. P., Blanken, P. D., Morse, J.F., & M. W. Williams (*In Review*) The relative contributions of alpine and subalpine ecosystems to the water balance of a mountainous, headwater catchment in Colorado, USA, *submitted to Hydrological Processes* August 2014.

Klaus, J., & J. J. McDonnell (2013) Hydrograph separation using stable isotopes: Review and evaluation, *Journal of Hydrology*, 505, 47-64.

Knop, A. (1878) Über die hydrographischen Beziehungen zwischen der Donau und der Aachquelle im badischen Oberlande. *N. Jb. Min. Geol. Pal.*, 350-363.

Lanphear, M. E. (1995) Geochemical characterization and subsurface flow path evaluation of mine drainage sources in Chalk Creek District, Colorado, *PhD Dissertation*, Colorado School of Mine.

Larsen, E. S. (1930) Recent mining developments in the Creede District, Colorado, U.S.G.S Bull. 811.

Larson, P. B. (1987) Stable isotope and fluid inclusion investigations of epithermal vein and porphyry molybdenum mineralization in the Rico Mining District, Colorado, *Economic Geology*, 82, 2142-2157.

Laudon, H. & O. Slaymaker (1997) Hydrograph separation using stable isotopes, silica and electrical conductivity: an alpine example, *Journal of Hydrology*, 201, 82-101.

Laul, D. & B. Peters (1967) Cosmic Ray Produces Radioactivity on the earth, *Encyclopedia of Physics*, 9(26), Flugge, S. (ed.). Springer-Verlag: New York 551-612

Lawaetz, A. J., & C. A. Stedmon (2009) Fluorescence Intensity Calibration Using the Ramen Scatter Peak of Water, *Applied Spectroscopy*, 63(8), 936-940.

Lavastre, V., La Salle, C., Michelot, J., Giannesini, S., Benedetti, L., Lancelot, J., Lavielle, B., Massault, M., Thomas, B., Gilibert, E., Bourles, D., Clauer, N. & P. Agrinier, (2010) Establishing constraints on groundwater ages with ^{36}Cl , ^{14}C , ^3H , and noble gasses: A case study in the eastern Paris basin, France, *Applied Geochemistry*, 25(1), 123-142.

Lawrence, C. R., Painter, T. H., Landry, C. C., & J. C. Neff (2010) Contemporary geochemical composition and flux of aeolian dust to the San Juan Mountains, Colorado, United States, *Journal of Geophysical research*, 115, G03007, doi:10.1029/2009JG001077.

Lee, G., Bigam, J. M., & G. Faure (2002) Removal of trace metals by coprecipitation with Fe, Al, and Mn from natural waters contaminated with acid mine drainage in the Ducktown Mining District, Tennessee, *Applied Geochemistry*, 17, 569-581.

- Leopold, M., Dethier D. P., Völkel J., Raab T., Rikert T.C., & N. Caine (2008) Using geophysical methods to study the shallow subsurface of a sensitive alpine environment, Niwot Ridge, Colorado Front Range, USA. *Arctic and Alpine Research*, 40 (3), 519–530.
- Leopold, M., Völkel, J., Dethier, D. P., Huber, J., & M. Steffens (2011) Characteristics of a paleosol and its implication for the Critical Zone development, Rocky Mountain Front Range of Colorado, USA, *Applied Geochemistry*, 26, 72–75.
- Leopold, M., Volkel, J., Dethier, D. P., & M. W. Williams (2013a) Changing mountain permafrost from the 1970s to today –comparing two examples from Niwot Ridge, Colorado Front Range, USA, *Zeitschrift für Geomorphologie, Supplementary Issue*.
- Leopold, M., Volkel, J., Huber, J., & D. Dethier (2013b) Subsurface architecture of the Boulder Creek Critical Zone Observatory from electrical resistivity tomography, *Earth Surface Processes and Landforms*, 38, 1417-1431.
- Lewis, W. M., & M. C. Grant (1979) Changes in the output of ions from a watershed as a result of the acidification of precipitation, *Ecology*, 60, 1093-1097.
- Lewis, W. S., Huskie, W. W., Wildow, C., & J. Emerick (1992) An Evaluation of Mining Related Metals Pollution in Colorado Streams, *Report to the Colorado Mined Land Reclamation Division by the Department of Environmental Sciences at the Colorado School of Mines*, Golden, Colorado.
- Lipman, P. W., Steven, T. A., and H. H. Mehnert (1970) Volcanic history of the San Juan Mountains, Colorado, as indicated by potassium-argon dating, *Geol. Soc. America Bull.*, 81, 2329-2352.
- Lipman, P. W., & D. A. Sawyer (1988) Preliminary geology of the San Luis Peak quadrangle and adjacent areas, San Juan Volcanic Field, southwestern Colorado: U.S. Geologic Survey Open-File Report 88-359, 33 p. and map.
- Lipman, P. W. (2000) Central San Juan caldera cluster: regional volcanic framework, *In Ancient Lake Creede: Its volcano-tectonic setting, history of sedimentation, and relation to mineralization in the Creede Mining District*, Bethke, P. M., & R. L. Hay (eds.), Boulder, Colorado, Geological Society of America Special Paper 346.
- Litaor, M. I. (1993) The influence of soil interstitial water on the physicochemistry of major, minor and trace metals in stream waters of the Green Lakes Valley, Front Range, Colorado, *Earth Systems Processes and Landforms*, 18, 489-504.
- Liu, F. J., Williams, M. W., & N. Caine (2004) Source waters and flow paths in an alpine catchment, Colorado Front Range, United States, *Water Resources Research*, 40, 16.

- Liu, F. J., Parmenter, R., Brooks, P. D., Conklin, M. H., & R. C. Bales (2008) Seasonal and interannual variation of streamflow pathways and biogeochemical implications in semi-arid, forested catchments in Valles Caldera, New Mexico, *Ecohydrology*, 1, 239-252.
- Lyons, R. G. (1993) Identification and separation of water tracing dyes using pH response characteristics, *Journal of Hydrology*, 152, 13-29.
- Manning, A. H., & J. S. Caine (2007) Groundwater noble gas, age, and temperature signatures in an Alpine watershed: Valuable tools in conceptual model development, *Water Resources Research*, 43(4), 1-16.
- Marchand, J. P., Jarrett, R. D., & L. L. Jones (1984) *Velocity profile, water-surface slope, and bed-material size for selected streams in Colorado*; Open-File Report 1984-733; U. S. Geological Survey: Lakewood, CO, USA, pp. 82.
- McClure, R., (2014) Rio Grand Silver, Inc.: Project Overview and Current Status, Oral presentation at the San Juan Mining Conference, April 25, 2014.
- McCulley, Frick & Gilman, Inc. (MFG) (1999a) Preliminary Characterization of the Willow Creek Watershed: Existing Conditions and Recommended Actions. April 1999.
- McCulley, Frick & Gilman, Inc. (MFG), (1999b) Site Specific Health and Safety Plan, Willow Creek Reclamation Project. July 1999.
- McDonnell, J. J., Sivapalan, M., Vache, K., Dunn, S., Grant, G., Haggerty, R., Hinz, C., Hooper, R., Kirchner, J., Roderick, M. L., Selker, J., & M. Weiler (2007) Moving beyond heterogeneity and process complexity: a new vision for watershed hydrology, *Water Resources Research*, 43, w07301, doi:10.1029/2006WR005467.
- McKnight, D. M., & G. L. Feder (1984) The ecological effect of acid conditions and precipitation of hydrous metal oxides in a Rocky Mountain stream, *Hydrobiologia*, 119, 129-138.
- McKnight, D. M. & K. E. Bencala (1989) Reactive iron transport in an acidic mountain stream in Summit County Colorado: A hydrologic perspective, *Geochim. Cosmochim. Acta*, 53, 2225-2234
- McKnight, D. M., & K. E. Bencala (1990) The chemistry of Iron, Aluminum, and dissolved organic material in three acidic, metal-enriched, mountain streams, as controlled by watershed and in-stream processes, *Water Resources Research*, 26, 3087-3100.
- McKnight, D. M., Kimball, B. A., & R. L. Runkel (2001) pH dependence of iron photoreduction in a rocky mountain stream affected by acid mine drainage, *Hydrological Processes*, 15, 1979-1992.
- McKnight, D. M., Boyer, E., Westerhoff, P., Doran, P., Kulbe, T., & D. Andersen (2001) Spectrofluorometric characterization of dissolved organic matter for indication of pre- cursor

organic material and aromaticity, *Limnol. Oceanogr.*, 46(1), 38–48.

McKnight, E. T. (1974) *Geology and ore deposits of the Rico district, Colorado*; Professional Paper 723; U.S. Geological Survey: Reston, VA, USA, pp. 100.

McCabe, G. J., & D. M. Wolock (2010) Long-term variability in Northern Hemisphere snow cover and associations with warmer winters, *Climate Change*, 99, 141-153.

Michel, R. L. (1989) *Tritium Deposition in the Continental United States, 1953-1989*; Water-Resources Investigations Report 89-4072; U.S. Geological Survey: Reston, VA, USA.

Michel, R. L. (1976) Tritium inventories of the world oceans and their implications, *Nature*, 263, 103–106.

Miller, M. P., McKnight, D. M., Cory, R. M., Williams, M. W., and R. L. Runkel (2006) Hyporheic exchange and fulvic acid redox reactions in an alpine stream/wetland ecosystem, Colorado Front Range, *Environ. Sci. Technol.*, 40(19), 5943-5949.

Minder, J. R. (2010), The sensitivity of mountain snowpack accumulation to climate warming, *Journal of Climate*, 23(10), 2634–2650, doi:10.1175/2009JCLI3263.1.

Molotch, N. P., Brooks, P. D., Burns, S. P., Litvak, M., Monson, R. K., McConnell, J. R. & K. Musselman (2009) Ecohydrological controls on snowmelt partitioning in mixed-conifer sub-alpine forests, *Ecohydrology*, 2(2), 129-142.

Monson, R. K., Turnipseed, A. A., Sparks, J. P., Harley, P. C., Scott-Denton, L. E., Sparks, K., & T. E. Huxman (2002) Carbon sequestration in a high-elevation, sub-alpine Forest, *Global Change Biology*, 8, 459-478.

Moore, J., J. Carrillo-Rivera, & M. Wireman (2012) *Field Hydrogeology 2nd Edition*, CRC press, Boca Raton, Florida, USA, 183 p.

Moses, A. L., referee (1902) Water District No. 2 Case 89-18, Appropriation Authority 1959-2, Costilla County, Colorado, 15 May 1902, court evidence vol. III, (claimants A. W. Weiss, J. W. Smith, J. Gredig and T. V. Wilson).

Mote, P. W., A. F. Hamlet, M. P. Clark, & D. P. Lettenmaier (2005) Declining mountain snowpack in western north America, *Bulletin of the American Meteorological Society*, 86(1), 39-52.

Munnich, K. O., (1957) Messungen des ¹⁴C-gehaltes von hartem grundwasser, *Naturwissenschaften*, 44, 32-33.

Murphy, E. M., Davis, S. N., Long, A., Donahue, D., & A. J. T. Jull (1989) Characterization and isotopic composition of organic and inorganic carbon in the Milk River aquifer, *Water Resources Research*, 25, 1893-1905.

- Naurath, L., Weidner, C., Rude, T. R., & A. Banning (2011) A New Approach to Quantify Na-Fluorescein (uranine) in Acid Mine Waters, *Mine Water Environment*, 30, 231-236.
- Nayak, A., Marks, D., Chandler, C. G., & M. Seyfried (2010) Long-term snow, climate, and steamflow trends at the Reynolds Creek Experimental Watershed, Owyhee Mountains, Idaho, United States, *Water Resources Research*, 46, W06519, doi:10.1029/2008WR007525.
- National Hardrock Mining Framework (1997) U.S. EPA 833-B-97-003, U.S. EPA Office of Water: Washington, DC.
- Nijssen, B., O'Donnell, G. M., Hamlet, A. F. & Lettenmaier, D. P. (2001), Hydrologic vulnerability of global rivers to climate change, *Climate Change*, 50, 143-175.
- Niyogi, D. K., Lewis, W. M. & D. M. McKnight (2002) Effects of stress from mine drainage on diversity, biomass, and function of primary producers in mountain streams, *Ecosystems*, 5, 554-567.
- Nolin, A. W., & C. Daly (2006) Mapping at risk snow in the Pacific Northwest, *Journal of Hydrometeorology*, 7(5), 1164–1171.
- Nordstrom, D. K., & C. N. Alpers (1999) Geochemistry of acid mine waters. *In*: The environmental geochemistry of mineral deposits, vol, 6A, Plumlee, G. S., & M. J. Logsdon (eds.), Society of Economic Geologists, Littleton, CO, pp. 133-160.
- Nordstrom, D. K. (2009) Acid rock drainage and climate change, *Journal of Geochemical Exploration*, 100, 97-104.
- Nordstrom, K. D. (2011) Hydrochemical processes governing the origin, transport and fate of major and trace elements from mine wastes and mineralized rock to surface waters, *Applied Geochemistry*, 26, 1777-1791.
- Olsen, I. U. (1970) The use of Oxalic Acid as a Standard, *In* I.U. Olsson, ed., Radiocarbon Variations and Absolute Chronology, Nobel Symposium, 12th Proc., John Wiley & Sons, New York, p. 17.
- Painter, T. H., Deems, J. S., Belnap, J., Hamlet, A. F., Landry, C. C., & B. Udall (2010) Response of Colorado River runoff to dust radiative forcing in snow, *Proceedings of the National Academy of Sciences of the United States of America*, 107, 17125-17130.
- Palumbo-Roe, B., & R. Dearden (2013) The hyporheic zone composition of a mining-impacted stream: Evidence by multilevel sampling and DGT measurements, *Applied Geochemistry*, 33, 330-345.
- Parlanti, E., Worz, K., Geoffroy, L., & M. Lamotte (2000) Dissolved organic matter fluorescence spectroscopy as a tool to estimate biological activity in a costal zone submitted to anthropogenic inputs, *Organic Geochemistry*, 31(12), 1765-1781.

- Pederson, G. T., Grey, S. T., Ault, T. et al. (2011a) Climate controls on the snowmelt hydrology of the Northern Rocky Mountain, *Journal of Climate*, 24, 1666-1687.
- Pederson, G. T., Grey, S. T., Woodhouse, C. A., et al. (2011b) The unusual nature of recent snow pack declines in the North American Cordillera, *Science*, 333, 332-335.
- Pielke, R. A. (2005) Land use and climate change, *Science*, 310(5754), 1625-1626.
- Plumlee, G. S., 1989, Processes controlling epithermal mineral distribution in the Creede Mining District, Colorado: Unpub. Ph.D. thesis, Harvard University, Cambridge, Ma, 378 p.
- Plummer, L. N., & P. D. Glynn (2013) Radiocarbon dating in groundwater systems, *In Isotope Methods for Dating Old Groundwater*, International Atomic Energy Agency, Vienna, p. 357.
- Polyakov, V. A., Medvedev S. A., & N. V. Pyatnitskij (1996) An isotopic and hydrochemical study of the groundwater inflow into the north-Muya tunnel, *Isotopes in water resources management*, Symposium proceedings of IAEA, Vienna, Austria.
- Raiber, M., Webb, J. A., & D. A. Bennetts (2009) Strontium isotopes as tracers to delineate aquifer interactions and the influence of rainfall in the basalt plains of southeaster Australia, *Journal of Hydrology*, 367 (3-4), 188-199.
- Rasmussen, R., Baker, B., Kochendorfer, J., Meyers, T., Landolt, S., Fischer, A. P., Black, J., Theriault, J. M., Kucera, P., Gochis, D., Smith, C., Nitu, R., Hall, M., Ikeda, K., & E. Gutmann (2012) How well are we measuring snow? The NOAA/FAA/NCAR winter precipitation test bed, *Bull. American Meteorological Society*, 93(6), 811-829.
- Regonda, S. K., Rajagopalan, B., Clark, M., & J. Pitlick (2005), Seasonal cycle shifts in hydroclimatology over the western United States, *Journal of Climate*, 18(2), 372–384.
- Riebsame, W. (1997) *Atlas of the New West: Portrait of a Changing Region*, W.W. Norton & Company, New York. 192 pp.
- Runkel, R. L., Kimball, B. A., McKnight, D. M., & K. E. Bencala (1999) Reactive solute transport in streams: a surface complexation approach for trace metal sorption, *Water Resources Research*, 35:3829-3840.
- Runkel, R. L., & B. A. Kimball (2002) Evaluating remedial alternatives for an acid mine drainage stream: Application of a reactive transport model, *Environmental Science and Technology*, 36, 1093-1101.
- Runkel, R. L., Kimball, B. A., Walton-Day, K., & P. L. Verplanck (2007) A simulation-based approach for estimating premining water quality: Red Mountain Creek, Colorado, *Applied Geochemistry*, 22, 1899-1918.

- Runkel, R. L., Bencala, K. E., Kimball, B. A., Walton-Day, K., & P. L. Verplanck (2009) A comparison of pre- and post-remediation water quality, Mineral Creek, Colorado, *Hydrological Processes*, 23, 3319-3333.
- Runkel, R. L., Walton-Day, K., Kimball, B.A., Verplanck, P.L., & D. A. Nimick (2013) Estimating instream constituent loads using replicate synoptic sampling, Peru Creek, Colorado, *Journal of Hydrology*, 489, 26-41.
- Sabatini, D. A., & T. A. Austin (1991) Characteristics of rhodamine WT and fluorescein as adsorbing ground-water tracers, *Ground Water*, 29, 341-349.
- Schemel, L. E., Cox, M. H., Runkel, R. L., & B. A. Kimball (2006) Multiple injected and natural conservative tracers quantify mixing in a stream confluence affected by acid mine drainage near Silverton, Colorado, *Hydrological Processes*, 20, 2727-2743.
- Schlaepfer, D. R., Lauenroth, W. K. & J. B. Bradford (2012) Consequences of declining snow accumulation for water balance of mid-latitude dry regions, *Global Change Biology*, 18, 1988-1997.
- Seager, R., & G. A. Vecchi (2010) Greenhouse warming and the 21st century hydroclimate of southwestern North America, *Proceedings of the National Academy of Sciences of the United States of America*, 107, 21277-21282.
- Serreze, M. C., Clark, M. P., Armstrong, R. L., McGinnis, D. A., & R. S. Pulwarty (1999) Characteristics of the western United States snowpack from snowpack telemetry (SNOTEL) data, *Water Resources Research*, 35, 2145-2160.
- Shapiro, A. M., Hsieh, P.A., & F.P. Haeni, (1999) Integrating multidisciplinary investigations in the characterization of fractured rock, U.S. Geol. Survey, Water Resources Investigation Report 99-4018C, pp. 669-680.
- Simpson, J. W. (1982) Creede project final evaluation report: unpub. company report, Chevron Resources Company, 48 p.
- Slymaker, O. (1988) Slope erosion and mass movement in relation to weathering in geochemical cycles, *In: Physical and chemical weathering in geochemical cycles*, Lerman, A., & M. Meybeck (eds.) *Springer*, Netherlands.
- Smart, P.L., & I. M. S, Laidlaw (1977) An evaluation of some fluorescent dyes used for water tracing, *Water Resources Research*, 13, 15-33.
- Smart, P. L. (1985) Applications of Fluorescent Dyes in the planning and hydrologic appraisal of sanitary landfills, *Quarterly Journal of Engineering Geology*, 18,275-286.
- Snow, D. T. (1973) Mountain Groundwater supplies, *Mountain Geology*, 10, 19-24.

- Stedmon, C. A., Markager, S., & R. Bro (2003) Tracing dissolved organic matter in aquatic environments using a new approach to fluorescence spectroscopy, *Marine Chemistry*, 82, 239-254.
- Stewart, I. T., Cayan, D. R. & M. D. Dettinger (2005) Changes toward earlier streamflow timing across western North America, *Journal of Climate*, 18, 1136-1155.
- Spencer, S., Anderson, A., Silins, U., Bladon, K., & A. Collins (2014) Towards understanding the spatial and temporal characteristics of stream, hillslope, and groundwater runoff processes in a Rocky Mountain headwater catchment in Alberta, Canada, *Geophysical Research Abstracts*, 16, EGU2014-4576.
- Sternberg, M., Holzapfel, C., Tielbörger, K., Sarah, P., Kigel, J., Lavee, H., Fleisher, A., Jeltsch, F., & M. Kochy (2011) The use and misuse of climatic gradients for evaluating climate impact on dryland ecosystems – an example for the solution of conceptual problems. *In: Gradients in Drylands: Linking Patterns and Processes and their Consequences for Biodiversity*, Veste, M., Linstädter, A., & S. W. Breckle (eds.). Springer, New York, USA
- Steven, T. A., & J. C. Ratte (1973) Geologic map of the Creede quadrangle, Mineral and Saguache Counties, Colorado: U.S. Geol. Survey Quadrangle Map GQ-1053, scale 1:62,500.
- Steven, T. A., & G. P. Eaton (1975) Environment of ore deposition in the Creede mining district, San Juan Mountains, Colorado: I. Geologic, hydrologic, and geophysical setting, *Economic Geology*, 70,1023-1037.
- Steven, T. A., & P. W. Lipman (1976) Calderas of the San Juan volcanic field, southwestern Colorado: U.S. Geol. Survey Prof. Paper 958, 35 p.
- Steven, T. A., & J. C. Ratte (1965) Geology and structural control of ore deposition in the Creede District, San Juan Mountains, Colorado: U.S. Geological Survey Prof. paper 487, 90 p.
- Steven, T. A., Mehnert, H. H., & J. D. Obradovich (1967) Age of volcanic activity in the San Juan Mountains, Colorado: U. S. Geological Survey Prof. Paper 575-D, p. D47-D55.
- Steven, T. A., & P. W. Lipman (1973) Geologic map of the Spar City quadrangle, Mineral County, Colorado: U. S. Geological Survey Quadrangle Map GQ-1052, scale 1:62,500.
- Stewart, I. T., Cayan, D. R. & M. D. Dettinger (2005) Changes toward earlier streamflow timing across western North America, *Journal of Climate*, 18, 1136-1155.
- Stuiver, M., & H. A. Polach (1977) Discussion: Reporting of ^{14}C data, *Radiocarbon*, 19, 355-363.
- Stuiver, M. (1980) Workshop on ^{14}C data reporting, *Radiocarbon*, 22, 964-966.

- Sueker, J. K., Ryan, J. N., Kendall C. & R. D. Jarrett (2000) Determination of hydrologic pathways during snowmelt for alpine/sub-alpine basins, Rocky Mountain National Park, Colorado, *Water Resources Research*, 36, 63-75.
- Swistock, B., DeWalle, D. & W. Sharpe (1989) Sources of acidic storm flow in an Appalachian headwater stream, *Water Resources Research*, 25(10), 2139-2147.
- Tague, C., Grant, C., Farrell, M., Choate, J. & A. Jefferson (2008) Deep groundwater mediates streamflow response to climate warming in the Oregon Cascades, *Climate Change*, 86(1-2), 189-210.
- Tague, C., Heyn, K. & L. Christensen (2009) Topographic controls on spatial patterns of conifer transpiration and net primary productivity under climate warming in mountain ecosystems, *Ecohydrology*, 2, 541-554.
- Tague, C., & G. E. Grant (2009) Groundwater dynamics mediate low-flow response to global warming in snow-dominated alpine regions, *Water Resources Research*, 45(7), DOI:10.1029/2008WR007179.
- Thurman, E. M. (1985) Organic Geochemistry of Natural Waters, *Eds. Martinus Nijhof, W. Junk*, New York.
- Thurman, E. M., & R. L. Malcom (1981) Preparative isolation of aquatic humic substances, *Environmental Science and Technology*, 15, 463-466.
- Thompson, T. B. (1992) Geology and mineral deposits of the Bondholder district, Colorado, USA, *Soc. Econ. Geologists Newsletter*, 8, 12-16.
- Thorn, C. E., & D. S. Loewenherz (1987) Alpine mass wasting in the Indian Peaks Area, Front Range, Colorado. *In: Geomorphic systems of North America (Centennial Special Vol. 2)*, Graft, W. L. (ed.), Geological Society of America; Boulder, Colorado; 238-247.
- Todd, A. S., Manning, A. H., Verplanck, P. L., Crouch, C., McKnight, D. M. & R. Dunham (2012) Climate-change-driven deterioration of water quality in a mineralized watershed, *Environmental Science and Technology*, 46, 9324-9332.
- Troldborg, L., Jensen, K. H., Engesgaard, P., Refsgaard, J. C., & K. Hinsby (2008) Using environmental tracers in modeling flow in a complex shallow aquifer system, *Journal of Hydrologic Engineering*, 13, 1037-1084.
- US EPA. (1997) EPA's National Hardrock Mining Framework, US EPA 833 B 97-003, US EPA Office of Water.
- Verhagen, B. T., Mazor, E., & J. P. F. Sellschop (1974) Radiocarbon and Tritium Evidence For Direct RainRecharge to Ground Waters in the Northern Kalahari, *Nature*, 249, 643-644.

Verplanck, P. L., Nordstrom, K. D., Bove, D. J., Plumlee, G. S., & R. L. Runkel (2009) Naturally acid surface and ground waters draining porphyry-related mineralized areas of the Southern Rocky Mountains, Colorado and New Mexico, *Applied Geochemistry*, 24, 255-267.

Viviroli, D., Archer, D. R., Buytaert, W., Folwer, H. J., Greenwood, G. B., Hamlet, A. F., Huang, Y., Koboltschnig, G., Litor, M. I., Lopez-Moreno, J. I., Lorentz, S., Schadler, B., Schreier, K., Schwaiger, M., Vuille, P. & R. Woods (2011) Climate change and mountain water resources: overview and recommendations for research, management and policy, *Hydrology and Earth Systems Sciences*, 15, 471-504.

Walton-Day, K., & E. Poeter (2009) Investigating hydraulic connections and the origin of water in a mine tunnel using stable isotopes and hydrographs, *Applied Geochemistry*, 24(12), 2266-2282.

Ward, Z. (2014) President of the Willow Creek Reclamation Committee, Creede, Colorado, *personal communication* on April 23, 2014.

Wassenaar, L., Aravena, R., Hendry, J., & P. Fritz (1991) Radiocarbon in Dissolved Organic Carbon, A possible Groundwater Dating Method: Case Studies from Western Canada, *Water Resources Research*, 27(8), 1975-1986.

Webber, K. L. (1988) The Mammoth Mountain and Wason Park tuffs: Magmatic evolution in the central San Juan volcanic field, southwestern Colorado: Unpublished Ph.D. Thesis, Rice University, Houston, Texas, 244 p.

Wels, C., Cornett, R. J., & B. D. Lazerete (1991) Hydrograph separation: a comparison of geochemical and isotopic tracers, *Journal of Hydrology*, 122, 253-274.

White, S. E. (1976) Rock glaciers and block fields: review and new data, *Quaternary Research*, 6, 77-97.

Williams, M. W., Brown, A. D., & J. M. Melack (1991) Biochemical modifications of snowmelt runoff in an alpine basin. *In* Hydrological interactions between atmosphere, soil and vegetation, Kienitz, G.; Milly, P. C. D., Van Genuchten, M. T., Rosbjerg, D., & W. J. Shuttleworth (eds.), International Association of Hydrological Sciences: Wallingford, UK, IAHS-AIHS Publication 204, pp. 457-465.

Williams, M. W. & J. M. Melack (1991a) Precipitation chemistry in and ionic loading to an alpine basin, Sierra Nevada, *Water Resources Research*, V 27, 1563-1574.

Williams, M. W. & J. M. Melack (1991b) Solute chemistry of snowmelt and runoff in an alpine basin, Sierra Nevada, *Water Resources Research*, V 27, 1563-1574.

- Williams, M. W., Brown, A. D., & J. M. Melack (1993) Geochemical and hydrologic controls on the composition of surface water in a high-elevation basin, Sierra Nevada, California, *Limnol. Oceanogr.*, 38(4), 775-797.
- Williams, M. W., Losleben, M., Caine, N. & D. Greenland (1996) Changes in climate and hydrochemical responses in a high-elevation catchment in the Rocky Mountains, USA, *Limnology and Oceanography*, 41, 939-946.
- Williams, M. W., Davinroy, T., & P. D. Brooks (1997) Organic and inorganic nitrogen pools in talus soils and water, Green Lakes Valley, Colorado Front Range, *Hydrologic Processes*, 11(13), 1747-1760.
- Williams, M. W., Cline, D., Hartmann, M., & T. Bardsley (1999) Data for snowmelt model development, calibration, and verification at an alpine site, Colorado Front Range, *Water Resources Research*, V 35, N 10, pp 3205-3209.
- Williams, M. W., Hood, E., & N. Caine (2001) The role of organic nitrogen in the nitrogen cycle of a high elevation catchment, Colorado Front Range, USA, *Water Resources Research*, 37(10), 2569-2582.
- Williams, M. W., Knauf, M., Caine, N., Liu, F. J. & P. L. Verplanck (2006) Geochemistry and source waters of rock glacier outflow, Colorado Front Range, *Permafrost and Periglacial Processes*, 17, 13-33.
- Williams, M. W., Seibold, C., & K. Chowanski (2009) Storage and release of solutes from a sub-alpine seasonal snowpack: soil and stream water response, Niwot Ridge, Colorado, *Biogeochemistry*, 95, 77-94.
- Williams, M. W., Barns, R. T., Parman, J. N., Freppaz, M., & E. Hood (2011) Stream water chemistry along an elevational gradient from the continental divide to the foothills of the Rocky Mountains, *Vadose Zone Journal*, 10, 900-914.
- Willow Creek Reclamation Committee (2003) Report on Surface and Mine Water Sampling and Monitoring in Willow Creek Watershed, Mineral County, CO (1999-2002) Creede, CO.
- Wireman, M. (2003) Characterization of ground-water resources in fractured-rock hydrogeologic settings. *Ground Water Monitoring and Remediation*, 23, 34-40.
- Wireman, M., Gertson, J., & M. W. Williams (2006) Hydrologic Characterization of Ground Waters, Mine Pools and The Leadville Mine Drainage Tunnel, Leadville, Colorado. Presented paper at the 2006 7th ICARD, Stylus, MO.
- Wireman, M., & B. Stover (2011) Hard-rock mining and water resources, *Ground Water*, 49(3), 310-316.

Wolkersdorfer, C. (2002) Mine water tracing. In *Mine Water Hydrogeology and Geochemistry*; Younger, P. L., & N. S. Robins (eds.), Geological Society: London, England; pp. 47-60.

Wolkersdorfer, C. (2008) Water Management at Abandoned Flooded Underground Mines—Fundamentals, Tracer Tests, Modeling, Water Treatment; Springer: Heidelberg, Germany; p. 466.

Wolkersdorfer, C., & J. LeBlanc (2012) Regulations, Legislation, and Guidelines for Artificial Surface Water and Groundwater Tracer Tests in Canada, *Water Quality Research Journal of Canada*, 47, 42-55.

Younger, P. L., & C. Wolkersdorfer (2004) Mining impacts on the fresh water environment: technical and managerial guidelines for catchment scale management, *Mine Water Environment*, 23, 2-80.

Zeliff, M. M. (2012) Hydrochemistry, residence time and nutrient cycling of groundwater in two, climate-sensitive, high-elevation catchments, Colorado Front Range, *Masters Thesis*, Department of Geography University of Colorado, Boulder, Colorado.

Zellweger, G. W. (1994) Testing and comparison of four ionic tracers to measure stream flow loss by multiple tracer injection, *Hydrologic Processes*, 8, 155-165.

Appendix 1

Field parameter data collected from 1999-2013.

Location	Date	pH	Temp (C)	DO (mg/l)	Discharge (cfs)	Discharge (gpm)	Elevation (water) (m)
Nelson Portal	9/18/99	3.8			0.77	345.576	
Nelson Portal	11/1/99					300	
Nelson Portal	11/15/99					300	
Nelson Portal	5/16/00	5.1					
Nelson Portal	1/22/01	4.3			0.58	260.304	
Nelson Portal	2/12/01				0.54	242.352	
Nelson Portal	2/12/01	4.3					
Nelson Portal	5/22/01	4.7					
Berkshire Shaft - 1	8/15/01		18.2				2815.2
Hospital Decline	8/15/01		20.7				
Drift above McClure	8/15/01	5	12.9				
Peak Drift Borehole	8/15/01	5	13				
McClure Drift	8/15/01	6	13.9				
Archimedes Raise	8/15/01		8.1				
North Comm raise	8/15/01		9.3				
Nelson Portal	5/2/02	4.2			0.49	219.912	
Nelson Portal	9/4/02	4.3					
Nelson Portal	11/7/02	4.4 4	17.1		0.39		
Nelson @ Bachelor	11/7/02	4.5	17.7				2804.5
Javelin Shaft	11/7/02	5.3 2	17				2808.1
Bachelor Shaft Proper	11/7/02	5.9 7	15.8				
McClure x-cut	11/7/02	6.2 8	12.7				
Peak Drift Borehole	11/7/02	6.1 2	13.5				
Daylight Winze	11/7/02	5.1	15.2				2808.1
Commodore shaft	11/7/02	5.7 9	16.1				2807.5

Nelson @ No Name	11/7/02	5.3 9	19.3			180*	2808.1
Amethyst shaft	11/7/02	6.7 4	11.4				
Berkshire Shaft	11/7/02	5.5 4	18.2				2815.7
Decline	11/7/02	4.0 5	17.4				2816.4
Nelson Portal	11/7/02	4.4			0.49	219.912	
Nelson Portal	5/8/03	4.1			0.47	210.936	
Nelson @ Bachelor	6/6/03	4.4 2	18.1			164.4*	2804.2
44 raise	6/6/03	5.1 3	9.5				
Daylight Winze	6/6/03	4.9	17.1				2809.3
Nelson @ No Name	6/6/03	5.2 1	19.1			233	2808.4
Park Regent	6/6/03	2.8 5	21.1			<5	
Commodore Adit	6/6/03	6.2 8	4.4				
Nelson Portal	5/6/04	4.7			0.65	291.72	
Nelson Portal	2/2/05	4.4			0.52	233.376	
Nelson Portal	2/15/05	4.3			0.52	233.376	
Nelson Portal	3/8/05	4.5			0.54	242.352	
Nelson Portal	4/5/05	4.5			0.53	237.864	
Nelson Portal	5/3/05	5.1			0.55	246.84	
Nelson Portal	6/3/05	4.9					
Bachelor Flume	8/2/05				0.63	282.744	
Nelson Portal	8/17/05	4.3					
Nelson Portal	9/21/05	4.3 2			0.29	130.152*	
Bachelor Flume	9/21/05				0.63	282.744	
Bachelor Flume	10/5/05				0.63	282.744	
Nelson Portal	10/29/05	4.3 5			0.29	130.152*	
Bachelor Flume	10/29/05				0.65	291.72	
Nelson Portal	11/16/05				0.63	282.744	
Bachelor Flume	11/16/05				0.63	282.744	
Bachelor Flume	12/20/05				0.63	282.744	
Bachelor Flume	1/25/06				0.63	282.744	
Bachelor Flume	1/31/06				0.67	300.696	
Nelson Portal	9/1/06				0.75	336.6	

Nelson Portal	9/1/06	4.4					
Nelson @ Bachelor	2/13/07	4.28	18.56	5.4			
Daylight Winze	2/13/07	4.78	18.19	2.4			
Nelson @ No Name	2/13/07	5.49	19.74	2.9			
Del Monte Raise	2/13/07	4.04	14.14	4.5			
Berkshire Shaft - 1	2/13/07	5.64	19.66	0.7			
Decline	2/13/07	3.66	19	0.6			
West Drift	2/15/07	4.04	14.14	4.5			
West Drift	2/15/07	6.9	17.26	4.1			
Nelson @ Bachelor	2/16/07	4.23	18.63	5.5			
Daylight Winze	2/16/07	4.69	18.19	2.4			
Nelson @ No Name	2/16/07	5.55	19.75	3.4			
Del Monte Raise	2/16/07	6.07	16.81	4.2			
Berkshire Shaft - 1	2/16/07	5.84	19.63	0.8			
Decline	2/16/07	3.73	18.9	0.9			
Nelson Portal	5/22/07	5.4			0.58	260.304	
Nelson Portal	5/22/07	5.2					
Nelson Portal	5/21/08	5.1					
Nelson Portal	7/1/08				0.69	309.672	
Peak Drift Borehole	6/1/09					2.7	
Nelson @ Bachelor	6/9/09	4.12					2803.9
Nelson Portal	6/9/09	4.37					2796.5
Nelson @ No Name	6/9/09	3.99					
Berkshire Shaft - 1	6/9/09	6.24					2817.3
Decline	6/9/09	3.99					
Del Monte Raise	6/9/09						2817.0

Peak Drift Borehole	6/9/09					5	
Nelson Portal	7/1/09				0.71	318.648	
Emerald Ranch Well	7/15/09	8.20					2817.3
Nelson Portal	1/1/10				0.65	291.72	
Nelson Portal	4/1/10				0.7	314.16	
Nelson Portal	8/13/10				0.54	242.352	
Berkshire shaft - 65	10/29/12	5.63	19.51	0.7	NA pool		
Berkshire shaft - 40	10/29/12	5.64	20.45		NA pool		
Nelson Portal	10/29/12	4.31	18.51	6.3		280	
Nelson @ Bachelor	10/29/12	4.58	19.44	5.7		218	
Nelson @ No Name	10/30/12	5.72	20.14	4.3			
Bachelor Shaft - 10	10/30/12	6.82	16.47	0.03	NA pool		
West Willow Creek	10/30/12	7.64	4.37	9.2	5		
HW-4 well	2/5/13	6.82	17.7				
Solomon adit	2/5/13	6.58	11.9			20	
East Willow Creek	2/5/13		2.5		5		
Bach Well	2/6/13	6.28	7.8			2.5	
*Discharge are noted as underestimates due to flume damage							

Appendix 2

Total recoverable and dissolved metals concentrations for samples collected from 2012-2013.

Sample Location	DATE	pH	Hardness	Tot Fe ug/L	Diss Fe ug/L	Tot Zn ug/L	Diss Zn ug/L	Diss Pb ug/L	Tot Pb ug/L	Diss Cd ug/L	Tot Cd ug/L	Diss Mn ug/L	Tot Mn ug/L	Diss Sr ug/L	Tot Sr ug/L
Berk Shaft - 40'	10/29/12	5.63	970	14900	9650	95800	95200	457	1550	207	209	36000	36400	3000	3040
Berk shaft -65'	10/29/12	5.64	985	13300	11400	95300	95600	929	1460	211	225	36300	36600	3030	3070
Berk shaft -60'	10/3/12	5.63	950	13000	11000	94200	93300	995	1450	219	222	35300	24100	2950	3000
Nelson @ bachelor	10/3/12	4.58	608	8170	2580	53200	54700	733	1000	110	118	18900	18900	2190	2190
Nelson @ no name	10/3/12	5.72	667	11600	9820	57400	58100	936	1260	117	124	20300	20000	2400	2380
Bachelor Shaft -15	10/3/12	6.82	61	1590	<1250	4180	4080	15	272	7.01	9.28	1720	1740	193	191
Nelson Portal	10/3/12	4.31	588	3050	<1250	51800	52600	578	818	114	111	18500	13900	2110	2090
W. Willow Creek	10/3/12	7.64	40	<500	<1250	265	311	4.86	8.47	3.21	3.21	<10	<10	150	147
Solomon Adit	2/5/13	6.58	193	2420	391	24300	24800	706	838	134	134	5460	5630	275	284
E. Willow Creek	2/5/13	NA	21	<100	<100	693	791	5.77	17.9	3.8	3.71	4.85	<2	40.1	40.5
Bach Well	2/6/13	6.29	32	7220	790	5430	4960	9.98	97	0.928	1.38	134	438	117	126
Bach Well	2/6/13	6.29	32	7420	386	5340	4930	8.01	98.7	0.908	1.43	119	428	117	124

Appendix 3

Stable Water Isotope for samples collected from 2007 to 2013.

Location	Date	$\delta^{18}\text{O}$ ‰	δD ‰	D ex
SOLOMON ADIT	20130205	-14.06	-104.53	7.95
BACHELOR SHAFT -15	20121030	-15.07	-110.76	9.78
CORKSCREW RAISE	20090609	-15.04	-112.00	8.36
PEAK DRIFT BOREHOLE	20090609	-15.48	-115.32	8.51
DEL MONTE RAISE	20090609	-14.93	-110.39	9.08
PARK REGENT	20090609	-15.52	-114.66	9.48
DEL MONTE RAISE	20081113	-14.46	-106.97	8.74
TELLER	20081113	-15.33	-113.52	9.12
CORKSCREW RAISE	20081113	-14.23	-104.68	9.14
BERKSHIRE -40	20121029	-14.86	-108.48	10.42
NELSON BACHELOR	20090609	-15.18	-112.30	9.16
NELSON PORTAL	20090609	-15.15	-111.47	9.70
BERKSHIRE -1	20090609	-15.11	-112.04	8.86
DECLINE	20090609	-15.06	-110.95	9.49
NESLON NO NAME	20090609	-15.18	-112.30	9.16
NELSON PORTAL	20101103	-14.85	-109.25	9.56
NELSON BACHELOR	20101103	-14.87	-108.98	9.96
BERKSHIRE -1	20101103	-14.83	-109.59	9.09

NELSON -NO NAME	20101103	-14.88	-108.71	10.30
NELSON - DECLINE	20101103	-14.84	-108.36	10.36
NELSON BACHELOR	20081113	-14.70	-108.12	9.48
NELSON PORTAL	20081113	-14.77	-108.43	9.75
NESLON NO NAME	20081113	-14.73	-108.71	9.10
DECLINE	20081113	-14.77	-108.07	10.07
BERKSHIRE -1	20081113	-14.71	-108.54	9.17
NELSON NO NAME	20081113	-14.72	-108.75	8.99
NELSON -BACHELOR	20070213	-14.68	-109	8.40
NELSON DAYLIGHT	20070213	-14.79	-110.1	8.30
NESLON NO NAME	20070213	-14.58	-109.2	7.50
BERKSHIRE -1	20070213	-14.62	-109.7	7.30
DECLINE	20070213	-14.59	-109.3	7.50
BERKSHIRE -65	20121029	-14.81	-108.34	10.18
BERKSHIRE -60	20121029	-14.89	-108.56	10.53
NELSON BACHELOR	20121030	-14.88	-108.70	10.33
NELSON NO NAME	20121030	-14.82	-108.57	9.95
NELSON PORTAL	20121030	-14.85	-108.58	10.21
NELSON PORTAL RAIN	20100828	-10.35	-75.41	7.43
NELSON PORTAL RAIN	20100828	-12.34	-88.70	10.05
NELSON PORTAL RAIN	20100928	-5.15	-35.62	5.59

NELSON PORTAL RAIN	20100928	-7.70	-47.66	13.91
NELSON SNOW	20100128	-19.31	-145.79	8.66
NELSON SNOW	20100428	-19.20	-148.28	
NELSON SNOW	20100428	-19.10	-146.30	
PROSPECT SNOW	20110502	-19.92	-150.09	10.78
EMERALD LAKE SPRING	20090610	-15.28	-112.37	9.87
WEAVER SPRING	20090610	-15.09	-111.92	8.84
MIDWEST SPRING	20090610	-14.68	-108.25	9.17
WEST WILLOW	20090609	-19.73	-153.10	4.78
WEST WILLOW	20081113	-14.42	-106.24	9.12
WEST WILLOW	20121030	-14.25	-103.25	10.74
East Willow creek	20120205	-14.82	-106.71	11.87
BULLDOG HW4 WELL	20130205	-15.03	-110.09	10.17
BULLDOG HW4 WELL	20130205	-14.96	-109.97	9.71
BACH WELL	20130206	-15.28	-113.34	8.92
BACH WELL	20130206	-15.26	-113.26	8.84
EMERALD RANCH WELL	20090609	-15.11	-112.04	8.86

Appendix 4

Tritium concentrations for samples collected from 2008 to 2013.

Location	Date	Tritium (TU)	SD (1 sigma)
NELSON PORTAL	20081113	1.34	
Emerald Ranch Well 2	20090609	9.3	
NELSON PORTAL	20090609	0.93	0.25
West Willow Creek	20090609	8.6	
Emerald Ranch Spring	20090610	8.5	
MID Spring	20090610	7.4	
WEAVER Spring	20090610	7.9	
Emerald Ranch well 1	20090715	1.34	0.19
NELSON SNOW	20100128	3.19	
DURANGO PRECIPITATION	20100415	4.92	0.29
DURANGO PRECIPITATION	20100415	3.49	0.27
DURANGO PRECIPITATION	20100517	14.00	0.80
DURANGO PRECIPITATION	20100711	8.70	0.40
DURANGO PRECIPITATION	20100711	8.60	0.40
DURANGO PRECIPITATION	20100802	4.97	0.20

DURANGO PRECIPITATION	20100802	5.60	0.21
DURANGO PRECIPITATION	20100802	7.10	0.30
DURANGO PRECIPITATION	20100810	5.90	0.30
DURANGO PRECIPITATION	20100810	9.20	0.70
EQUITY PRECIPITATION	20100810	5.90	
NELSON PRECIPITATION	20100810	5.10	
DURANGO PRECIPITATION	20100817	5.30	0.40
DURANGO PRECIPITATION	20100818	3.70	0.40
DURANGO PRECIPITATION	20100830	4.20	0.30
DURANGO PRECIPITATION	20100830	4.10	0.40
EQUITY PRECIPITATION	20100930	5.80	
NESLON PRECIPITATION	20100930	5.30	
Berkshire shaft -1	20101103	0.00	0.40
CREEDE-NO NAME	20101103	-0.20	0.40
DECLINE	20101103	-0.30	0.40
NELSON BAHELOR	20101103	0.90	0.30
Nelson Portal	20101103	0.60	0.30
TELLURIDE RAIN	20110719	3.9	
RICO SNOW	20111007	13.7	0.7
Berkshire Shaft -40'	20121029	0.44	0.23
Berkshire shaft -65'	20121029	0.74	0.24

Bachelor Shaft -15	20121030	0.02	0.20
Berkshire shaft -60'	20121030	0.92	0.24
NELSON BAHELOR	20121030	1.10	0.24

Appendix 5

Carbon isotopes for DOC and DIC from samples collected from 2009 to 2013. Abbreviations: DOC, dissolved organic carbon; DIC, dissolved organic carbon; pMC, percent modern carbon; DOM, dissolved organic matter.

Site	Date	DIC pMC	DIC pMC error	DIC Age	DIC Age error	DIC $\delta^{13}\text{C}$	DIC $\Delta^{14}\text{C}$	DOC pMC	DOC pMC Error	DOC Age	DOC Age Error	DOC $\delta^{13}\text{C}$ ‰	DOC Type
Berk Shaft -40'	10/29 2012	0.1392	0.0011	15850	65	-8.02	-861.8	0.394	±0.0013	7,485	±30	-22.0	Fulvic acid
Berk shaft -65'	10/29 2012	0.1325	0.0009	16250	55	-8.91	-868.4	0.314	±0.0013	9,305	±35	-22.0	Fulvic acid
Berk shaft -60'	10/29 2012	0.1349	0.0009	16100	55	-8.83	-866.2	NA	NA	NA	NA	NA	NA
Nelson @ Bach	10/30 2012	0.2841	0.0011	10100	30	-11.07	-718.0	NA	NA	NA	NA	NA	NA
Nelson @ no name	10/30 2012	0.1986	0.0011	13000	45	-8.89	-802.9	0.3934	±0.0015	7,495	±35	-22.7	Fulvic acid
Bachelor Shaft -15	10/30 2012	0.2671	0.0011	10600	35	-9.85	-734.9	0.42	±0.0014	6,970	±30	-21.6	Fulvic acid
Nelson Portal	10/30 2012	0.333	0.002	8830	50	-10.15	-669.5	0.381	±0.0016	7,750	±35	-23.3	Fulvic acid
West Willow Creek	10/3 2012	0.99	0.0106	80	85	-2.67	-17.35	0.8828	±0.0020	1,000	±20	-28.0	Fulvic acid
HW 4 Well	2/5 2013	0.1992	0.001	12950	40	-8.04		0.4568	0.0012	6,295	30	-27.2	Fulvic acid
Salomon Adit	2/5 2013	0.7018	0.0032	2840	35	-11.96		NA	NA	NA	NA	NA	NA
East Willow	2/5 2013	1.0153	0.003	>Modern		-4.95		NA	NA	NA	NA	NA	NA
HW 4 Well Dup	2/5 2013	0.2185	0.0012	12200	45	-6.51		0.3861	0.0013	7645	30	-31.4	Fulvic acid
Bach Well	2/6 2013	0.9723	0.0028	225	20	-16.81		0.5346	0.0013	5,030	20	-28.8	Fulvic acid
Nelson @ Bach	6/9 2009	0.2438	0.0016	11350	50	-10.35		0.2509	± 0.0013	11,105	±40	-36.0	Whole DOM
Nelson Portal	6/9 2009	0.3086	0.0019	9440	50	-10.67		NA	NA	NA	NA	NA	NA
Nelson @ no name	6/9 2009	0.2124	0.0014	12450	55	-10.21		NA	NA	NA	NA	NA	NA
Berk Shaft -1	6/9 2009	0.2827	0.0019	10150	55	-10.89		0.1942	± 0.0007	13,165	±30	-39.3	Whole DOM
Emerald Ranch Well	7/15 2009	0.5446	0.0021	4880	30	-14.60		NA	NA	NA	NA	NA	NA

Appendix 6

Loadings, components, and fluorescence indices results from fulvic acid fractions of dissolved organic mater isolated from mine samples. Loadings (LC) and components (%C) are based on the Cory-McKnight parallel factor analysis model while indices were calculated from the resulting EEMs.

Sample	LC1	LC2	LC3	LC4	LC5	LC6	LC7	LC8	LC9	LC10	LC11	LC12	LC13	SU M
Berk Shaft -40	2.28 E+01	6.48 E+01	4.14 E+01	1.09 E+01	5.59 E+00	4.28 E+01	4.32 E+00	8.40E +01	2.28E +01	2.26 E+01	3.56 E+01	1.69 E+02	0.00 E+00	526 .64
Berk Shaft -65	1.99 E+01	5.20 E+01	3.93 E+01	1.71 E+01	3.66 E+00	3.01 E+01	6.05 E+00	5.92E +01	1.84E +01	2.25 E+01	2.97 E+01	1.23 E+02	2.17 E+00	422 .93
Nelson @ Bach	2.48 E+01	6.91 E+01	3.52 E+01	3.59 E+01	6.54 E+00	2.87 E+01	1.12 E+01	4.51E +01	1.67E +01	1.93 E+01	3.30 E+01	1.02 E+02	1.44 E+01	442 .42
Bachelor shaft	5.03 E+01	1.05 E+02	3.60 E+01	9.66 E+01	2.03 E+01	5.92 E+01	1.70 E+01	6.29E +01	1.35E +01	7.34 E+01	7.05 E+01	1.33 E+02	2.39 E+01	762 .07
Nelson Portal	2.84 E+01	6.81 E+01	3.77 E+01	4.32 E+01	6.34 E+00	1.25 E+01	1.58 E+01	5.37E +01	5.16E +00	2.75 E+01	3.98 E+01	1.00 E+02	6.54 E+01	503 .72
HW4 Well	7.75 E+01	1.93 E+02	1.13 E+02	1.77 E+02	1.68 E+01	3.71 E+01	4.19 E+01	1.65E +02	2.75E +01	9.38 E+01	1.22 E+02	2.89 E+02	1.40 E+02	149 3.6
East Willow	1.72 E+02	2.73 E+02	1.14 E+02	3.33 E+02	9.23 E+01	1.08 E+02	8.00 E+01	8.27E +01	8.15E +01	8.28 E+01	1.36 E+02	2.34 E+02	1.27 E+01	180 1.5
Bach Well	3.24 E+01	7.09 E+01	3.45 E+01	6.85 E+01	9.99 E+00	0.00 E+00	1.47 E+01	8.37E +01	2.54E +00	1.24 E+01	2.91 E+01	7.40 E+01	1.31 E+02	563 .35
Nelson Portal	1.44 E+02	2.68 E+02	1.51 E+02	1.50 E+02	3.60 E+01	8.90E +01	7.40 E+01	2.17E +02	5.25E +01	9.37 E+01	1.18 E+02	2.99 E+02	1.91 E+01	171 0.1 39
	%C1	%C2	%C3	%C4	%C5	%C6	%C7	%C8	%C9	%C10	%C11	%C12	%C13	
Berk Shaft -40	4%	12%	8%	2%	1%	8%	1%	16%	4%	4%	7%	32%	0%	
Berk Shaft -65	5%	12%	9%	4%	1%	7%	1%	14%	4%	5%	7%	29%	1%	
Nelson @ Bach	6%	16%	8%	8%	1%	6%	3%	10%	4%	4%	7%	23%	3%	
Bachelor shaft	7%	14%	5%	13%	3%	8%	2%	8%	2%	10%	9%	17%	3%	
Nelson Portal	6%	14%	7%	9%	1%	2%	3%	11%	1%	5%	8%	20%	13%	
HW4 Well	5%	13%	8%	12%	1%	2%	3%	11%	2%	6%	8%	19%	9%	
East Willow	10%	15%	6%	18%	5%	6%	4%	5%	5%	5%	8%	13%	1%	
Bach Well	6%	13%	6%	12%	2%	0%	3%	15%	0%	2%	5%	13%	23%	
Nelson Portal	8%	16%	9%	9%	2%	5%	4%	13%	3%	5%	7%	17%	1%	
	FI	% Protein	RI	Max Emis 370	Abs 254	HIX	FIX BIX	DOC mg/L	SUVA L/mg -M					
Berk Shaft -40	1.64 E+00	16%	0.1391 42694	4.48 E+02	7.47 E-03	1.61 E+00	8.67 E-01	0.47	1.58					
Berk Shaft -65	1.74 E+00	15%	0.1809 57335	4.50 E+02	2.21 E-03	2.11 E+00	8.34 E-01	0.32	0.68					
Nelson @ Bach	1.53 E+00	13%	0.2559 62546	4.48 E+02	8.77 E-03	2.68 E+00	8.41 E-01	0.12	7.41					

Bach Shaft below Nelson	1.36 E+00	11%	0.3229 65175	4.72E +02	1.89E -02	2.52 E+00	5.69 E-01	0.26	7.37					
Nelson Portal	1.47 E+00	24%	0.2531 00619	4.64E +02	6.39E -03	4.50 E-01	8.32 E-01	0.18	3.61					
HW4 Well	1.48 E+00	20%	0.3036 52005	4.58E +02	5.38E -02	1.18 E+00	7.74 E-01	2.21	2.43					
East Willow	1.41 E+00	5%	0.4769 28004	4.60E +02	8.30E -02	4.86 E+00	6.55 E-01	0.91	9.15					
Bach Well	1.41 E+00	38%	0.3548 88997	3.00E +02	1.13E -01	5.40 E-01	7.95 E-01	0.90	12.57					
Nelson Portal	1.63 E+00	14%	0.3129 34855	4.58E +02	6.78E -02	2.00 E+00	7.84 E-01							